

Copyright

by

Abdelhakim Bouadi

1994

**USE OF ECCENTRICALLY BRACED FRAMES (EBFS) FOR SEISMIC
STRENGTHENING OF REINFORCED CONCRETE FRAMES**

by

ABDELHAKIM BOUADI, M.Sc.

DISSERTATION

Presented to the Faculty of the Graduate School of

The University of Texas at Austin

in Partial Fulfillment

of the Requirements

for the Degree of

DOCTOR OF PHILOSOPHY

THE UNIVERSITY OF TEXAS AT AUSTIN

August 1994

**USE OF ECCENTRICALLY BRACED FRAMES (EBFs) FOR SEISMIC
STRENGTHENING OF REINFORCED CONCRETE FRAMES**

Approved by

Dissertation Committee:

Michael W. Dwyer

Richard E. Meyer

James D. Gusa

Joe W. Roedel

[Signature]

To my dear wife, Lila Ghemri

ACKNOWLEDGEMENTS

The author gratefully acknowledge financial support provided by the National Science Foundation Grant N° BCS-8820502.

I wish to express my deepest and sincere gratitude to Dr. Michael D. Engelhardt for his patience, guidance, support, and encouragements. I feel very fortunate to have worked under the supervision of Dr. Engelhardt who has enriched my education and has been a great source of motivation. Deepest thanks are extended to Dr. J. O. Jirsa who provided helpful suggestions and additional guidance in this research. I am also very indebted to Dr. Jirsa for all his guidance throughout my graduate program. Special thanks are extended to Dr. M. E. Kreger, Dr. J. M. Roesset, and Dr. S. Kyriakides who accepted to be member of the dissertation committee and to review this work. The help and friendship of Dr. Jose Pincheira, a Ferguson Laboratory graduate, are appreciated .

Special thanks are extended to the staff of Phil M. Ferguson Structural Engineering Laboratory. The author wishes to particularly thank Ryan Green, April Jenkins, and Laurie Golding.

I wish to thank all my fellow graduate students who made working at Ferguson Laboratory a joyful experience. In particular, the author wishes to thank Ryad Aboutaha, Todd Helwig, Khaled Kahhaleh, Carin Roberts, Karen Ryals, and Raj Valluvan.

Finally, and of course, my deepest gratitude goes to my wife, Dr. Lila Ghemri, for her love and continual support, for taking time to read this dissertation and suggesting changes, for providing me with so much needed support and encouragements, and simply -and more importantly- for being herself.

USE OF ECCENTRICALLY BRACED FRAMES (EBFS) FOR SEISMIC STRENGTHENING OF REINFORCED CONCRETE FRAMES

Publication No _____

Abdelhakim Bouadi, Ph.D.

The University of Texas at Austin, 1994

Supervisor: Michael D. Engelhardt

Older reinforced concrete structures are often found inadequate to resist seismic loading. These structures are characterized by limited strength and stiffness and by low ductility. The risk of potential structural failures in these buildings indicates the need for seismic retrofit.

In the present research conducted in this project, the feasibility of using steel EBFs to retrofit existing nonductile reinforced concrete frames is investigated. EBFs are a well recognized seismic lateral resisting system for new steel buildings. However, up to now little research effort has been devoted to the use of EBFs as a retrofit scheme. EBFs exhibit high stiffness and strength, large ductility, and stable hysteretic behavior under cyclic load.

This investigation consists of an analytical study of medium rise and low rise reinforced concrete buildings, representative of the 1950s and 1960s west coast construction. The response of the buildings to strong motion earthquake records are investigated both before and after being retrofitted with steel EBFs. A number of variables affecting the bracing retrofit schemes are investigated, including bracing configuration, strength, strength distribution with height, and link length. Some additional analyses are conducted on the buildings retrofitted with steel concentrically braced frames, for comparison with the EBFs. The existing and retrofitted structures are analyzed under static and dynamic load.

The research shows that EBFs constitute an effective retrofit scheme, can control drift, and provide an increase in strength, stiffness, and ductility. The use of EBFs with very short links was found to be advantageous. Reducing the strength and stiffness of the EBFs along the building height in an attempt to match the seismic force demands, results in better behavior. The study shows that EBFs alone may not be sufficient in preventing column shear failure. For a building exhibiting low column shear strength, in addition to the EBFs, it is necessary to either increase the shear capacity of the columns or change their mode of failure to a ductile flexural mode. Finally, simple design recommendations for EBF retrofit schemes are presented.

TABLE OF CONTENT

CHAPTER 1: INTRODUCTION	1
1.1 Introduction	1
1.2 Objectives	2
1.3 Scope	2
CHAPTER 2: LITERATURE REVIEW	4
2.1 Introduction	4
2.2 Evaluation of Existing Buildings	4
2.3 Selected Seismic Retrofit Techniques	6
2.3.1 General	6
2.3.2 Steel Bracing	7
2.3.3 Addition of Infill Walls	10
2.3.4 Jacketing	11
2.3.5 Connections and Interface	12
2.3.6. Column Splice Retrofit	15
2.3.7 Observations on Retrofit Techniques	15
2.4 Background on EBFs for Seismic Design	16
2.4.1 General	16
2.4.2 Influence of Link Length	17
2.4.3 EBF Energy Dissipation Mechanism	18
2.4.4 Selection of EBF Configuration	19
2.4.5 Link Behavior	19
2.4.6 Selected Tests on EBFs	20
2.5.7 Connection Details and Lateral Supports	21
2.4.7 Summary on EBFs	22
CHAPTER 3: ANALYTICAL MODELING	39
3.1 General	39

3.2 Program Design	39
3.3 Analysis Method	41
3.4 Integration Procedure	41
3.5 Damping	42
3.5.1 DRAIN-2D Formulation	42
3.5.2 Effect of Viscous Damping on EBFs	43
3.5.3 Changes in Damping Formulation in DRAIN-2D	44
3.6 Details of Selected DRAIN-2D Element Subroutines	45
3.6.1 General	45
3.6.2 Reinforced Concrete Element	45
3.6.3 Beam Column Element	48
3.6.4 Shear Link Element	49
3.6.5 Brace Buckling Element	50
3.7 Evaluation of Shear Link Element	52
3.7.1 Introduction	52
3.7.2 Comparison with an Experiment on an Isolated Link	53
3.7.3 Comparison with an Analytical Study of an EBF	54
3.7.4 Conclusion	56
3.8 Evaluation of the Brace Buckling Element	56
3.9 Additional Discussion on Analytical Modeling of EBFs and CBFs	58
3.9.1 Analytical Modeling of EBFs	58
3.9.2 Analytical Modeling of CBFs	59
3.9.3 Concluding Remarks	60
CHAPTER 4: GROUND MOTIONS AND ANALYSIS OF A SIMPLE FRAME	78
4.1 Introduction	78
4.2 Ground Motion Selected	78
4.2.1 Acceleration Records	78
4.2.2 Elastic Spectral Responses	79
4.3 Analysis of a Two-Story Frame	80

4.3.1 Introduction	80
4.3.2 Original Structure	80
4.3.3 Retrofitted Structure	82
4.3.4 Static Elastic Analysis	87
4.3.5 Static Inelastic Analysis	88
4.3.6 Dynamic Analysis	89
4.3.7 Concluding Remarks	90
CHAPTER 5: THREE-STORY BUILDING	107
5.1 General	107
5.2 Structural Details	107
5.3 Analytical Modeling	109
5.3.1 Modeling of the Columns	109
5.3.2 Modeling of the Beams	110
5.4 Static Inelastic Analysis of the Original Building	110
5.5 Dynamic Analysis of the Original Building	111
5.6 Concluding Observations on the Original Building	112
5.7. Description of EBF Retrofit Schemes	113
5.8 Modeling of EBF Retrofit Schemes	115
5.9 Static Analyses of EBF Retrofit Schemes	115
5.10 Dynamic Analysis of EBF Retrofitting Schemes	119
5.10.1 Period of Vibration	119
5.10.2 Maximum Interstory Drift of the Retrofit Structures	119
5.10.3 Roof Displacements	122
5.10.4 Plastic Deformations of the Structure	122
5.10.5 Axial Load at the Building Foundation	130
5.10.6 Distribution of Lateral Load	132
5.11 Summary on the Three Story Building	134

CHAPTER 6: SEVEN-STORY BUILDING	183
6.1 General	183
6.2 Details of Structural Members	183
6.3 Analytical Modeling	185
6.3.1 General	185
6.3.2 Column Modeling	185
6.3.3 Beam Modeling	186
6.4 Static Analysis of the Original Building	186
6.5 Dynamic Analysis of the Original Building	187
6.6 Concluding Observations	188
6.7 Retrofit Schemes I: Column Shear Failure Prevented	189
6.7.1 Description of Retrofit Schemes I	189
6.7.2 Modeling of Retrofit Schemes I	190
6.7.3 Static Analysis of Retrofit Schemes I	192
6.7.4 Dynamic Analysis of Retrofit Schemes I	194
6.7.5 Concluding Remarks	196
6.8 Retrofit Schemes II: Shear Failure Prevented	197
6.8.1 General	197
6.8.2 Static Analysis of Retrofit Schemes II	197
6.8.3 Dynamic Analysis of Retrofit Schemes II	198
6.8.4 Concluding Observations	201
6.9 Retrofit Schemes III: Weaker Spandrels	202
6.9.1 Modeling of Retrofit Schemes III	202
6.9.2 Static Analysis of Retrofit Schemes III	203
6.9.3 Dynamic Analysis of Retrofit Schemes III	204
6.10. Retrofit Scheme IV: Minimum Requirements	210
6.10.1 Static Analysis of Retrofit Scheme IV	211
6.10.2 Dynamic Analysis	211
6.10.3 Summary on EBF4W	212
6.11. Summary on the Study of the Seven-Story Building	213

CHAPTER 7: DISCUSSION OF RESULTS AND DESIGN RECOMMENDATIONS	250
7.1 Introduction	250
7.2 General Observations	250
7.3 Comparison of EBF and CBF schemes	253
7.3.1 Introduction	253
7.3.2 Analytical Behavior of EBF and CBF Retrofit Schemes	253
7.3.3 Analytical Modeling of EBFs and CBFs	256
7.3.4. Review of Experimental Behavior of EBFs and CBFs	257
7.3.5 Post Earthquake Repair in EBFs and CBFs	258
7.3.6 Conclusions	259
7.4 Comparison of Analytical Results to ATC 22 provisions	260
7.4.1 Introduction to ATC 22	260
7.4.2 Evaluation of Case Study Building by ATC 22	261
7.5 Preliminary Design Recommendation for EBF Retrofit Schemes	264
7.5.1 Introduction	264
7.5.2 Estimation of Required Strength	264
7.5.3 Estimation of Ultimate Drift	266
7.5.4 Estimation of Maximum Link Rotation	268
7.5.5 Estimation of Maximum Axial Load in the Columns	270
7.5.6 Summary of Suggested Design Procedure	274
7.5.7 Observations on Link Connections Details	274
CHAPTER 8: CONCLUSIONS	290
8.1 Summary	290
8.2 Conclusions	292
8.3 Need for Further Research	294
REFERENCES	295
VITA	302

CHAPTER 1:

INTRODUCTION

1.1. Introduction.

Reinforced concrete structures built according to the 1950s and 1960s standards are often found inadequate to resist seismic loading. These structures are characterized by limited strength and stiffness due to low design force requirements, and by low ductility due to poor detailing procedures. Past earthquakes have subjected such structures to heavy damage, indicating their poor seismic performance. As an example, the 1970 San Fernando earthquake caused severe damage to a number of buildings including the Olive View Hospital which was provided with poorly designed columns and a soft first story (Lew et al., 1971). More recently, the 1989 Loma Prieta led to a dramatic failure of the Cypress Viaduct that was poorly detailed.

The risk of potential structural failures in older buildings has triggered the need for seismic retrofit. Retrofit projects are performed to either repair a building that was damaged by an earthquake, or to strengthen a building to improve its behavior in future earthquakes. A significant research effort has already been devoted to developing retrofit techniques. A number of examples of actual building retrofit projects are documented in the literature, including the Durango Building in Mexico City (Foutch et al., 1989) or the University Hall in Berkeley, California (Wyllie, 1991). Existing retrofit techniques consider either improving the behavior of isolated elements or providing a new lateral load resisting system. The first type of retrofit scheme includes concrete and steel jackets. The second type of retrofit technique includes the addition of infill walls, or steel bracing.

Several studies have been conducted on the use of steel concentrically braced frames (CBFs) to retrofit existing buildings. CBFs have also been used to retrofit existing buildings in seismic areas. CBFs can provide an increase in strength and stiffness and help improve the seismic behavior of existing buildings. However, CBFs are also known to exhibit strength and stiffness deterioration following brace buckling. Brace buckling limits the energy dissipation

capacity of the structure and imposes very large forces and deformations on the brace connections.

Steel eccentrically braced frames (EBFs) can overcome such deficiencies since they are designed to prevent brace buckling. In EBFs, inelastic action is limited to the links, and the remaining members, including the braces, are designed to behave elastically. This design concept provides EBFs with a combination of high stiffness and strength and excellent energy dissipation capacity. EBFs are known to exhibit stable cyclic behavior to large drifts.

EBFs have become a well recognized and widely used seismic lateral resisting system for new steel buildings. Up to now however, little research effort has been devoted to the use of EBFs as a retrofit scheme. The present research aims at investigating the feasibility of using steel EBFs to retrofit existing nonductile reinforced concrete frames.

1.2 Objectives.

As mentioned above, the main objective of this study is to investigate the possibility of using steel EBFs as a retrofit scheme for reinforced concrete frames that are inadequately designed to resist seismic loading. The study will identify the range of applicability of EBFs as a retrofit scheme along with potential merits and inadequacies. The seismic performance of EBF retrofit schemes will be compared to the performance of CBF retrofit schemes. The study will also aim at providing practical design guidelines for EBFs in retrofit applications.

1.3 Scope.

The seismic performance of EBF retrofit is evaluated using the computer program DRAIN-2D (Kanaan and Powell, 1975). DRAIN-2D allows for nonlinear analysis of two-dimensional frames under seismic excitation.

The research is limited to reinforced concrete moment resisting frames designed according to the 1950s and 1960s standards. Two prototype buildings are selected for the analysis: a three-story low rise building and a seven-story medium rise building. The medium rise building is characterized by short columns with low shear strength and deep spandrel beams. The low rise building has inadequate column lap splices, insufficient embedment lengths of the bottom reinforcement in the beams, and poor confinement.

The two reinforced concrete buildings are retrofitted with either steel eccentrically braced frames (EBFs) or steel concentrically braced frames (CBFs). To limit building disruption during construction, the bracing system is added to the external frames only. The schemes considered variation in strength, stiffness, and configuration. Effects of the link length are also evaluated.

The buildings are analyzed under static and dynamic load. The static analyses are conducted by subjecting the structures to a lateral incremental load. The dynamic analyses are performed using a set of three firm soil earthquake records and two soft soil earthquake records.

CHAPTER 2: LITERATURE REVIEW

2.1 Introduction.

Extensive effort has been devoted in the past two decades to seismic retrofitting of existing reinforced concrete structures. Retrofit procedures are undertaken to either strengthen inadequately designed structures or to repair buildings damaged by an earthquake. The objective of seismic retrofit is to increase the stiffness, strength, and/or, ductility of a building in order to improve its performance in future earthquakes.

A variety of retrofit techniques have been developed. Some of these techniques, such as column jacketing, tend to improve the behavior of the structure by increasing the strength and ductility of some structural elements. Other methods, such as the addition of bracing or walls, provide for an alternate lateral resisting system. Bracing techniques used for seismic retrofit include steel concentrically braced frames (CBF) and post-tensioned cables. As yet however, steel eccentrically braced frames (EBFs) have received little attention as a retrofit scheme, although they are a well recognized lateral load resisting system for new steel buildings.

This chapter will review some procedures available to evaluate the ability of existing structures to perform satisfactorily under an earthquake. The most widely used techniques to retrofit reinforced concrete frames are then presented. Finally research performed to investigate the behavior of EBFs will be summarized.

2.2 Evaluation of Existing Structures

Structural evaluation is the first step undertaken to decide whether to seismically retrofit an existing building. To evaluate the structure, the designer needs to obtain information on the member dimensions, material properties, and steel reinforcing detailing. The original

drawings can be a good resource. However, because these drawings may not be available or because of possible discrepancies between the construction and the drawings, an on-site inspection is necessary. Once the structural information is gathered, the seismic evaluation of the structure can be performed. Several documents are available to assist the engineer in the evaluation of existing buildings. The procedures most widely used in the U.S. and in Japan are summarized below.

In the United States, ATC 22 recommendations (Applied, 1989) constitute the main tool used to evaluate the seismic performance of existing buildings. The primary objective of these provisions is to determine if a structure, or structural components, present an "unacceptable risk to human life" under severe ground motions. A structure is considered adequate if its lateral strength at "first significant yield" is higher than a minimum specified lateral load. ATC-22 lateral load is taken equal to $(LF) C_s W$, where LF is a load factor, W is the building weight, and C_s is a base shear coefficient that depends on the building's location, and lateral load resisting system. The load factor, LF , provides for an increase in the lateral load for structures with low ductility. Further details of the ATC-22 procedure and its application can be found in Chapter 7.

The Japan Building Disaster Association (JBDA) published a standard for evaluation of existing reinforced concrete buildings in 1977, and presented a revised version in 1990 (Japan, 1990). These standards are limited to low and medium rise reinforced concrete buildings and are based on a concept initially developed by Okada and Bresler (1976).

The seismic safety of an existing building is evaluated by a performance index I_s defined as:

$$I_s = E_0 G S_D T \quad (2.1)$$

where G is a soil profile parameter, S_D is a structural index that depends on the building configuration, on the stiffness distribution over the building height, and on the type of lateral

load resisting system. T considers the long term effects such as creep and shrinkage, and E_o measures the energy dissipation capacity of the structure, and is defined as:

$$E_o = C F \quad (2.2)$$

where F is a ductility index, and C is the shear strength of the level considered divided by the weight of the floors above that level.

A building is considered adequate if the structural index, I_s , exceeds a specified minimum value I_o . The value of I_o depends on the building location, the type of soil, the building use, and the type of lateral load resisting system.

Umemura (1980) summarized two studies conducted to verify the application of the Japanese evaluation method. In the first study, the behavior of a large number of single story buildings was analytically investigated under dynamic earthquake loading. The second study dealt with the observed behavior of 39 buildings that experienced severe earthquakes. Both studies showed good correlation between the behavior of the structures studied or the observed damage and the value of their seismic performance index, I_s .

2.3 Selected Seismic Retrofit Techniques.

2.3.1 General. As mentioned earlier, extensive research work has been performed in the last two decades to develop retrofit techniques for seismically inadequate structures. A report published by the Federal Emergency Management Agency (FEMA) summarized many techniques used to retrofit a wide range of buildings (Federal, 1989). The report, based on a literature review, discusses the merits and disadvantages of the techniques presented and provides a substantial reference list. The discussion in this section will be limited to the major techniques used to retrofit reinforced concrete moment frames.

2.3.2 Steel Bracing. The seismic performance of existing reinforced concrete frames can be greatly improved by the addition of steel braces. Bracing provides a substantial increase in stiffness and strength with a minimum increase in weight. Furthermore, the braces can limit disruption to the building during the construction process since they are often attached to the external frames only. The use of braces as a retrofit, however, can induce additional axial forces in the columns and foundation. If these forces are too high, strengthening of the columns and foundations can be required. Also, braces alter the architectural configuration of the building and may obstruct windows and access ways.

Jones and Jirsa (1986) conducted an experimental study on the use of steel concentric bracing to retrofit a reinforced concrete frame with deep spandrel beams and short columns with low shear strength (Fig. 2.1). The braces were made of wide flange sections and were designed to carry all the lateral load due to current seismic design codes. Attachment of the steel bracing to the existing concrete frame was provided by means of steel collectors that were attached with epoxy grouted dowels into the existing beams and columns. Welded connections were used between the braces and the collectors. The tests were performed under static cyclic load.

The test results showed that adding an concentric bracing system greatly improved the behavior of the original building. The retrofitted specimen carried a lateral load three times higher than the design load and about six times higher than the strength of the original reinforced concrete frame. The capacity of the retrofitted frame was limited by a welded connection failure. The vertical collectors increased the stiffness and strength of the columns. The increase in the column shear strength was, however, difficult to predict analytically and may not be sufficient to prevent column shear failure (Bush, 1987).

Badoux (1987) conducted an analytical study to further investigate the adequacy of steel concentrically braced frames (CBFs) as a retrofit scheme for reinforced concrete frames. A parametric study was included to consider the effect of the braces slenderness ratio. The research showed that the bracing system can be adjusted to provide for different design

objectives that include drift control and collapse prevention. Columns and foundations may need to be strengthened due to the load increase introduced by the added CBF. Brace buckling was found to produce large deformations and a reduction in the energy dissipation capacity. To limit the effects of brace buckling, the study recommended that the slenderness ratio of the braces be kept below 80. For frames with columns having inadequate shear strength, Badoux (1987) showed that the increase in stiffness provided by the added CBF may not necessarily prevent column shear failure.

Steel bracing was used to repair the Durango building (Fig. 2.2), a twelve-story reinforced concrete structure located in Mexico City and damaged by an earthquake in 1970 (Foutch et al., 1989). The external frames had deep spandrel beams and short columns. The bracing configuration was the same throughout the building height except for the ground level, in order not to hinder building access. Vertical steel collectors were attached to the external face of the existing reinforced concrete columns. New footings and piles were placed under the vertical steel collectors. To ensure monolithic behavior, the added footings were attached to the original foundation. The repair scheme increased the strength and stiffness of the building. Due to the shape of the response spectra of Mexico city earthquakes, the increase in stiffness led to a substantial reduction in the seismic force demands which helped improve the performance of the building under the 1985 Mexico city earthquake. A study of this structure by Foutch et al. (1989) concluded that this scheme would require additional strengthening of the columns if used for a building on the stiff soils of California.

A reinforced concrete building, at the Tohoku Institute of Technology in Sendai, Japan was repaired by the addition of steel concentric bracing (Fig. 2.3) (Kawamata and Ohnuma, 1980). The building is an eight-story structure with external deep spandrel beams and short columns with low shear strength. The repair was performed following the 1978 Miyagi-Ken-Oki earthquake that caused shear failure of several columns.. The retrofit scheme included weakening the beams by coring the concrete in the vicinity of the columns. Beam weakening was performed to force hinging into the beams and to protect the columns against shear failure. To assess the effectiveness of the method, Kawamata and Ohnuma (1980) conducted an

experimental program on a beam-column subassemblage. The tests showed that the retrofit scheme increased the stiffness and strength of the building to an acceptable level of safety, and effectively prevented column shear failure.

Miranda (1990) conducted an analytical study on the use of post tensioned bracing to retrofit a low rise building located on soft soil in Mexico City. Post tensioned braces were found to significantly increase the strength and stiffness of the original building, and to improve the building's performance. However, it was noted that the braces introduced an increase in the column's axial load, and consequently column strengthening may be required.

Pincheira (1992) conducted an analytical study that considered the use of high strength post-tensioned steel braces to retrofit low and medium rise reinforced concrete buildings. The research examined the performance of the original buildings and retrofit schemes under static and earthquake load. Post tensioned braces are characterized by their high slenderness ratio, and were envisioned as an alternate to CBFs which introduce large forces and deformations in the connections due to brace buckling. The study by Pincheira (1992) concluded that post tensioned bracing successfully controlled lateral drift and prevented collapse. Better performance was observed for low rise buildings on soft soils. Initial prestressing of the bracing was found to help improve the seismic performance. The energy dissipation capacity was maximized for an initial prestress level of 50%. Initial prestressing, however can introduce large forces in the original building. If, the original frame is governed by column shear failure, the addition of post tensioned braces alone was found to be insufficient. In this case, it was recommended to strengthen the columns or to modify their failure mode to a more ductile failure. The research also found that the post tensioned bracing introduced large axial load in the columns and suggested the use of jackets to increase the column's capacity. Finally it was found that for low and medium rise buildings, the performance of post-tensioned bracing is comparable to concentric bracing.

2.3.3 Addition of Infill Walls. The addition of infill walls to a structure has the advantage of providing a substantial increase in stiffness and strength. The ductility of the structure can also be improved if the added walls are detailed to fail in flexure and if slip between the infill wall and the existing frame is minimized (Jimenez, 1989). The new infill wall can be connected to the existing frame with epoxy grouted dowels or other type of anchors.

Gaynor (1988) conducted experimental research to investigate the behavior of nonductile reinforced concrete frames retrofitted by the addition of shotcreted infill walls. The columns of the original frame were designed according to the standards of the 1950s. This resulted in inadequate splice length at the base of the columns and in widely spaced transverse reinforcement. The study considered the use of three types of infill walls: a full infill wall, an infill wall with a door opening, and an infill wall with a window opening (Fig 2.4). The shotcreted walls were connected to the exiting frames using epoxy grouted dowels.

The tests by Gaynor (1988) showed that the strength of the repaired structure was limited by the nonductile columns of the original frame. The capacity of the specimen with the solid wall and the wall with a door opening was controlled by a splice failure at the base of the non ductile columns. The wall with a window opening failed by a combined shear failure of the columns and concrete crushing at the opening's corners.

Jimenez (1989) continued the experimental work initiated by Gaynor (1988), and tested a non ductile reinforced concrete frame retrofitted by a cast-in-place wall. The study used the same boundary frame as the one used by Gaynor (1988). The cast-in-place wall was eccentric with respect to the original frame and was connected to the existing beams and columns with epoxy grouted dowels (Fig. 2.5). To avoid premature failure of the non ductile frame, the columns were provided with a reinforced concrete jacket.

The tests showed that the jackets were very effective in improving the behavior of the system and in preventing splice or shear failure in the original columns. The strength and ductility of the eccentric wall were much higher than the shotcreted infill walls tested by Gaynor

(1988). The capacity reached by the system was in excess of the maximum strength predicted by ACI 318.

2.3.4 Jacketing. Jacketing is performed by encasing the original structural elements with a reinforced concrete member or steel elements. The jackets improve the performance of the retrofitted members without modifying the lateral load resisting system. This technique does not require major changes in the architectural configuration of the building and may require only minor or no changes in the foundations. However, concrete jacketing may not be cost effective because of the difficulty associated with providing transverse reinforcement (Federal, 1989, Alcocer and Jirsa, 1991).

Bett (1985) conducted an experimental program to study the behavior of short columns repaired or strengthened with reinforced concrete jackets. The research included testing an original short column designed according to the standards of the 1950s and 1960s. The specimen was repaired by the addition of a concrete jacket and tested again under cyclic loads. Two additional short columns were strengthened with concrete jackets and tested under cyclic loads. The original column experienced a brittle shear failure at a drift ratio of about 1%. The retrofitted specimens exhibited greater ductility, strength, and stiffness than the original column. In addition, the retrofitted specimens failed in a more ductile manner and exhibited stable hysteretic behavior under cyclic load.

Alcocer and Jirsa (1991) tested a reinforced concrete beam-column subassembly representing an interior joint designed according to the US and Mexican practice of the 1950's (Fig. 2.6). The joint was not detailed for ductile behavior. The beams and slab were designed for heavy gravity load and the columns were designed for low lateral forces. This resulted in a joint with strong beams and a weak column. The original specimen was tested to failure, repaired with a concrete jacket and tested again. Three other strengthened specimens were tested. Two of them considered jacketing the column only. The third one considered jacketing the beams and column. For all retrofitted specimens, a steel jacket was used to confine the

joint region. Figure 2.7 shows typical results of the study. The original specimen exhibited poor performance and experienced a large amount of damage in the column. The repaired and strengthened specimens showed a major improvement in the response and exhibited higher strength and better energy dissipation. The repaired specimen (initially damaged) exhibited double the strength of the original one but had less stiffness than the strengthened specimens (initially not damaged). The best performance was obtained for the strengthened specimen that included with jacketing of the beams and column.

Aboutaha and Engelhardt (1994) are currently conducting an experimental investigation at the University of Texas at Austin to assess the effectiveness of using steel jackets to retrofit existing reinforced concrete columns. The program involves testing a series of unretrofitted and retrofitted large scale columns with inadequate shear strength or inadequate lap splice. The retrofit schemes consisted of the addition of steel jackets or steel collars (Fig. 2.8). Figure 2.9 shows some experimental results of the tests on columns with low shear strength.

The tests by Aboutaha and Engelhardt (1994) showed that the addition of thin rectangular jackets constitutes a very effective strengthening scheme. The added steel jackets enhanced the performance of the column and increased its strength and stiffness. In addition, the retrofitted column exhibited good energy dissipation and showed no degradation until very large drifts. The use of collars to retrofit columns with low shear strength did not prove to be as effective as the solid steel jackets. The tests on columns with inadequate splices showed the jackets to be an effective retrofit scheme. The added steel jacket however, had to be of adequate height and had to be stiffened with an appropriate number of adhesive anchor bolts. The use of collars provided some improvements but was not as effective as the jackets.

2.3.5 Connections and Interface. As noted above, infill walls or concrete jackets are widely used to retrofit existing reinforced concrete frames. For this type of retrofit technique, proper shear transfer between the new and existing concrete is essential to insure monolithic behavior.

Bass (1985) conducted an experimental study to investigate the strength and behavior of the interface between new and existing concrete. 33 push-off specimens representing a column and an added wall were tested. Figure 2.10 shows a typical specimen. The parameters studied included surface preparation, amount and embedment depth of the interface reinforcement, reinforcement details in the new and existing elements, and the compressive strength of the new and old concrete.

The main results of the tests can be summarized as follow:

- 1) The current ACI 318 recommendations on the strength and embedment of the dowels are conservative.
- 2) A deeper embedment provided higher shear capacity at large drifts.
- 3) Specimen with no interface preparation showed the lowest shear capacity. For deep surface preparation, such as chipping to 1 in. deep shear keys, higher base block concrete strength resulted in higher shear capacity. For sandblasted surfaces, the concrete strength had no effect on the interface shear capacity.
- 4) Reinforcement details in the new and added elements did not have a significant effect on the interface shear capacity.

Valluvan (1993) continued the experimental work cited above on shear transfer across new and existing concrete and tested a series of similar push off specimens. The variables investigated included type of shear loading, i.e. monotonic or cyclic, level of compression on the interface, number of dowels across the interface surface, and concrete strength. The tests showed that the shear transfer capacity should be based on the dowel contribution only. The presence of permanent compression across the interface improved the interface capacity in direct shear. However, cyclic compression across the interface surface did not have a substantial influence on the interface performance. Consequently, unless permanent, compression across the interface should not be considered in computing the shear capacity. The tests also showed that dowels provided as shear connectors must be anchored on both sides of the interface to develop the dowel's yield strength. Otherwise, a higher number of dowels must be provided to compensate for premature pull out. Finally, the test results were

compared to the current provisions on shear transfer specified in Section 11.7 of ACI 318-89 code. These provisions were found not to reflect the behavior of test specimens, and modification to the current code were proposed.

Repair techniques often involve attaching steel members to existing reinforced elements. Such attachments can be found for example in schemes that consider the use of steel braces, or the addition of steel jackets. For such schemes, an effective procedure for force transfer between the existing concrete and the added steel is needed.

Jimenez-Pacheco (1992) conducted an experimental program to investigate the behavior of steel plates connected to a concrete member using epoxy-grouted steel anchors. 36 specimens were tested to investigate the behavior of single anchor steel-to-concrete connections. In the tests, a steel channel was connected to a concrete block by a threaded anchor, epoxy grouted into the concrete (Fig. 2.11). The variables studied included clamping force provided by the tightened anchor bolt, type of material used to fill the void between the rod and the steel hole and between the concrete and the steel, thickness of interface material, type of fastening methods (standard or spring washer), and type of loading (cyclic and monotonic).

Figure 2.12 show some typical plots of load versus slip between the steel and concrete. Test Results on monotonically loaded specimens showed that, in general the use of filler material increased the initial slip load but decreased the deformation capacity of the connection. The combination of epoxy in the annulus and a clamping force in the anchor proved to be very effective in increasing the initial slip load. Thick grout interface increased the deformation capacity of the connection. Cyclically loaded specimens showed the same type of initial response as the monotonically loaded specimens and similar peak strengths. After initial slip, however the cyclic response showed stiffness degradation. The use of spring loaded washers was found to limit stiffness degradation.

2.3.6. Column Splice Retrofit. One of the deficiencies identified in existing reinforced concrete buildings is the tensile capacity of lap splices in the columns. Generally, a short lap splice are used at the column base. Valluvan (1993) conducted an experimental study on retrofit techniques for columns splices. In the study a non-strengthened column specimen was first tested to provide a basis for comparison. Two specimens were strengthened by welding the bars together to provide a continuous force transfer along the steel. Nine specimens were strengthened by confining the lap splice region. This was accomplished by adding external steel straps and angles, by providing external ties, or by placing additional internal ties in the splice region after removal of concrete cover.

Valluvan's tests showed that welding the bars to provide a continuous load path enabled the longitudinal bars to reach yield in tension. For this scheme to perform satisfactorily, however, it was necessary to provide additional internal ties to control the thrust due to the eccentricity between the spliced bars. The addition of external ties or steel elements around the splice region significantly improved the splice performance. The external ties or steel straps need to be grouted to allow for proper confinement. Finally, it was observed that the addition of internal ties was not an effective retrofit scheme. It was inferred that removal of external cover (to place the ties) may have resulted in microcracking of the concrete core.

2.3.7 Observations on Retrofit Techniques. Several techniques can be used to retrofit reinforced concrete frames that are inadequately designed to resist seismic loading. Some of the most widely used of these procedures were discussed above. Additional methods can be found in a report published by the Federal Emergency Management Agency (Federal, 1989). The selection of a retrofit solution is usually a unique problem and depends on the building configuration and the requirements set by the owner.

To help assess the effectiveness of several retrofit techniques Sugano (1982) presented typical load-displacement relations for different retrofit schemes (Fig. 2.13). These plots were based on tests performed on more than 100 strengthened frames and 40 strengthened columns

in Japan. The plots indicated the level of strength, stiffness and ductility that can be gained by a given scheme. In the figure the strength of a monolithic reinforced concrete wall with boundary elements is represented by Q_w , and the strength of the original frame is represented by Q_F . The plots showed that the addition of infill walls with adequate connections resulted in the largest increase in strength. The infill wall, however, resulted in the lowest level of ductility and deformation capacity. The addition of steel concentric bracing or multiple precast panels resulted in a lesser increase in strength but provided higher ductility.

2.4. Background on EBFs for Seismic Design.

2.4.1. General. The purpose of this research is to investigate the use of steel eccentrically braced frames (EBFs) as a retrofit scheme for reinforced concrete buildings. Although EBFs have received little attention as a retrofit scheme, they are widely used as a lateral load resisting system for new steel buildings. Extensive research work was conducted on the seismic behavior of EBFs starting in the early 1970s at the University of California at Berkeley. In the following sections a summary of this research is presented. Additional information can be found in an overview of EBFs made by Popov and Engelhardt (1988).

Eccentrically braced frames (EBFs) can be defined as a bracing system in which at least one end of every brace is attached to a small beam element, of length e , referred to as a link (Fig. 2.14). In EBFs, energy dissipation is limited to the links. The remaining members are designed to behave elastically under the maximum forces generated by the strain hardened links. By designing the links to be the weak element of the structure, brace buckling is precluded. Brace buckling is known to cause degradation of strength and stiffness under cyclic loading for concentrically braced frames (CBFs).

The advantages of an EBF are illustrated by Figure 2.15 which shows lateral load versus deflection curves of three types of steel frames: a moment resisting frame (MRF), a concentrically braced frame, and an EBF. MRFs exhibit good ductility but low stiffness, and require large displacement to achieve significant energy dissipation. CBFs have a high initial

stiffness but experience reduction in strength and stiffness following brace buckling. EBFs combine the high stiffness of CBFs and the good energy dissipation capacity of MRFs.

2.4.2. Influence of Link Length. The stiffness and strength of EBFs were found to vary with the link length (e). Figure 2.16 shows typical results of a parametric study conducted by Hjelmstad and Popov (1984) on the effect of link length on the stiffness of EBFs. The figure suggests that short links lead to the largest stiffness and that for a ratio of e/L , L being the span length, higher than about 0.5, almost no additional stiffness is gained from the use of EBFs. The link length was also found to influence the strength of EBFs as demonstrated by a study by Kasai and Popov (1986c). Figure 2.17 shows the variation of the frame ultimate strength with the ratio e/L for a three-story EBF assuming elastic perfectly plastic behavior. The graph indicates that the EBF's strength increases with a decrease in e/L . From these studies, it appears that keeping the link length short, maximizes the gain in stiffness and strength. However, the link length cannot be made too short because of the increasing inelastic link rotation demands. The effect of the link length on the rotation demands will be discussed in the Section 2.4.3.

Under frame lateral loading, links are subject to high shear forces along their entire length and to high moments at their ends (Popov and Engelhardt, 1988). In general, long links tend to yield primarily in bending and short link tends to yield primarily in shear. Experimental studies have shown that EBFs with short links, yielding primarily in shear, exhibit better performance than EBFs with long links (Hjelmstad and Popov, 1983a, Hjelmstad and Popov, 1983b). For a predominately shear yielding link Kasai and Popov (1986b, 1986c) recommend that link length, e , be limited according Equation 2.3.

$$e \leq 1.6 \frac{M_p}{V_p} \quad (2.3)$$

In this equation, M_p is the plastic moment capacity, and, V_p is the plastic shear capacity of the link section.

The subsequent discussion will be limited to links that satisfy Equation 2.3 and that were found to have the best performance under cyclic loading.

2.4.3 EBF Energy Dissipation Mechanism. Links can be considered as the most critical member in an EBF structure. Energy dissipation under seismic loading is limited to the links and the capacity of an EBF is controlled by the link's strength and deformation capacity. Proper estimation of link rotation is thus essential. In current practice, plastic link rotations are estimated using energy dissipation mechanisms. Figure 2.18 shows typical mechanisms for two types of EBFs. These mechanisms assume rigid plastic behavior. Furthermore, shear hinges are assumed to form in the links and flexural hinges are assumed to form at the base of the building. Note that, with the exceptions of flexural hinges at the building base, inelastic action is limited to the links. This can be ensured by designing the link for specified forces (code level forces for example) and designing the other steel members for the forces generated by the fully strain hardened links as mentioned in Section 2.4.1.

For the EBFs shown in Figure 2.18, the plastic rotation of the links is related to the plastic drift ratio of the floor, θ by the following equation:

$$\gamma = \frac{L}{e} \theta \quad (2.4)$$

where L is the bay length, and e is the link length.

The relationship between the floor and the link plastic rotation depends on the EBF configuration. Equation 2.4 is valid only for the configurations shown in Figure 2.18.

Figure 2.19 shows the variation of the link plastic rotation with e/L . The link rotation is seen to increase rapidly with a reduction in the link length. Short links that satisfy Equation 2.3 are found to exhibit better seismic performance, as explained above. The links however cannot be made too short to avoid excessive rotation demands.

2.4.4 Selection of EBF Configuration. Links in EBFs are typically located either at the beam midspan or adjacent to a column as shown in Figure 2.14. If the link is placed next to a column, the link will transmit large moments to the adjoining column. These large moments must be considered in the design of the columns and the link-to-column connection. Large link end moments can cause premature failure at the link-to-column connection (Engelhardt and Popov, 1989b). EBFs with the links at midspan of the beams avoid potential problems associated with link-to-column connections.

2.4.5 Link Behavior. Hjelmstad and Popov (1983a, 1983b) tested a series of 15 links, 13 of which were designed as short shear yielding links. The main objectives of the tests was to understand the cyclic behavior of the links and to study the effects of web buckling. Figure 2.20 shows the experimental behavior of selected specimens. Inelastic web buckling was found to cause a degradation in link stiffness and strength. The link that was not provided with any stiffener showed very poor energy dissipation capacity. The addition of one stiffener improved the observed behavior, but web buckling still caused some degradation in strength and stiffness. The addition of a sufficient number of stiffeners successfully controlled web buckling and allowed the link to achieve large inelastic deformations while maintaining stable hysteretic loops.

In a subsequent study, Malley and Popov (1983, 1984) tested a series of 13 isolated links. One of the objectives of this experimental study was to determine the effects of stiffener details and spacing on the cyclic behavior of links. The study confirmed that to control web buckling and ensure good performance, links need to be provided with a number of properly spaced stiffeners. It was also shown that it was sufficient to provide only one side of the link web with stiffeners. The use of one sided stiffeners results in lower fabrication costs. Based on these tests, Kasai and Popov (1986a, 1986c) developed simple formula for spacing of stiffeners.

The tests summarized above showed that well detailed links can sustain a maximum plastic rotation, γ , under cyclic loading of about 0.10 rad. Beyond such rotation, links are found to experience web buckling or even web fracture, leading to rapid deterioration of stiffness and strength. The plastic shear rotation of the links can be simply approximated as the ratio of the end relative displacement over the link length. Throughout this study a plastic link rotation of 0.10 rad. was considered to represent link failure.

2.4.6 Selected Tests on EBFs. Roeder and Popov (1977, 1978) conducted a research program to investigate the behavior of EBFs under cyclic loads. For the first part of the study, a nonlinear dynamic analysis was conducted on a 20-story EBF prototype. This was followed by an experimental study on the cyclic performance of two one-third scale EBF frames. Each frame was three stories high. The study demonstrated the excellent performance of EBFs under cyclic loading. The results showed that EBFs possess high stiffness and high ductility. Stable hysteretic loops were observed to very large displacements.

In another study, a full scale six-story steel EBF was tested at the Building Research Institute (BRI) in Tsukuba, Japan as part of the US-Japan cooperative earthquake research program (Nishiyama et al., 1988, Foutch 1989). The building was designed to reflect the US and Japanese practices. The EBF was tested under the 1952 Taft earthquake record scaled to a peak ground acceleration of 0.5g. The structure survived well the simulated earthquake with minor damage and showed excellent ductility throughout the loading. The EBF was then subjected to larger lateral forces until a gusset plate at a brace-to-link connection, failed at the second floor. Despite the connection failure, the prototype EBF exhibited excellent ductility and stable hysteretic behavior. The tests demonstrated the need for proper detailing and design of the connections.

In a subsequent study, Whittaker et al. (1987) tested a one-third scale model that replicated the structure tested at BRI, but the detailing of the connections was improved. Connection failure was prevented and the building exhibited excellent behavior under a

number of simulated strong earthquake records. Lee and Lu (1989) conducted quasi static tests on a similar one-third scale model. These tests also showed very stable hysteretic behavior and high ductility of EBFs. The capacity of the structure was limited by link web fracture which occurred when the links reached a rotation of around 0.10 rad.

2.4.7 Connections Details and Lateral Support. Connection details of EBFs have been studied in a number of experimental investigations, and design guidelines are well established. Tests by Malley and Popov (1983, 1984) on isolated shear links indicated that link-to-column connections should be all welded to prevent premature connection failures. Subsequent tests by Engelhardt and Popov (1989b) showed all welded connections did not perform satisfactorily for long links that exceeded the limit of Equation 2.3. Current codes prohibit the use of links attached to columns when link length exceeds the limit of Equation 2.3. For links satisfying Equation 2.3, codes require all welded connections as shown in Figure 2.21. As noted earlier, potential problems at the link-to-column connection are completely avoided by placing the link at midspan of the beam.

Design of the brace-to-link connection also requires some special consideration in EBFs. As described above, a brace-to-link connection failed at a gusset plate during tests conducted on a full scale six-story EBF in Japan. An improved connection detail was developed and experimentally verified by Engelhardt and Popov (1989b). The improved detail is illustrated in Figure 2.21a. Additional recommended brace-to-link connection details are reported by Engelhardt and Popov (Engelhardt and Popov, 1992).

Lateral bracing must be provided at the top and bottom flanges of each link end of a link (Fig. 2.21.). Experimental tests (Engelhardt and Popov, 1989b) have shown the importance of this bracing for maintaining the stability of the link. The beam is subject to large bending moments and axial forces, and lateral braces may be required to maintain the stability of the beam. The need for lateral bracing can be checked using the beam-column stability design criteria of AISC-LRFD specifications (AISC 1990b).

2.4.8 Summary on EBFs. Eccentrically braced frames (EBFs) constitute an excellent lateral load resisting system for structures under seismic load. They have the advantage of combining large stiffness and strength and high ductility. In an EBF the energy dissipation is limited to the links, while the braces and other members are designed to remain elastic. This precludes brace buckling and avoids strength and stiffness deterioration observed in concentrically braced frames (CBFs).

Tests have shown that better behavior was observed with short links that yield primarily in shear. Furthermore, the links need to be provided with a sufficient number of stiffeners to avoid local web buckling and ensure good behavior. A well detailed link can achieve rotations of about 0.10 rad. under cyclic load. Particular attention should also be given to connection detailing. However, experimentally verified connections details are well established for EBFs.

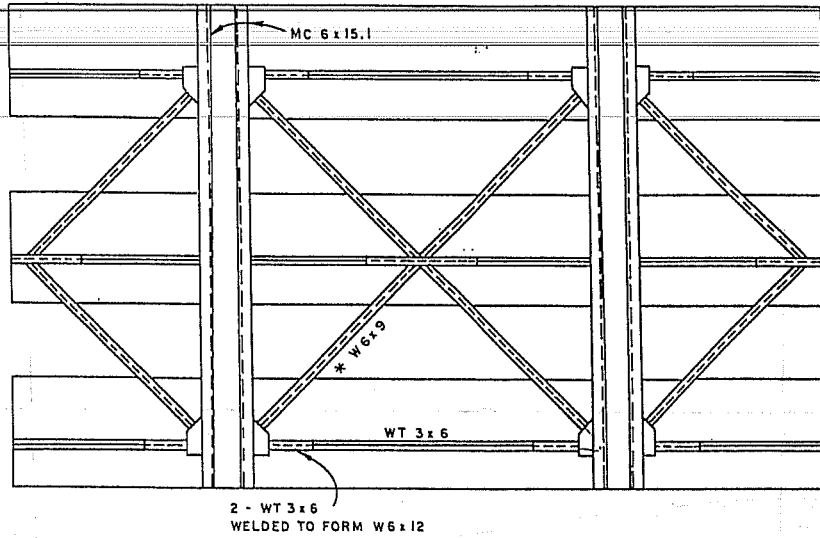


Figure 2.1 Reinforced Concrete Frame Specimen Retrofitted with Steel CBFs
(Jones and Jirsa, 1985)

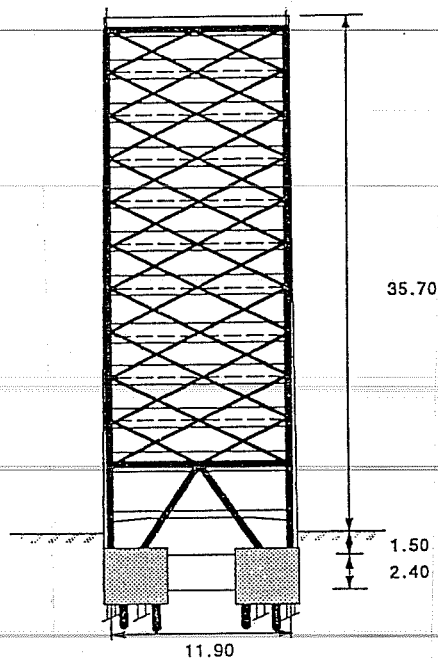


Figure 2.2 The Durango Building Retrofitted with Steel CBFs
(Foutch et al., 1989)

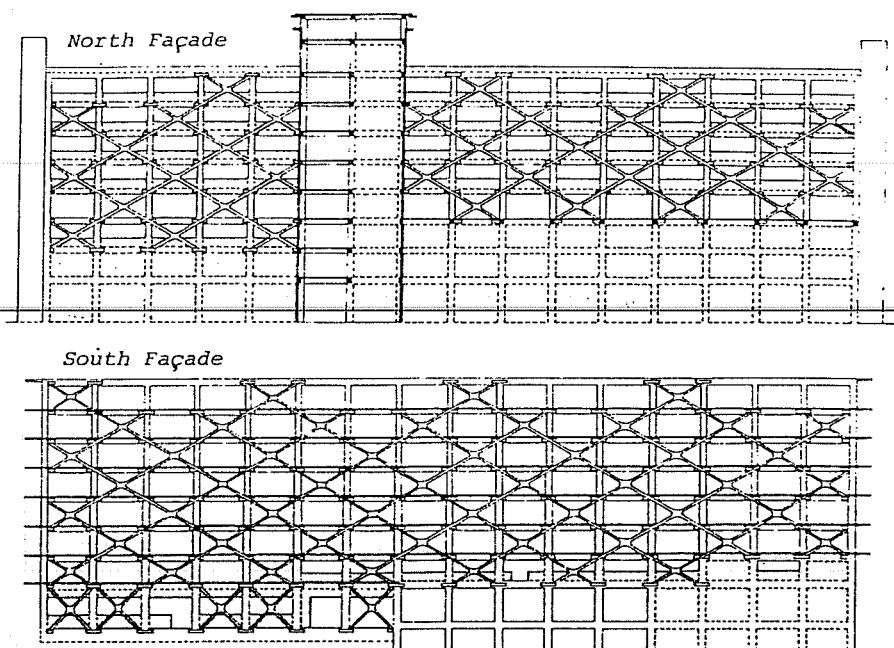
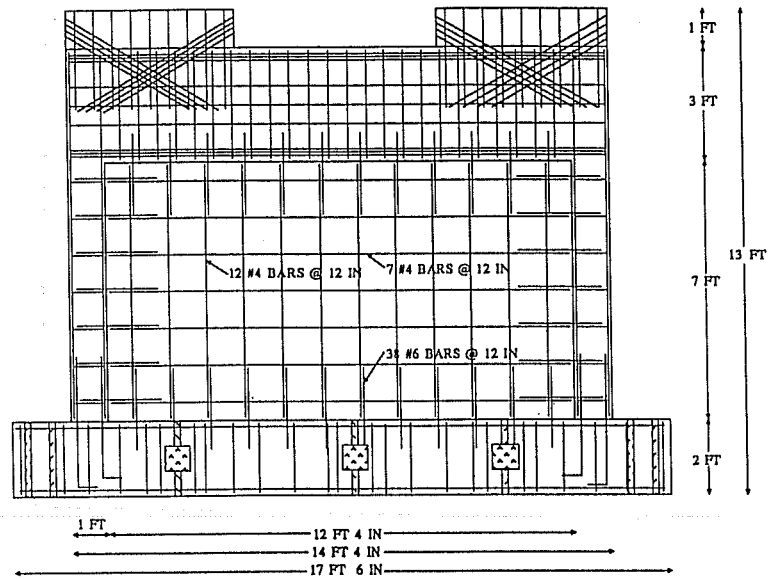
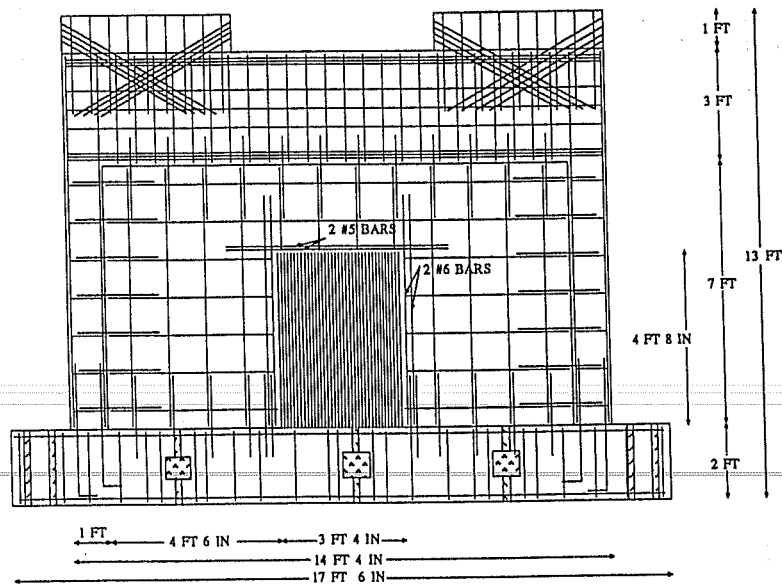


Figure 2.3 A Japanese Building Retrofitted with the Addition of Steel Bracing Combined with Beam Weakening (Kawamata and Ohnuma, 1980)

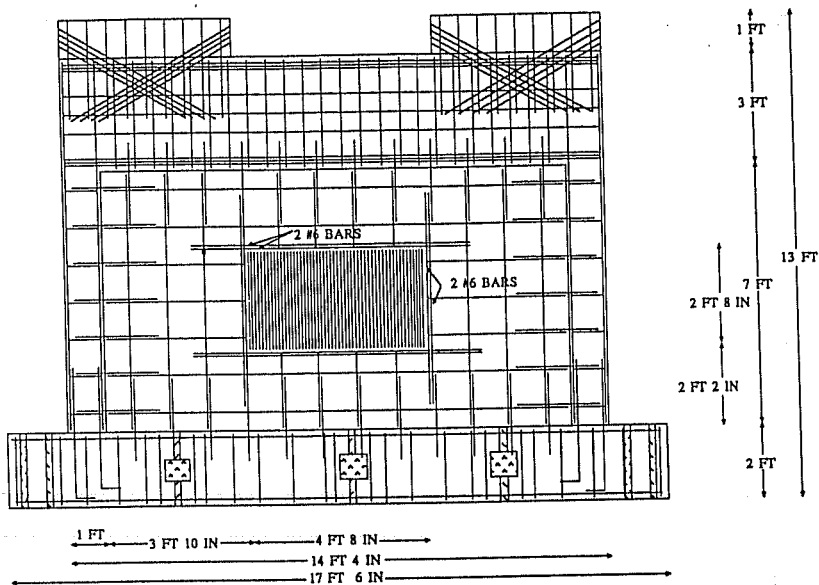


(a) Full Infill



(b) Infill with Door Opening

Figure 2.4 Reinforced Concrete Frame Retrofitted with Infill Wall (Gaynor, 1988)



(c) Infill with Window Opening

Figure 2.4 Reinforced Concrete Frame Retrofitted with Infill Wall (Cont'd) (Gaynor, 1988)

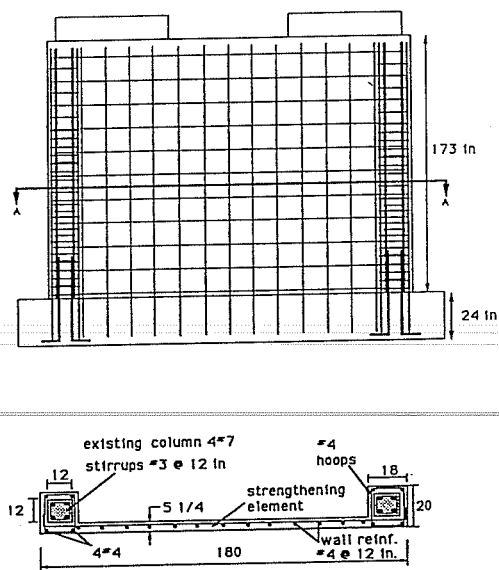
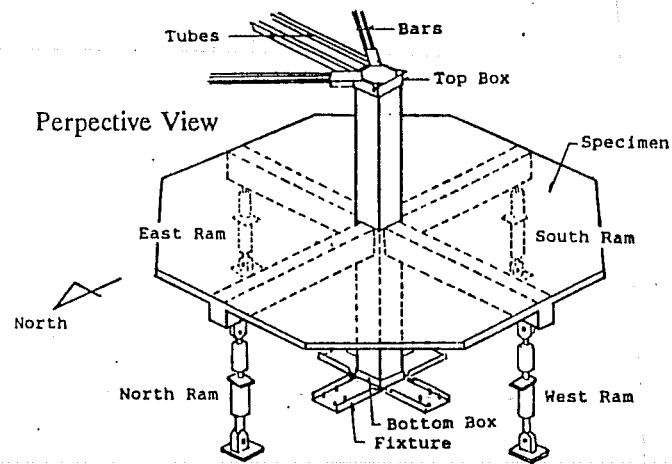
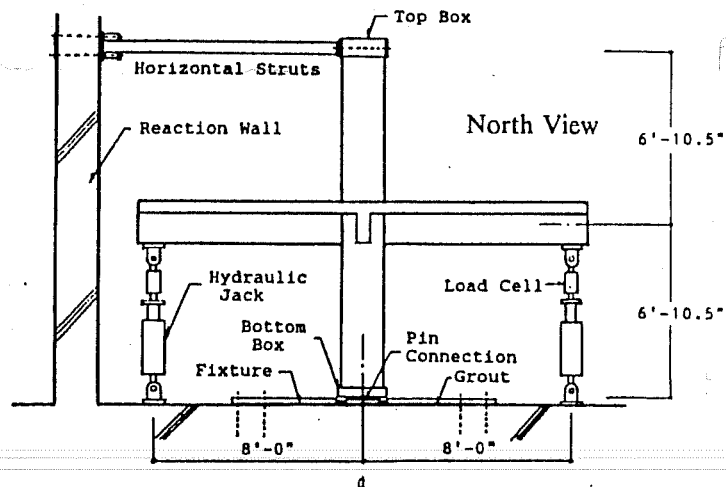


Figure 2.5 Reinforced Concrete Frame Retrofitted with Eccentric Wall and Column Jackets (Jimenez, 1989)

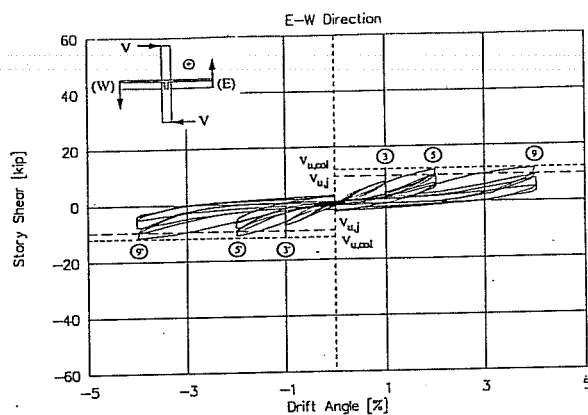


(a) Perspective View

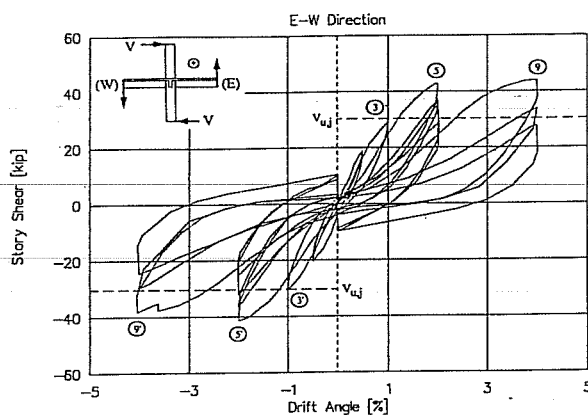


(b) North View

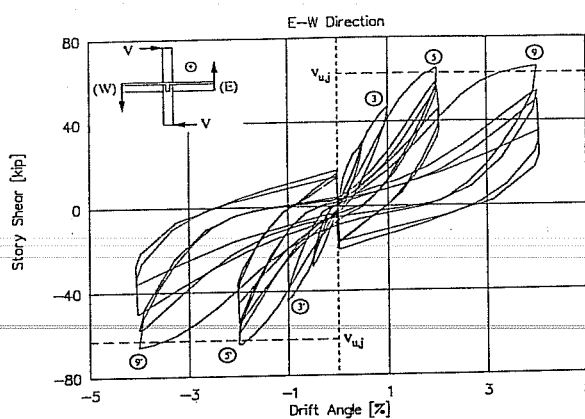
Figure 2.6 Specimen and Test Set Up of an Interior Joint Subassembly Retrofitted by Jacketing (Alcocer and Jirsa, 1991)



(a) Original Specimen



(b) Specimen Retrofitted with Column Jacking



(c) Specimen Retrofitted with jacking of Beams and Column

Figure 2.7 Hysteretic Behavior of Original and Two Retrofitted Interior Joint Subassembly Specimens Tested by Alcocer and Jirsa (1991)

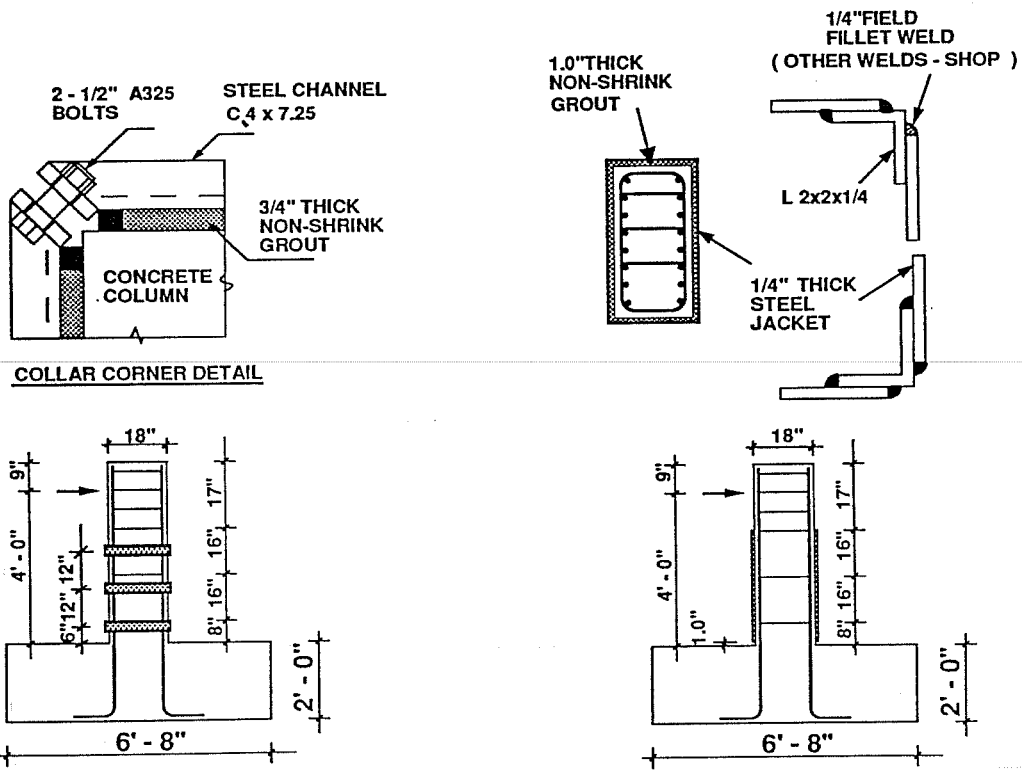
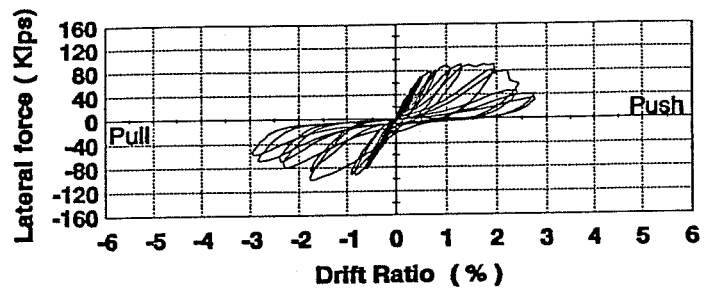
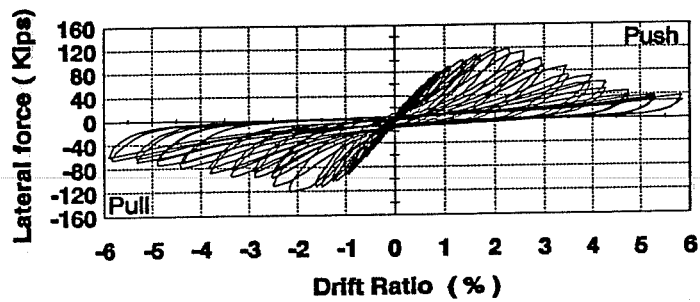


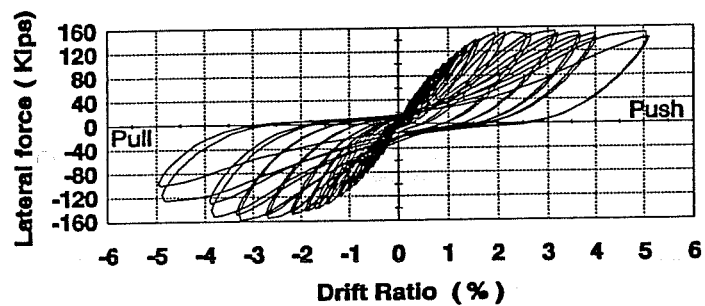
Figure 2.8 Reinforced Concrete Columns Retrofitted with Steel Jacket or Steel Collars (Aboutaha and Engelhardt, 1994)



(a) Original Column



(b) Column Retrofitted with Steel Collars



(c) Column Retrofitted with a Steel Jacket

Figure 2.9 Hysteretic Behavior of Columns Retrofitted with Steel Jacket or Steel Collars (Aboutaha and Engelhardt, 1994)

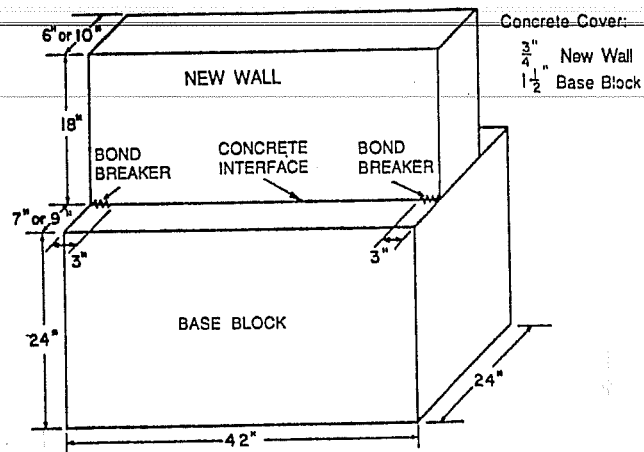


Figure 2.10 Test Specimen Used to Investigate the Interface Between New and Old Concrete (Bass, 1985)

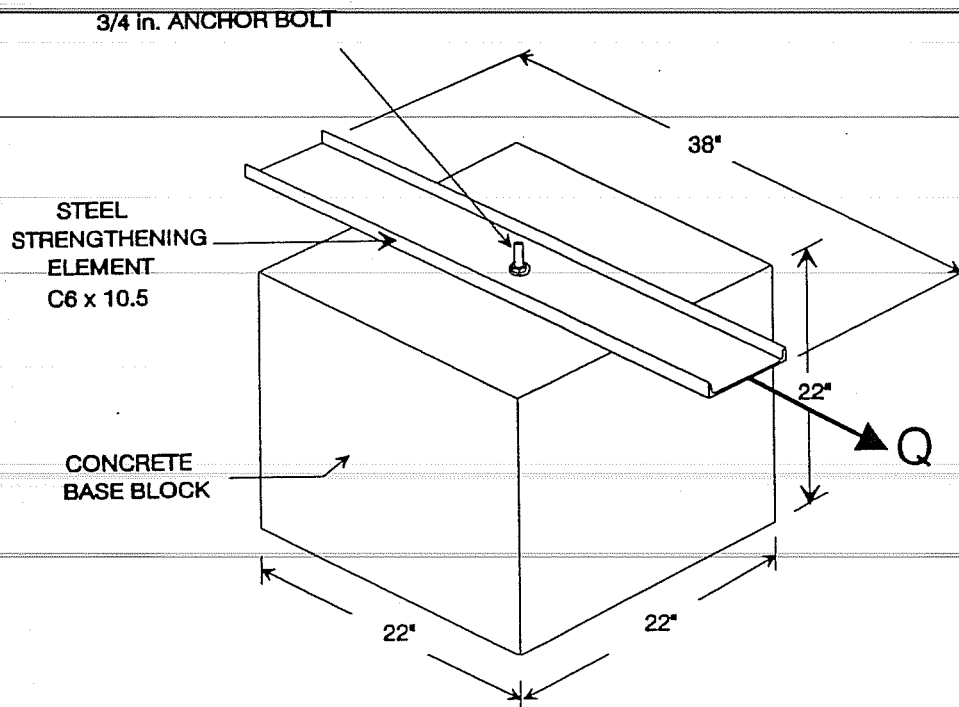
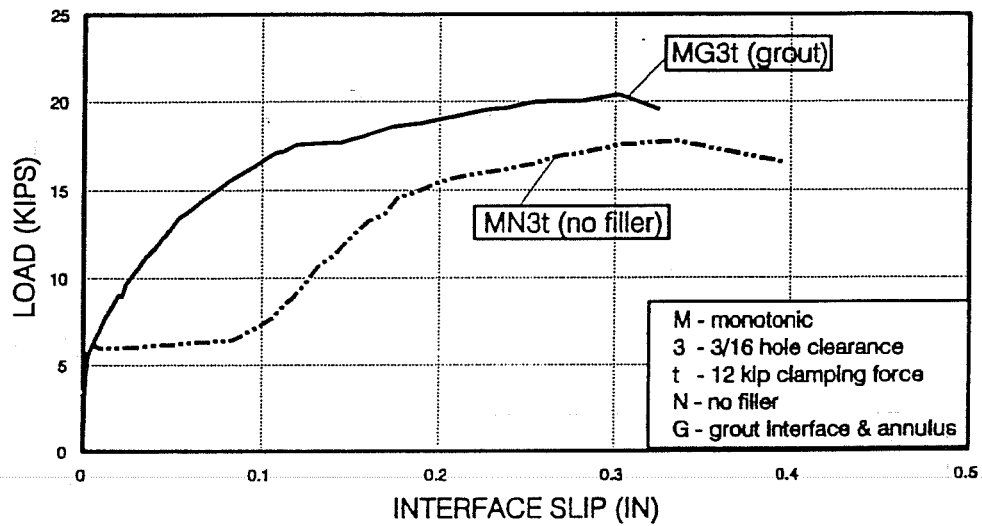
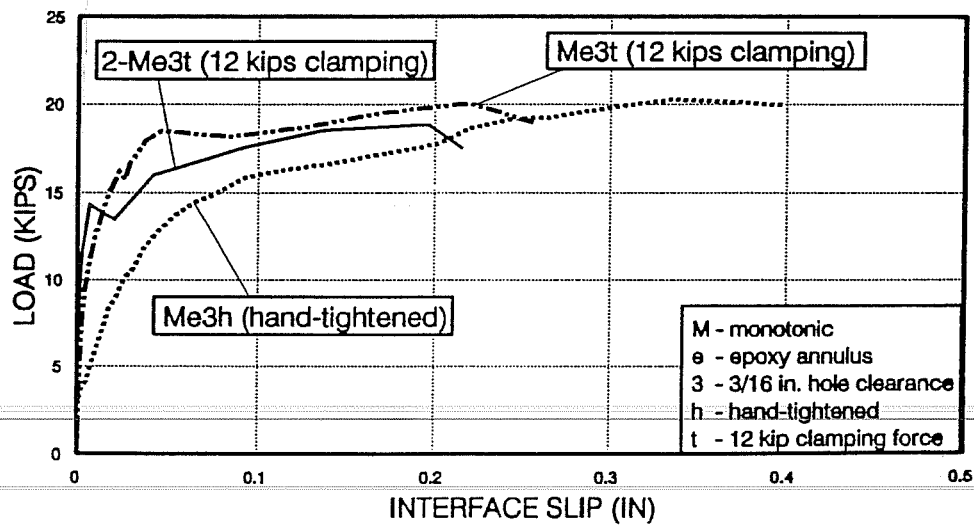


Figure 2.11 Specimen Used in Tests on Steel-to-Concrete Connections (Jimenez-Pacheco, 1992)



(a) Effect of Filler Material



(b) Effect of Clamping Force

Figure 2.12 Selected Results of Jimenez-Pacheco's (1992) Tests on Steel-to-Concrete Connections

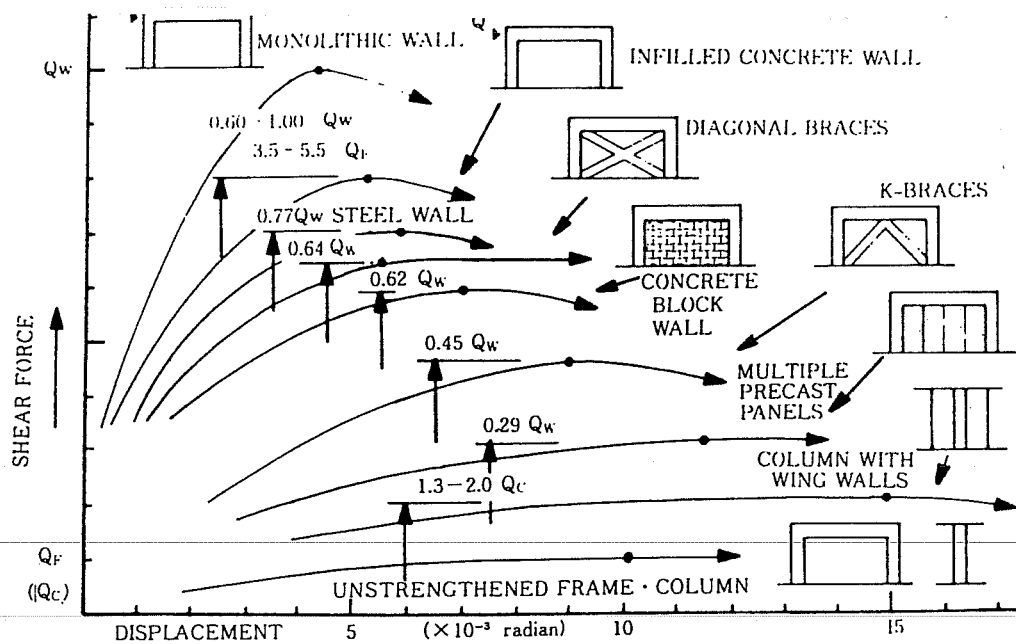


Figure 2.13 Load-Displacements Relationships for Selected Retrofit Schemes (Sugano, 1982)

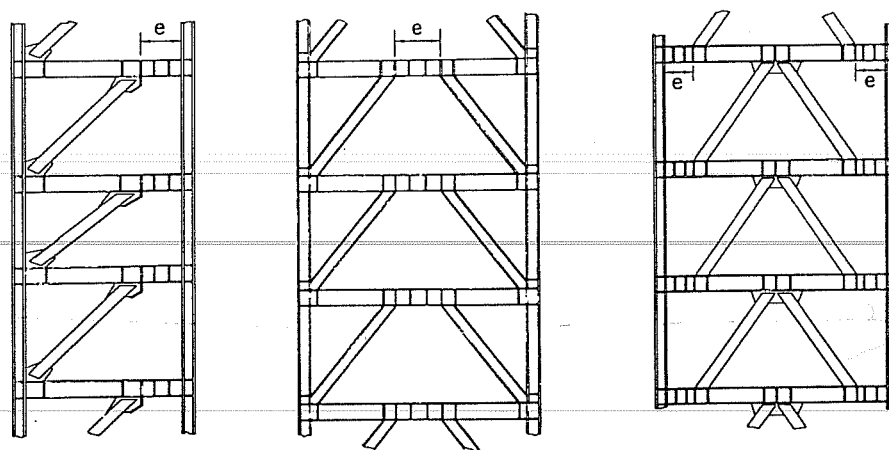


Figure 2.14 Some Typical Arrangements for Steel EBFs

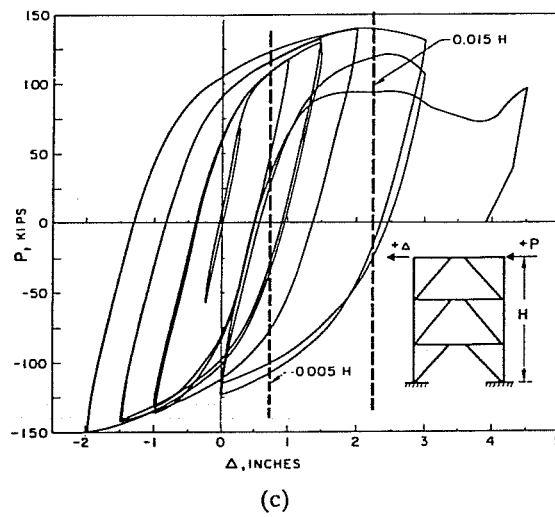
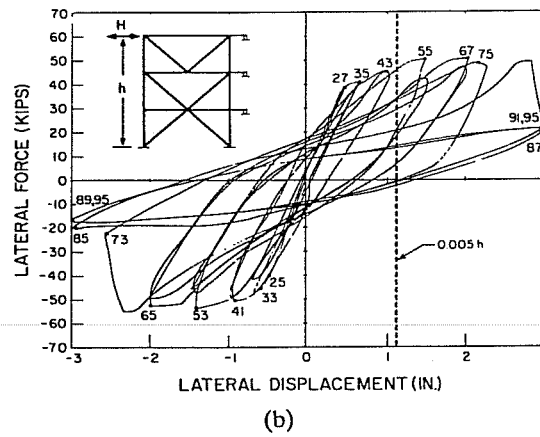
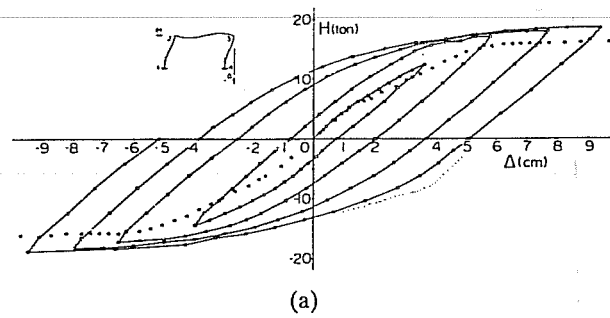


Figure 2.15 Typical Hysteretic Behavior of Steel Frames Under Lateral Load:
 (a) MRF, (b) CBF, (c) EBF (Popov and Engelhardt, 1988)

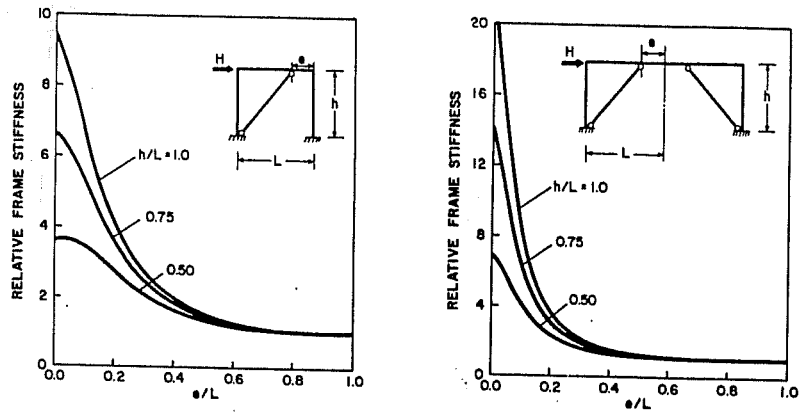


Figure 2.16 Variation of Stiffness with Link Length (Hjelmstad and Popov, 1984)

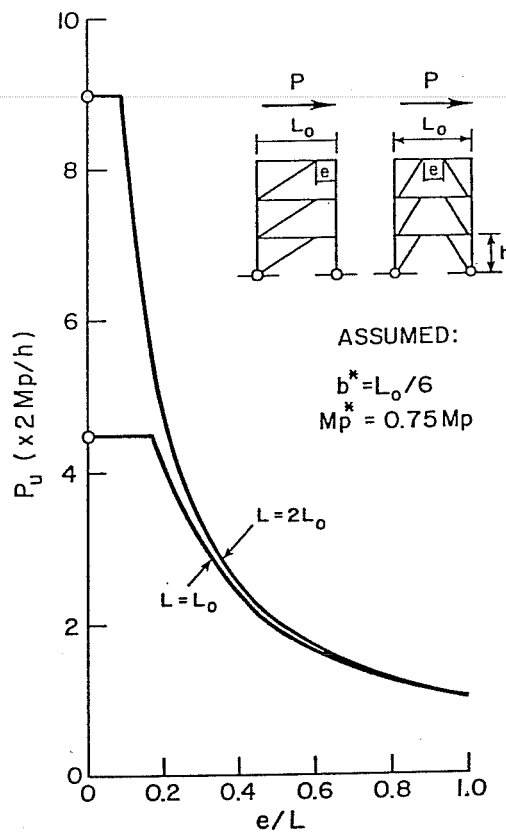


Figure 2.17 Variation of Strength with Link Length (Kasai and Popov, 1986c)

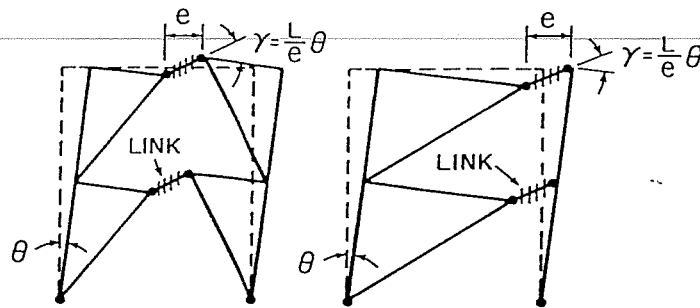


Figure 2.18 Energy Dissipation Mechanisms for EBFs
(Popov and Engelhardt, 1988)

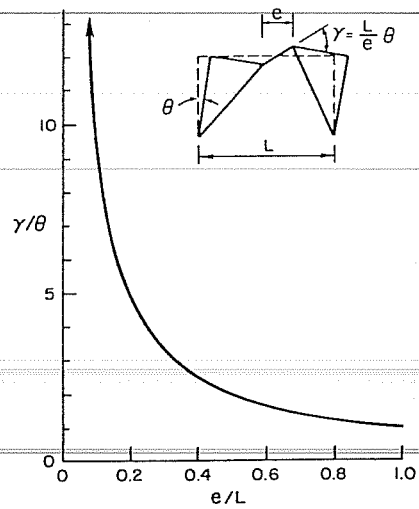
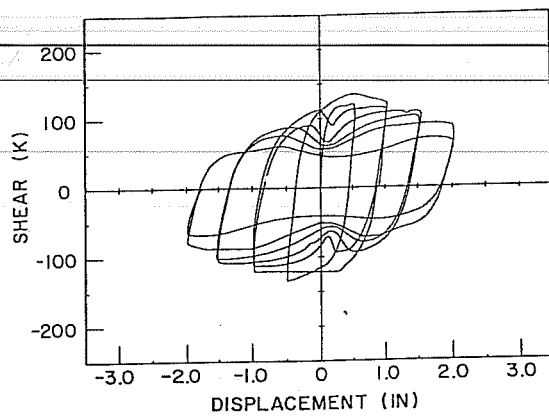
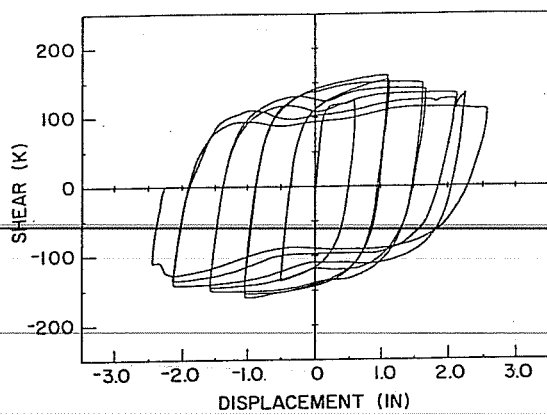
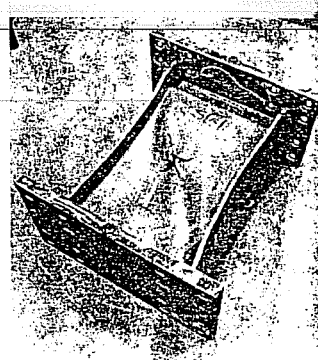


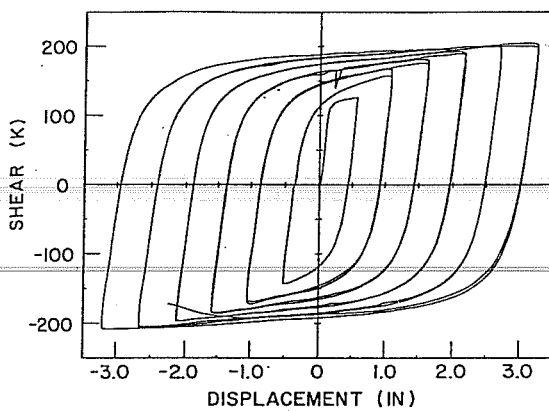
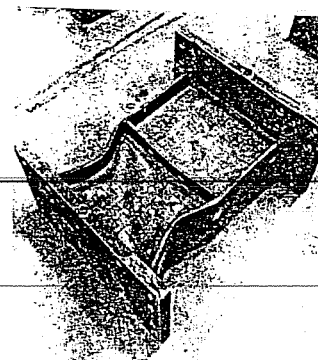
Figure 2.19 Variation of Link Rotation Demand with Link Length
(Engelhardt and Popov, 1988)



(a) Link with No Stiffeners



(b) Link with One Stiffener



(c) Well Detailed Link

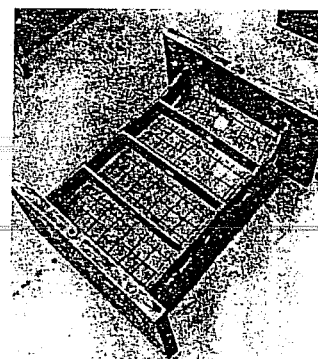
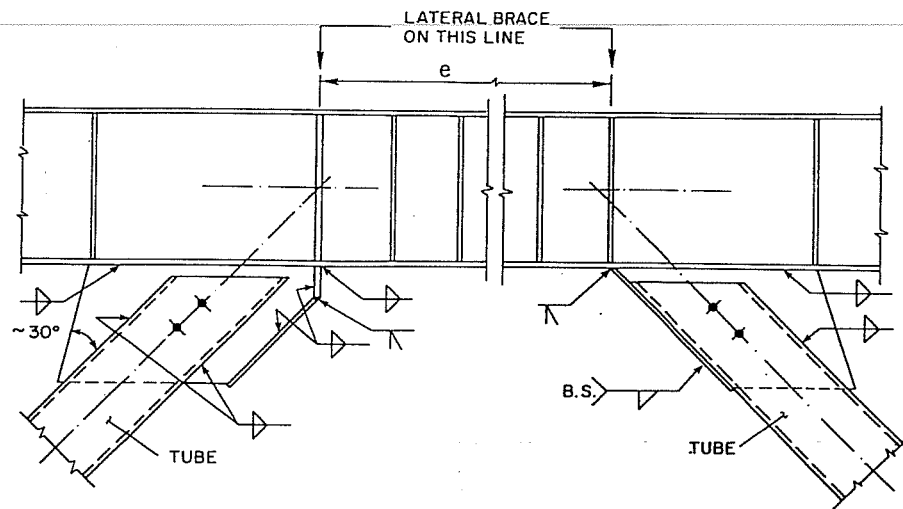
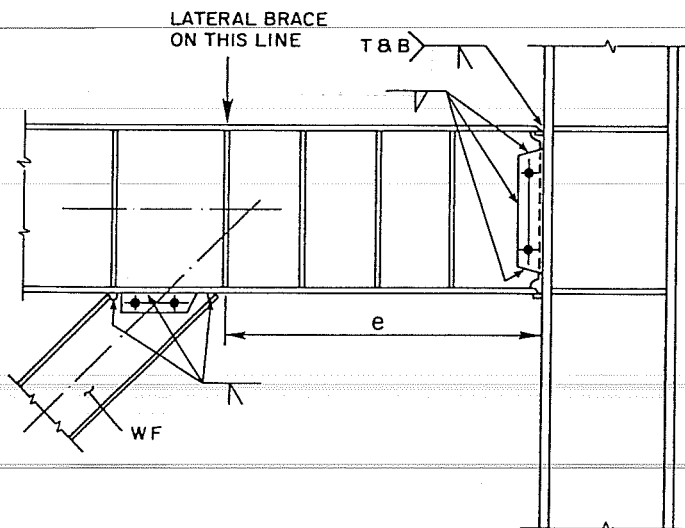


Figure 2.20 Experimental Behavior of Links and Appearance After Failure (Hjelmstad and Popov, 1983b)



(a) Link at Midspan of Beam



(b) Link Adjacent to Column

Figure 2.21 Typical Connection Details for EBFs (Popov and Engelhardt, 1988)

CHAPTER 3: ANALYTICAL MODELING

3.1 General.

The structural analyses conducted in this study were performed using the computer program DRAIN-2D, initially developed by Kanaan and Powell (1975). The program allows for nonlinear analysis of two dimensional frames under earthquake excitation. Gravity loads can be applied prior to the earthquake loads. However yielding under these initially applied gravity loads is not permitted.

3.2 Program Design.

The program is composed of a base program and a number of element subroutines. The base program assembles the global structural stiffness matrix, the mass matrix, and the load matrix and computes the structure's response. Member input and output information, member stiffness, and member state computations are carried out within the element subroutines. Each element subroutine models a specific type of member. The program is designed to allow for new subroutines to be easily added. Currently, the library of elements includes the following:

1) Truss Element

This element can be used to model members subject to axial load only. The inelastic deformations are modeled by taking a bi-linear relation between the axial load and the axial deformation (Kanaan and Powell, 1975).

2) Beam-Column Element

This element has axial and flexural stiffness and considers all plastic deformations to be concentrated at the element ends as flexural hinges. Inelastic behavior is considered by having a bi-linear relation between the end moments and the end rotations. The beam-column element allows for a moment-axial load interaction to model the influence of axial load on the yield moment (Kanaan and Powell, 1975).

3) Infill Panel Element

This element has shear stiffness only and can be used to simulate the behavior of infill panels, masonry walls, or inelastic shear beams. The relationship between shear strain and shear stress is bi-linear (Kanaan and Powell, 1975).

4) Semi-Rigid Connection Element

This element can be used to model connections in which significant changes of angle occur between two members connected to a node. The relationship between the moments transmitted by the element and the relative rotation between the connected nodes is bi-linear (Kanaan and Powell, 1975).

5) Beam Element

This element is identical to the beam column element but does not consider any interaction between the yield moment and the axial load (Kanaan and Powell, 1975). It can be used to model beams under pure bending.

6) Shear Link Element

This element is used to model short shear yielding links of eccentrically braced frames. Yielding of this element is controlled by the shear force. Flexural yielding is not considered. The shear link element does not consider any interaction between shear and moment or between shear and axial load. The inelastic behavior is modeled by considering a bi-linear relation between the shear and the relative end displacement (Tang and Goel, 1988).

7) Buckling Element

This element was based on the truss element and was developed to model the hysteretic behavior of axially loaded pin-ended bracing members (Tang and Goel, 1988).

8) End Moment Buckling Element

This element is a combination of the beam column element and the buckling element. It was developed to model brace members that are also subject to bending moments (Tang and Goel, 1988).

9) Reinforced Concrete Element

This element allows the modeling of reinforced concrete members. The element exhibits degrading stiffness properties with each cycle (Kanaan and Powell, 1975). The model was later changed to include stiffness softening to simulate bond loss (Pincheira, 1992).

3.3 Analysis Method.

In DRAIN-2D, the structure is modeled as a planar assemblage of members connected at the nodes which may have up to three degrees of freedom. The structural analysis is based on the direct stiffness method. The member element stiffness $[k]$ is established for each element and then assembled in the global stiffness matrix $[K]$ of the structure. The program permits static loads to be applied prior to dynamic loading. These loads are either applied at the node or on the element. In the later case, they are converted to equivalent nodal loads. Dynamic loads representing inertia and damping effects are assembled as described below.

3.4 Integration Procedure.

The incremental equations of dynamic equilibrium of the structure can be written as:

$$[M] \{\Delta \ddot{u}\} + [C] \{\Delta \dot{u}\} + [K_T] \{\Delta u\} = -[M] \{\Delta \ddot{u}_g\} \quad (3.1)$$

in which $\Delta \ddot{u}$, $\Delta \dot{u}$, Δu are respectively the acceleration increment vector, the velocity increment vector, and the displacement increment vector between the previous time step ($t-\Delta t$) and the current time step (t); $[M]$ is the mass matrix of the structure; $[C]$ and $[K_T]$ are the damping matrix and the tangent stiffness matrix at the current step. $\Delta \ddot{u}_g$ is the increment of the ground acceleration.

The dynamic equations of motion (Eq. 3.1) is solved using the constant average acceleration method. In this method, the acceleration is assumed to remain constant during

each time step. This method is unconditionally stable and does not introduce numerical damping in the solution (Newmark, 1959).

The size of the time step needed to obtain accurate analytical response depends on the period of vibration, the nonlinear properties of the structure and the rate of variation of the acceleration record. The size of the time step was chosen using a trial and error procedure. A set of structures which are representative of the buildings investigated in this research were analyzed under the same earthquake records used in the study. These structures had different vibration periods and were analyzed using different time steps. A comparison between the results showed that a time step less than 0.005 s did not increase the solution accuracy while a larger time step sometimes resulted in an inaccurate response. A time step of 0.005 s was therefore used in the analyses.

If the state of the structure does not change within a time step, then structural equilibrium will be satisfied at the end of that time step. However when changes occur within a time step, dynamic equilibrium at the end of the step will not be satisfied and equilibrium unbalance is, thus, introduced. To avoid accumulation of such errors, a load, opposite to the unbalanced load, is applied to the structure in the subsequent time step.

3.5 Damping.

3.5.1 DRAIN-2D Formulation. DRAIN-2D uses the Rayleigh formulation for viscous damping. The damping matrix is taken as a linear combination of the mass matrix and the tangent stiffness matrix according to the following equation:

$$C_T = \alpha M + \beta K_T + \beta_0 K \quad (3.2)$$

where M is the structure's mass matrix of the structure, K_T is the structure's tangent stiffness matrix, and K is the structure's initial elastic stiffness matrix. The parameters α and β can be specified by the user and the parameter β_0 is set equal to zero in the original version of the

program. Since the tangent stiffness matrix (K_T) is time dependent, the amount of damping introduced in the structure may vary during the analysis.

3.5.2 Effect of Viscous Damping on EBFs. Ricles and Popov (1987) studied the influence of Rayleigh damping on the analytical behavior of steel EBFs. For their study, they analyzed the response of a six-story EBF subjected to the 1940 El Centro earthquake ground motion record. The floor masses were concentrated at the nodes and an elasto-plastic model was assumed for the links. Their investigation showed that the EBFs modeled with Rayleigh damping developed unrealistically high axial forces in the braces. These high brace forces were attributed to large velocities developed by the nodes at the link ends. The results suggested that the conventional Raleigh damping formulation could result in significant errors in the inelastic dynamic analysis of EBFs.

A modified damping formulation which avoids the above problem was developed by Ricles and Popov (1987) as follows:

$$C_T = \alpha \sum M_{elem\ i} + \sum \beta_0\ elem\ i\ K_{elem\ i} \quad (3.3)$$

where $M_{elem\ i}$ and $K_{elem\ i}$ are the mass and the initial stiffness matrix of element (i). The viscous damping matrix is expressed as a combination of the mass matrix and the initial stiffness matrix and is not dependent on the nonlinear deformations of the structure. Furthermore, the same study (Ricles and Popov, 1987) suggested that damping for the shear link elements should be taken as proportional to the mass only (i.e. $\beta_0 = 0$ for the links). With the above formulation (Eq. 3.3), a different damping coefficient can be specified for each element making it possible to set the stiffness proportional coefficient (β_0) equal to zero for the links and specify a non zero stiffness proportional coefficient for the remaining structural members.

3.5.3 Changes in DRAIN-2D Damping Formulation. The viscous damping formulation in DRAIN-2D was changed to conform to Equation 3.3. Viscous damping was taken proportional to the mass matrix and to the initial stiffness matrix. The program was modified to permit the user to select an α value for the structure and a β_0 value for each type of element. If the system is uncoupled into normal modes, the amount of damping, as a ratio of critical can be defined for two vibration modes (i) and (j) as (Clough and Penzien, 1975):

$$\xi_i = \frac{\alpha T_i}{4 \pi} + \frac{\beta_0 \pi}{T_i} \quad (3.4)$$

and

$$\xi_j = \frac{\alpha T_j}{4 \pi} + \frac{\beta_0 \pi}{T_j} \quad (3.5)$$

Solving for α and β_0 yields:

$$\alpha = \frac{4\pi (T_j \xi_j - T_i \xi_i)}{(T_j^2 - T_i^2)} \quad (3.6)$$

$$\beta_0 = \frac{(T_j \xi_j - T_i \xi_i)}{\pi (T_j^2 - T_i^2)} \quad (3.7)$$

The values of α and β_0 used in the analyses, were obtained assuming a viscous damping equal to 2% of critical damping for the two first modes of vibration.

3.6 Details of Selected DRAIN-2D Element Subroutines.

3.6.1 General. The DRAIN-2D elements which were extensively used in this study are:

- 1) Reinforced Concrete Element
- 2) Shear Link Element
- 3) Beam-Column Element
- 4) Brace Buckling Element

The formulation and features of these elements are described below.

3.6.2 Reinforced Concrete Element. The reinforced concrete element was initially developed by Kanaan and Powell (1975) to model the behavior of concrete members that are known to exhibit degrading stiffness. The element has both flexural and axial stiffness but does not consider an interaction between axial load and moment. Shear deformation and rigid zones at the member's ends can be considered.

The one-component model, initially developed by Giberson (1969), was adopted by Kanaan and Powell (1975) to model inelastic deformations. The model consists of a linear elastic member with non linear rotational springs at both ends (Fig. 3.1). All plastic deformations are concentrated in the end springs.

The moment-rotation relationship of the reinforced concrete element is a modified version of the Takeda model (Takeda et al. 1970). Features of the moment rotation relationship are as follow:

- 1) A reduction in the unloading stiffness (Fig. 3.2), K_u that depends on the previous maximum plastic rotation θ_p can be modeled. K_u is controlled by the input parameter α which typically varies between zero and 0.4.
- 2) The reloading stiffness, K_r , (Fig. 3.3) depends on the previous maximum plastic rotation and is controlled by the input parameter β . Typically the value of β varies between zero and 0.6.

The reinforced concrete element model was further modified (Pincheira, 1992) to represent splice failure which is characterized by a sudden loss of flexural strength. The stiffness of the member after splice failure is defined by the user. The hysteresis rules of the model are shown in Figure 3.4. First, the member is loaded in the elastic range between point 0 and 1. After the member reaches yield at point 1, a hinge forms at the members' end and the moment-rotation curve follows 1-2. At point 2, the member reaches its peak moment capacity (splice failure) and further loading results in the curve 2-3. If the load is reversed the member will follow slope 3-4 and 4-5. Notice that stiffness degradation can be considered by having the slope of segment 3-4 different from the one of 0-1. Further negative loading causes the member to follow paths 5-6 and 6-7. Reloading of the member follows the path 7-8 and 8-9. Point 9 represents the maximum rotation of the member in the previous stage (point 3).

3.6.2.1 Reinforced Concrete Members with Shear Failure.

A simple model to

include shear failure in reinforced concrete members was proposed by Pincheira (1992) and was adopted for this study. Experimental studies have shown that column shear failure is followed by a rapid reduction in strength and stiffness of the member (Umehara and Jirsa, 1982). The model adopted here assumes that after a shear failure, the member loses completely its lateral strength but can carry axial load. Such assumption appears reasonable for small deformations only. Thus, the model assumes that after shear failure, a column behaves essentially, as a pin ended element. To satisfy equilibrium, the lateral forces resisted by the column that failed in shear are transferred to the remaining members of the structure in the subsequent time step.

The purpose of the simple model adopted here is to provide some indication of the behavior of the structure after some reinforced concrete members have failed in shear. However, it does not attempt to model the post shear failure behavior of these members.

3.6.2.2 Modeling Procedure and Input Parameters.

Input parameters of the DRAIN-2D reinforced concrete model element require defining the basic moment-rotation

relationship of the member to model. To derive this relationship, first the moment curvature diagram for the member end sections are obtained using the computer program RCCOLA (Mahin and Bertero, 1972). The stress-strain relationship proposed by Park and Kent (1977) was used to model the concrete (Fig. 3.5). For this stress-strain curve, the ascending branch is represented by a second degree parabola. The maximum concrete stress (f'_c), and the maximum concrete strain (ϵ_{\max}) are defined by the user. For this study ϵ_{\max} was based on the expression proposed by Scott et al. (1982) which considers the effect of concrete confinement and is defined by Equation 3.8. The reinforcing steel was idealized as shown in Figure 3.6. Table 3.1 summarizes the values of the different parameters used to define the steel stress-strain diagram.

$$\epsilon_{\max} = .004 + .9 \rho_s \frac{f_{yh}}{43.5} \quad (3.8)$$

where ρ_s is the ratio of the total volume of the transverse reinforcement over the concrete core measured to the outside of the hoops, and f_{yh} is the yield stress of the transverse reinforcement in ksi.

The continuous moment curvature diagram obtained from RCCOLA for the cross section being considered is represented by a bi-linear relationship (Fig. 3.7). In the bi-linear relationship, the initial stiffness (EI), and the ultimate moment and ultimate curvature are taken equal to the same values as for the continuous curve. The yield point (M_y, ϕ_y) and the inelastic stiffness are obtained by equating the area under the continuous graph and the linear fit. The moment-rotation relationship (Fig. 3.8) of the member is then derived assuming that the member is bent in double curvature and the inflection point is located at mid-span. Such a moment distribution corresponds approximately to the static lateral loading case.

The maximum moment and rotation capacity that can be developed by a well detailed reinforced concrete section is usually limited by concrete crushing or steel fracture. However, if the longitudinal bars have short lap splices or small embedment length, as is often the case in older buildings, the maximum capacity of the section may be limited by splice failure. In this

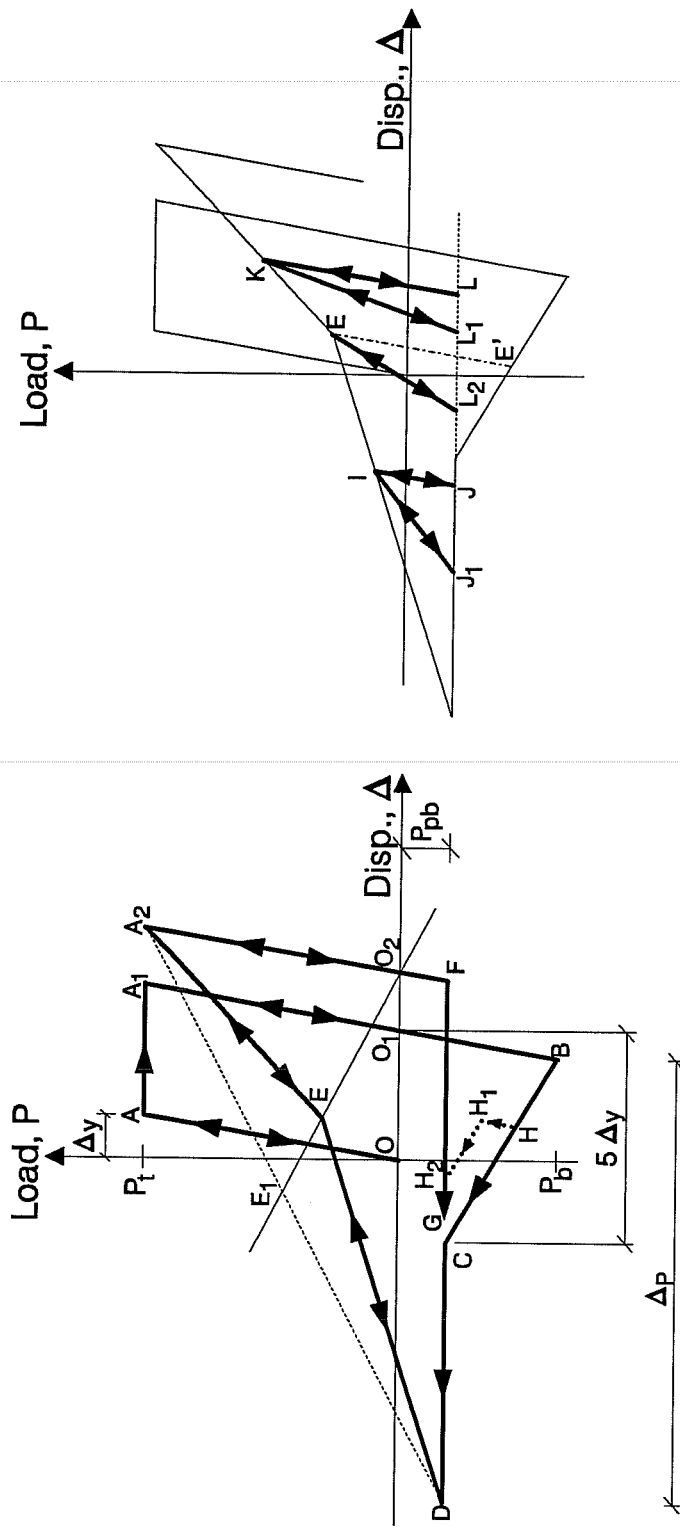


Figure 3.13 Hysteretic Rules for the Brace Buckling Element
(Adapted from Tang and Goel, 1988)

case, the user needs to specify the moment at splice failure (point 2 in Figure 3.4) and the slope of the descending branch (slope 2-10 in Figure 3.4).

The largest steel stress that can develop in a reinforcing bar with a short development length can be estimated using the following equation (Orangun et al., 1977):

$$f_s = 4 \frac{l_{db}}{d_b} \sqrt{f_c} \left(1.2 + 3 \frac{c}{d_b} + 50 \frac{d_b}{l_{db}} + \frac{A_{tr} f_{yt}}{500 s d_b} \right) \quad (3.9)$$

In the above equation f_s is the longitudinal steel stress at splice failure., l_{db} is the available development length of the bars., f_c is the compressive strength of the concrete, c is the cover parameter, d_b is the bar diameter, A_{tr} is the area of transverse reinforcement resisting splitting failure., f_{yt} is the yield strength of the transverse reinforcement, and s is the spacing of the transverse reinforcement.

Knowing the steel stress at splice failure, the moment capacity of the section can be evaluated.

3.6.3 Beam Column Element. This element models structural members under combined bending and axial load. The user may specify an effective shear area to consider shear deformations. Rigid zones can be specified at the element's ends to account for the joint dimensions. Geometric stiffness can be included to model $P\Delta$ effects.

Inelastic deformations are considered by using a two-component model (Giberson, 1969). Element response is the sum of an elastic component and an elasto-plastic component (Fig. 3.9). After the hinge yields the moment in the elastic component continues to increase, however the moment in the elasto-plastic component remains constant.

Three types of axial force-moment interaction curves are possible for this element :

- 1) No interaction

- 2) Steel type (Fig. 3.10a)
- 3) reinforced concrete type (Fig. 3.10b).

The element is assumed to be elastic if a combination of axial load and moment lies within the yield interaction surface. A plastic hinge is introduced at an end of the element, if the load combination at the element end lies on or outside the yield surface. Combinations outside the yield surface introduce an unbalanced load that is compensated for by applying a load equal in magnitude and of opposite sign in the subsequent time step.

3.6.4 Shear Link Element. The shear link element, developed by Tang and Goel (1988), models short shear yielding links of eccentrically braced steel frames. The element is valid only for short links that satisfy the following equation (Kasai and Popov, 1986b and Kasai and Popov, 1986c):

$$e \leq \frac{1.6 M_p}{V_p} \quad (3.10)$$

where e is the link length, M_p is the plastic moment of the section and is defined by $M_p = ZF_y$, V_p is the fully plastic shear capacity of the section and is defined by $V_p = 0.55 F_y d t_w$, d is the section depth and t_w is the web thickness.

Links that satisfy Equation 3.10 yield primarily in shear with little flexural hinging.

Yielding of the DRAIN-2D shear link element is controlled by the shear force. The relation between the shear at the element ends (V) and the relative end displacement (Δ) is assumed to be bi-linear (Fig. 3.11). A combination of kinematic and isotropic hardening is considered for cyclic loading (Fig. 3.12).

Experimental research (Kasai and Popov, 1986b) has shown that there is little or no influence of the bending moment on the shear yield force in a short link. Hence the yield

surface assumed for the member does not involve an interaction between moment and shear. The interaction between axial load and shear is also not included in the model. Shear axial load interaction is significant for large axial link forces (Kasai and Popov, 1986b). However for all EBFs considered in this study, link axial forces were always small.

The load carrying capacity of links deteriorates rapidly after web buckling. Properly detailed shear links can sustain angular plastic deformations, γ , of up to 0.10 rad. for cyclic loading (Malley and Popov, 1984; Hjelmstad and Popov, 1983). The angular deformation, γ , measures the average shear strain for links and can be computed as the relative end displacements divided by link length, e . The link element of DRAIN-2D does not model the behavior of links following inelastic web buckling. Inelastic web buckling was taken in this study as the failure for the link and was considered reached if the plastic link rotation attains 0.10 rad.

3.6.5 Brace Buckling Element. This element was developed by Jain and Goel (1978) to model the behavior of steel braces under axial load. The cyclic behavior modeling of this element was based largely on experimental data. It assumes an elastic perfectly-plastic behavior in tension and a stiffness and strength reduction after first buckling in compression. However the element does not consider the influence of local buckling on the hysteretic behavior.

Figure 3.13 shows the hysteretic behavior of the brace element. If the member is first loaded in tension, it follows elastically the segment OA. The member yields at A, and upon further loading follows segment AA₁. If the loading is reversed at A₁, the member unloads elastically along segment A₁B parallel to the initial slope. After reaching its first cycle buckling load at point B, the member deforms along segment BC. Point C is located at a displacement equal to five times the yield displacement ($5\Delta_y$), measured from point O₁ as shown. The compressive load at point C is equal to the post buckling load capacity (P_{pb}). The segments BC and CD indicate a gradual reduction of the buckling load with repeated cycles. If the

displacement is reversed at H, the member follows HH_1 which is parallel to the initial loading slope OA. If the displacement is reversed at H_1 , the member follows segment H_1H_2 which is parallel to BC. After the member reaches the post buckling load at point C (or H_2), it follows segment CD (or H_2D). If the load is reversed at point D, the member follows the segment DEA_2 . This segment indicates a gradual gain in stiffness. Under tension load the member, that had deformed under buckling, is being straightened. The elongation A_1A_2 (Δ_R) is a function of the previous maximum displacement (Δ_p) and the slenderness ratio (KL/r) and can be estimated by the following equation (Jain and Goel, 1978):

$$\frac{\Delta_R}{L} = .0175 \left(.055 \frac{\Delta_p / \Delta_y}{KL/r} + .002 (\Delta_p / \Delta_y)^2 \right) \quad (3.11)$$

The elongation (Δ_R) indicates that the member experienced permanent plastic deformation. These deformations were caused by the combined effect of compressive load and moment (due to P- Δ effect) in the previous cycle. The point E is obtained by drawing a line from the new origin (point O_2) at a slope of 1/3 of the initial elastic slope (OA). The distance O_2E is taken as $60/(KL/r)$ times the distance O_2E_1 . The line EE' , parallel to the initial elastic loading segment (OA) distinguishes between the two regions of loading history.

If the load is reversed along DE, the member unloads along the segment IJ which is parallel to the initial loading segment OA. Further compression results in segment JJ_1 . The member reloads along segment J_1I . If the load is reversed along EA_2 , the member follows the segment KL. Further compression results in either L_1 or L_2 . If load reversal occurs at L_1 , the member follows L_1K , however if load reversal occurs at L_2 , reloading follows L_2E .

These complex hysteretic rules were developed by Jain and Goel (1978) to mimic the very complex experimental behavior of braces subject to cyclic loading.

3.6.5.1 Input Parameters. The main input parameters required to model braces using the element described above include the initial buckling load, the post buckling load and

the effective length factor. The initial buckling load can be calculated using the recommendations of Load and Resistance Factor Design (LRFD) specification (AISC, 1990a). The effective length factor (K) depends on the restraint at the member ends. In this study, tubular braces with simple connections were used. In practice, a value of 1.0 is used for K of simple connections. For similar braces as the ones used in this study, Lee and Goel (1987), obtained an experimental value of K of about 0.85, indicating that connections designed as simple provide some restraint. A value of 0.9 was adopted in this research. The post buckling load capacity depends on the slenderness ratio of the member and on the initial buckling load. For a tubular section Lee and Goel (1987) recommended Equation 3.12. for estimating post buckling capacity. This equation is based on experimental data.

$$F_r = \frac{P_{pb}}{P_b} = 0.4 - 0.0025 \frac{KL}{r} \quad (3.12)$$

where F_r is the cyclic buckling strength reduction factor, P_{pb} is the post buckling compressive load capacity, P_b is the initial buckling load, K is the effective length factor, L is the unbraced length, and r is the radius of gyration.

3.7 Evaluation of the Shear Link Element.

3.7.1 Introduction. Two analyses were conducted to evaluate the suitability of the link element used in DRAIN-2D program. The element is intended to model properly detailed links of length less than $1.6 M_p/V_p$, i.e. links that yield primarily in shear. Firstly, an isolated shear link was analyzed and the results of the analysis compared to an experimental study. Secondly, a six-story EBF building was analyzed to evaluate the effect of the model on the overall behavior of a structure. These results were compared to another analysis that used a more sophisticated link model.

3.7.2 Comparison with an Experiment on an isolated Link. Hjelmstad and Popov (1983) conducted an experimental program to evaluate the behavior of the links used in EBFs. In their experiment, a shear link was isolated and subjected to a cyclic lateral displacement (Fig. 3.14) to reproduce the behavior of a link in a structure subject to seismic loading. Full details about the experimental program can be found in Hjelmstad and Popov (1983a and 1983b).

The experimental response of Hjelmstad and Popov's specimen 4 was compared to the response predicted by the DRAIN-2D shear link element. This specimen was selected because it was well detailed with adequate stiffeners to develop maximum link plastic rotation. The specimen was provided with appropriately spaced transverse stiffeners to control web inelastic buckling and to allow for good energy dissipation. Table 3.2 summarizes the experimental properties of the specimen. In this Table σ_y is the yield stress of the steel material, σ_u is the ultimate stress, ϵ_{sh} is the strain at onset of strain hardening and ϵ_u is the strain at ultimate.

Table 3.3 gives the parameters used for the analytical modeling of the link. These parameters were derived from the experimental properties summarized above. The section area (A) and the moment of inertia (I) were taken from AISC tables of section properties. The shear area (A_s) was taken as the depth of the section times the web thickness. The plastic shear force of the section (V_p) was computed as $0.55 F_y \text{ web } d t_w$. The strain hardening stiffness was computed from the stress-strain properties of the material. Finally, Poisson ratio (ν) was taken as 0.3 for steel. Poisson ratio is required by the program to compute the elastic and inelastic shear stiffness of the section.

The link shear force versus link end displacement obtained from the analysis and from the experiment are shown in Figure 3.15. The limitation of the model imposed by the simplified hardening law and by the assumption of bi-linear behavior are apparent from these plots. The plots show that more accurate results may be obtained with a tri-linear element. Nevertheless, the DRAIN-2D link element appears to capture the basic load-deformation response in a reasonable manner.

3.7.3 Comparison with an Analytical Study of an EBF.

3.7.3.1 General. A six-story EBF structure was analyzed using DRAIN-2D and the results compared to an analysis conducted by Ricles and Popov (1987). Figure 3.16 shows a plan and an elevation view of the structure. The external frames of the building were made of EBFs and were assumed to resist all the lateral load. All links in the EBFs were short shear yielding links.

The analysis by Ricles and Popov (1987) was conducted using the analytical program ANSR (Mondkar and Powell, 1975). Their model implemented a more sophisticated and rigorously developed link element as compared to the DRAIN-2D link element. The ANSR element included both shear and flexural yielding, multi-linear inelastic response and an improved hardening law.

Two of the analyses conducted by Ricles and Popov (1987) were duplicated. The first analysis was performed on a steel frame with representative strain hardening. The second analysis was conducted on the same frame assuming an elastic perfectly plastic (EPP) behavior for all members to assess the effect of strain hardening. The structure was subjected to the 1940 El Centro earthquake scaled by 1.5 to a maximum ground acceleration of 0.5g. The viscous damping was assumed to be 5% of critical.

Full details about the structure and the ANSR modeling assumptions can be found in Ricles and Popov (1987). The analysis presented here, conducted using DRAIN-2D, attempted to duplicate the same analytical behavior. The beams and braces were modeled using the beam-column element. Moment-axial load interaction followed the recommendations of the LRFD code (AISC, 1990a) code for doubly and singly symmetric sections under flexure and axial load (Equation H1-1 in the LRFD code). For the strain hardening case, the inelastic stiffness was taken as 1.5% of the initial stiffness. The floor masses were concentrated at the nodes. A vertical translational mass was applied at the link nodes. The links were modeled with

the DRAIN-2D shear link element described above. Figure 3.17 shows the relationship between the shear force and the link end displacement used for the ANSR analysis. DRAIN-2D modeling permits only a bi-linear behavior for the links. The bi-linear curve was selected so that the area under the shear-displacement curve is the same for both models (Fig. 3.18).

3.7.3.2 Analytical Results. The results of the DRAIN-2D analyses were compared to the ones obtained using ANSR (Ricles and Popov, 1987). Selected overall building response parameters and member behavior are shown here to assess the suitability of the analytical modeling used in DRAIN-2D. Figure 3.19a shows that the floor lateral displacements for the strain hardening case obtained using DRAIN-2D are very close to the results of the ANSR analysis. The comparison was limited to the first floor and to the roof to avoid cluttering the Figure. Figure 3.20 shows the frame's lateral floor displacements for the elastic perfectly plastic case. In general, DRAIN-2D analysis resulted in slightly higher displacements and showed larger permanent deformations than the ANSR analysis. However the difference was small and the agreement between the two analyses can be considered satisfactory. The maximum shear force in the links for the elastic perfectly plastic case are shown in figure 3.21. Very close agreement was obtained for this case. For the strain hardening case, DRAIN-2D predicted smaller forces however the difference was within acceptable limits. Figure 3.22 shows the axial force in the brace from the two analyses (DRAIN-2D and ANSR) for the elastic-plastic case and the strain hardening case. The figure shows a very close agreement between the two analyses. The axial force in the brace was of particular concern in this analysis. As discussed previously, nonlinear deformation of EBFs affects the damping formulation and introduces high velocities at the link ends. These high velocities may result in unrealistically high brace forces. Figure 3.23 shows the relative end displacement of the first level link obtained using DRAIN-2D and ANSR. The results between the two analyses for the strain hardening case are very close. For the elastic perfectly plastic case, the agreement between the two analyses is satisfactory but larger displacement are predicted by DRAIN-2D. DRAIN-2D, thus may yield more conservative results.

The analytical results summarized here for the analysis of an EBF steel frame showed that overall the response predicted by DRAIN-2D using a simple link element was in close agreement with the one predicted by ANSR using a more sophisticated element.

3.7.4 Conclusion. To evaluate the suitability of the link element of DRAIN-2D to model the behavior of shear links, two analyses were conducted. First, an isolated link was analyzed and the results compared to an experimental study. Second, a six-story steel EBF was analyzed and the results compared to an analytical study that used a more rigorously developed link element.

The analysis conducted on the isolated link showed reasonable correlation with experimental data despite the limitation imposed by the simple hardening laws and the assumption of bi-linear behavior. The inelastic dynamic analysis of a six-story EBF structure using DRAIN-2D element showed close agreement with a more rigorous analysis using the ANSR computer program. Consequently, it appears that the shear link element used in DRAIN-2D provides satisfactory prediction of the behavior of shear link elements. Additional discussion on EBF modeling is presented in Section 3.9.

3.8 Evaluation of the Brace Buckling Element.

In this research, retrofit schemes using concentric bracing were analyzed. The accuracy of the analytical response of such structures depends largely on the hysteretic modeling of the braces. In this section, the response of the brace element used in the computer analysis is compared to available experimental data to provide an indication of the accuracy of the modeling.

Two rectangular tube braces which were tested by Lee and Goel (1987), designated as specimens 5 and 6, were selected for this analysis. Lee and Goel (1987) subjected these brace specimens to cyclic loading until brace fracture or local buckling. The brace properties that were experimentally measured, are summarized in Table 3.4. Tubular sections were

selected since only this type of member was used in the analyses conducted for this research. Hysteretic rules for the brace element of DRAIN-2D were based on tests conducted on braces with Kl/r higher than 60 (Jain and Goel, 1978).

The braces were analyzed using the brace buckling element of DRAIN-2D. The loading history was simulated by conducting a displacement controlled analysis. The initial buckling load, P_b was calculated according to the recommendations of LRFD specification (AISC, 1990a). The post buckling load capacity, P_{pb} was computed using Equation 3.12. Table 3.5 shows the computed initial buckling load and cyclic load strength reduction factors used for the analyses.

Figure 3.24 and Figure 3.25 show the experimental and analytical results for the brace with Kl/r less than 60 and for the brace with Kl/r higher than 60 respectively. The element gives a good estimation of the tension envelop curve and the compression envelop curve. However the cyclic load deterioration is not very closely modeled by the brace buckling element. After the member buckles, the model element assumes that the compressive load capacity drops to the post buckling load. While the experimental results show a more gradual decrease in the load capacity. This is particularly apparent for the brace with KL/r less than 60. For Kl/r larger than 60, the approximation in the load capacity decrease is rather within acceptable limits. For Kl/r larger than 60, the reloading stiffness is properly estimated. However, for the brace with KL/r less than 60, the reloading stiffness used in the model is rather higher than the experimental one. Consequently, the element predicts a somewhat larger energy dissipation capacity.

Based on this limited comparison it appears that the DRAIN-2D brace buckling element gives generally a satisfactory modeling of a brace cyclic behavior for tubular braces with KL/r larger than 60. However, for braces with Kl/r smaller than 60, the model predicts larger energy dissipation.

It is worth mentioning that the model exhibits some inherent limitations: local buckling and brace fracture are not modeled. Tests have shown that brace local buckling is followed by a considerable reduction in strength and stiffness (Tang and Goel, 1987). The current model cannot reproduce such strength degradation. Brace capacity is usually limited by brace fracture which cannot be predicted by the model used here. Additional discussions on the limitations of the brace model elements is presented below.

3.9 Additional Discussion on Analytical Modeling of EBFs and CBFs.

Existing research work related to modeling of EBFs and CBFs is reviewed here. This review will help assess the accuracy and limitations of the elements used in this study to model braced steel buildings.

3.9.1 Analytical Modeling of EBFs The analytical modeling of EBFs depends mainly on the shear link modeling. Numerous test data of link behavior are available (Hjelmstad et al. 1983, Kasai et al., 1986b, Malley et al., 1984). These data indicate that the hysteretic behavior of links is stable and predictable and can be represented with a simple model (Roeder and Popov, 1977). The model used in this study assumed a bi-linear behavior and was developed by Tang and Goel (1988)

Lee and Lu (1989) used the link model developed by Tang and Goel (1988) to analyze a structure that was previously tested under cyclic loading. The structure considered in that study was a 1/3 scale model of a six-story steel EBF prototype. Their investigation showed that the use of the simple model led to a good agreement between the analytical and experimental results. Lee and Lu (1989) noted however that a tri-linear model may lead to even better analytical results. Similar conclusions were reached in this study (see Section 3.7).

Lee and Lu's study (1989) also showed that the ductility and energy dissipation capacity of an EBF could be analytically predicted. The ductility of the building was limited by link

failure which occurred at a link plastic rotation of 0.10 rad. This failure criteria is in agreement with previous test data, summarized in Chapter 2 and serves as a good indication of the structure's deformation capacity.

3.9.2 Analytical Modeling of CBFs The performance of CBFs is primarily controlled by the brace behavior which is generally more complex and not as well understood as shear links (Khatib et al., 1988, Popov et al. 1993). Brace behavior depends on several parameters that include slenderness ratio, local buckling, type of cross section and brace fracture. The influence of each parameter on behavior and modeling of braces will be discussed below.

The most important parameter influencing brace behavior is the slenderness ratio, Kl/r (Black and Popov, 1981). This ratio depends on the section properties and on the restraint provided by the brace connections. Connection restraint is, however, difficult to estimate. As yet, little information is available on the behavior of heavy bracing connections with the brace subject to inelastic buckling (Popov et al., 1993, Tremblay, 1992). Tang and Goel (1987) showed that for rigid end connections, the experimental value of the effective length factor, K varied between 0.6 and 1.0. Experimental research conducted in Japan (Nakashima, 1992) showed similar variations in the experimental value of the effective length factor. Hysteretic brace behavior in existing models is controlled by the member's slenderness ratio. However, uncertainties and complexity involved in estimating this ratio makes brace modeling uncertain.

Brace behavior was also found to be influenced by local buckling. Local buckling was experimentally observed even in sections that satisfy compact section requirements, such as tubular members (Tang and Goel, 1987). Popov and Black (1981) tested 22 specimens with different sectional shapes and slenderness ratios and found that all struts, except thick walled pipes, experienced premature local buckling. Experimental data have shown that this type of buckling leads to considerable reduction in stiffness and strength and eventually to brace fracture (Tang and Goel, 1987). Brace local buckling and its effect on the strut behavior is not,

as yet, incorporated in known brace models including the one used in this study. This limits the ability of the brace model to properly predict strut behavior and can result in overestimating the energy dissipation capacity.

Experimental research showed that the cyclic behavior of the braces depends also on the type of section (Popov and Black, 1981, Jain and Goel, 1978). The brace model used in this study and in the study conducted by Pincheira (1992) was developed by Jain and Goel (1987) to model the behavior of tubular sections with Kl/r larger than 60. Hence, it can not be readily applied to other brace sections.

3.9.3 Concluding Remarks. Currently available analytical models can satisfactorily predict EBF behavior but present some limitations in predicting the inelastic behavior of CBFs due to the complexity of modeling. In particular, energy dissipation capacity, an essential feature in seismic design, cannot be predicted with confidence for CBFs. Also, stiffness and strength reduction due to local buckling, brace fracture, and connection failure which limits the deformation capacity of CBFs, cannot be yet modeled with confidence.

Table 3.1. Parameters Defining the Stress-Strain Curve for the Reinforcing Steel

Grade	σ_y (ksi)	σ_u (ksi)	E (ksi)	E_{sh} (ksi)	ϵ_{sh}	ϵ_u
40	40	70	29000	1000	.015	.1
50	50	80	29000	1200	.01	.1
60	60	100	29000	1200	.008	.1

Table 3.2. Experimental Properties of the Link Specimen

Section	Length (in)	Location	σ_y (ksi)	σ_u (ksi)	ϵ_{sh}	ϵ_u
W18x40 A36 Steel	28.0	web	39.5	60.1	.018	.22
		flange	35.0	58.5	.014	.24

Table 3.3. Properties Used for DRAIN-2D Link Element

E_s/E	A (in ²)	I (in ⁴)	A_s (in ⁴)	V (k)	ν
.009	11.8	612	5.64	122	.3

Table 3.4. Properties of the Braces Tested by Lee and Goel (1987)

Specimen	Section	KL/r	F_y (ksi)	F_u (ksi)
5	TS 4x4x1/4	77	74.0	85.6
6	TS 4x4x1/4	45	74.0	85.6

Table 3.5. Buckling Load Parameters Used in the Analysis of Test Specimen

Specimen	P_b (kips)	$F_r = P_{pb}/P_b$
5	152	.21
6	213	.29

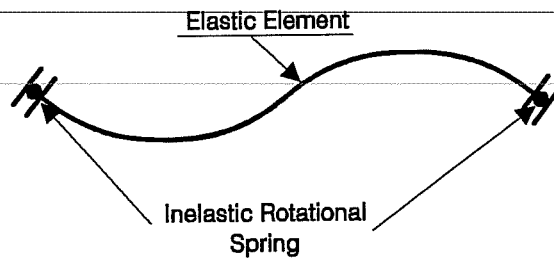


Figure 3.1. One Component Model for a Nonlinear Beam

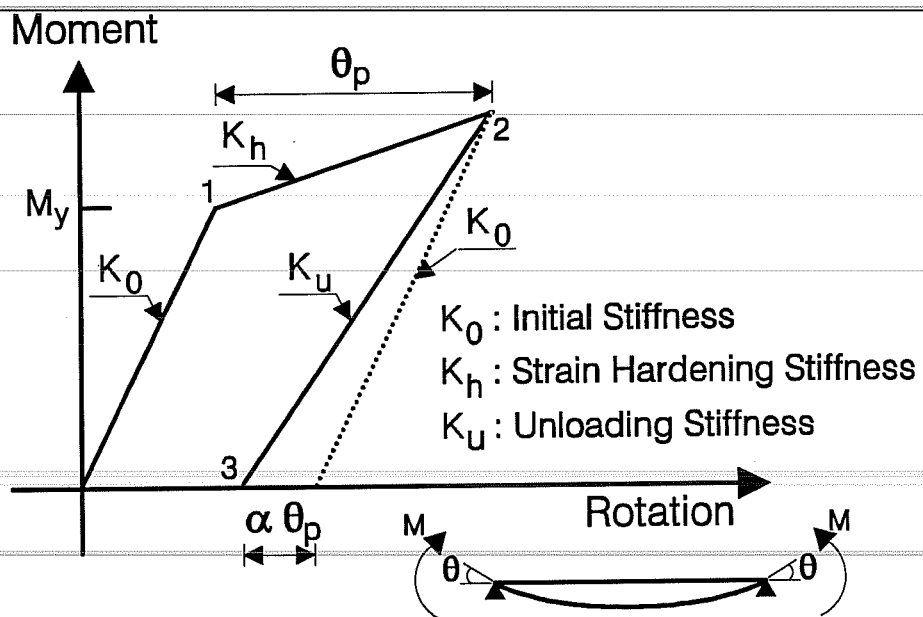


Figure 3.2. Initial, Strain Hardening, and Unloading Stiffness for the Reinforced Concrete Model Element

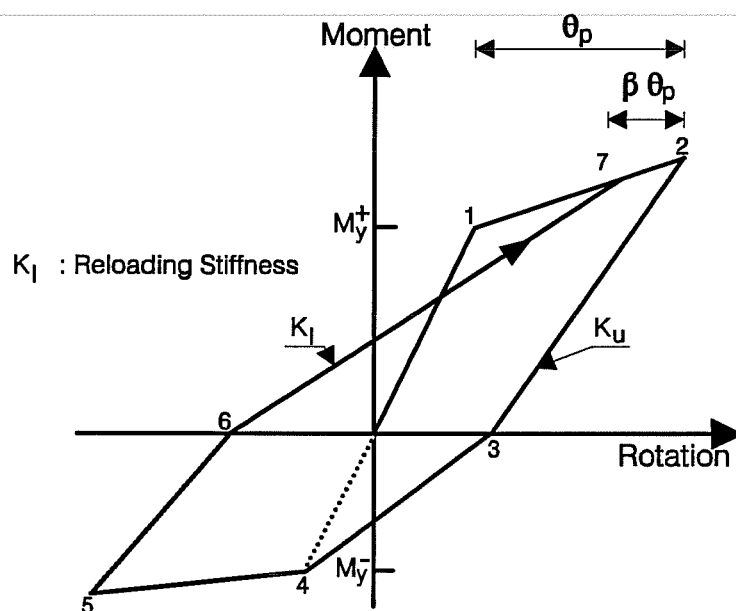


Figure 3.3. Reloading Stiffness for the Reinforced Concrete Model Element

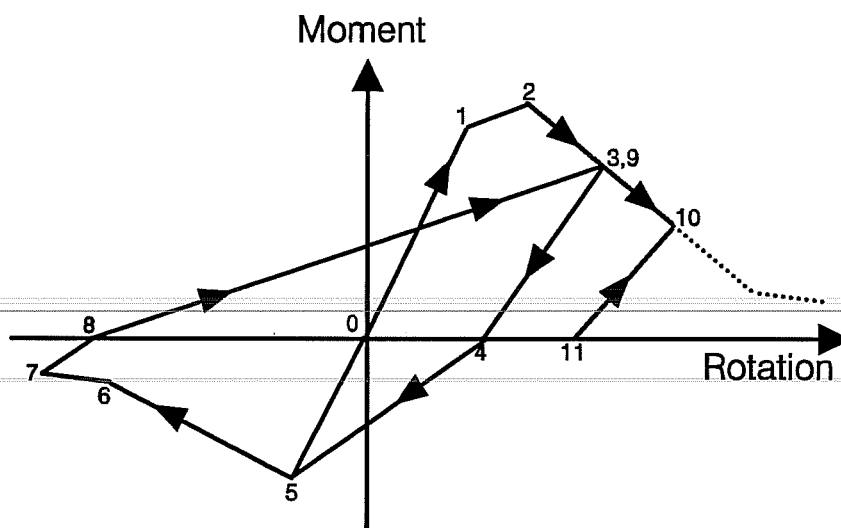


Figure 3.4. Hysteretic Rules for the Reinforced Concrete Model Element

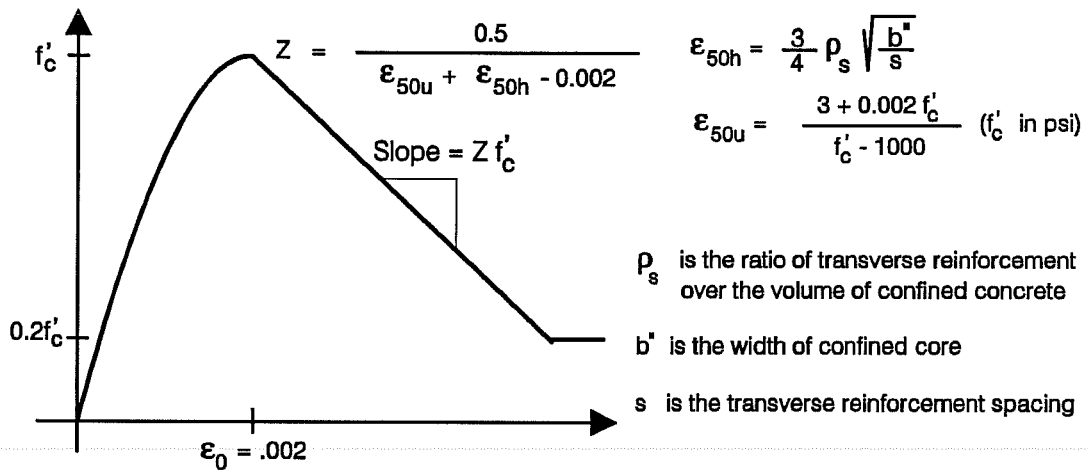


Figure 3.5 Stress-Strain Diagram for Confined Concrete
(Adapted from Kent and Park, 1970)

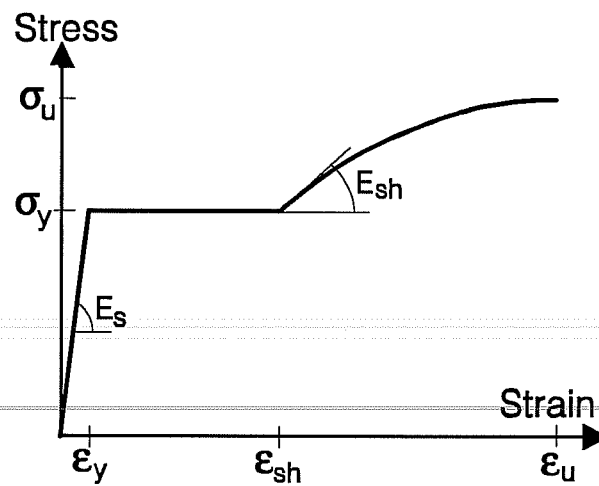


Figure 3.6 Strain-Stress Diagram for Reinforcing Steel

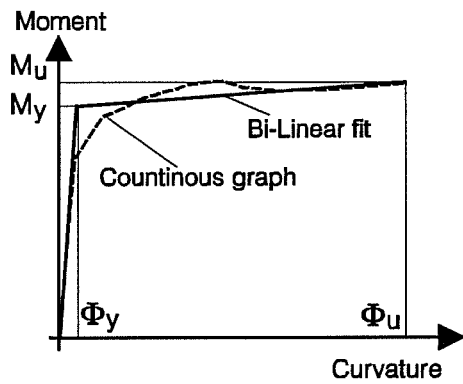


Figure 3.7 Bi-Linear Fit for the Moment Curvature Diagram for Reinforced Concrete Sections

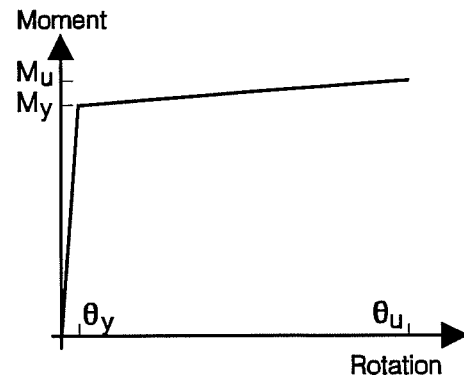


Figure 3.8 Moment Rotation Diagram Assumed for Reinforced Concrete Sections

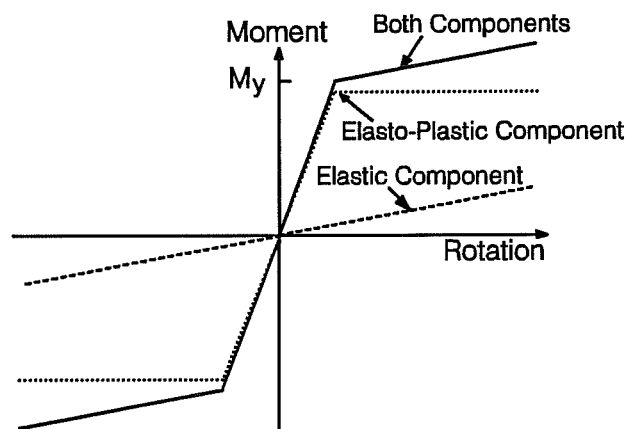


Figure 3.9 Moment-Rotation Diagram of the Beam-Column Model Element

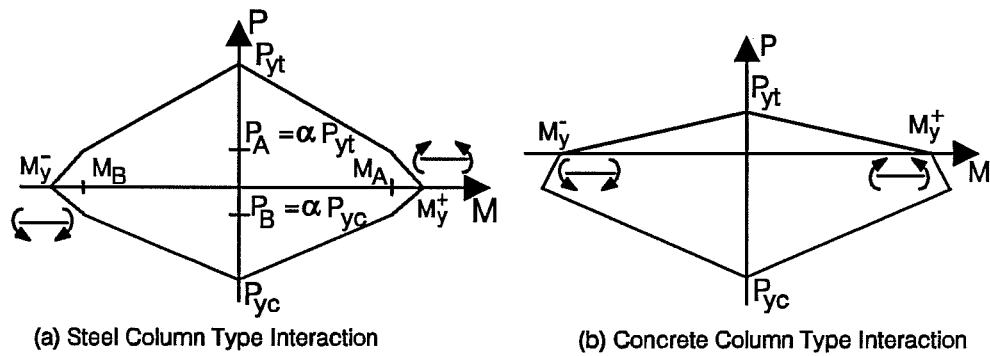


Figure 3.10 Interface Surfaces for the Beam-Column Element

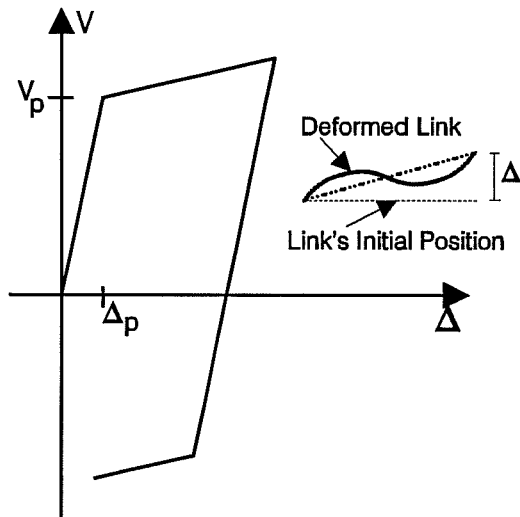


Figure 3.11 Force Displacement Relationship for the Shear Link Element

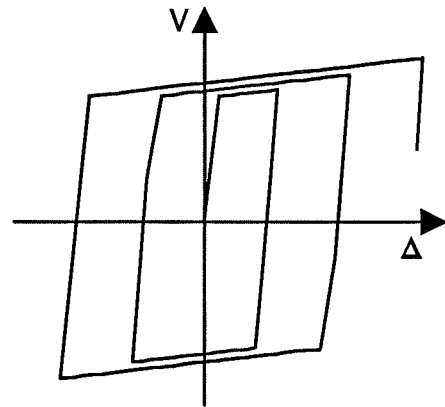


Figure 3.12 Hysteretic Behavior of the shear Link Element

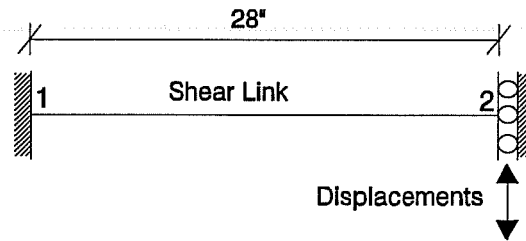
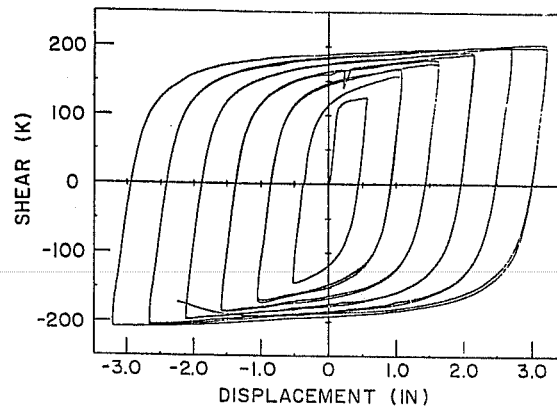
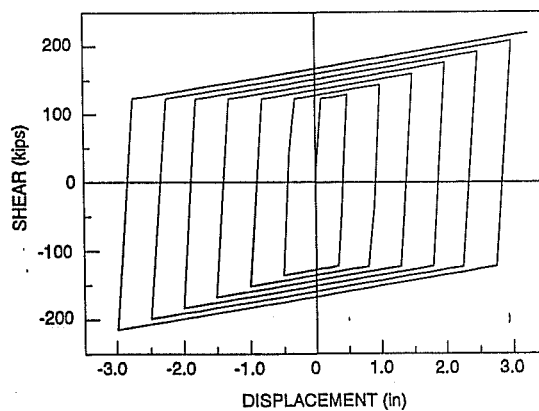


Figure 3.14 Test on An Isolated Shear Link

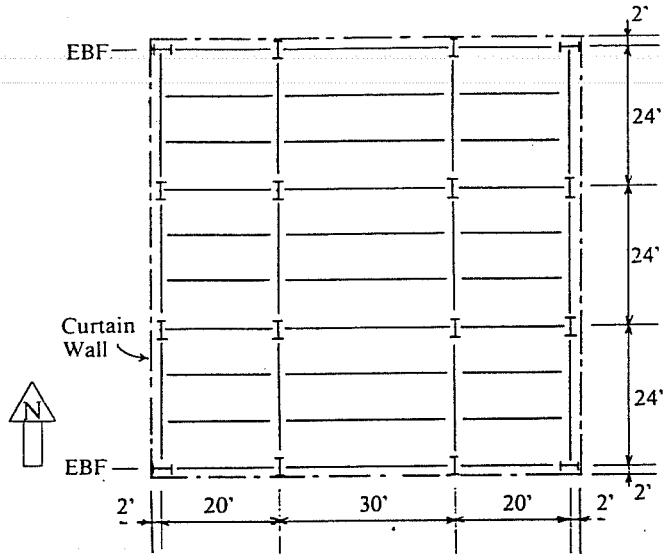


(a) Experimental Behavior (Hjemstad and Popov, 1983)

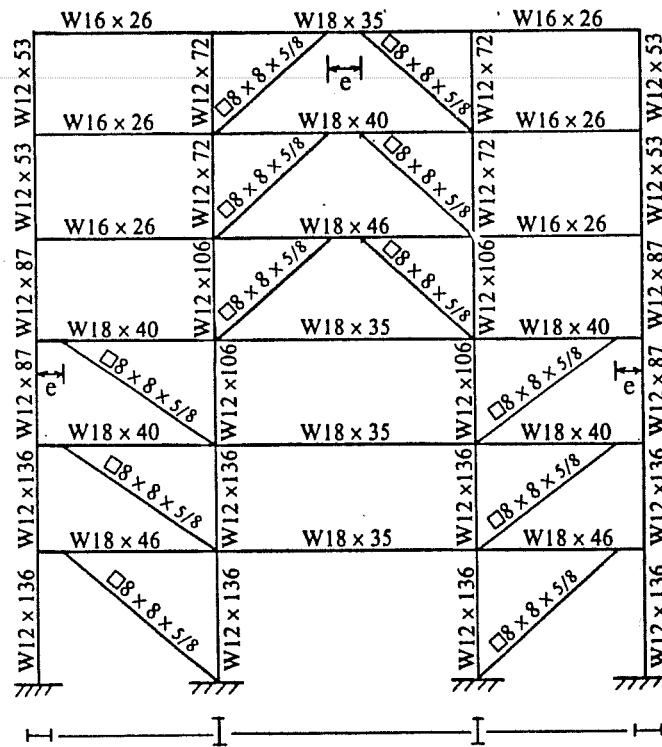


(b) Analytical Behavior

Figure 3.15 Comparison Between the Experimental and Analytical Behavior of an Isolated Shear Link



(a) Plan View



(b) Elevation View of External Frame

Figure 3.16 Plan and Elevation View of the Six-Story Steel EBF Building (Ricles and Popov, 1983)

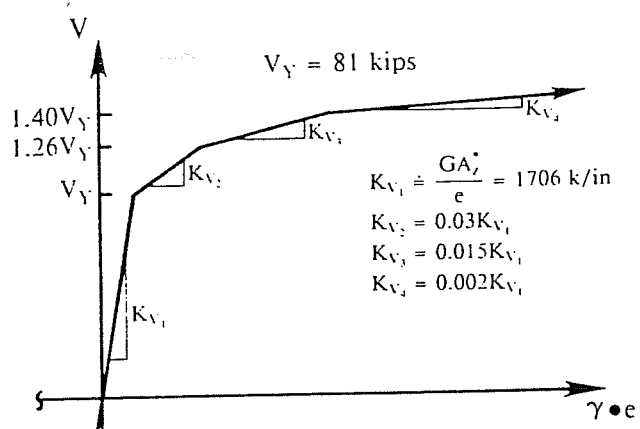


Figure 3.17 Modeling of Shear Link Behavior in Ricles and Popov (1983) Analysis

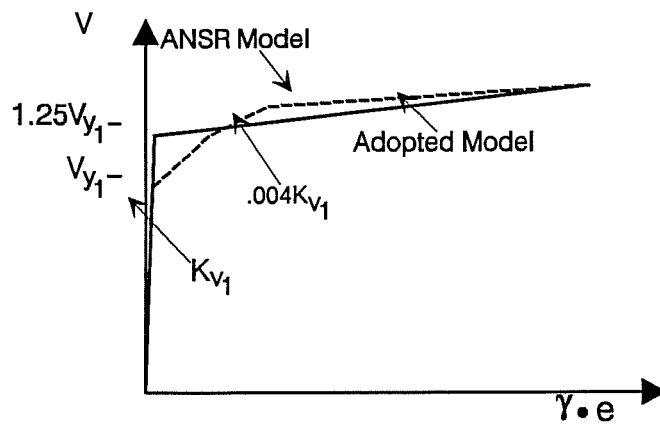
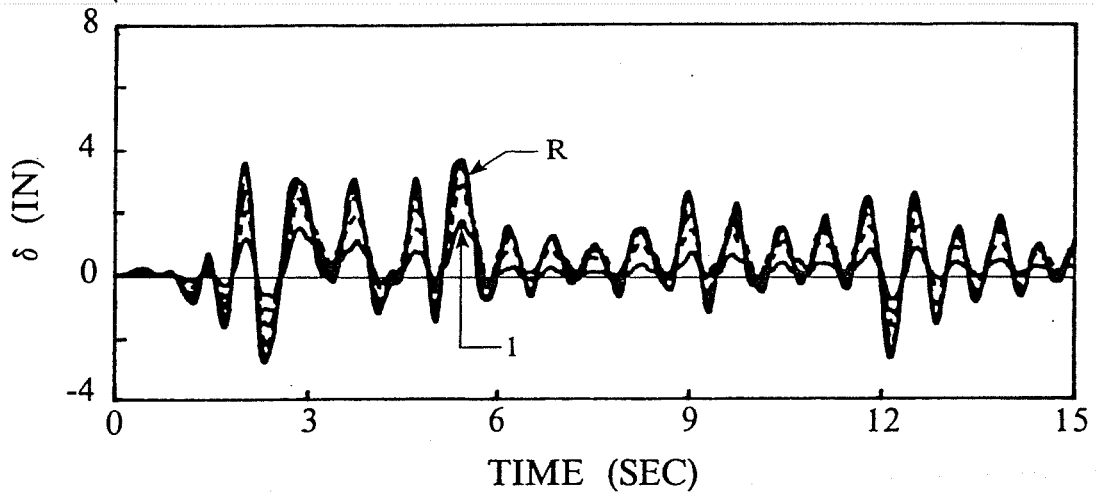
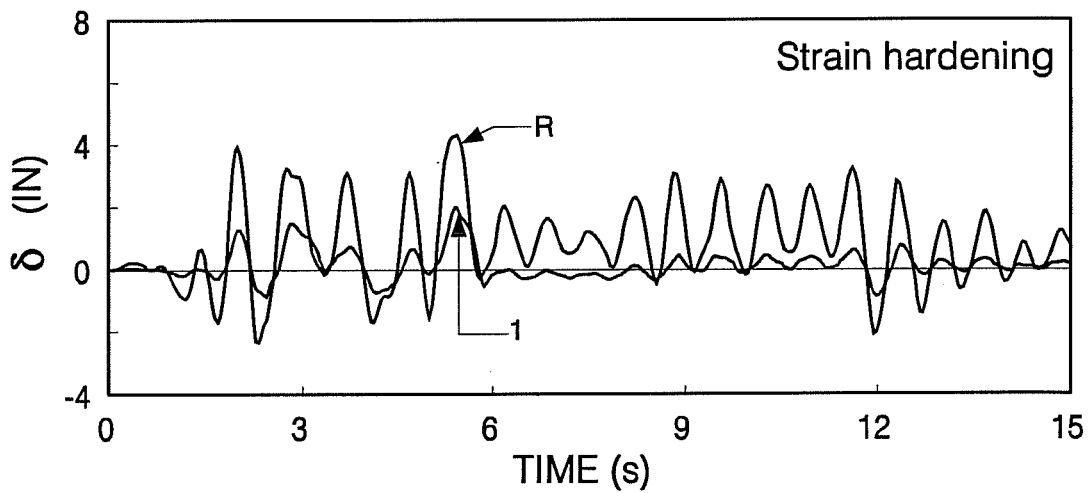


Figure 3.18 Shear Force - End Displacement Relation Used in the DRAIN2D Analysis

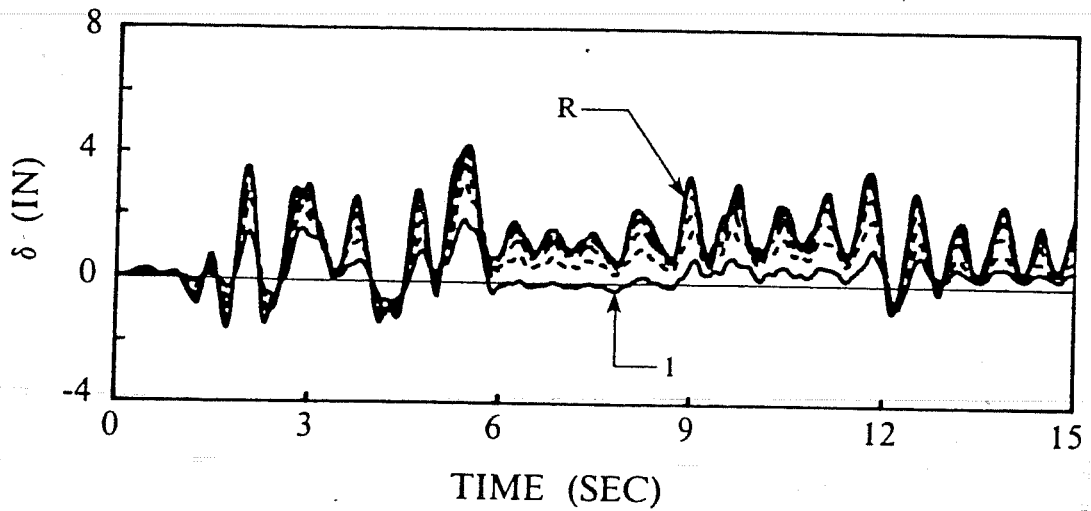


(a) ANSR Analysis (Ricles and Popov, 1987)

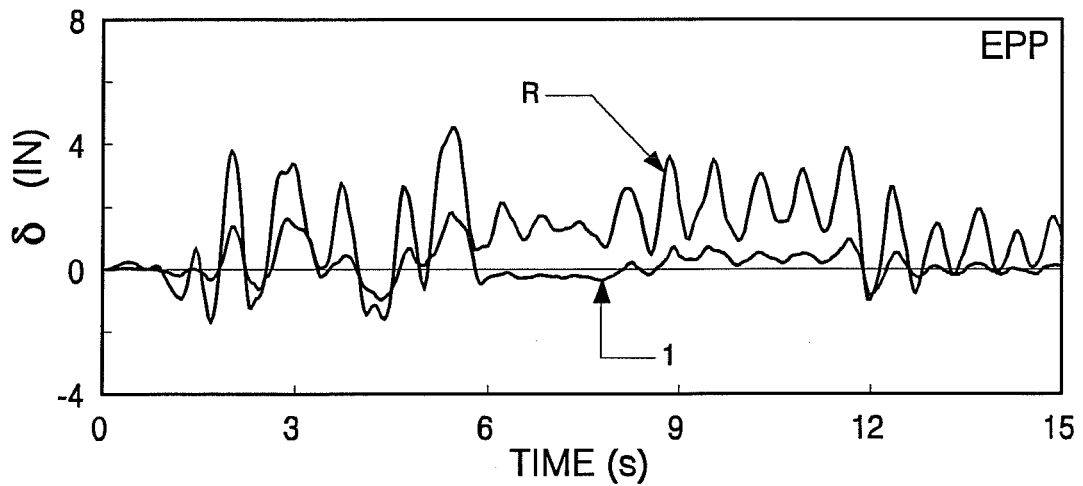


(b) DRAIN2D Based Analysis

Figure 3.19 Lateral Floor Displacements of the Six-Story EBF Building for the Strain Hardening Case

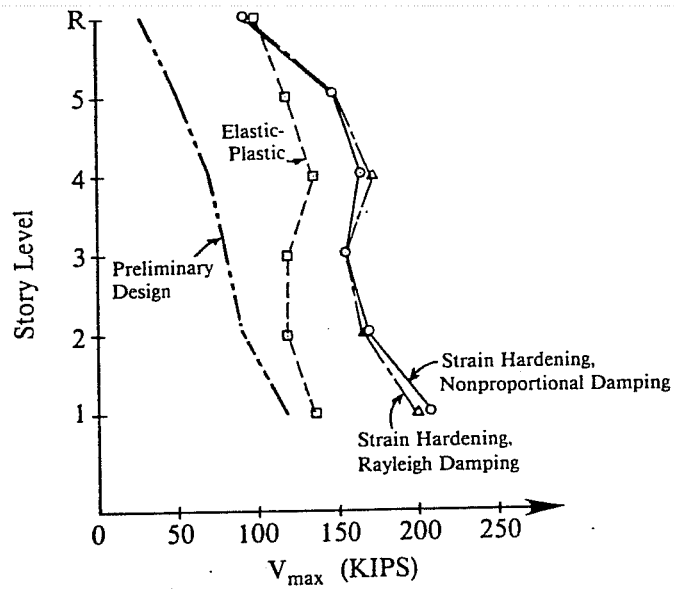


(a) ANSR Analysis (Ricles and Popov, 1987)

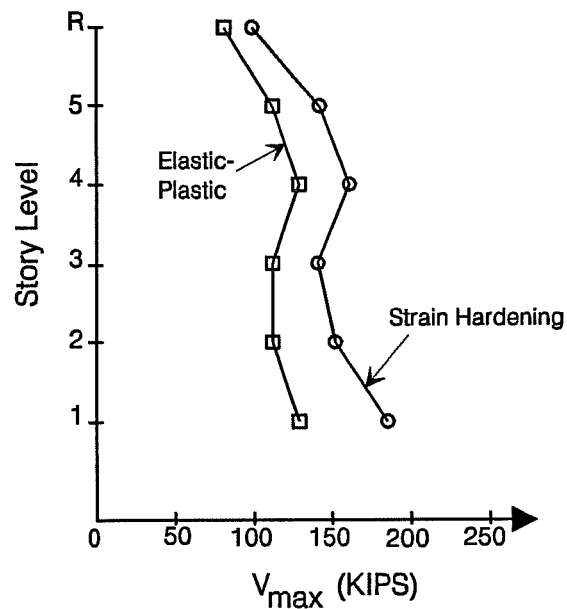


(b) DRAIN2D Based Analysis

Figure 3.20 Lateral Floor Displacements of the Six-Story EBF Building for the Elastic-Perfectly Plastic Case

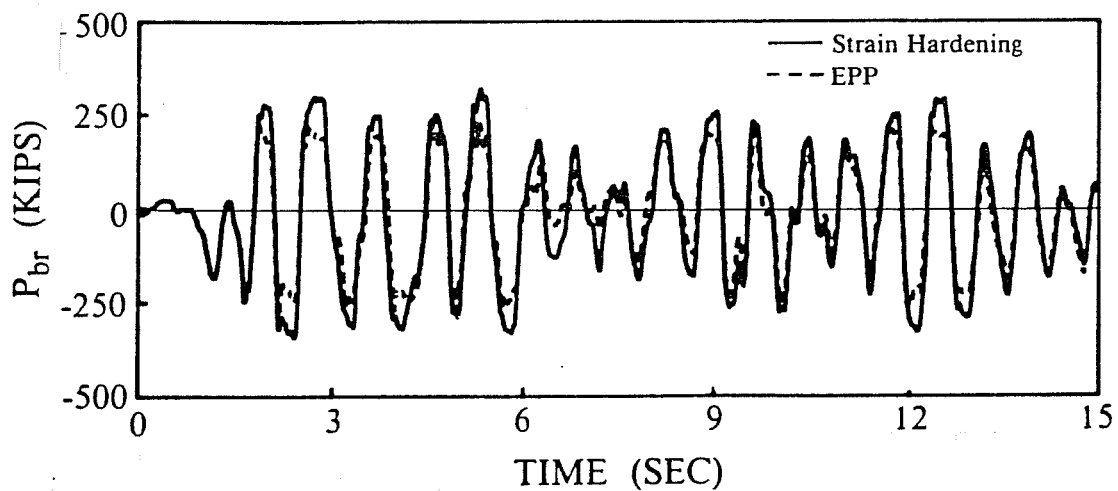


(a) ANSR Analysis (Ricles and Popov, 1987)

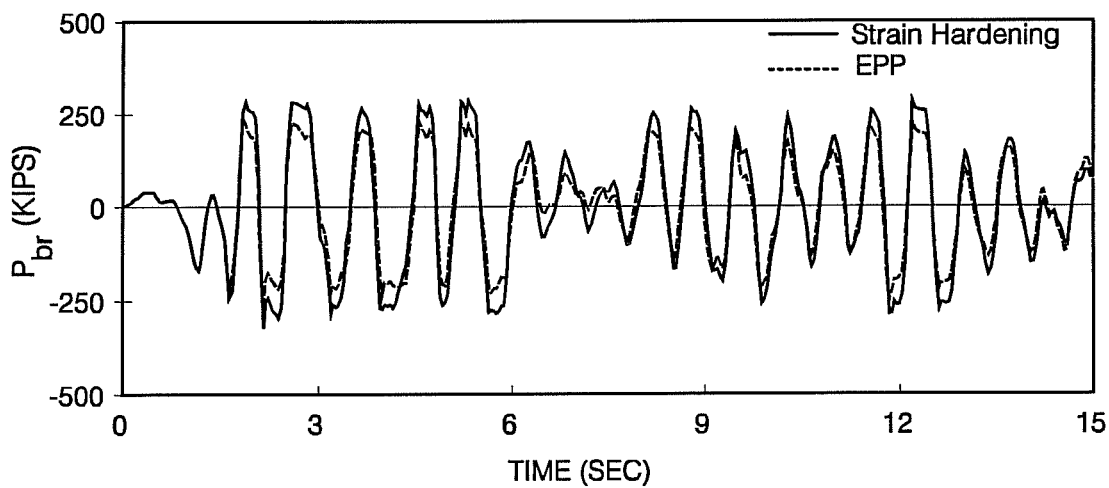


(b) DRAIN-2D Analysis

Figure 3.21 Maximum Link Shear Force for the Six-Story EBF Building

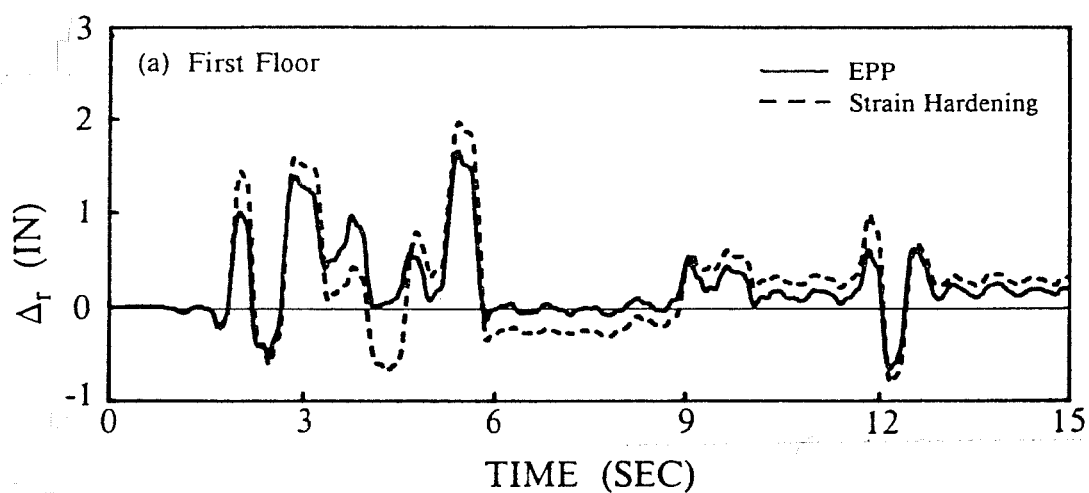


(a) ANSR Analysis (Ricles and Popov, 1987)

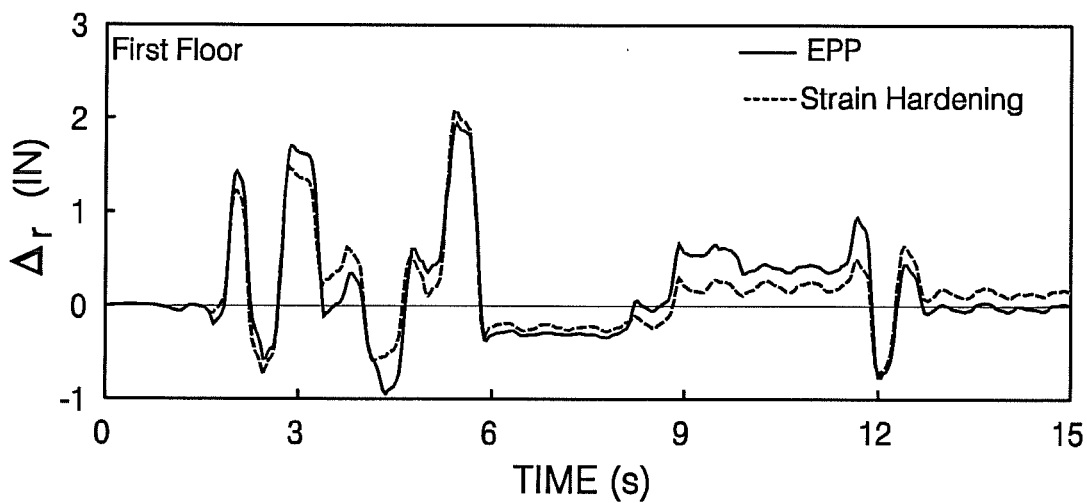


(b) DRAIN2D Analysis

Figure 3.22 Axial Force in the First Floor Brace for the Six-Story EBF Building Subjected to 1.5 El Centro Earthquake Record

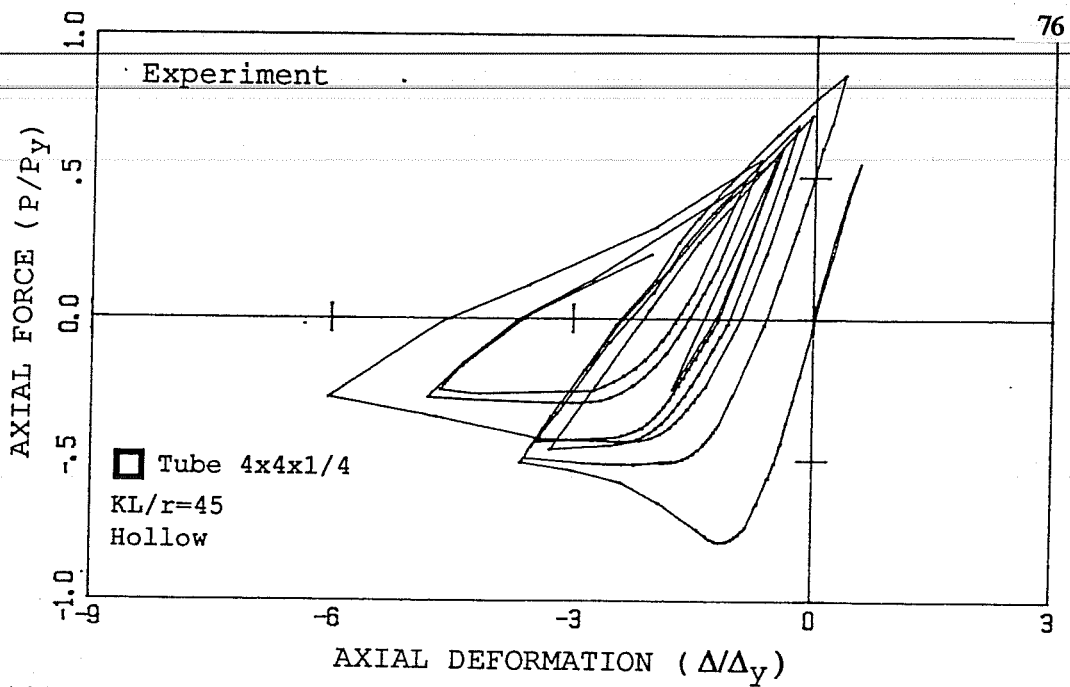


(a) ANSR Analysis (Ricles and Popov, 1987)

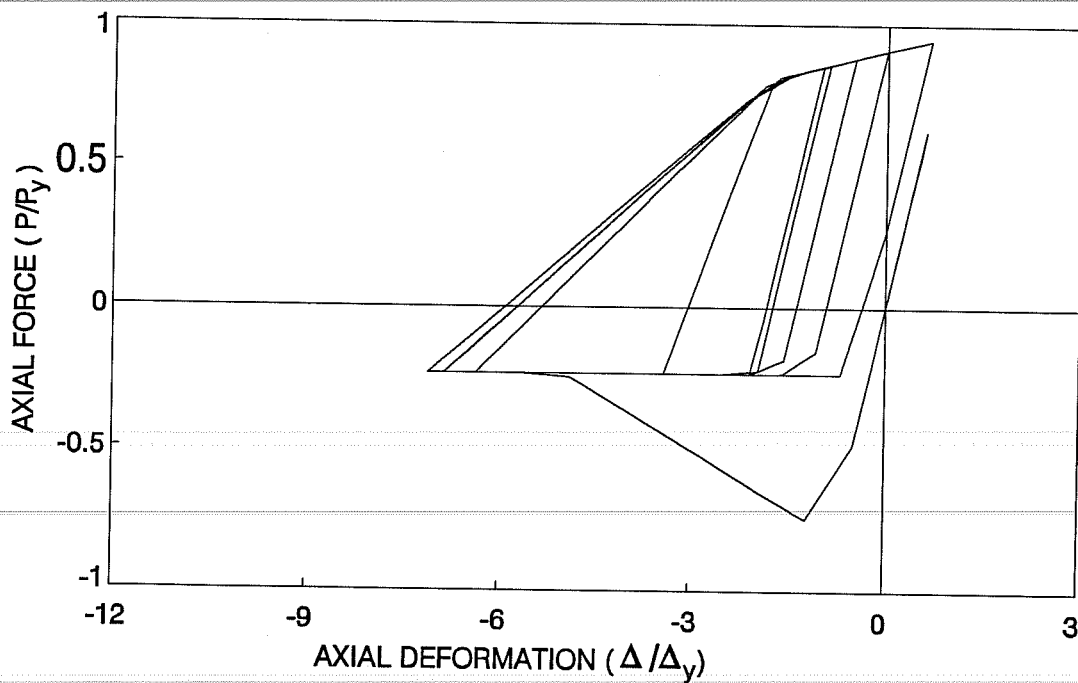


(b) DRAIN2D Analysis

Figure 3.23 Relative End Displacement for the Shear Links of the Six-Story EBF Building Subjected to 1.5 El Centro Earthquake Record

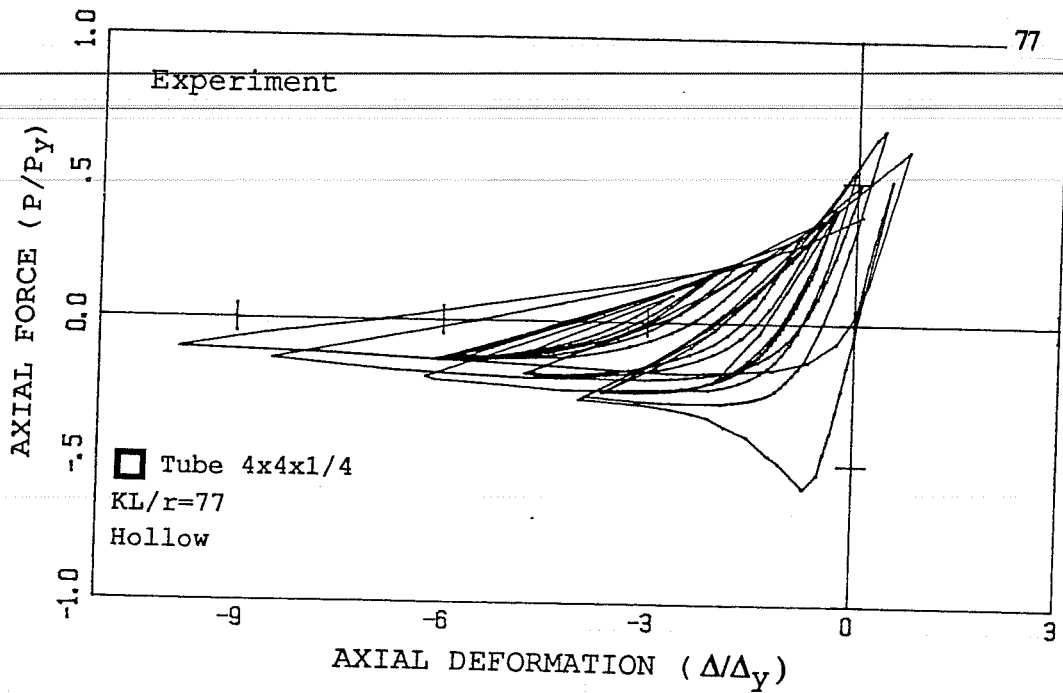


(a) Experimental Behavior (Tang and Goel, 1987)

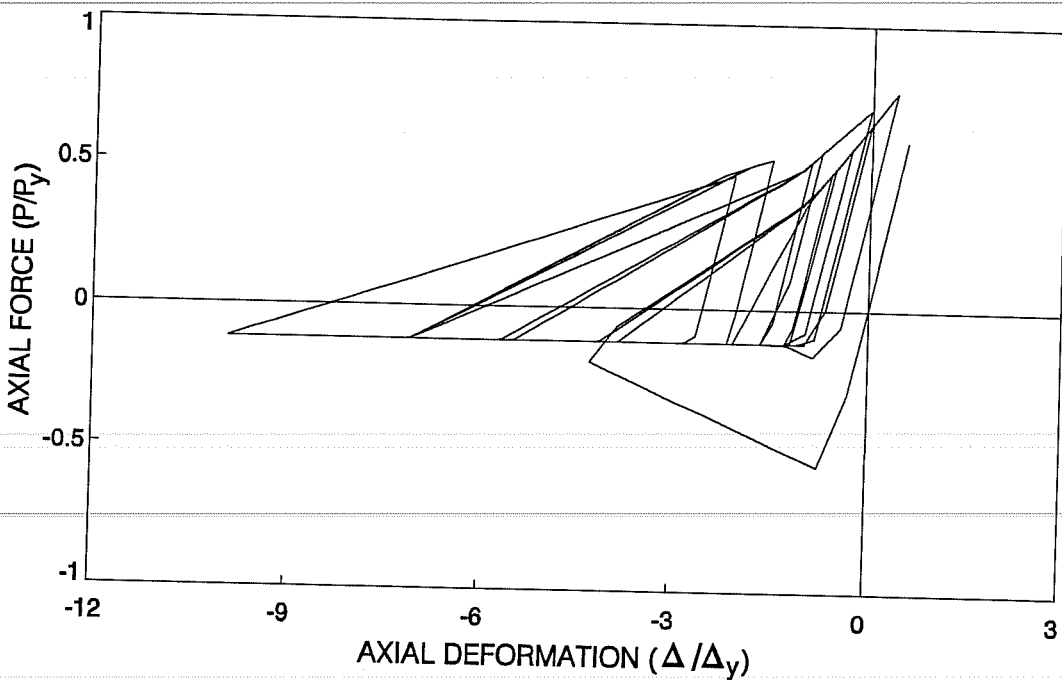


(b) Analytical Behavior

Figure 3.24 Experimental and Analytical Behavior of a Brace with KL/r less than 60



(a) Experimental Behavior (Tang and Goel, 1987)



(b) Analytical Behavior

Figure 3.25 Experimental and Analytical Behavior of a Brace with KL/r larger than 60

CHAPTER 4:
GROUND MOTIONS AND ANALYSIS OF A SIMPLE FRAME

4.1 Introduction.

Reinforced concrete buildings, representative of low and medium rise 1950s and 1960s west coast construction, were selected for this study. The design of these buildings was based on older codes that are not as rigorous as the current standards. Consequently the buildings may not have sufficient strength or ductility to sustain the earthquake loading. To improve their seismic behavior, the selected structures were retrofitted, mainly by the addition of eccentrically braced frames (EBFs). The performance of the original and retrofitted buildings were analytically evaluated under static loading and dynamic loads. The static analysis was performed by applying a lateral incremental load and the dynamic analysis was performed using a number of earthquake records.

4.2 Ground Motions Selected.

4.2.1 Acceleration Records. Five strong ground motions were selected for the dynamic analyses conducted in this study. Three were recorded on firm soil and two on soft soil. One of the records was from the 1985 Mexico City earthquake, while the remaining ones were from US west coast earthquakes. The three records on firm soil were:

- **1940 El Centro, N00E component.**

This record has been extensively used in other studies, thus making it possible to compare the results obtained here to those of other studies. Note that El Centro acceleration record was scaled to a peak ground acceleration of 0.5g.

- **1989 Corralitos, N00E component.**

The Corralitos record was taken during the Loma Prieta earthquake of 1989. It was recorded very close to the fault and constitutes a strong earthquake on stiff soil.

- **1966 Parkfield, N65E component.**

The Parkfield record shows a strong motion within a short duration and resembles an impulse type of load.

The two soft soil earthquake records were as follow:

- **1985 Mexico, N90E component.**

The Mexico record shows a long duration of strong shaking with a large predominant period.

- **1989 Oakland.**

This was one of the strongest records measured on soft soil during the Loma Prieta earthquake.

Table 4.1 provides some information for the selected records and Figure 4.1 show the time history of these records.

4.2.2 Elastic Spectral Responses. Figure 4.2a shows the elastic acceleration response spectra for the selected records on firm soil at 2% damping. The largest spectral acceleration for these records were obtained for low to medium periods with the Corralitos record, reaching a peak of 2.74 g. The acceleration response spectra for the soft soil records is shown in Figure 4.2b The largest response for the Mexico earthquake is obtained for periods ranging from 1.8 s to 2.6 s with a peak pseudo acceleration of 1.65 g at 2s. The spectral accelerations for the Oakland record were not as large as for Mexico record, and the largest spectral accelerations occurred at lower periods. The peak spectral acceleration for the Oakland record occurred at a period of 0.6s and measured about 0.9g.

Figure 4.3a shows the spectral displacement for the records on firm soil at 2% damping. In general, the Parkfield record resulted in the largest spectral displacement for the firm soil records. The spectral displacements for the soft soil records at 2% damping are

shown in Figure 4.3b. The Oakland record maintains a spectral displacement averaging 17 in. for periods above 2s. The Mexico record imposes extremely large spectral displacements for periods ranging between 1.7s and 4s. The peak spectral displacement for Mexico record was equal to 71.6 in. and was reached at a period of 2.7 s.

4.3 Analysis of a Two-Story Frame.

4.3.1 Introduction. A two-story frame was analyzed to provide an initial indication of the capabilities and advantages of steel Eccentrically Braced Frames (EBFs) for seismic strengthening of reinforced concrete frames. To that end, the behavior of the original frame and the frame retrofitted with a steel EBF were compared based on a static elastic analysis, a static inelastic analysis, and a dynamic analysis. This small frame will also be used to illustrate the modeling procedure and the typical steps followed in the preliminary selection and design of an EBF retrofit scheme.

4.3.2 Original Structure.

4.3.2.1 General. The two-story, one bay frame considered here was based on a larger structure used in an earlier study (Bush, 1987). Figure 4.4 shows the frame's configuration and the member reinforcement. The frame has six feet deep spandrel beams. The story height is 10 ft but due to the deep spandrel beams, the clear height of the columns is only four ft. Grade 50 steel was used for the longitudinal reinforcement and Grade 40 for the transverse reinforcement. The concrete compressive strength is specified as 3000 psi.

The transverse reinforcement in the columns followed the recommendations of ACI 318-56 (ACI, 1956) code and was provided to resist the shear due to the design lateral forces of UBC 55 (International, 1955). The applications of these codes resulted in a widely spaced transverse reinforcement that is not adequate to permit the development of flexural hinges prior to shear failure. Consequently the columns are expected to experience a brittle shear failure. Also, the column transverse reinforcement does not satisfy the current code (ACI318-89)

recommendations on confinement. For these columns, a spacing of 4 in. is required in the vicinity of the beam-column joint, while the actual spacing was equal or larger than 12 in.

The columns were provided with short compression splices in accordance with the recommendations of the 1956 ACI code. However, the splices started at the slab level (Fig. 4.4c.) and due to the presence of the deep spandrel beams, the actual splice length was larger than the intended length. The splices had adequate length to allow for development of the longitudinal steel capacity.

4.3.2.2 Structural Modeling. The beams and columns were modeled using the reinforced concrete element described in Section 3.6.2.. The moment curvature diagrams for the beams and columns were obtained using the RCCOLA program, as described in Section 3.6.2.2. The moment curvature diagram for the columns was computed assuming an axial load level corresponding to the gravity loading. Axial load was neglected in calculating the moment curvature diagram for the beams. The continuous moment curvature diagram was fit to a bi-linear relationship. The moment rotation relationship for the beams and columns were derived from the moment curvature diagram as explained in Section 3.6.2.1. The shape of these moment rotation relationship is shown in Figure 4.5. Table 4.2 shows the yield and ultimate points for the moment curvature diagrams, and Table 4.3 gives the value of the moment and rotation at yield and at ultimate for the columns and the beams.

Column shear strength was computed according to the ACI 318-89 recommendations and was found equal to 51 kips for a resistance factor, ϕ of one. Column shear failure was anticipated for the frame under lateral load. The occurrence of column shear failure was considered to define the failure of the unretrofitted frame.

4.3.3 Retrofitted Structure.

4.3.3.1 Introduction. The original structure was retrofitted by the addition of a steel eccentrically braced frame (EBF). The design procedure of the EBF consisted of first, selecting the EBF geometry and then sizing the links based on the lateral design forces. The other steel structural members were then designed to remain essentially elastic under the forces generated by the fully yielded and strain hardened shear links (Popov and Engelhardt, 1988). Inelastic rotational capacity of the links is checked by examining the DRAIN-2D analysis output. Experimental research (Hjelmstad and Popov, 1983) has shown that properly detailed shear links can undergo rotations of 0.1 rad under cyclic loading. Exceeding a link rotation of 0.1 rad. was considered to constitute failure of the EBF in the retrofitted frame.

4.3.3.2 Selection of EBF geometry. Two configurations can be envisioned for the added EBF: one with the link at the beam mid-span, the other with the link at the end of the beam. In the second configuration, the links transfers large moments to the columns. These large moments may adversely affect the existing concrete columns and may lead to difficulties in the design of the link to column connections as explained in Section 2.4. The first configuration, with the link in the middle of the beam was therefore used (Fig. 4.6a). The forces from the EBF are transferred to the columns through channels doweled to the column's face (Fig. 4.6b and 4.6c)

4.3.3.3 Selection of EBF's member sizes. The equivalent lateral load procedure of the 1991 edition of the UBC (International, 1991) was selected as a method for preliminary sizing of the added EBF. For the retrofitted frame, the concrete was assumed to carry vertical load only, with all the lateral load resisted by the EBF. The design base shear was computed assuming that the building was located in seismic zone four and was resting on firm soil. The force reduction factor (R_w) was taken equal to 10. The period of vibration, T was computed using the procedure outlined in the 1991 UBC.

The base shear was distributed to each floor level, in accordance with the 1991 UBC lateral load procedure. EBF member design followed the LRFD specifications (AISC, 1990a) rather than the allowable stress procedure of UBC 91. Using a load factor of 1.5, as specified by the LRFD code for earthquake forces, the lateral force at the second and first level were found equal to 40 kips and 20 kips respectively.

- **Link Size**

The same member size was used for both links. The most heavily loaded shear link is the one at the first level. The shear force in the link, V_{link} at a given floor level of an EBF can be estimated from the following simple relation suggested by Kasai and Popov (1986c):

$$V_{link} \approx \frac{h}{L} V_{cum} \quad (4.1)$$

where L is the bay width, h is the story height, V_{cum} is the accumulated story shear at the level under consideration. This relation was derived by summing the moments about point A in the simplified free body diagram shown in Figure 4.7.

V_{link} was found equal to 57 kips. A W12x30 of A36, with a plastic shear capacity of 64 kips, steel was selected.

To obtain the maximum stiffness and strength from the EBF, short links that yield primarily in shear are used. The length of shear links need to be less than $1.6 M_p/V_p$, where M_p is the plastic moment and V_p is the plastic shear strength. For the link selected $1.6 M_p/V_p$ is equal to 36 in. The link length of the added EBF was taken as 15 in.

After selecting the shear link, the other EBF members are sized for the forces generated by the yielded and strain hardened shear link. The beam section is the same as the link section (W12x30), a square tube of 5x5x1/2 A500 Gr. B was selected for the braces. Verification of adequacy of these members is provided below.

● **Axial Forces in the Braces and Beam.**

The maximum shear force that develops in a fully yielded and strain hardened link (V_{ult}) is taken as $1.5 V_p$, based on recommendation from EBF research (Engelhardt and Popov, 1989). For the W12x30 A36 link, V_{ult} equals 96 kips. The axial force generated in the brace (P_{brace}), and in the beam segment outside the link (P_{beam}) due to a link of V_{ult} can be estimated by one of the following two methods:

- a) Compute the ratios P_{brace}/V_{link} and P_{beam}/V_{link} from an elastic analysis. Use these ratios, shown to remain constant for an EBF in both the elastic and inelastic range (Hjelmstad and Popov, 1983b), to compute P_{brace} and P_{beam} for V_{link} equal to V_{ult} .
- b) Use the following approximate formulas that are based on frame equilibrium at the beam-link-brace joint (Engelhardt, 1987):

$$P_{brace} = \frac{\frac{e}{2L_{beam}} + 1}{\sin \alpha} V_{link} \quad (4.2)$$

$$P_{beam} = \frac{\frac{e}{2L_{beam}} + 1}{\tan \alpha} V_{link} \quad (4.3)$$

In these equations, V_{link} is the shear force in the link (taken as $V_{ult} = 1.5 V_p$), L_{beam} is the length of the beam segment outside of the link and α is the angle between the beam and the brace.

Using the second method, the axial forces in the brace and beam generated by a link shear of V_{ult} of 96 kips were computed as $P_{brace} = 138$ kips, and $P_{beam} = 92$ kips.

● **Moment in Brace and Beam.**

The maximum moment generated at the end of a fully yielded and strain hardened link is computed from static equilibrium, as follows:

$$M_{link} = \frac{e V_{link}}{2} \quad (4.4)$$

This moment must be resisted by the beam segment outside the link, and by the brace. Assuming that the beam and the brace are designed to remain essentially elastic, the distribution of link end moment to the beam and brace can be estimated by one of the following methods:

- a) Compute the ratios M_{beam}/M_{link} and M_{brace}/M_{link} from an elastic frame analysis and use these ratios to compute M_{beam} and M_{brace} for a link moment equal to M_{ult} .
- b) Use approximate formulas for M_{beam} and M_{brace} based on simplified elastic analysis of the beam and brace. These approximate formulas (Engelhardt, 1987) are:

$$M_{beam} = \frac{(I_{beam} / L_{beam})}{(I_{beam} / L_{beam}) + (I_{brace} / L_{brace})} M_{link} \quad (4.5)$$

$$M_{brace} = \frac{(I_{brace} / L_{brace})}{(I_{beam} / L_{beam}) + (I_{brace} / L_{brace})} M_{link} \quad (4.6)$$

In these equations, I is the moment of inertia, L is the length of the member considered, and M_{link} is the link end moment (taken as $M_{ult} = e V_{ult}/2$)

For the W12x30 link, with $e = 15$ in. and $V_{ult} = 96$ kips, the ultimate link end moment is $M_{ult} = 720$ k-in. M_{beam} and M_{brace} were estimated using the approximate formulas, and were found equal to 700 k-in and 20 k-in respectively.

The brace and the beam are under combined moment and axial load. The strength check for these members was performed following the equation H1-1 of LRFD specifications taking the effective length factor (K) equal to one for the brace and to 0.7 for the beam. The moment amplification factor (B_2) was set equal to one for both members. Both members were found to satisfy the LRFD equation H1-1. Note that the effective length KL, was taken assuming the brace was simply supported, and the beam was fixed at its ends. Smaller values of KL can however, be used. The brace connections provide some rotational restraint, resulting in lower K values. Also, the beam can be provided with intermediate lateral support reducing the unbraced length.

- **Strengthened Columns.**

A C7x14.75 channel made of A36 steel is attached on each side of the existing columns using epoxy grouted dowels. The main purpose of these channels is to act as vertical collectors for the load transferred by the added EBF members to the existing frame. The channel section was selected based on the following two criteria:

- a) The channel should resist the maximum force that can be transmitted by the braces to the columns. For this type of EBF configuration, the maximum axial force transferred to the columns is equal to $1.5 V_p$.
- b) The channel need to be deep enough to allow for the attachment of the added steel beams.

4.3.3.4 Modeling of the Retrofitted Structure. The columns in the braced bays were attached to the vertical steel collectors using epoxy grouted dowels. In flexure, full composite action is considered between the reinforced concrete columns and the vertical collectors. The shape of the moment rotation diagram used for these columns is shown in Figure 4.4 and Table 4.4 gives the moment and end rotation at yield and ultimate for these strengthened columns. The added steel beams were connected to the existing reinforced

concrete frame at the beam-column joint and at the link ends only. The steel beam and the link were considered to deform independently of the reinforced concrete beam.

In an experimental study conducted on a similar reinforced concrete frame retrofitted with steel concentrically braced frame, Bush (1987) showed that the addition of steel channels increased the shear strength of the existing columns. This increase was however difficult to quantify. For the purposes of this study, an estimate of the shear strength of the strengthened columns was taken as the sum of the reinforced concrete column shear strength and the channel's shear strength.

The links were modeled using the shear link element. The beams and braces were modeled using the beam column element. The braces were designed to remain elastic under the fully strain hardened shear links and were not expected to yield or buckle.

4.3.4 Static Elastic Analysis. A static elastic analysis was conducted on the original and the retrofitted frames. The purpose of this analysis was to compare the initial stiffness, the distribution of the lateral load, and the period of both structures during the elastic response phase.

To evaluate the elastic stiffness of the structure, a lateral load was applied at the floor level. Two analyses were conducted. In the first analysis, the load was applied at the second floor only and in the second analysis, the load was applied at the first floor only (Fig. 4.8). The stiffness coefficients of the structures were computed as the ratio of the load over displacement. The EBF strengthening scheme was found to increase the stiffness of the existing structure by a factor of about four (Table 4.5). The increase in stiffness was accomplished with little increase in the mass of the structure since the weight of the added steel members is negligible compared to the weight of the concrete members.

An additional static elastic analysis was performed on both structures by applying a triangularly distributed lateral load. A lateral force of 40 kips was applied at the second level, and a lateral force of 20 kips was applied at the first level. Table 4.6 gives the forces acting on the columns for the original reinforced concrete frame and the retrofitted frame. This table shows that the added EBF reduced the shear acting on the first level columns by a factor of more than two. This indicates that more than half the base shear acting on the retrofit frame is resisted by the added braces and the demand on the reinforced concrete columns is reduced.

The first and second periods of vibration of both structures was also evaluated. To compute the periods, transnational masses were lumped at the nodes. These lumped masses were based on the tributary area of the floor slab of the original building (Bush, 1987) from which the simple two-story, one bay frame was derived. The period of the strengthened frame decreased from 0.40s to 0.19s reflecting the gain in the structure's stiffness. The acceleration response spectra for El Centro and Parkfield (Fig. 4.2a) show that this decrease in period of vibration may result in an increase in the seismic force demand on the retrofitted structure. Hence, under these records, the base shear acting on the retrofitted frame may be higher than the one acting on the original frame. This increase in demand may or may not impose higher demands on the reinforced concrete columns since the base shear is also resisted by the added EBF as shown above.

4.3.5. Static Inelastic Analysis. The purpose of the static inelastic analysis was to estimate the strength, ductility, and sequence of inelastic events in the frames. The analysis was conducted by applying static incremental load at the roof level. Figure 4.9 shows the relationship between the roof displacement and the base shear. This figure indicates that the retrofit scheme provided an increase in strength, stiffness and ductility. The original structure experienced column shear failure at a roof drift ratio of about 0.6% corresponding to a base shear of a 100 kips or 0.28 W, where W is the building weight. This mode of failure is expected to be brittle and is assumed to define the failure of the frame.

The retrofitted structure behaved elastically until the link at the first level yielded at a drift ratio of about 0.13%. Further decrease in the stiffness of the structure occurred at a roof drift ratio level of about 0.5%, upon yielding of the second level link. At a drift ratio of 1%, the inelastic rotation capacity of the link at the first level was reached. This was assumed to define failure of the retrofitted frame. The maximum lateral load capacity of the retrofitted frame was equal to 255 kips and represented 0.70 W. Overall, based on the static analysis, the retrofitted frame had approximately four times the initial elastic stiffness, 2.5 times the ultimate strength, and 1.7 times the deformation capacity of the original frame.

4.3.6 Dynamic Analysis. A nonlinear dynamic analysis was conducted to evaluate the response of the original reinforced concrete frame and the retrofitted frame subjected to earthquake loading. The El Centro and the Parkfield acceleration records were used for this analysis. Both of these records were on firm soil. The Parkfield record had a strong acceleration pulse as indicated by Figure 4.1c.

Figure 4.10 and Figure 4.11 show the base shear acting on the original and retrofitted frames under the El Centro and Parkfield records respectively. These figures indicate an increase in base shear for both records. The increase is on the order of 30% for El Centro and 60% for Parkfield.

The nonlinear dynamic analysis showed that the retrofitting scheme reduced building deflections. The roof drift (Fig. 4.12 and 4.13) of the original structure reached a maximum value of about 3.6 in. (drift ratio of 1.5%) for El Centro and 4.8 in. (drift ratio of 2%) for the Parkfield acceleration record. The roof drift of the retrofitted structure was kept below 0.6 in. (0.25% drift ratio) and 1.2 in. (0.5% drift ratio) respectively.

Figure 4.14 and Figure 4.15 show the shear in the first story columns of the original and retrofitted frames for the El Centro and Parkfield records. The column shear in the original frame was in excess of the shear strength of the columns. The dynamic analysis

predicts a column shear failure in the original frame. The shear in the columns of the retrofitted frame was about the same level as the shear acting on the columns of the original frame, but the added vertical collectors are assumed to provide sufficient shear strength. The high column shear for the retrofit structure, despite the low drift, is due to the increased stiffness of the retrofitted columns. In the analytical model a full flexural interaction was considered between the reinforced concrete column and the added vertical collectors.

4.3.7 Concluding Remarks. A small reinforced concrete frame that was not adequately designed to sustain earthquake loading was retrofitted using a steel eccentrically braced frame (EBF) to provide a preliminary assessment of the feasibility of the EBF as a retrofit scheme. The retrofit scheme and the original frame were analyzed under static and dynamic loading. The addition of the EBF was found to provide sufficient increase in strength and stiffness to permit the retrofitted frame to survive the selected earthquake records. The retrofit also dramatically reduced the drift of the structure. The static analysis showed that the added EBF provided a level of ductility to the structure, while the original frame failed in a brittle manner. A simple measure of ductility (Fig. 4.9) can be taken as the ratio of the inelastic drift (i.e maximum drift minus drift at yield) over the drift at yield. The EBF was not successful, however in reducing the maximum shear forces developed in the columns under earthquake loading. Although the EBF resisted a large portion of the base shear, the stiffening effect of the EBF caused a substantial increase in base shear under dynamic loading.

Table 4.1 Essential Data for The Selected Earthquake Records

Earthquake Date Station	Comp.	Richter Magn.	Epicentral Distance (km)	Peak Acc. (g)	Site Description
Imperial Valley, Ca. ¹ April 1940 El Centro	N00E	6.7	11.5	.35	Alluvium
Loma Prieta October 1989 Corralitos	N00E	7.1	7	.64	Landslide Deposit
Parkfield June 1966 Cholame, Array 5	N65E	5.6	56.1	.49	Alluvium
Loma Prieta October 1989 Oakland Harbor Wharf	N35E	7.0	95	.29	Bay Mud
Mexico September 1985 Mexico City SCT-1	N90E	8.1	400	.16	Deep Alluvial Lake Deposit

(1) The El Centro acceleration record was scaled to a peak acceleration of .5g

Table 4.2 Moment and Curvature for the Columns and Beams at Yield and Ultimate

	M_y (k-in)	ϕ_y (1/in.)	M_u (k-in)	ϕ_u (1/in.)
Columns	2780	.025 10^{-2}	3100	.620 10^{-2}
Spandrel Beams	11,830	.007 10^{-2}	13,220	.170 10^{-2}

Table 4.3 Moment-Rotation Diagram and Stiffness Properties for The Columns and Beams

	M_y (k-in)	θ_y (rad)	M_u (k-in)	θ_u (rad)
Columns	2780	5.25 10^{-3}	3100	30.05 10^{-2}
Beams	11,830	4.41 10^{-3}	13,220	15.46 10^{-2}

Table 4.4 Properties of the Retrofitted Column

	M_y (k-in)	ϕ_y (1/in.)	θ_y (rad.)	M_u (k-in)	ϕ_u (1/in.)	θ_u (rad.)
Retrofitted Column	3106	$0.108 \cdot 10^{-3}$	$2.29 \cdot 10^{-3}$	7051	$0.977 \cdot 10^{-2}$	$13.75 \cdot 10^{-3}$

Table 4.5 Stiffness of the Original and Retrofitted Frame

	$K_{11} = \frac{F_1}{\Delta_{11}}$ (k/in.)	$K_{12} = \frac{F_2}{\Delta_{12}}$ (k/in.)	$K_{22} = \frac{F_2}{\Delta_{22}}$ (k/in.)
Original Structure	188.7 k/in.	151.5	95.6
Retrofitted Structure	901.1	714.3	357.1

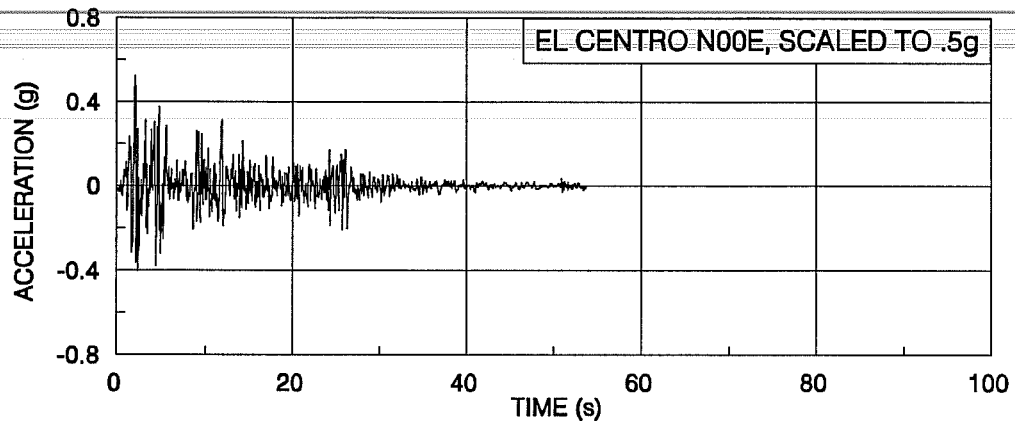
where (Fig. 4.8): F_1 = Lateral load at level 1, F_2 = Lateral force at level 2
 Δ_{12} = Lateral displacement at level 1 due to F_2
 Δ_{22} = Lateral displacement at level 2 due to F_2
 Δ_{11} = Lateral displacement at level 1 due to F_1

Table 4.6 Forces in the First Level Columns of Both Structures

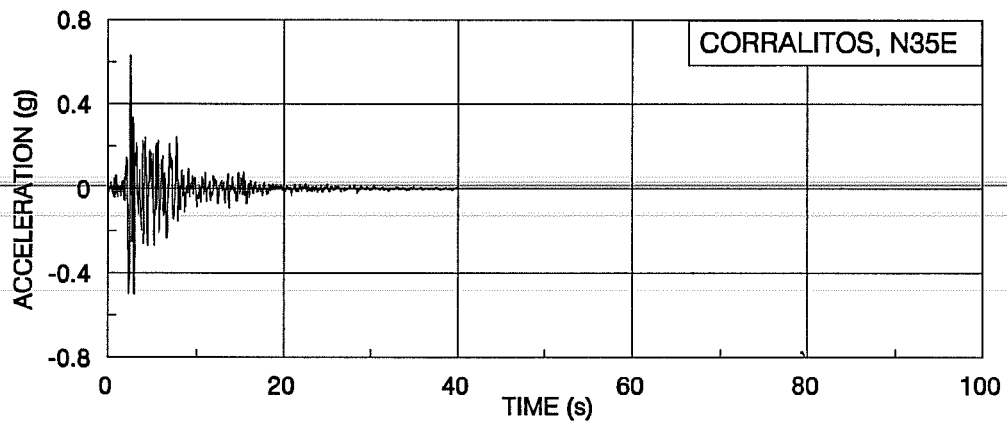
	1st Level Column		2nd Level Column	
	V (k)	M (k-in)	V (k)	M (k-in)
Original Structure	30.0	1568	20.0	692
Retrofitted Structure	13.4	760	4.2	380

Table 4.7 Period of Vibration of the Original and retrofit Frames

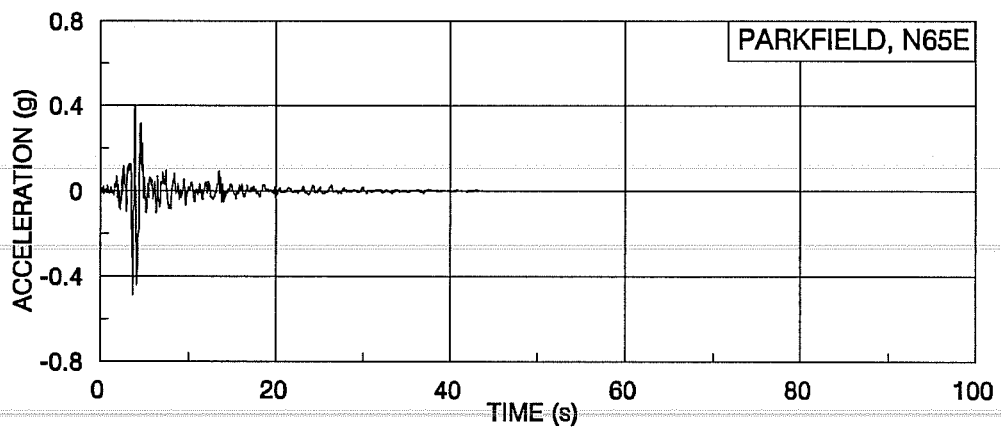
	Period (s)	
	1st Mode	2nd Mode
Original Structure	0.40	0.13
Retrofitted Structure	0.19	0.07



(a) N00E Component of the 1940 El Centro, Scaled to 0.5g

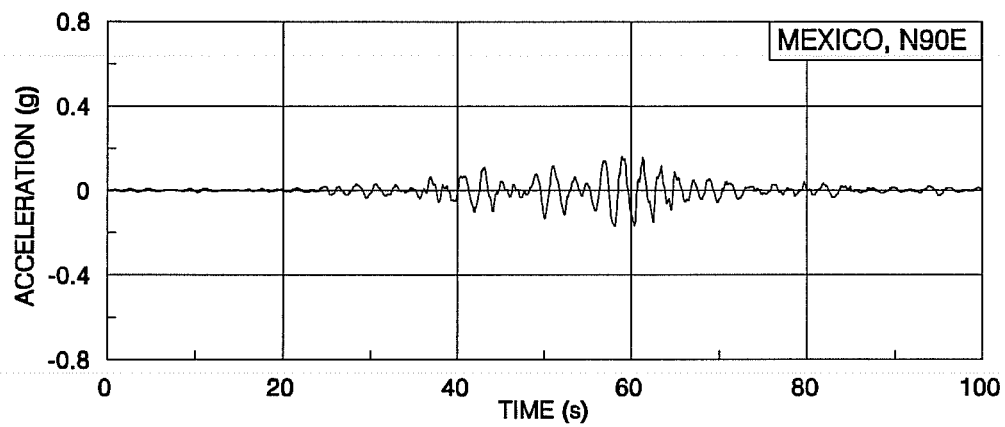


(b) N35E Component of the Corralitos Record

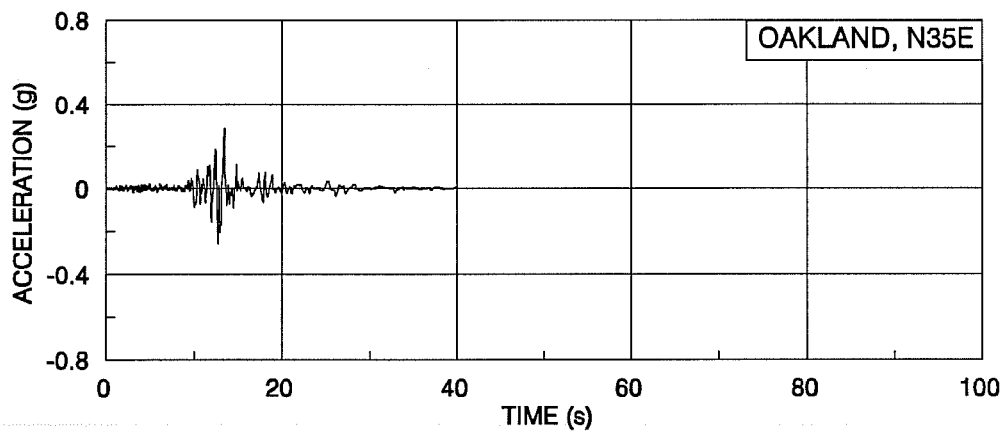


(c) N65E Component of the Parkfield Record

Figure 4.1 Time History for the Selected Earthquake Records

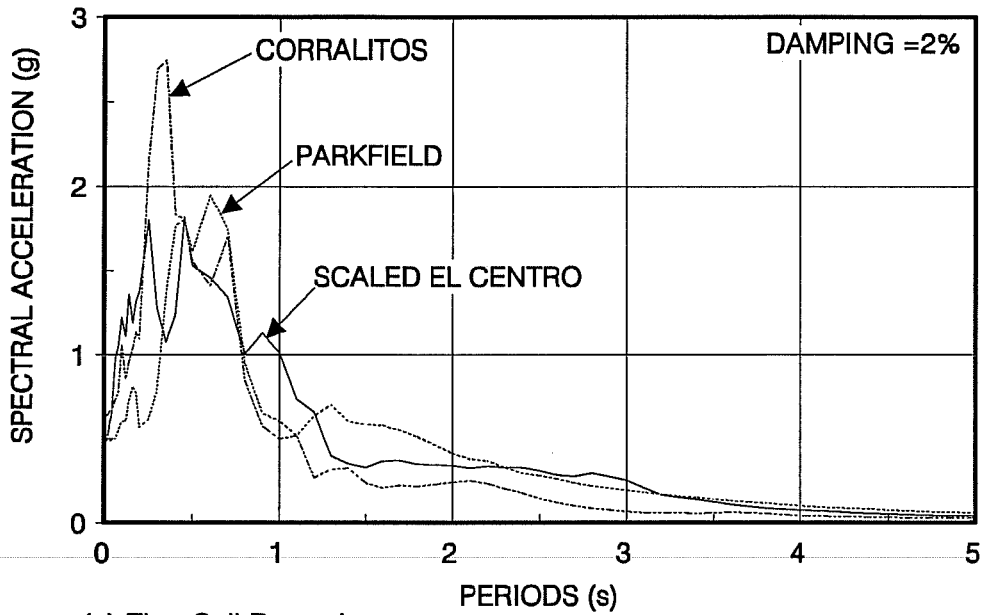


(d) N00E Component of the 1940 El Centro, Scaled to 0.5g

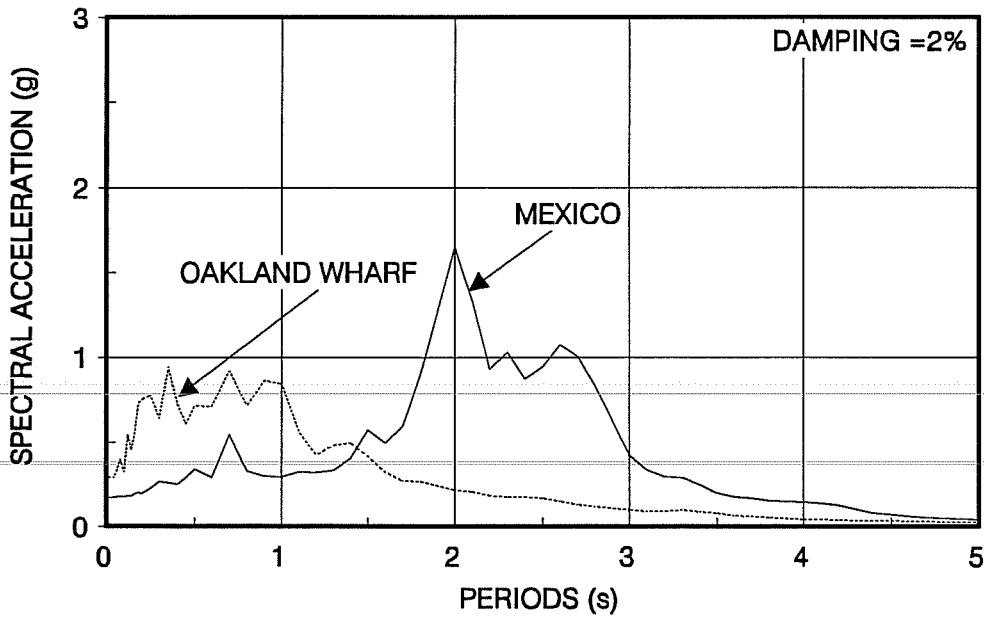


(e) N00E Component of the 1940 El Centro, Scaled to 0.5g

Figure 4.1 (Cont'd) Time History for the Selected Earthquake Records

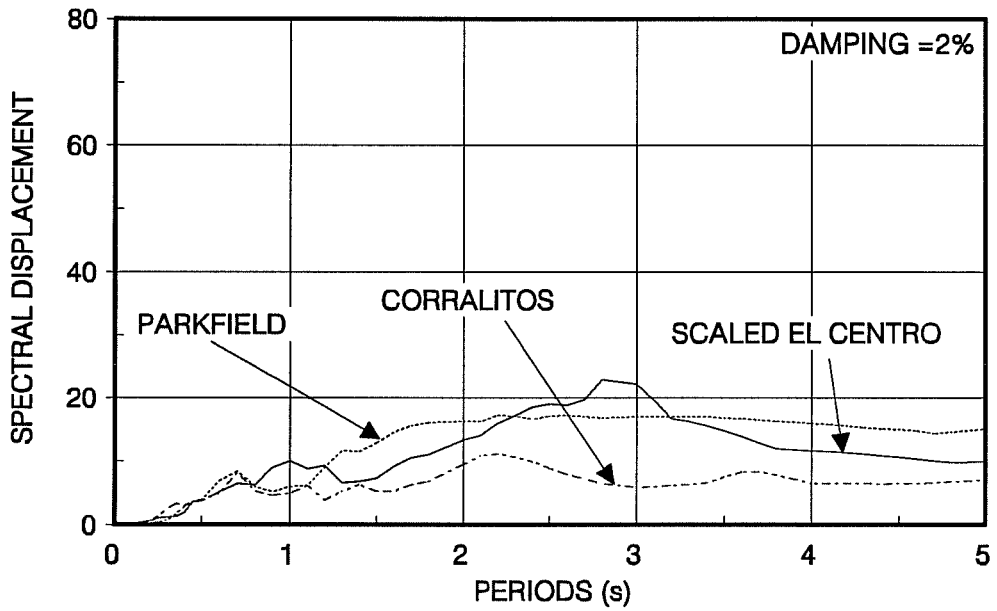


(a) Firm Soil Records

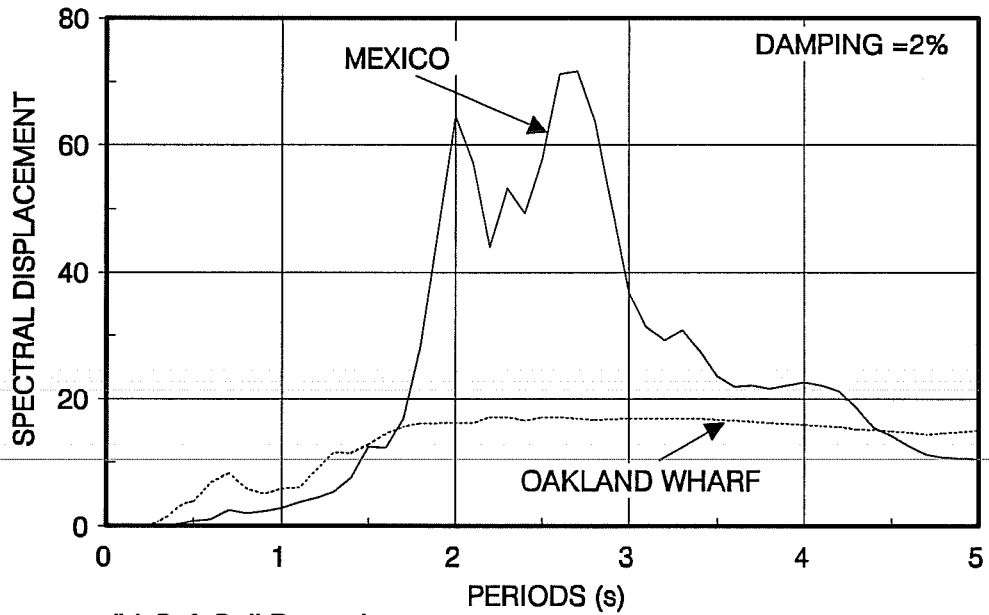


(b) Soft Soil Records

Figure 4.2 Elastic Spectral Acceleration for the Selected Earthquake Records



(a) Firm Soil Records



(b) Soft Soil Records

Figure 4.3 Elastic Spectral Displacement for the Selected Earthquake Records

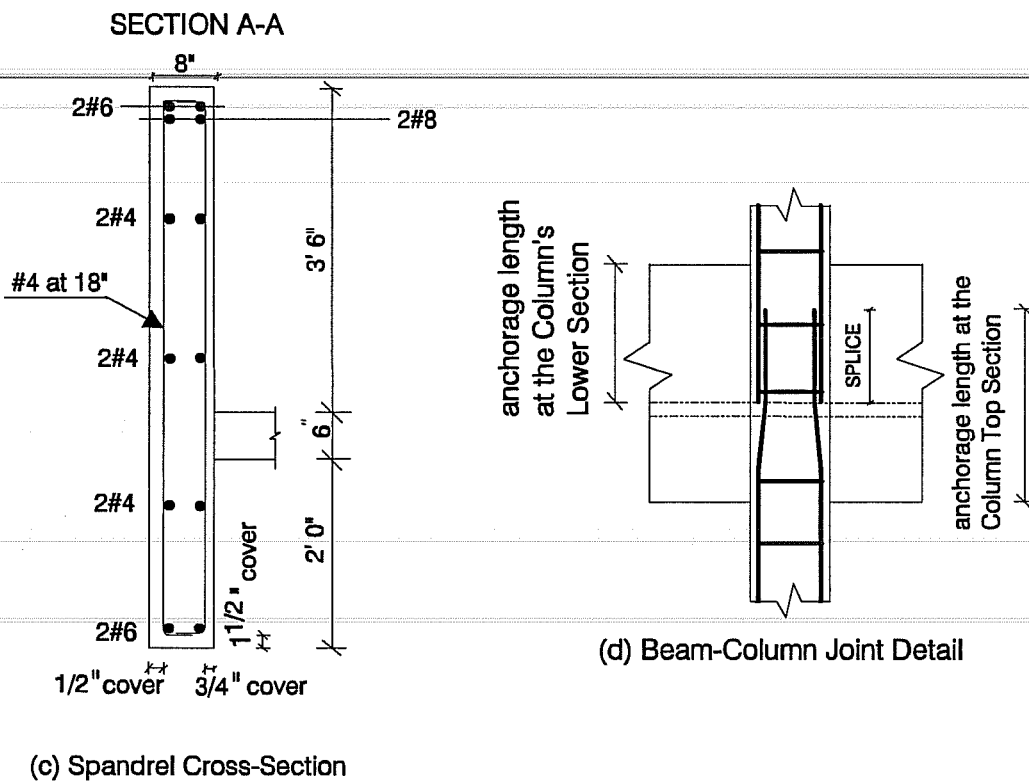
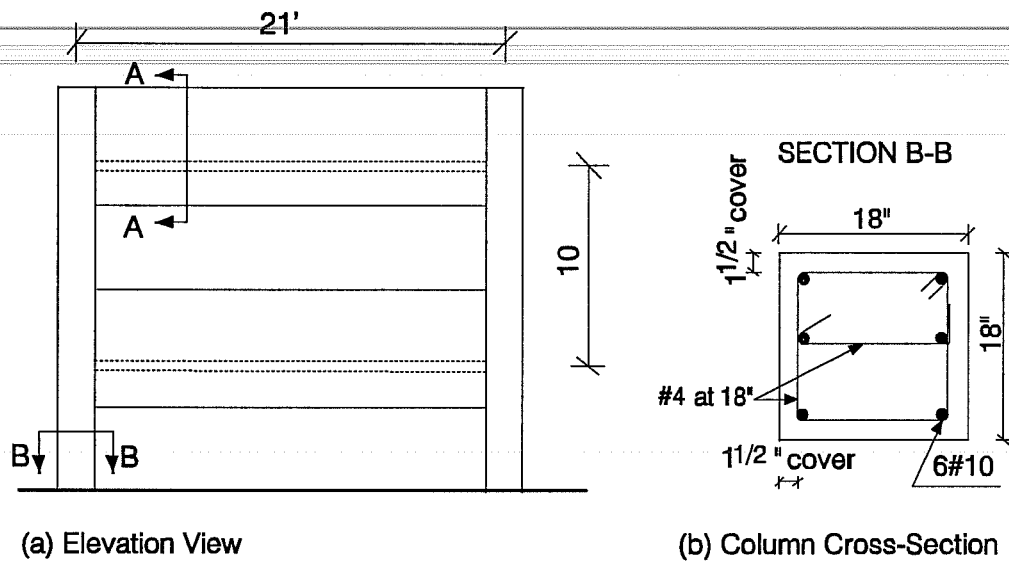


Figure 4.4 Configuration of the Two-Story, One-Bay Frame

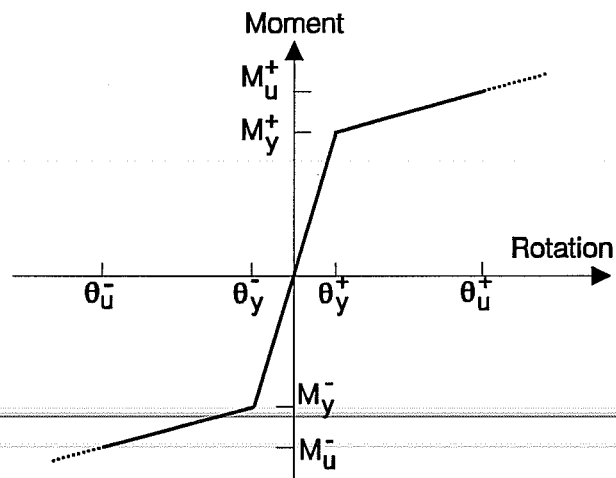
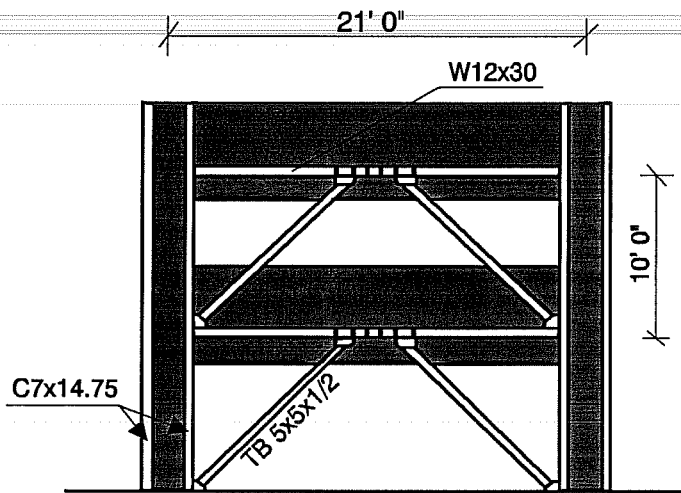
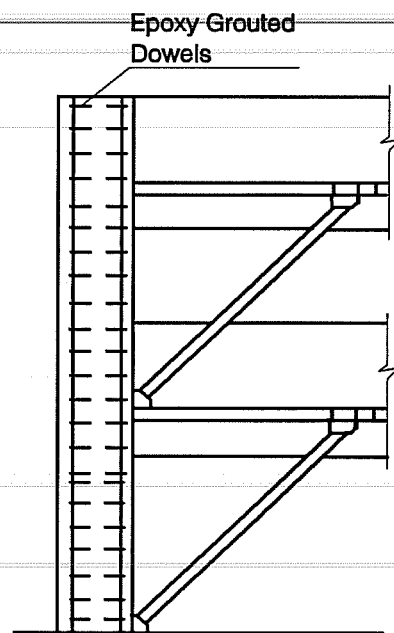


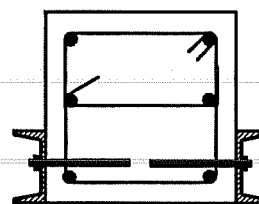
Figure 4.5 Shape of the Moment-Rotation Envelope for the Columns and Spandrel Beams of the Two-Story Frame



(a) Elevation View



(b) Attachment to Column
Elevation View



(c) Attachment to Column
Cross Section

Figure 4.6 Configuration of the Retrofitted Frame

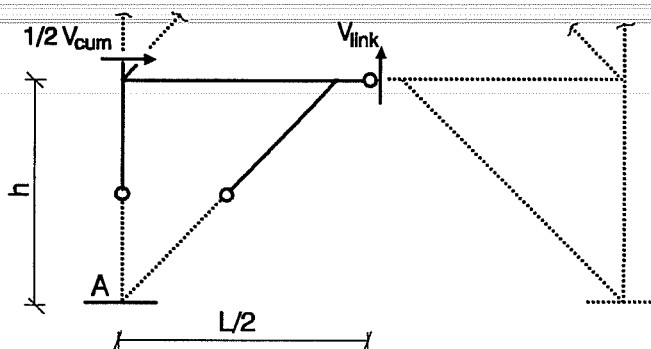


Figure 4.7 Simplified Free Body Diagram Used to Evaluate Link Shear Force (Adapted from Popov and Engelhardt, 1988)

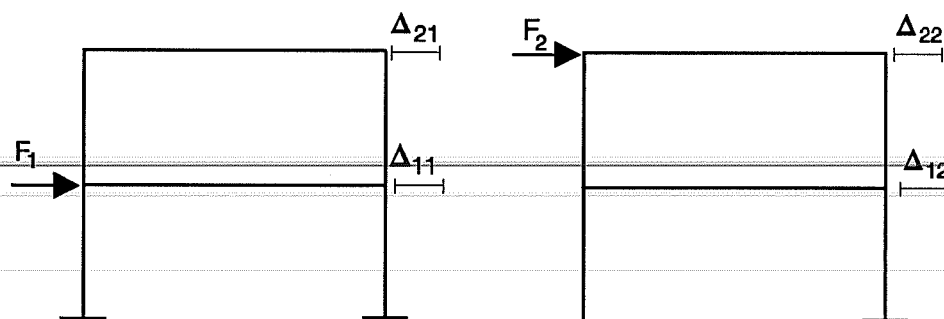


Figure 4.8 Force Application and Corresponding Displacement for the Static Analysis

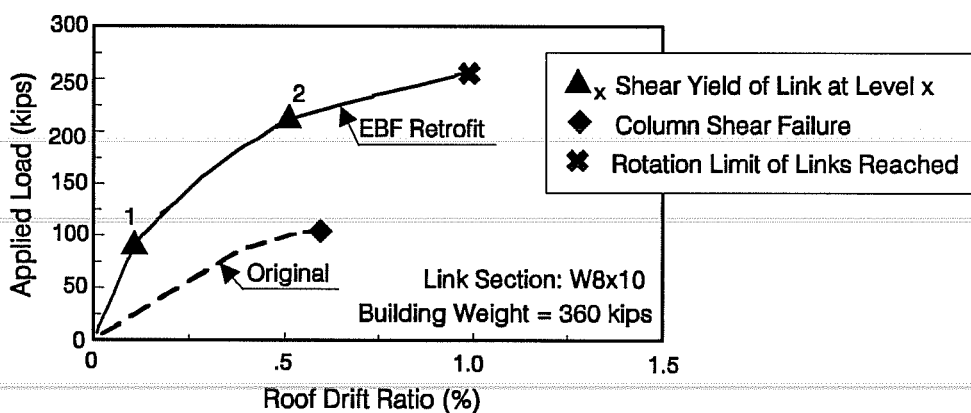
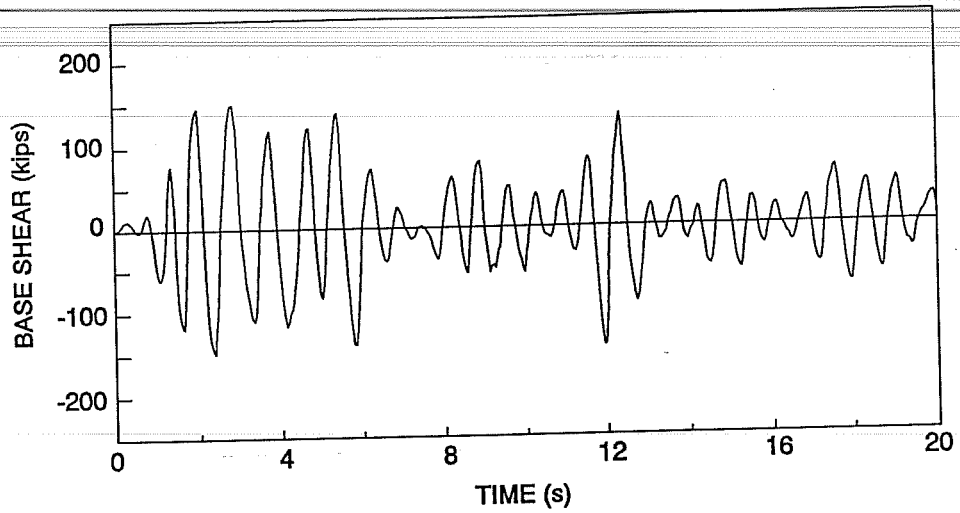
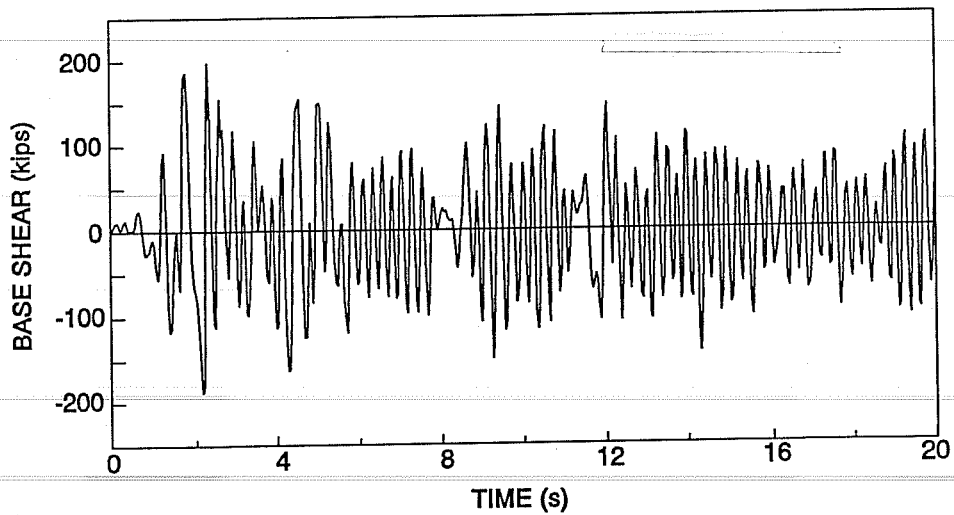


Figure 4.9 Roof Drift Ratio for the Original and Retrofitted Frame Subjected to Static Load

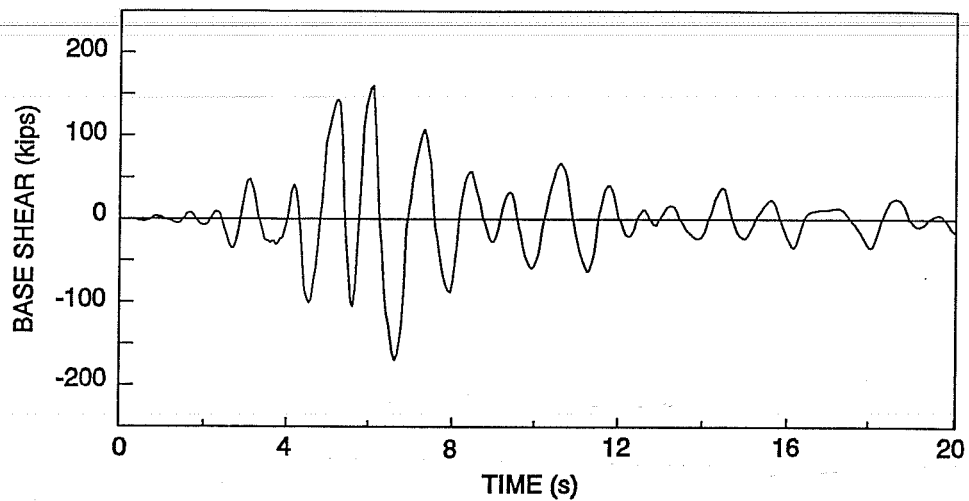


(a) Original Frame

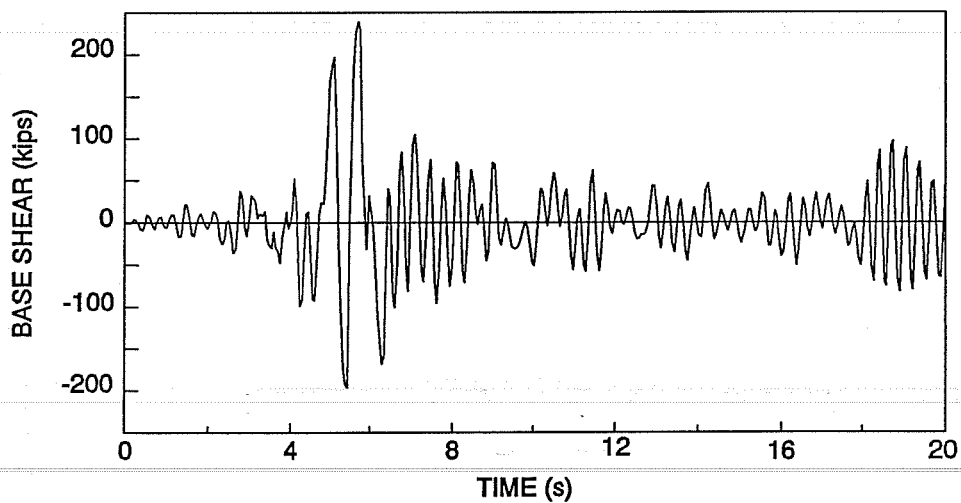


(b) Retrofitted Frame

Figure 4.10 Base Shear of The Original and Retrofitted Two Story, One Bay Frame Subject to the Scaled El Centro Record

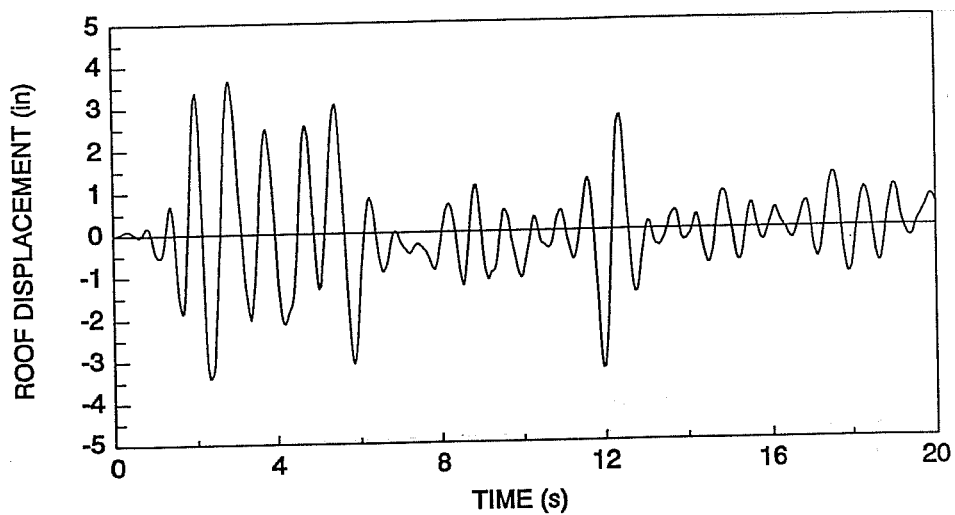


(a) Original Frame

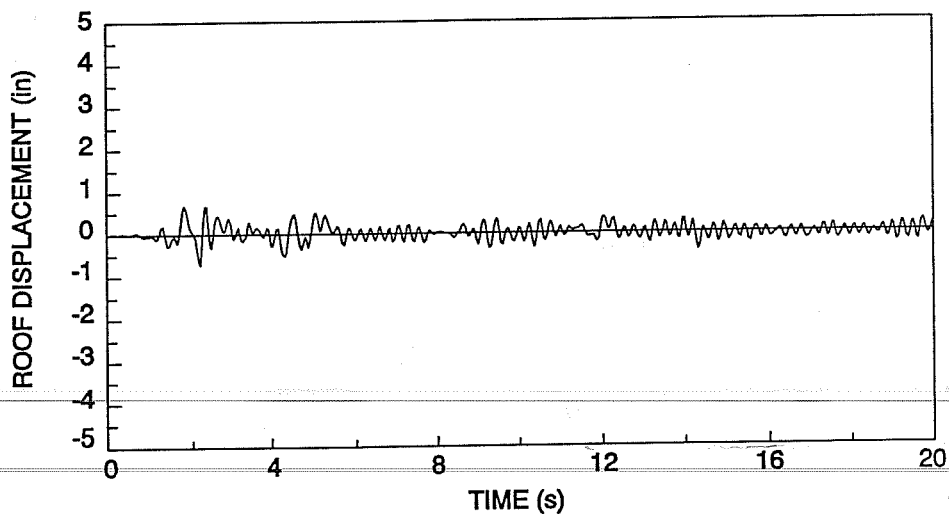


(b) Retrofitted Frame

Figure 4.11 Base Shear of The Original and Retrofitted Two Story, One Bay Frame Subject to The Parkfield Record

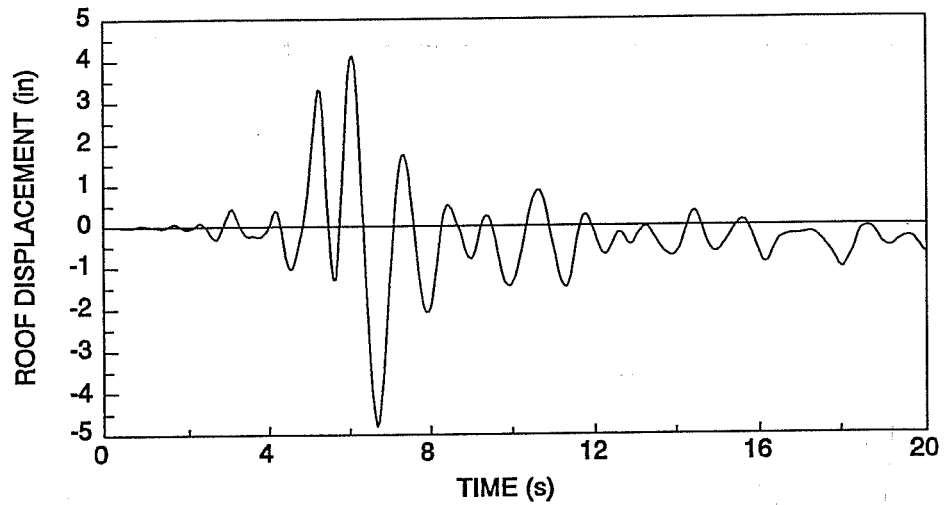


(a) Original Frame

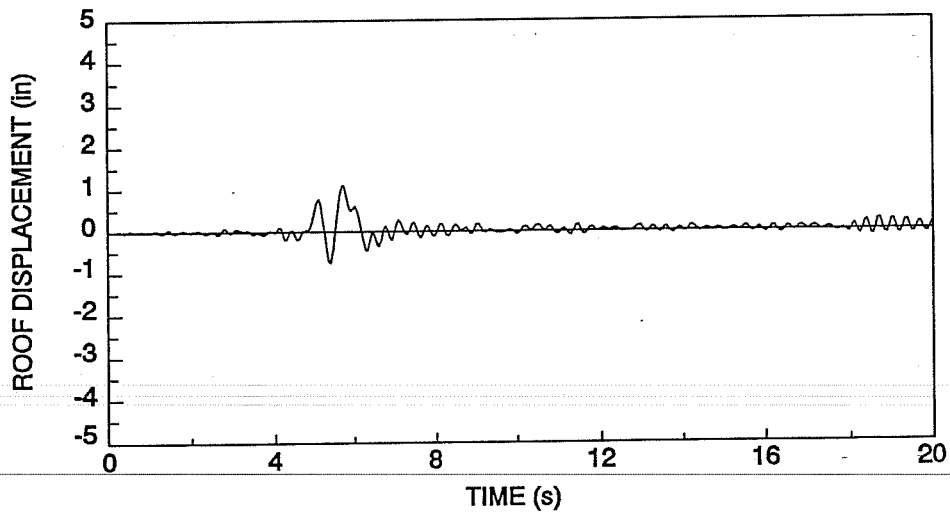


(b) Retrofitted Frame

Figure 4.12 Roof Displacement of The Original and Retrofitted Two Story, One Bay Frame Subjected to the Scaled El Centro Record

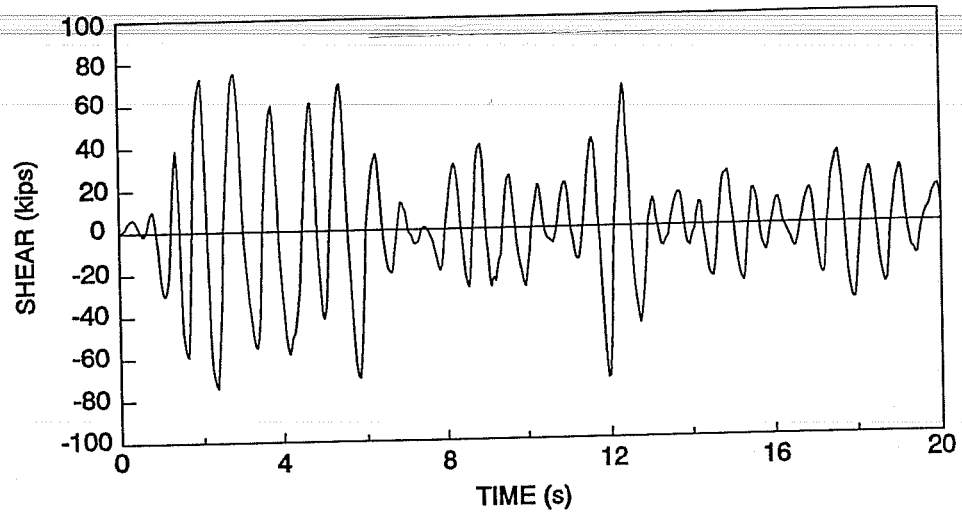


(a) Original Frame

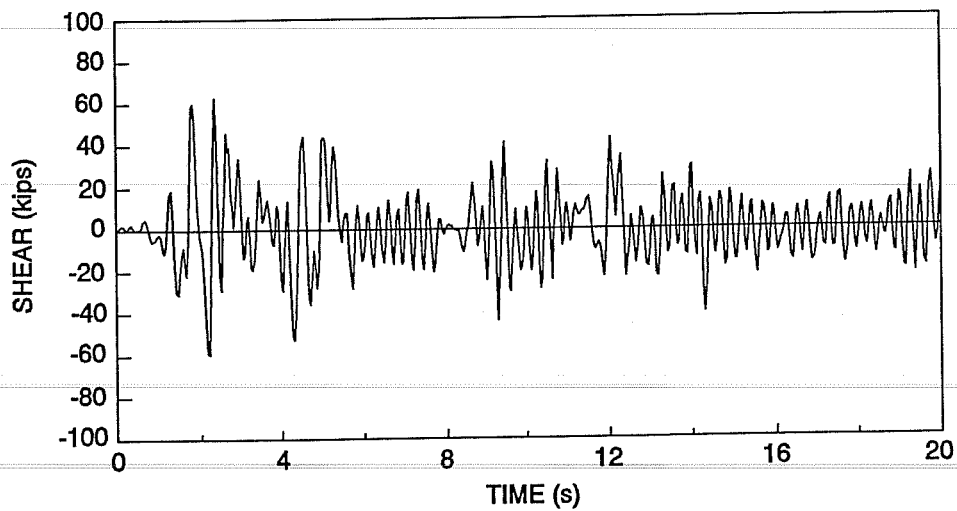


(b) Retrofitted Frame

Figure 4.13 Roof Displacement of The Original and Retrofitted Two Story, One Bay Frame Subjected to the Parkfield Record

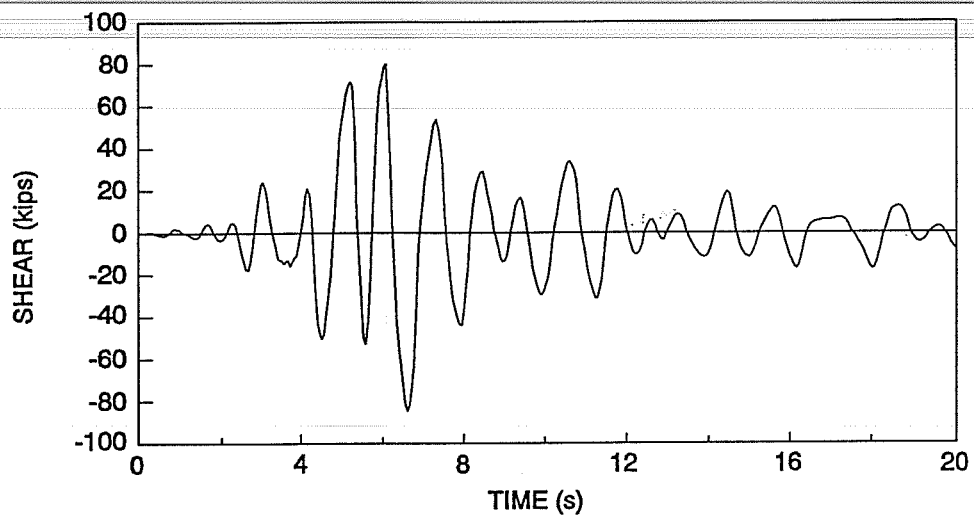


(a) Original Frame

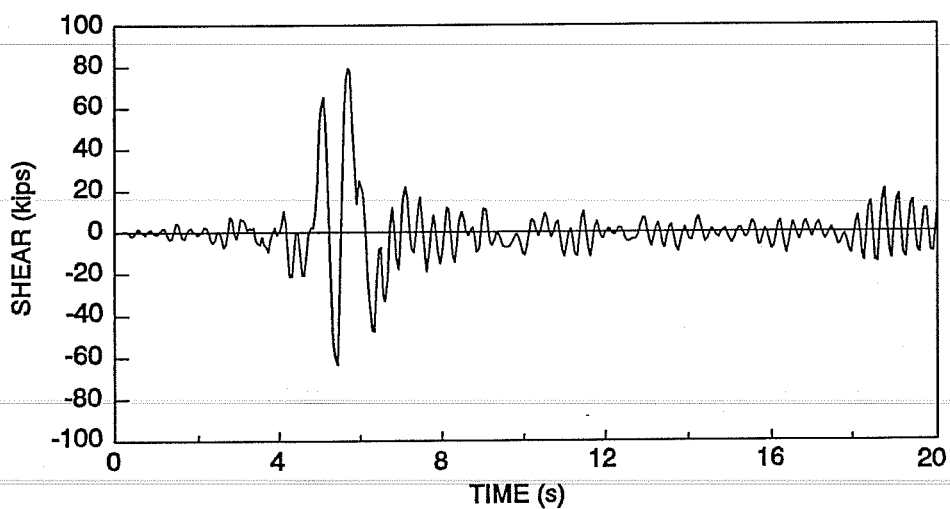


(b) Retrofitted Frame

Figure 4.14 First Floor Column Shear for The Original and Retrofitted Two Story, One Bay Frame Subjected to the Scaled El Centro Record



(a) Original Frame



(b) Retrofitted Frame

Figure 4.15 First Floor Column Shear for The Original and Retrofitted Two Story, One Bay Frame Subjected to the Parkfield Record

CHAPTER 5: THREE-STORY BUILDING

5.1 General.

The first building considered for this study is a three-story reinforced concrete structure (Fig. 5.1) representative of the US west coast low rise construction of the 1950s and 1960s. The lateral load resisting system consists of ordinary reinforced concrete moment frames in both directions. The building has three bays in the transverse direction and five bays in the longitudinal direction. The columns are 18 in. by 18 in., the beams are 14 in. wide and 20 in. deep, and the slab thickness is 7in. Normal weight concrete with a specified compressive strength of 3000 psi was used and all reinforcing steel was Grade 60. Only the behavior in the longitudinal direction was analyzed in this study.

5.2 Structural Details.

The seismic forces used in the design of this structure were based on the 1964 edition of the UBC. The detailing and design of the reinforced concrete members followed the recommendations of the 1963 edition of the ACI 318 code. Because of the low lateral force requirements of the 1964 UBC, gravity loads governed the structure design. The building was provided with low lateral strength and poor detailing by today's standards. Figure 5.2 and Figure 5.3 show the reinforcing details of the columns and beams respectively. The beam to column connection detail is shown in Figure 5.4. The main structural details of the structure are as follow:

- **Columns Splice.** Since the design was controlled by the gravity loads, tension was not expected in the columns. The columns were therefore, provided with a compression lap splice of 24 bar diameter (d_b) only in accordance with the recommendations of ACI 318-63 code. The splice was located just above the slab level (Fig. 5.4). According to the current recommendations of ACI 318, the splice length required to develop the full capacity

of the reinforcing bars used for these columns is equal to $33 d_b$. The short lap splice limits the flexural capacity at the base of the columns. Spalling of concrete and early hinging of the column base is expected. Based on Orangun's equation (Eq. 3.9) (Orangun et al., 1977), splice failure was estimated to occur when the steel stress in the longitudinal reinforcement reaches 55 ksi for the columns of the internal frames and about 60 ksi for the columns of the external frame. The anchorage provided at the top section of the columns appeared satisfactory. As shown by Figure 5.4, longitudinal steel anchorage started at the top of the slab and extended 24 bar diameter above the slab level. The extra length of longitudinal bars provided within the beam depth resulted in a sufficient development length for the top sections of the columns.

● **Confining Reinforcement.** The potential hinging areas of the columns were not well confined. The transverse reinforcement was widely spaced since it was provided only to resist the shear due to the low design forces. Under current provisions (ACI 318-89) for confinement, three #3 bars spaced at 3.5 in. are required for the column potential hinging area. For this building, the external frame columns are provided with three #3 bars spaced at 12 in. and the internal frame columns are provided with three #3 bars spaced at 14 in. The poor concrete confinement limits the rotational capacity of the columns and the columns may not be able to sustain large deformations or repeated cyclic load reversals.

● **Anchorage of Beam Bottom Reinforcement.** Since the design was controlled by gravity loading, positive bending was not expected at the beam end sections. The bottom longitudinal bars in the beams were embedded only 6 in. into the joint, in accordance with the minimum requirements of the ACI 318-63 code. As a result the beams had very limited positive moment capacity at the joint. Earthquake loads are expected to induce moment reversal and cause premature pull out of the bottom reinforcement in the beams. Calculations based on Orangun's equations (Orangun et al., 1977) showed that pullout of the bottom longitudinal reinforcement in the beams would occur when the steel stress reaches 23 ksi for the beams of the internal frames and 20 ksi for the beams of the external frames.

● **Shear Reinforcement.** Although the shear reinforcement in the beams and columns was low and widely spaced, it was sufficient to develop the flexural capacity of these members. Shear failure of the structural members was therefore, not anticipated. The shear capacity, ΦV_n , of the first level columns estimated using ACI equations was found equal to 50 kips for the external frames and to 47 kips for the internal frames. While the shear strength required for the development of column flexural hinging, assuming equal end moments, was found equal to 30 kips and 45 kips respectively. Similar observations were made for the columns of the upper floors. The shear strength of the beams was estimated equal to 46 kips for the external frames and to 64 kips for the internal frames. The shear strength required for the development of flexural hinges in the beams was found equal to 18 kips and 28 kips respectively.

5.3 Analytical Modeling.

The beams and columns of the three-story building were modeled using the reinforced concrete element of DRAIN-2D. Anchorage failure was simulated and the moment at splice failure was computed based on Orangun's equation (Orangun et al., 1977). The moment rotation envelopes were derived from the moment curvature diagrams of the sections. More details on the modeling procedure are given in Section 4.3.2.

5.3.1 Modeling of the Columns. The moment curvature diagrams of the columns were computed assuming the columns are subject to an axial load level corresponding to the effect of gravity loading. Figures 5.5 shows the shape of the moment rotation diagram at the base and at the top of the columns. At the top of the columns, the longitudinal steel was properly anchored and the ultimate moment can be developed. A bi-linear envelope for the moment rotation was assumed. At the base, the moment capacity was limited by splice failure which was predicted to occur just before yielding. Splice failure is followed by strength and stiffness degradation. Very limited information is currently available on the modeling of strength degradation rate following splice failure. In this study, an ongoing experimental

research project (Aboutaha and Engelhardt, 1994) provided a basis for estimating the slope of the descending branch. Table 5.1 and Table 5.2 provide the numerical values for the moment rotation diagram of the columns of the internal and external frames.

5.3.2 Modeling of the Beams. Figure 5.6 shows the shape of the moment rotation relationship assumed for the beams. The top reinforcement at the beam end had sufficient anchorage length. Therefore in negative bending, the section was assumed to develop yielding and strain hardening. The positive flexural capacity of the beams at the joint was however, limited by bar pullout. Bond failure in the beams was found to occur at a relatively low stress level. In positive bending, the beams were assumed to behave elastically until cracking. Further loading leads to splice failure and strength degradation. Similarly to reinforced concrete columns, limited information is available for the modeling of the post splice failure behavior of beams subjected to cyclic load. Tests conducted on similar beams by Pessiki et al. (1990) provided a basis for the modeling adopted here. Table 5.3 and Table 5.4 provide the values used to define the moment-rotation envelopes for the beams of the internal and external frames.

5.4 Static Inelastic Analysis of Original Building.

A static inelastic analysis was conducted to estimate the lateral stiffness and strength of the structure. For this analysis, a static incremental lateral load, applied at the floor levels and uniformly distributed with height, was applied to the structure. Note that gravity loading was applied prior to lateral load.

Figure 5.7 shows the relationship between the base shear coefficient and the maximum interstory drift which was found to occur at the first level. The base shear coefficient is defined as the total base shear (i.e. the lateral load) divided by the weight of the building. The figure indicates that the building has high flexibility, low lateral strength, and a low level of ductility.

The building behavior was essentially elastic until anchorage failure of the bottom reinforcement in the beams at a lateral drift ratio of about 0.45%, corresponding to a lateral load of 0.12 W; W being the weight of the building. Continued loading caused a splice failure in some columns of the first floor at a drift ratio of about 0.6% and at a lateral load of about 0.15 W. This was followed by a significant decrease in lateral stiffness. At 0.75% interstory drift, corresponding to a load of 0.16 W, all columns of the first floor experienced a splice failure resulting in a rapid degradation in strength and stiffness. This event can be considered as defining the maximum deformation capacity of the building. Note that after the drift ratio of 0.75%, the analytical solution became unstable, indicating strength degradation or excessive deformation. Strength degradation will result in a negative pivot in the global structural matrix. The analytical solution in DRAIN-2D diverges if a negative pivot is present in the structure's stiffness matrix, or if the deformations reach high values.

Figure 5.7 shows also the yield strength required by the ATC 22 recommendations. The building was considered as an ordinary moment-resisting frame (OMRF) resting on firm soil. The minimum strength required by ATC 22 exceeds the yield strength of the three-story building by a factor of approximately 2.5. Thus, according to ATC 22, the building has a low lateral strength and cannot survive the expected seismic load. Further discussions on the application of ATC 22 recommendations are presented in Chapter 7.

5.5 Dynamic Analysis of the Original Building.

A dynamic analysis under the effect of the earthquake records listed in Section 4.2 was conducted. For this analysis the floor mass was assumed lumped at the nodes, the viscous damping was taken as 2% of critical, and the floor diaphragm was assumed rigid. Gravity loading was applied prior to earthquake load. The fundamental period of vibration was found equal to 1.05s. This long period for a three-story building reflects the large flexibility of the structure.

Figure 5.8 shows the maximum interstory drifts for the structure subjected to the different earthquake acceleration records. In general, the records on soft soil caused higher drifts. Interstory drifts in excess of 3% were predicted for both Oakland and Mexico earthquake records. Such large drifts can cause extensive damage and may lead to the collapse of the structure.

The firm soil records also subjected the building to high drifts, causing severe damage. Maximum interstory drift for the scaled El Centro and Parkfield records occurred in the first level and was in the vicinity of 2% and 2.5% respectively. The maximum drift for the Corralitos record occurred in the second level and was around 1.8%. For the three records on firm soil, splice failure was predicted for all columns at the first level and for some columns at the second level. Pullout of the bottom bar reinforcement in the first level beams was also predicted. Severe damage can be expected and the ability of this structure to sustain the large drifts due to the firm soil records, without collapse appears doubtful.

5.6 Concluding Observations on the Original Building.

The static analysis showed that the three-story building was very flexible and had low strength and ductility. The dynamic analysis indicated a poor seismic performance for the building. The soft soil records were found to be most damaging. The structure appeared also, unable to sustain the dynamic loading due to these firm soil records. Large drifts and extensive damage are expected for both soft and firm earthquake records. The large interstory drifts predicted for the structure suggest a possibility of collapse.

5.7 Description of EBF Retrofitting Schemes.

The three-story building was retrofitted by several EBF schemes. To limit disruption to the building, the EBFs were added to the external frames only. Several configurations with various levels of strength and stiffness were considered. These configurations are as follows:

- EBF1-x (Fig. 5.9a): where x represents the ratio $e/(M_p/V_p)$. e is the link length, M_p is the plastic moment capacity, and V_p is the plastic shear capacity of the links. As noted in Section 2.4.2, this ratio must be less than 1.6 for a shear yielding link. The links and beams were formed by W24x55 sections made of A36 steel, the braces were formed by tubular section TS7x7x1/2, A500 Gr. B steel ($F_y = 46$ ksi). The vertical collectors, attached to the external face of the columns, were made of W10x19 sections of A570 Gr. 50 steel. Three link lengths were selected: 18 in., 24 in., and 40 in. representing approximately $0.75 M_p/V_p$, M_p/V_p and $1.5 M_p/V_p$ respectively. The corresponding EBF retrofit schemes were labeled EBF1-.75, EBF1-1, and EBF1-1.5. For these schemes, the braces were distributed over several bays and the overall lateral strength of the added EBF decreased with height to allow for uniform yielding of the links at the different levels.
- EBF1-1S: (Fig. 5.9b) EBF1-1S had the same configuration as EBF1. However smaller member sizes were selected in an attempt to provide the minimum lateral strength required to resist the selected ground motions. A W14x38 A36 section was selected for the links and the beams. The link length was taken equal to 24 in., representing approximately M_p/V_p . The braces were formed by tubes TS7x7x5/16 A500 Gr. B steel, and the vertical collectors were formed by W12x14 sections of A36 steel.
- EBF2: Figure 5.9c shows the configuration EBF2. Only the internal bays were braced and the same member size was provided along the height of the structure. The links, the collector beams and the braces were the same as the ones for EBF1-1, however the size of the vertical collectors was increased due to the expected increase in the vertical force transferred to the columns. The link length was taken equal to 24 in.

- **EBF3:** The bracing system of EBF3 (Fig. 5.9d.) is distributed over several bays and the lateral strength was reduced with height. Two member sizes were selected for each of the shear links, the collector steel beams, and the vertical steel collectors. Compared to the other schemes, a larger number of braced bays was provided at the first floor where higher forces are usually expected.
- **EBF4:** EBF4 configuration (Fig. 5.9e) has the advantage of limiting the retrofit work to one bay since only the middle bay was braced. The link section were formed by W 24x76 sections made of A572 Gr. 50 steel. The braces and vertical collectors were formed by TS10x10x1/2 A500 Gr.B steel sections, and W16x89 A572 Gr.50 steel sections respectively. The link length was equal to 24 in. and represented approximately M_p/V_p .
- **EBF4-S:** (Fig. 5.9f) uses the same configuration as EBF4, however smaller member sizes are used to provide only the minimum lateral strength needed to resist the earthquake load due to the selected earthquake records. The link section was formed by W24x55 sections of A36 steel and the link length was taken as 24 in. representing approximately M_p/V_p . The braces and vertical collectors were formed by TS8x8x1/2 A500 Gr.B steel sections, and a W12x58 A572 Gr. 46 steel sections, respectively.
- **EBF4-H** (Fig. 5.9g) EBF4-H has the same configuration as EBF4 but uses smaller member sizes and the lateral strength was reduced with height to allow for a more uniform yielding of links with height. The link sections at the first, second and third level were formed respectively by a W24x76, A572 Gr. 50 steel, a W24x55 A36 steel and, a W14x38 A36, steel. The link length was maintained at 24 in. for all three levels. The braces and the vertical collectors were formed by a TS10x10x1/2 A500 Gr. B steel section, and a W16x89 A572 Gr.50 steel section, respectively.

The design of the above retrofit schemes consisted first in selecting a link section, then sizing the braces and beams for the forces generated by the fully strain hardened shear links. The vertical collectors are designed to transmit the vertical load transferred to the columns by

the strain hardened links. Detailed calculation procedures are outlined in Section 4.3.3. For all the schemes presented above, the vertical collectors were attached to the external face of the columns.

EBF1-1S, EBF4, EBF4-S and EBF4-H retrofit schemes were designed in an attempt to provide the minimum strength required to resist the seismic loads due to the selected earthquake records. Their design was based on a trial and error procedure. The trials were evaluated with a dynamic inelastic analysis. Link sizes were progressively reduced until the link plastic rotation limit of 0.10 rad. was reached under an earthquake record.

5.8 Modeling of EBF Retrofit Schemes.

The reinforced concrete members (beams and columns) were modeled as explained for the original structure. The horizontal steel beams, the vertical steel collectors and the braces were modeled using the beam-column element of DRAIN-2D and assuming a steel-beam type interaction between the moment and axial load. The beam-column element was deemed appropriate since these members were designed to behave elastically. The analysis output was checked to verify that the assumption of linear behavior for these members was satisfied throughout the loading history. No composite action was considered between the reinforced concrete columns and the vertical collectors. It was assumed that the only connections transferring load between the original frame and the steel bracing system occurred at the columns. The steel beams, links, and braces were otherwise assumed to be able to deform independently of the concrete frame. The links, designed to yield primarily in shear, were modeled with the shear link element.

5.9 Static Analyses of EBF Retrofit Schemes.

A static analysis was performed to evaluate the lateral stiffness and strength of the retrofit schemes. The analysis was performed by applying a lateral incremental load uniformly distributed with height. The load was applied at the floor level.

Figure 5.10 shows the relationship between the maximum interstory drift and the base shear coefficient for the EBF1-1 retrofit scheme. First and second level links yielded at 0.22% drift corresponding to 0.67 W; W being the building weight. Further loading resulted in yielding of the third level link at a drift of 0.34%. Splice failure of the first level columns and pull out of bottom reinforcement of the beams occurred at a drift of about a drift of 0.6% and 0.8% respectively. The rotational capacity of the first level link was reached at an interstory drift of 1.16% corresponding to a lateral strength level of 0.96 W. This condition indicated that the structure reached its ultimate capacity.

The behavior of EBF2 retrofit scheme under static lateral load is summarized in Figure 5.11. Initially the structure behaved elastically until yielding of the first and second level links at a drift of about 0.2%, corresponding to a lateral load of 0.65W. Splice failure of the first level columns occurred at a drift of 0.7%. Ultimate strength capacity of the structure was reached at a drift of 0.9% and was found equal to 0.96 W. The static analysis showed that the third-level link did not yield, indicating that this link may have a shear strength that is too large and may not contribute to the structure's energy dissipation capacity.

Under static loading, EBF3 behaved elastically until yielding of the first level link which occurred at a drift of about 0.2% corresponding to a lateral load of 0.9W (Fig. 5.12). Further loading resulted in yielding of the second and third level links. Pullout of the beam bars and column splice failure occurred at drift levels of 0.55% and 0.8% respectively. Ultimate lateral load capacity of the structure was estimated equal to 1.28W and was reached at a drift of 1.1%.

EBF1-1, EBF2, and EBF3 provided a significant increase in stiffness, strength, and ductility. These schemes did not prevent anchorage and splice failure in the beams and columns of the reinforced concrete frame. However, failure in the reinforced concrete members had little impact on the building behavior, since the added EBF acted as the primary lateral load resisting system. The original reinforced concrete frame still acts as the primary gravity load resisting system.

Figures 5.13 and 5.14 summarize the static behavior of EBF1-.75, and EBF1-1.5. These two schemes were similar to EBF1-1 except for the link length, e . The ratio of the link length over M_p/V_p was set approximately equal to 0.75, 1.0 and 1.5 for EBF1-.75, EBF1-1, and EBF1-1.5, respectively.

Inelastic action in EBF1-.75 started at a drift of 0.22% upon yielding of first level link. This drift corresponded to a base shear of about 0.7 W. The third level link yielded at about 0.3% interstory drift ratio. The maximum strength of the EBF1-.75 was reached at a drift of 0.9%, and was equal to 0.97W. EBF1-1.5 behaved elastically until yielding of the first and second level links at a drift of 0.31% corresponding to a lateral load of 0.7W. At a drift of approximately 0.6%, the third level link yielded. This led to a further reduction in the stiffness of the structure. The links failed at an interstory drift ratio of 2% and the ultimate lateral capacity of EBF1-1.5 was estimated equal to 0.91W.

A comparison between EBF1-.75, EBF1-1 and EBF1-1.5 shows that increasing the link length resulted in a stiffness decrease and in a substantial gain in ductility for the frame. The deformation capacity of the structure was found to increase with the link length. Larger link lengths correspond to larger e/L ratios, L being the bay width. As discussed in Section 2.4.3, the relationship between link plastic rotation and interstory drift can be estimated as $\gamma = (L/e)\theta$ or $\theta = (e/L)\gamma$. Thus, when the link rotation limit of $\gamma = 0.10$ rad. is achieved, a larger plastic frame drift is possible with a larger e/L ratio.

Figure 5.15 shows the response of EBF1-1S under static loading. This scheme, kept the same configuration as EBF1 but had smaller member sizes. Yielding of first and second level links was predicted at a drift level of 0.18% and yielding of the third level link occurred at a 0.28% drift. These drift levels correspond respectively to a lateral load of 0.34W and 0.38W. At a drift of 1.1% rotational capacity of the links was reached indicating failure of the structure. The maximum lateral strength of EBF1-1S scheme was found equal to 0.53W.

Compared to EBF1-1, EBF1-1S had a significantly smaller strength and stiffness as expected. Yielding of the structure and maximum capacity occurred at a similar drift level for both retrofit schemes.

Figure 5.16, 5.17, and 5.18 show the static response of EBF4, EBF4-S and EBF4-H. Note that EBF4-S and EBF4-H had smaller members than EBF4. In addition EBF4-H featured a reduction in strength and stiffness with height. The maximum interstory drift capacity of these three retrofit schemes is approximately the same (1.13%). The lowest strength capacity was predicted for of EBF4-S, and was equal to 0.45W. Note that in EBF4, the third level link did not yield.

The behavior of EBF4 and EBF4-H was essentially similar although EBF4-H had smaller member sizes. The lateral strength of both schemes was approximately equal to 0.6W. The analysis showed that for EBF4 only the two lower links yielded, while for EBF4-H, all three links yielded in shear. Inelastic activity in EBF4 and EBF4-H started at a drift of around 0.2%.

Table 5.5 summarizes the main results of the static analysis. The static analysis showed that EBF1-S, EBF4-1, EBF4-H and EBF4-S essentially increased the strength of the original building by a factor of about three, and increased the initial stiffness of by a factor of about six. While the remaining schemes provided a more substantial increase in both stiffness and strength. All schemes are shown to behave elastically until first shear yield of the links which was observed to occur at around 0.25%. Splice and anchorage failure occurred at somewhat different drift levels for the different retrofit schemes but did not have significant effect on the stiffness of the structure. For comparable retrofit schemes, increasing the link length was shown to result in lower stiffness but higher frame ductility.

5.10 Dynamic Analysis of EBF Retrofitting Schemes.

The retrofitted structures were analyzed under the ground motions listed in Section 4.2. The results of the dynamic inelastic analyses are presented below.

5.10.1 Period of Vibration. Table 5.6 shows the period of vibration for the first and second modes for the original and retrofitted structures. The retrofitting schemes, which consisted of the addition of structural steel members, caused only a negligible change in the mass of the existing building. Hence, a change in the fundamental vibration period can only be attributed to a stiffness change. A reduction in the vibration period of the structure indicates a stiffness increase. The fundamental period of vibration of the retrofitted structures varied between 0.27s (EBF3) and 0.46s (EBF4-S) while the original structure had a period of 1.05s. Thus all retrofit schemes provided a substantial increase in stiffness, as also indicated by the static analysis. The acceleration response spectra for the firm soil records (Fig. 4.2a) indicate that the first period of vibration of the retrofit schemes falls in the area of peak spectral response while the first period of vibration of the original building is located in an area of relatively low spectral acceleration. This indicates that, for these records, the retrofit schemes will cause an increase in the force demand on the structure. For the records on soft soil, no firm conclusion can be drawn about the eventual change in the demands.

5.10.2 Maximum Interstory Drift of the Retrofit Structures. Figures 5.19, 5.20, and 5.21 show the maximum interstory drift for EBF1-1, EBF2, and EBF3 subjected to the selected ground motions. All three retrofit schemes provided a substantial improvement in the behavior of the structure (interstory drift for the original structure is shown in Figure 5.8). For both the firm and soft soil records, the retrofit schemes in a number of cases reduced interstory drifts by a factor in excess of 10, as compared to the original building. For the records on firm soil, maximum interstory drift ratios for the three schemes was below 1%. The largest drifts occurred under Corralitos record. The largest drifts under the firm soil earthquake records occurred at the first level for EBF2 and at the second or third level for EBF1-1 and EBF3.

This indicates that for the EBF2, the first mode of vibration may be dominating the dynamic response, while for the EBF1-1 and EBF3 schemes higher mode of vibration may have some influence on the response of the structure. For the records on soft soil (Mexico, Oakland), these retrofit schemes appeared very effective. Interstory drift ratio was kept below 0.1% and 0.25% for Mexico record and Parkfield record respectively. As a comparison, the original building experienced drift in excess of 3% for these two records.

Maximum interstory drift for EBF1-.75 and EBF1-1.5 are shown in Figures 5.22 and 5.23. In general the interstory drift were higher for EBF1-1.5 than for EBF1-1 or EBF1-.75. This is in agreement with the static analysis that showed that an increase in the link length resulted in a reduction in stiffness. For the firm soil record, the interstory drift ratios for EBF1-.75 were kept below 0.6%. Maximum interstory drift ratio for EBF1-1.5 remained below 0.8% for the Parkfield record and below 0.7% for the scaled El Centro record. The maximum interstory drift for EBF1-1.5 under the Corralitos record was in the vicinity of 1%. Very low drift levels were predicted for EBF1-.75 and EBF1-1.5 for the records on soft soil.

Maximum interstory drift ratios for EBF1-1S are shown in Figure 5.24. For the record on soft soil, the interstory drifts were very low and comparable to those of EBF1-1. For the records on firm soil, larger drifts were predicted for EBF1-1S. However, these drift levels remained within acceptable limits. The largest drift ratios occurred for the Corralitos record and measured approximately 1%. Based on the interstory drifts, EBF1-1S appears adequate to resist the seismic load due to the selected records. This scheme is more economical than EBF1-1 since it provides the needed strength but requires less material. The lower strength of EBF1-1S is also advantageous in limiting the loads on the foundations as will be discussed in Section 5.10.5.

Figure 5.25 shows the maximum drifts for the EBF4 retrofit scheme which had only one braced bay. The EBF4 retrofit scheme greatly improved the behavior of the building under the soft soil records. The drift ratios were kept below 0.5% for Oakland and below 0.2% for Mexico. Under the firm soil records, the drifts were relatively high but within acceptable limits.

The largest interstory drift occurred for the Parkfield record and was in the vicinity of 1.4%. Under the records on firm soil, the highest drifts are observed at the first floor. Low drifts are predicted at the third level.

Interstory drifts for EBF4-S and EBF4-H are shown in Figures 5.26 and 5.27, respectively. These schemes had the same configuration as EBF4 but smaller member sizes. In addition, the strength and stiffness of EBF4-H was reduced with height to better match the dynamic demands. EBF4-S and EBF4-H were very effective in controlling drifts for the soft soil records. Under the Parkfield record, maximum interstory drift ratios for EBF4-S and for EBF4-H were in the vicinity of 0.6% and 0.5% respectively. Under the Mexico record, the drift ratios were kept below 0.2%. Firm soil records subjected both schemes to relatively large drifts. The maximum drift ratio at the first level of EBF4-S was in the vicinity of 1.5% under Corralitos, and in excess of 1.5% under Parkfield record, indicating that significant damage may be expected in the structure. Note that interstory drifts exceeding 1.5 % may be considered unsafe for the building. Of particular concern are the low ductility of the existing columns and the possibility of punching shear failure at the slab-column connection of internal frames. The drift for EBF4-H under firm soil records remained within acceptable limits. The largest drifts occurred under Corralitos and Parkfield and were in the vicinity of 1%.

Note that the deformations for EBF4 and EBF4-S were essentially concentrated in the first floor while the deformations of EBF4-H were distributed amongst the three stories of the structure. This indicates that for the latter, the upper floor links had a greater contribution to the frame's deformation and energy dissipation, while for the former inelastic deformation, tended to create a soft first story. Reducing the strength and stiffness with height promoted uniform yielding with height and resulted in a better seismic performance.

In summary, plots of the maximum drifts indicated that the retrofit schemes provided a substantial improvement in the seismic behavior of the building. The different schemes significantly reduced interstory drifts. The reduction in the drifts were particularly substantial for the earthquake records on soft soil. A reduction of the link size with height promoted a

more uniform contribution of the different levels to the structure's dissipation capacity, and resulted in a higher performance. EBF1-1S, EBF4 and EBF4-H were shown to be the most economical schemes in preventing collapse under the dynamic loading due to the selected records. These schemes require a minimum amount of material and maintain the drifts within acceptable limits. EBF4-S, however, may not be adequate to resist the seismic load due to Parkfield record.

5.10.3 Roof Displacements. Figure 5.28 shows the roof displacements for the original structure and for EBF1-1 and EBF4-H retrofit schemes subjected to the Corralitos record. Corralitos record was selected since it was shown to impose relatively high demands on the structures. EBF1-1 had a relatively high stiffness and strength, while EBF4-H had a relatively low strength and stiffness. These retrofit schemes reduced the roof displacement by a factor of approximately two, indicating a substantial improvement in the building behavior. The largest roof displacement for the original structure measured 5.5 in. (1.4% overall drift), while maximum roof displacement for EBF1-1 and EBF4-H was respectively 2.7 in. (0.6% overall drift) and 3in. (0.7% overall drift).

5.10.4 Plastic Deformations of the Structure.

5.10.4.1 General. The amount of plastic deformation of the structural members can help assess the structure performance, estimate the damage level and indicate the ability of the building to withstand the earthquake loading. In this section, plastic rotation of the links and rotational demands on the reinforced concrete members will be presented. Comparison between the deformations of the original building and the retrofit schemes will be made to assess possible benefits of the added EBFs

5.10.4.2 Plastic Rotation of the Links. Plastic deformations of EBFs are primarily limited to the links. The maximum plastic rotations of the retrofit schemes are shown in Figure 5.29 to 5.37. These figures show that in general the soft soil records imposed low plastic rotations on the links. As indicated earlier, well designed and detailed links can sustain plastic rotation of 0.10 rad. under cyclic loading.

Figure 5.29 shows the maximum plastic rotation for the links of EBF2. The links remained elastic under the soft soil records. Under the firm soil records, plastic deformations were concentrated at the first level and the links at the third level remained elastic. Under the Corralitos record, a relatively large rotation of 0.052 rad was predicted at the first level. For the scaled El Centro record, the maximum link rotation was below 0.025 rad. at the first floor and was negligible at the second level. Under Parkfield, only the first floor link experienced plastic rotation, however this rotation was very low. The results indicate that the link sizes could be reduced for EBF2, particularly at the second and third level.

Maximum plastic link deformations for EBF3 (Fig. 5.30) indicate that this scheme remained essentially elastic under the soft soil records. Under the firm soil records, the largest plastic link deformations occurred at the second floor. The link at the first and third level remained elastic except for the Corralitos record where a low plastic rotation of 0.01 rad. was predicted.

The link deformations of EBF1-.75 (Fig. 5.31), EBF1-1 (Fig. 5.32), and EBF1-1.5 (Fig. 5.33) suggest that the maximum link plastic rotation increased somewhat with a reduction in the link length, despite the fact that the frame stiffness increases with a reduction in link length. This can be attributed to the relationship between story drift and link rotation as discussed in Section 5.9. The shorter links result in larger L/e ratios, and correspondingly result in larger link rotations for the same drift.

The largest link deformations for EBF1-1 occurred at the second level and the distribution of the plastic rotation over the height indicates a participation of higher vibration

modes in the response. The Corralitos record imposed the largest link rotations for the EBF1-1. Under this record, a maximum link rotation of 0.051 rad. was predicted, well within the link's rotation capacity of 0.10 rad. Under the scaled El Centro record and the Parkfield record, relatively low plastic rotations were expected. The demands under the soft soil record were very small. Maximum link rotation under Parkfield record was below 0.02 rad, and the links remained elastic under the Mexico record.

Under the firm soil records, links at all levels of EBF1-.75 experienced relatively large rotations. The maximum rotation under Corralitos and Parkfield occurred at the second level and was equal to 0.58 rad. and 0.31 rad. respectively. The largest rotation under the scaled El Centro record was predicted at the first level link and was equal to 0.038 rad. The soft soil records imposed low plastic rotations on the links of EBF1-.75. Under the Oakland record, the plastic link rotations were kept below 0.02 rad and the structure remained elastic under the Mexico record.

Figures 5.34 and 5.35 show the maximum plastic rotation for EBF4 and EBF4-H which have only one bay braced and similar strength and stiffness. In EBF4-H, link size was reduced with height to better match the seismic demands. EBF4-H appears to have a better overall performance under dynamic loading. The maximum link rotations were lower for EBF4-H than for EBF4. In general, the link rotation of EBF4 were concentrated at the first level while, they were more evenly distributed among all floors of EBF4-H. EBF4 showed the tendency toward the formation of a soft first story. The dynamic behavior of EBF4-H shows that decreasing the link size with the building height promoted link yielding at the different floors and reduced the rotational demands on the first floor links. In EBF4-H, the maximum link rotations were on the order of 20 to 30 percent less than in EBF4.

The maximum link rotation for EBF4 under Parkfield was equal to 0.13 rad, exceeding the limiting value of 0.10 rad. This scheme may be considered inadequate to resist the Parkfield record. Under the Corralitos record, a maximum link rotation of around 0.10 rad. was predicted at the first floor. The rotation at the second level was equal to 0.03 rad, and the

rotation at the third level was very low. For the El Centro record, only the two lower level links experienced plastic rotations. These rotations were moderately large and measured 0.054 rad. at the first level and to 0.032 rad. at the second level.

Under the stiff soil records, very large link rotations were predicted at all levels of EBF4-H. These rotations were however below the limiting value of 0.10 rad. The largest rotation under the Corralitos occurred at the first level and was equal to 0.084 rad. Link rotations at the second and third floors were equal to 0.043 rad. Under the Parkfield record, the link rotation decreased somewhat with height. The largest rotation was predicted at the first level and was equal to 0.087 rad. Under El Centro a moderately large rotation of 0.043 rad. was predicted for all level links. Low plastic link rotations were predicted for the building on the soft soil records. Under the Oakland record, the second floor link remained elastic and the third and first level link rotations were below 0.02 rad. The links remained elastic under the Mexico record.

Maximum plastic link rotations of EBF4-S (Fig. 5.36) show that this scheme may be inadequate to resist the load due to most of the records on firm soil. Under the Corralitos record and the Parkfield record, the maximum link rotations were largely in excess of 0.10 rad. Under the scaled El Centro record, the maximum link rotation slightly exceeded 0.10 rad. and can be considered acceptable. The links remained elastic under the Mexico record. Under the Oakland record, first level and second level links experienced plastic rotation. The maximum rotation of these links were respectively below 0.06 rad. and 0.03 rad.

Figure 5.37 shows the maximum plastic link rotations of EBF1-1S which had the same geometric configuration as EBF1-1 but a lower lateral strength and stiffness. This scheme had several braced bays and was characterized by a reduction of stiffness and strength with height. The static analysis showed that the strength and stiffness of EBF1-S were comparable to the ones of EBF4-H and EBF4.

Under the stiff soil records, the links of EBF1-S were subjected to relatively large plastic rotations. These rotations remained however, within acceptable limits. The maximum rotation under Corralitos and Parkfield were close to 0.10 rad. The maximum link rotation under the scaled El Centro record measured 0.084 rad. The reduction in strength with height in EBF1-S allowed the higher levels to participate in energy dissipation and helped maintain acceptable link rotations.

Note that EBF1-S appears to provide the minimum strength required to sustain the selected earthquake records. The link plastic rotations were very close to the rotation capacity (0.10 rad.). Schemes with smaller link sizes were analyzed and were found inadequate to resist the firm soil earthquake records, without exceeding link rotation limits.

Figures 5.38 and 5.39 show the link rotation as a function of time for EBF1-1 and EBF4-1H subjected to the Corralitos ground motion. These plots allow for a comparison of link rotations throughout the loading history rather than at maximum displacement only. Maximum plastic rotations occurred early in the records. The largest rotation was reached at 2.64s for EBF4-1H and at 2.76s for EBF1-1. The figures indicate that seismic loading caused permanent plastic deformations in the links of both structures. The permanent plastic rotations are on the order of 0.01 rad., and are quite small. For the 24 in. link length used in these frames, one end of the link will be permanently displaced with respect to the other by approximately 0.25 in. The EBF should require little or no repair after these severe earthquakes.

In summary, the plots of link rotations of the retrofit scheme show the following:

- The use of EBF retrofit schemes with a short link ($e = 0.75 M_p/V_p$) was found more advantageous than EBF retrofit schemes with long links ($e = 1.5 M_p/V_p$). In general, short link transmits lower moments to the braces and adjoining steel beam. The lower beam moments are advantageous for minimizing the need for lateral braces in the

beam segment outside of the link. The lower brace moments reduce the required brace size and simplify the brace end connection details. On the other hand, reducing the link length results in an increased link rotation demands. However, the dynamic analysis showed that due to the increase in strength, the plastic link rotation of EBFs with short links remained within acceptable levels.

- A reduction of strength with height promoted uniform link yielding with height and resulted in a better seismic performance.
- All the proposed schemes resulted in a significant decrease of the demand for the soft soil records. For these records, the gain in stiffness was sufficient to control the deformations and to adequately strengthen the building to resist the seismic loading.
- EBF4, EBF4-H and EBF1-S were found to provide the minimum strength and stiffness required to resist the selected earthquake records. EBF4-S was found inadequately designed. EBF2 and EBF3 provided the greatest strength and stiffness of all the retrofit schemes, maintained the lowest interstory drifts, and provided the greatest degree of damage control.

5.10.4.3 Ductility Demands of the Reinforced Concrete Members.

This section will present the rotational ductility demands of the reinforced concrete members for the original building and for the retrofit schemes EBF1-1 and EBF4-H subjected to the Corralitos record and to the scaled El Centro record. Analytical results indicated that these records imposed relatively high demands on the structures. EBF1-1 has a relatively high stiffness and strength, while EBF4-H has a minimum level of stiffness and strength. The rotational ductility demand is measured as the maximum rotation of the member divided by the rotation at the onset of inelastic action in the member.

Rotational ductility demand was selected as an indicator of the level of damage and the ability of the reinforced concrete members to sustain the seismic load. Other indicators involving more computation efforts can be utilized (Banon et al., 1981 and Bracci et al., 1989). However, the rotation ductility was shown to give acceptable analytical prediction of damage for reinforced concrete members (Banon et al., 1981). The rotation ductility demand will be used here to help assess the damage level in the reinforced concrete members. The discussion below is limited to the external frames of the three-story building, since the EBFs were added to these frames only.

It is in general difficult to define damage analytically. To make a qualitative assessment of the damage level, the rotational ductility demands can be compared to the ductility needed for the section to reach its ultimate capacity. The reinforced concrete members can still carry load beyond their ultimate capacity. This will however result in a reduction in strength and in damage of the member.

Based on the values in Table 5.2, the top section of the columns are found to reach their ultimate capacity at a rotation ductility of about 1.5 to 1.6. The lower sections reach their ultimate capacity at a rotational ductility of 1.0. The beams reach their ultimate load carrying capacity at a rotation ductility of about 2.25 in negative bending and at about 1.1 in negative bending (Table 5.4).

Figure 5.40 and 5.41 show the maximum rotation ductility demands of the reinforced concrete members of the original structure subjected to the scaled El Centro record and to the Corralitos record respectively. Note that "yield" in the figures refers actually to the onset of inelastic deformation in the members. Inelastic action in the reinforced concrete members is caused by member yielding or by anchorage or splice failure. The figure indicates that both records caused pullout of the bottom beam reinforcement and large ductility demands in the beams. In addition most columns of the building experienced splice failure.

The largest rotations for the columns were expected at the base of the building. At the bottom of the first level columns, the rotation ductility demands under the Corralitos record ranged between 3.3 and 4.5, indicating extensive damage. In the upper floor, the maximum rotational demand was around two, indicating low damage. Under the scaled El Centro record, the columns were subject to larger rotations. Rotational ductility demands were greater than six at the base of the first level columns, and varied between 4.5 and 6.3 at the second level. This indicates very heavy damage at the first and second level columns.

Most of beams experienced pullout of the bottom reinforcement in positive bending. Under the scaled El Centro record, the rotation ductility demand ranged between 10 and 14.6 at the first level and between 8 and 12 at the second level. Under the Corralitos record, the rotational ductility demands varied between 6 and 9 at the first level and was around 9 at the second floor. Although these rotational values appear high, they correspond to low moments in the beams and are due to the very small embedment length of the bottom bars.

The rotational ductility demands of the reinforced concrete members of the original building indicate that the structure may be unable to sustain the selected earthquake records. Extensive damage was expected for the columns.

Figure 5.42 shows the maximum ductility demands of the reinforced concrete beams for the EBF1-1 retrofit scheme under the Corralitos record. The reinforced concrete members (beams and columns) remained elastic under the scaled El Centro record. Under Corralitos record, the columns remained elastic. The plastic deformation were limited to the second level beams only and the rotation ductility demands at this floor were limited to relatively low values which ranged between 1.2 and 3.1.

Figures 5.43 shows the ductility demands of the reinforced concrete members of EBF4-H under the scaled El Centro record and Corralitos records. Under the scaled El Centro record, the columns remained elastic. Plastic deformation were limited to the first level floor

beams in positive bending. The largest rotational ductility demand was equal to 3.4. This rotation ductility demand can be considered low for the beams.

Under the Corralitos record all beams of the first level and some beams of the higher floors were subjected to plastic deformations (Fig. 5.44). A maximum rotational ductility demand of 5 was predicted at the first floor beams in positive bending. Column splice failure was predicted for the first level. The rotational ductility demands in these columns varied between 1.4 and 2.6.

In summary, both retrofit schemes successfully reduced the rotation demands on the reinforced concrete members. Retrofit scheme EBF1-1 prevented pullout of the beam reinforcement and considerably reduced the beam rotations. Also, this scheme prevented column splice failure for both strong records. Compared to the original structure, the EBF4-H retrofit scheme reduced the number of hinges in the reinforced concrete members and the amount of plastic deformation. Under the Corralitos record, hinge rotations in the beams were reduced by a factor of two. Some columns experienced splice failure. However the rotational demands on these columns were relatively small. Under the Scaled El centro record, splice failure in the columns was prevented. In general the plastic rotations and the number of hinges were higher in EBF4-H than in EBF1-1.

5.10.5 Axial Load at the Building Foundation. The addition of a bracing system to an existing structure may cause an increase in the axial load on the existing columns and on the foundation. Such a load increase could require strengthening the foundation.

Figure 5.45 shows the maximum axial load on the foundation of the original building and on three retrofit schemes subjected to the Corralitos record. The three retrofit schemes for which foundation load is shown are EBF1-1, EBF1-S, and EBF4-H. The axial loads shown in this figure are due to the combined effect of gravity and earthquake loading. It is worth mentioning, that there is no available information about the foundation design of the three-

story building. Hence, the adequacy of the foundation cannot be properly assessed and only general and qualitative observations can be made.

The EBF retrofit schemes increased the compression load on the foundation. For EBF1-1, the increase in compression load under the Corralitos record, averaged 180% for the external columns and varied between 70% and 120% for the internal columns. EBF1-S also led to an increase in the foundation compressive load. This load was however smaller than the load for EBF1-1. Note that EBF1-S has the same configuration as EBF1-1 but lower strength. For EBF1-S, the compression on the external foundations increased by 80% compared to the original building. The increase in compression load for the internal foundations varied between 40% and 70%. The most dramatic increase in compression load was observed for EBF4-H retrofit scheme. EBF4-H had only one bay braced. While the load on the unbraced bays remained about the same, the compression load under the braced bay increased by more than 500%.

While the foundation of the original building was not subjected to tensile loading, the use of EBF retrofit schemes introduced tension load in the foundation. The tension load on the external foundation of EBF1-1 was equal to about 130 kips. In EBF1-S, the corresponding load averaged 40 kips. A very large axial load was imposed on the braced bay foundations of EBF4-H. The load reached a value of 625 kips.

Like most retrofit schemes, EBFs are found to cause an increase in the axial load acting on the foundation. Keeping the strength and stiffness of the EBF to a minimum, while distributing the bracing to several bays (EBF1-1S) allowed for the lowest increase in the axial load. For the case shown, EBF4-H which had only one braced bay, caused the largest increase in the axial load. For this scheme, the ability of the columns in the braced bay to resist the imposed axial load appeared doubtful and column strengthening may be required. Due to the increase in axial load, the use of EBF retrofit schemes may require foundation strengthening.

5.10.6 Distribution of Lateral Load.

5.10.6.1 General. The distribution of lateral load between the original reinforced concrete frame and the added EBF can help assess the effectiveness of the EBFs as a retrofit scheme. The distribution of the lateral load is discussed below for the static and dynamic analyses of EBF1-1 and EBF4-H.

5.10.6.2 Static Analysis. Figure 5.46 and Figure 5.47 show the distribution of the base shear between the added EBF and the reinforced concrete frame for EBF1-1 and EBF4-H retrofit schemes subjected to static incremental loading. Previous results showed that EBF1-1 has a relatively high stiffness and strength, while EBF4-H has a low stiffness and strength. Both schemes have an adequate level of lateral strength to resist the load due to the selected records.

The portion of the total base shear resisted by the bracing system was around 90% for EBF1-1 and around 80% EBF4-H during the initial loading stages. This ratio remained essentially constant until shear yielding of the links which resulted in a stiffness reduction of the EBF. The stiffness decrease caused a reduction in the lateral load carried by the added EBF. The minimum base shear resisted by EBF1-1 and EBF4-H was equal to 80% and 70% of the total base shear respectively. Splice failure in the reinforced concrete columns led to a decrease in the base shear resisted by the concrete frame, and to an increase in the base shear resisted by the EBF. This was due to a reduction in the reinforced concrete column stiffness. In general, the fraction of the total base shear resisted by EBF1-1 was higher than that resisted by EBF4-H, reflecting the higher stiffness of EBF1-1.

The static analysis indicated that the added EBF are significantly stiffer than the original frame. In the retrofitted structures, the EBFs resist 70% to 90% of the total load.

5.10.6.3 Dynamic Analysis. Figures 5.48 and 5.49 show the distribution of the base shear between the reinforced concrete frame and the added EBFs for EBF1-1 and EBF4-H under the Corralitos record which imposed high demands on the three-story building. These figures show that most of the lateral load is resisted by the added EBFs. The EBFs appear to resist about 70% to 80% of the base shear in EBF4-1 and about 80% to 90% of the base shear in EBF1-1. These results are in agreement with the ones of the static analysis. The maximum base shear resisted by the concrete frame in EBF1-1 and in EBF4-H was $0.13W$ and $0.19W$ respectively; W being the building weight.

The added EBF schemes increased the stiffness of the building and reduced its fundamental period of vibration. A change in the building dynamic properties may affect the demand due to a given ground record. To examine the effect of the addition of an EBF retrofit scheme on the base shear demand, the base shear in the original building is plotted (Fig. 5.50) and compared to the base shear in EBF1-1 (Fig. 5.48) and in EBF4-H (Fig. 5.49). These figures show that the retrofit schemes led to a significant increase in the lateral load. The maximum base shear in the original building was equal to $0.21W$ but reached $0.60W$ in EBF4-H and $0.80W$ in EBF1-1. The base shear increase is mainly due to the higher strength of the retrofitted structure.

Note that the maximum shear acting on the reinforced concrete columns of the original building and of EBF4-H is, essentially, of the same magnitude. Compared to the original building, EBF1-1 reduced the shear in the reinforced concrete columns to about half. EBF1-1 scheme had higher stiffness and lower fundamental period of vibration than EBF4-H. These results indicate that for retrofit schemes with a fundamental period of vibration in the medium range, increasing the stiffness of the added EBF may reduce the column shear.

The ratio of the base shear resisted by the added EBF was shown to average 80% of the total base shear. This appears to justify designing the added EBF retrofit scheme to resist all of the base shear. However, it is important to notice that an increase in stiffness due to the added EBF scheme may be accompanied with an increase in the demand under dynamic load.

The increase in the demand may keep the same shear level on the columns. For retrofit schemes with a period of vibration in the medium range, EBFs with a high level of stiffness appeared to be preferable in reducing the base shear in the columns than EBF system with a relatively low stiffness.

5.11 Summary on the Three-Story Building.

A three-story reinforced concrete building representative of the 1950s and 1960s low rise construction was analyzed. The design forces for this building were based on the 1964 edition of the UBC and the member design and detailing followed the recommendations of the ACI 381-63 recommendations. Due to the low lateral loads of the 1964 UBC, the building design was governed by gravity loading only. Consequently the building was provided with low lateral strength and poor detailing. The splices provided in the columns were inadequate by current standards and splice failure was expected. The bottom beam reinforcement was embedded only six inches into the joint, hence the beams were not expected to resist moment reversal due to seismic loading. The concrete was not well confined and the members (columns and beams) were expected to have limited rotational capacity.

A static analysis showed that the building had very low lateral strength and little ductility. A dynamic analysis was conducted using a set of three earthquake records on firm soil and two records on soft soil. The peak ground accelerations varied between 0.49 g and 0.64 g for the firm soil records and between 0.16 g and 0.29 g for the soft soil records. The dynamic analyses indicated that the original building may not be adequate to resist the earthquake loadings due to the selected records. Large displacements and extensive damage were expected.

To enhance its seismic performance, the building was strengthened with several EBF retrofit schemes. The parameters that were varied for these schemes include stiffness and strength of the added EBF, bracing configuration, link length, and variation of stiffness and strength with height.

Reducing the link size with height to better match the distribution of the lateral force, was found to promote uniform yielding and to improve the performance of the structure. Variation in the link length was found to affect the response of the building. The use of EBF retrofit schemes with short link was found more advantageous than EBF retrofit schemes with long links.

The added EBFs were found to cause an increase in the axial load on the columns and on the foundation. The axial load introduced by the added EBF may require strengthening of the columns and/or of the foundation. Keeping the strength of the EBF to a minimum and distributing the braces to several bays was found to minimize the increase in column axial load.

The study showed that most of the base shear is resisted by the added EBF. This may justify designing the EBF to resist all of the base shear. Note however, that the addition of an EBF to an existing reinforced concrete building leads also to an increase in the seismic demands as was shown for the case studies.

Table 5.1 Moment Rotation Relationship for the Columns of the Internal Frames

Lev.	Location	Bottom Section		Top Section			
		M_p (k in)	θ_p (rad.)	M_y (k in)	M_u (k in)	θ_y (rad.)	θ_u (rad.)
1	Ext. Col.	2054	.00481	2595	2794	.00604	.00777
	Int. Col.	2561	.00428	2908	3151	.00483	.00651
2	Ext. Col.	1821	.00441	2368	2605	.00570	.00803
	Int. Col.	2355	.00430	2649	2970	.00483	.00651
3	Ext. Col.	1614	.00467	2216	2413	.00637	.00876
	Int. Col.	1821	.00441	2595	2794	.00604	.00777

Table 5.2 Moment Rotation Relationship for the Columns of the External Frames

Lev.	Location	Bottom Section		Top Section			
		M_p (k in)	θ_p (rad.)	M_y (k in)	M_u (k in)	θ_y (rad.)	θ_u (rad.)
1	Ext. Col.	1667	.00460	1852	2033	.00508	.00814
	Int. Col.	2008	.00603	2231	2330	.00665	.00779
2	Ext. Col.	1591	.00520	1768	1929	.00573	.00858
	Int. Col.	1742	.00521	1936	2138	.00575	.00846
3	Ext. Col.	1484	.00520	1649	1832	.00574	.00940
	Int. Col.	1591	.00520	1768	1929	.00573	.00858

Table 5.3 Moment Rotation Relationship for the Beams of the Internal Frames

		Positive Bending Direction				Negative Bending Direction			
		M_{cr} (k in)	M_p (k in)	θ_{cr} (rad.)	θ_p (rad.)	M_y (k in)	M_u (k in)	θ_y (rad.)	θ_u (rad.)
Outside Beams	Ext. Joint	551	579	.00150	.00158	3195	3512	.00870	.01368
	Int. Joint	551	579	.00150	.00158	3561	3833	.00969	.01322
Inside Beams		551	579	.00145	.00153	3561	3833	.00939	.01293

Table 5.4 Moment Rotation Relation for the Beams of the External Frames

		Positive Bending Direction				Negative Bending Direction			
		M_{cr} (k in)	M_p (k in)	θ_{cr} (rad.)	θ_p (rad.)	M_y (k in)	M_u (k in)	θ_y (rad.)	θ_u (rad.)
Outside Beams	Ext. Joint	432	454	.00175	.00185	1877	2226	.00762	.01926
	Int. Joint	432	454	.00175	.00185	2037	2375	.00826	.01828
Inside Beams		432	454	.00170	.00179	2037	2375	.00800	.01803

Table 5.5 Summary of the Static Analysis of the Three-Story Building

	Initial Stiffness (kips / % drift)	Ultimate Strength (kips)	Drift Ratio Capacity (%)
Original	488	300	.75
EBF1-.75	5823	1770	.90
EBF1-1	5573	1760	1.16
EBF1-1.5	4132	1660	2.12
EBF2-1	5948	1750	.89
EBF3-1	8235	2340	1.10
EBF4-1	2897	1120	1.16
EBF1-S	3457	980	1.08
EBF4-S	2643	820	1.11
EBF4-H	3023	1110	1.14

Table 5.6 Two First Vibration Periods for the Original Three-Story Building and for the Retrofit Schemes

Structure	Period of Vibrations	
	First Mode	Second Mode
Original	1.050	.340
EBF1-.75	0.335	0.144
EBF1-1	0.345	0.148
EBF1-1.5	0.380	0.160
EBF2-1	0.297	0.106
EBF3-1	0.273	0.108
EBF4-1	.410	.148
EBF1-S	0.432	0.179
EBF4-S	0.460	0.165
EBF4-H	.412	.149

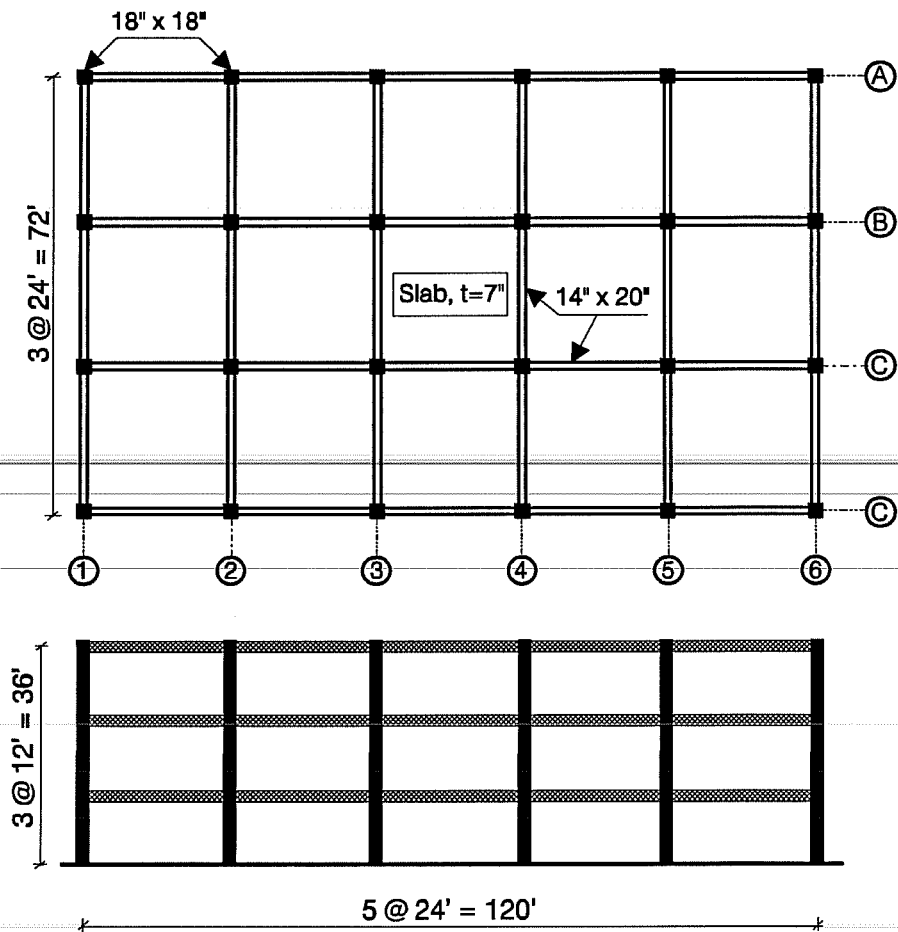
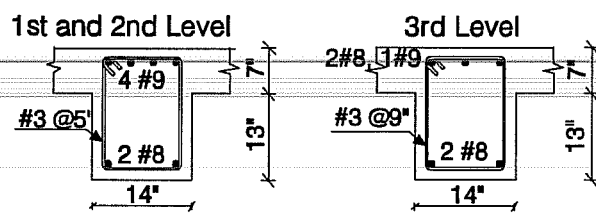
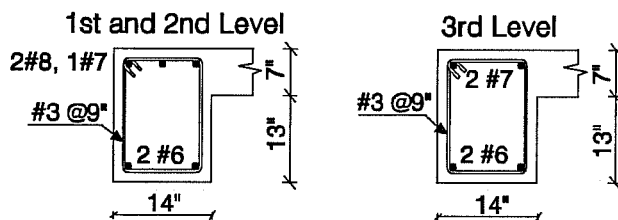


Figure 5.1 Elevation and Plan View of the Three Story Building



(a) Internal Frame Beams



(b) External Frame Beams

Figure 5.2 Cross Sections of the Beams

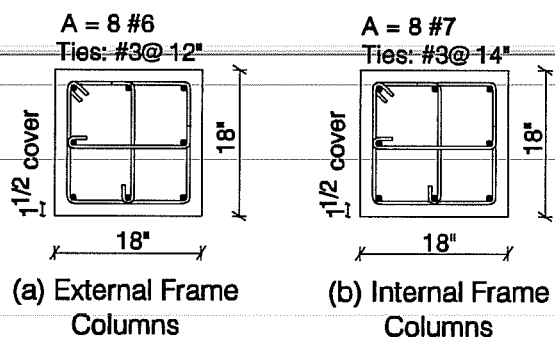


Figure 5.3 Column Cross Sections

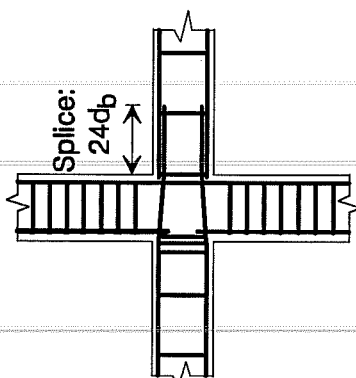
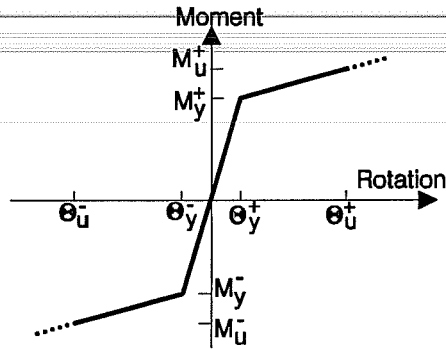
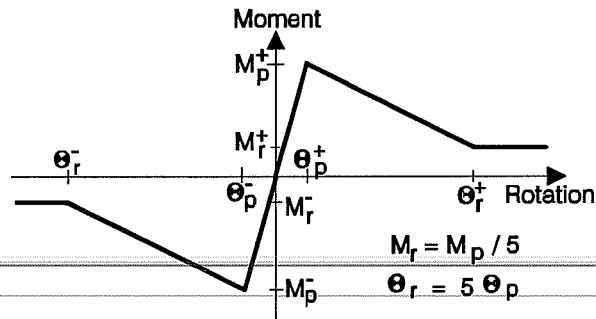


Figure 5.4 Beam and Column Reinforcement at the Joint



a) At top of the columns



a) At the base of the columns

Figure 5.5 Envelope of the Moment-Rotation Relationship for the Columns of the Three-Story Building

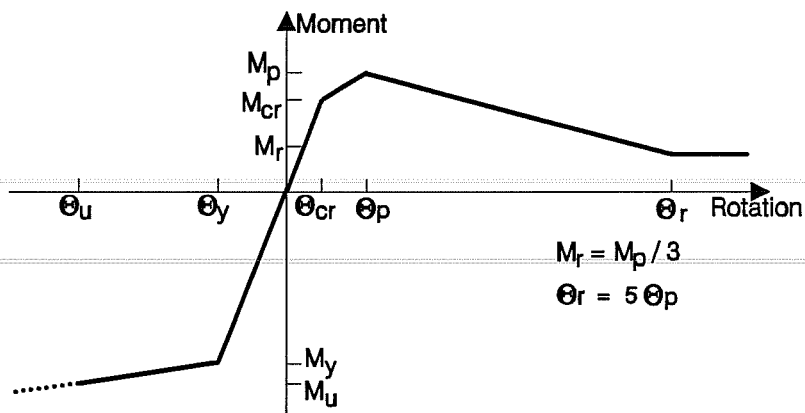


Figure 5.6 Envelope of the Moment-Rotation Relationship for the Beams of the Three-Story Building

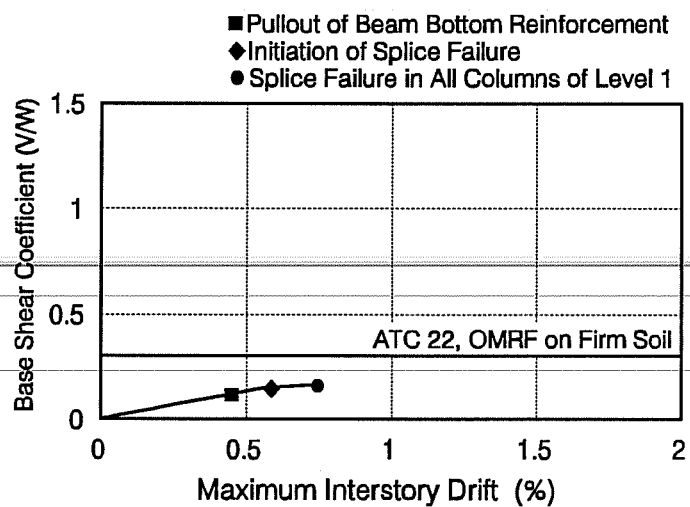


Figure 5.7 Maximum Interstory Drift for the Original Three-Story Building Under Static Load

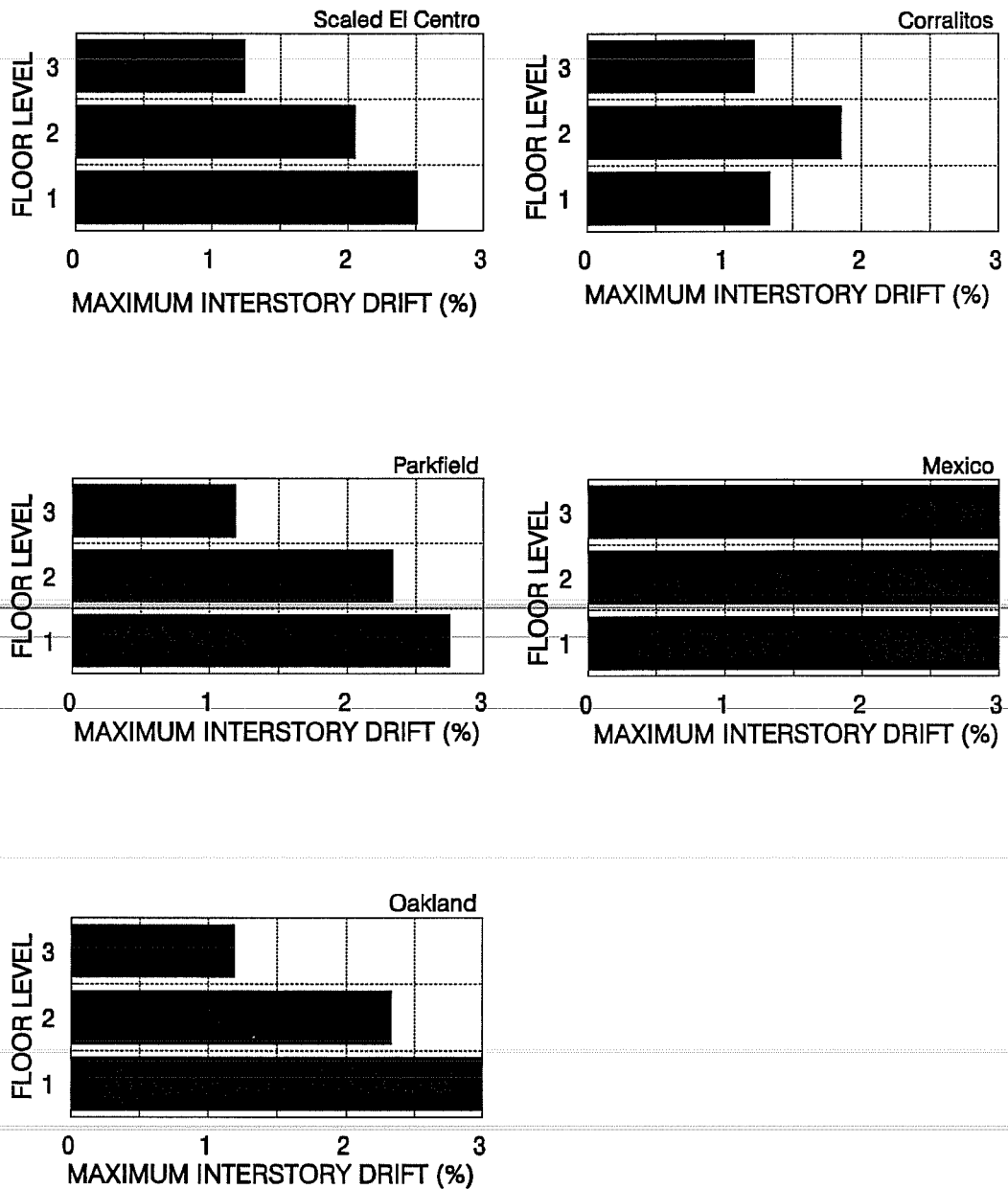
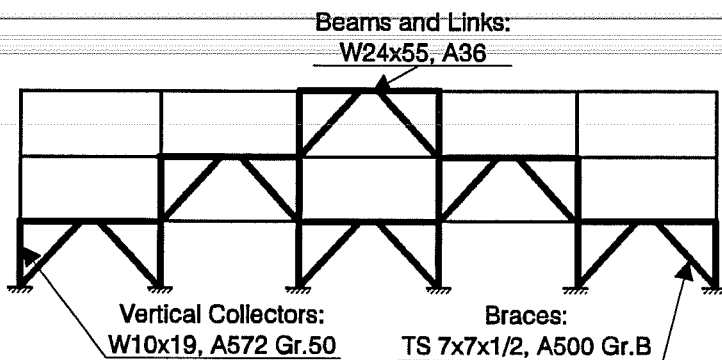
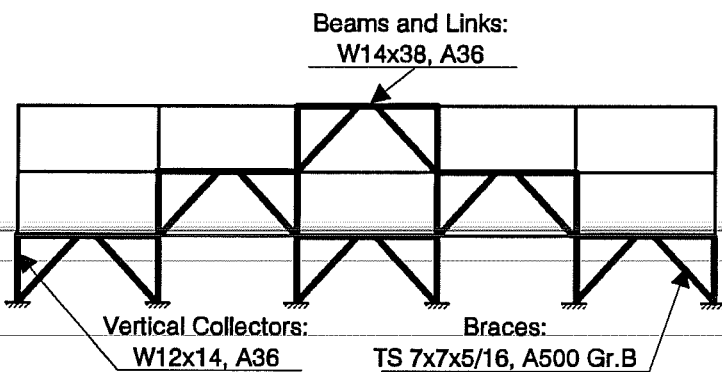


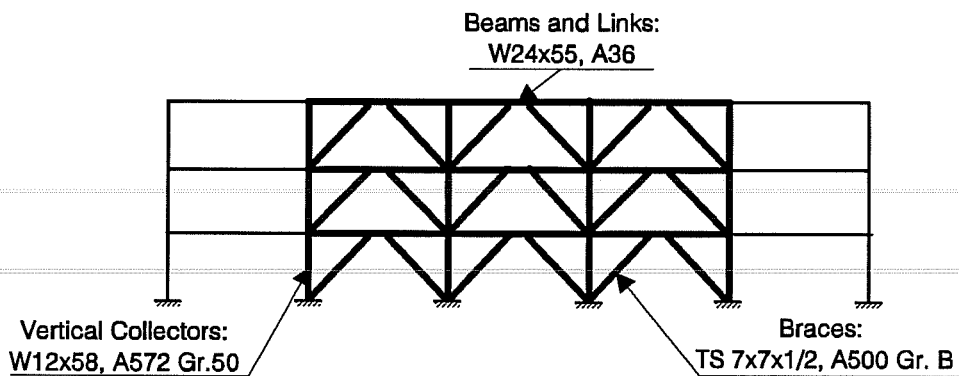
Figure 5.8 Maximum Interstory Drifts for the Original Three-Story Building Subjected to the Selected Acceleration Records



(a) EBF1 Configuration

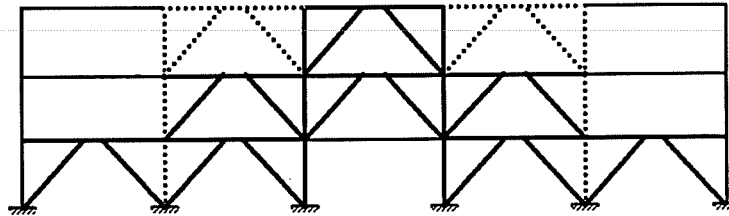


(b) EBF1-1S Configuration



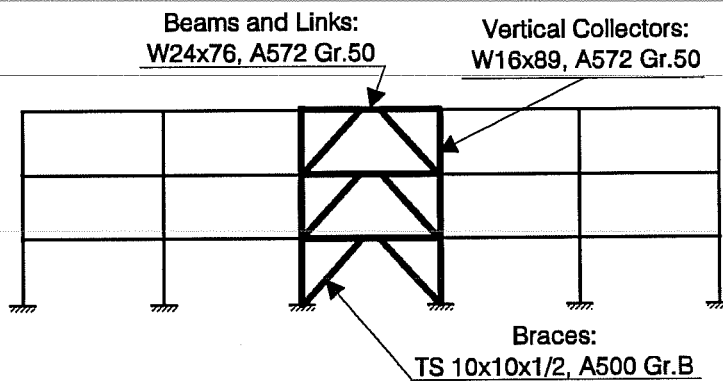
(c) EBF2 Configuration

Figure 5.9 Configuration of EBF Retrofit Schemes



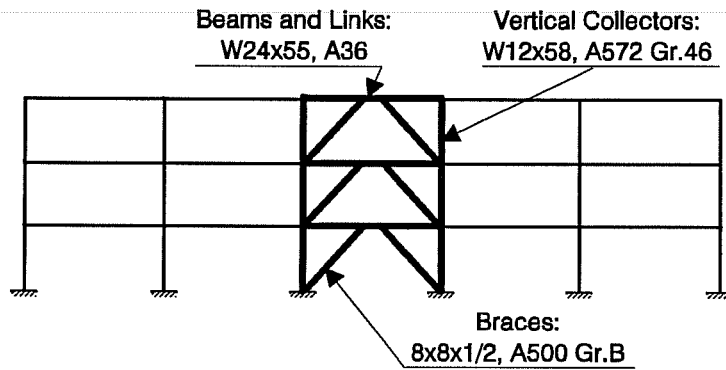
Braces:	Vertical Collectors:	Beams and Links:
— TS 7x7x1/2, A500 Gr.B	— W12x19, A578 Gr.50	— W24x55, A36
..... TS 7x7x1/4, A500 Gr.B W12x30, A578 Gr.50 W14x38, A36

(d) EBF3 Configuration

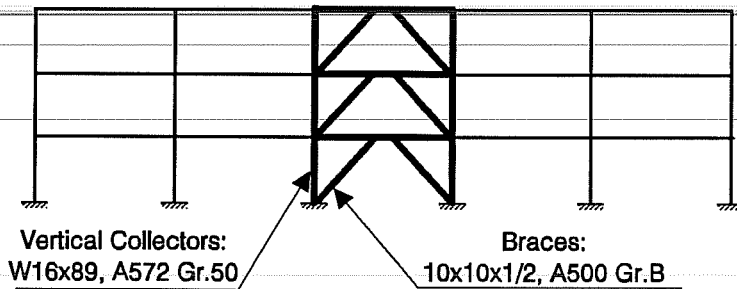


(e) EBF4 Configuration

Figure 5.9 Configuration of EBF Retrofit Schemes (Cont.)



(f) EBF4-S Configuration



	Beams and Links
Level 1	W24x76, A572 Gr.50
Level 2	W24x55, A36
Level 3	W14x38, A36

(g) EBF4-H Configuration

Figure 5.9 Configuration of EBF Retrofit Schemes (Cont.)

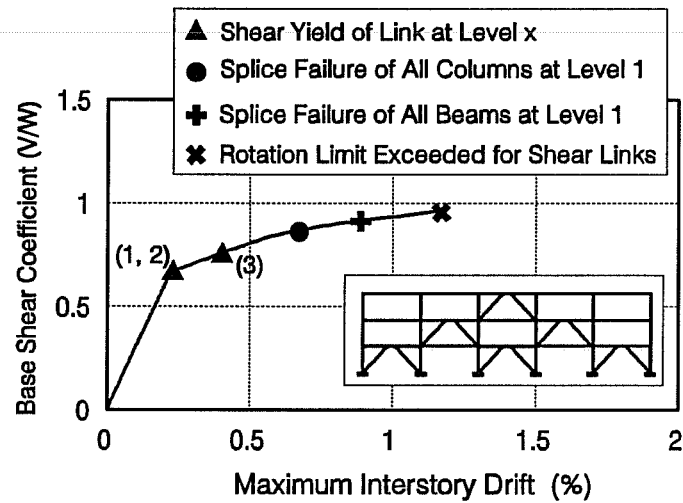


Figure 5.10 Maximum Interstory Drift for EBF1-1 Retrofit Scheme Subjected to Static Load

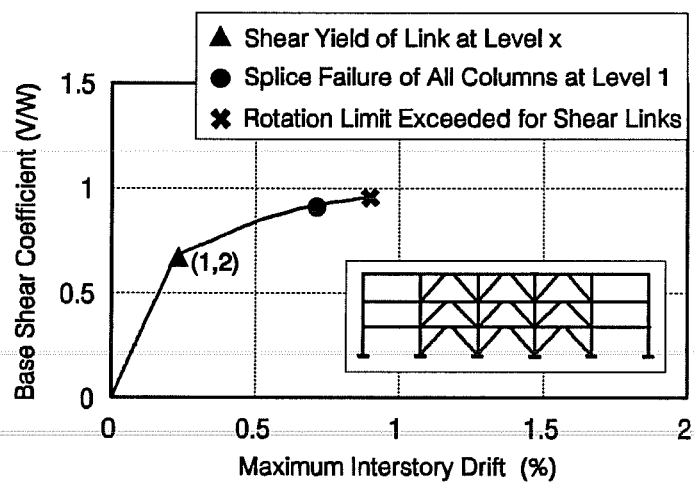


Figure 5.11 Maximum Interstory Drift for EBF2-1 Retrofit Scheme Subjected to Static Load

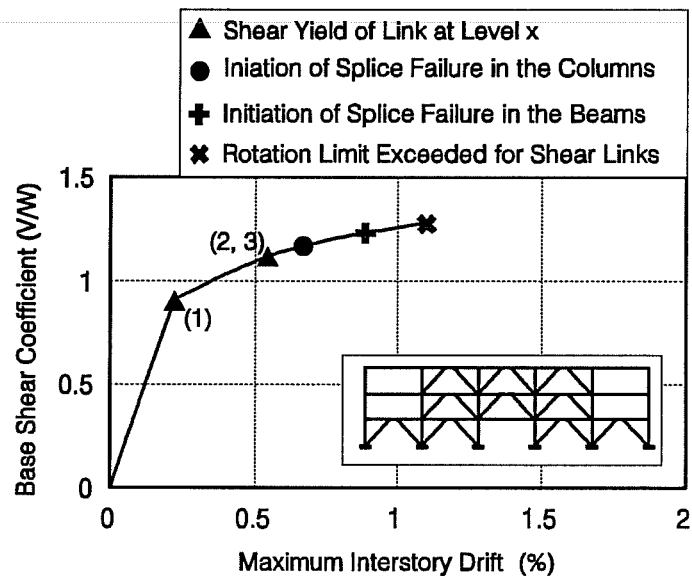


Figure 5.12 Maximum Interstory Drift for EBF3-1 Retrofit Scheme Subjected to Static Load

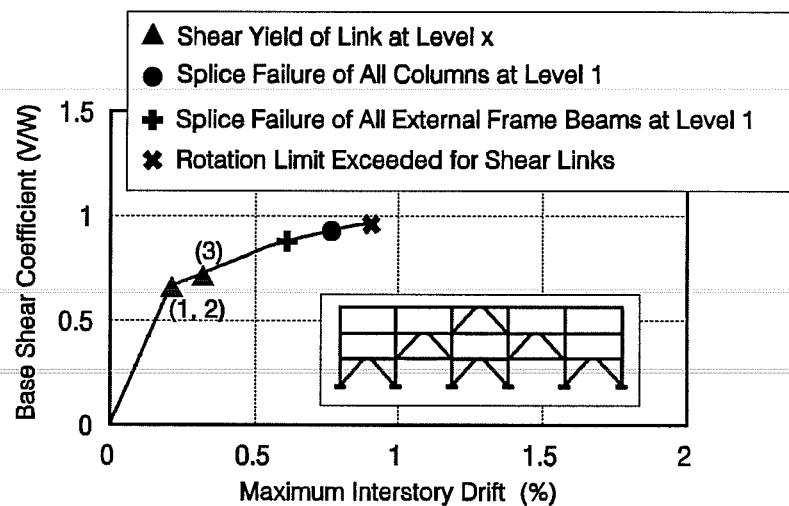


Figure 5.13 Maximum Interstory Drift for EBF1-.75 Retrofit Scheme Subjected to Static Load

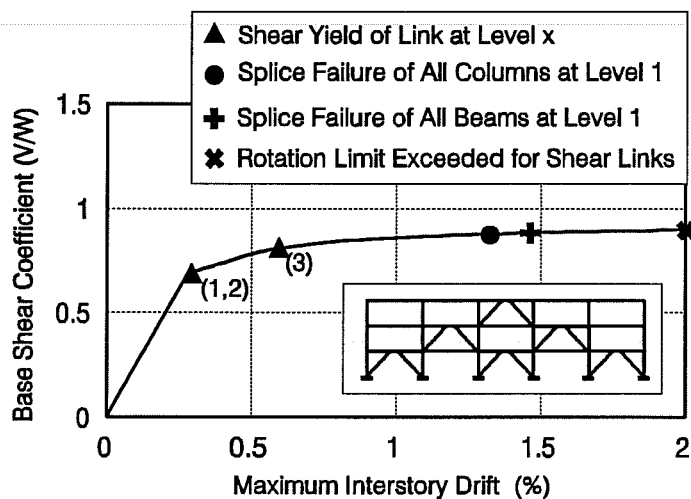


Figure 5.14 Maximum Interstory Drift for EBF1-1.5 Retrofit Scheme Subjected to Static Load

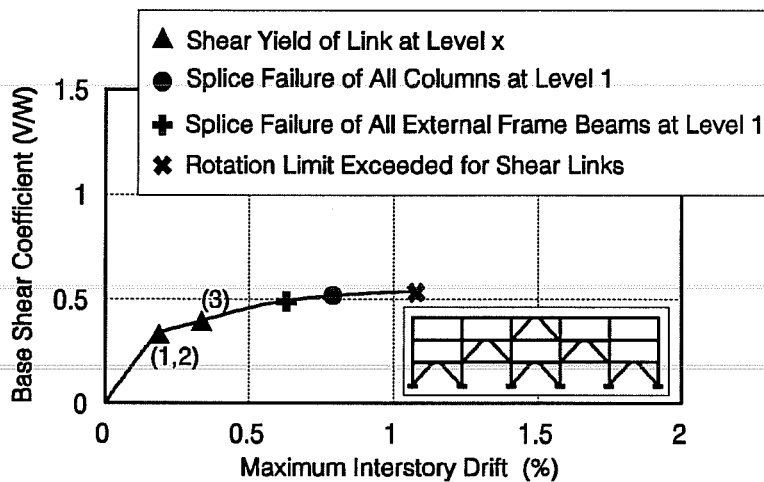


Figure 5.15 Maximum Interstory Drift for EBF1-1S Retrofit Scheme Subjected to Static Load

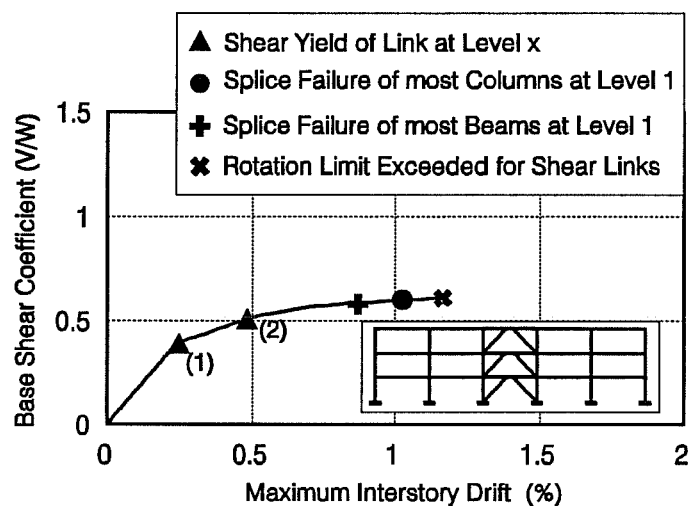


Figure 5.16 Maximum Interstory Drift for EBF4
Retrofit Scheme Subjected to Static Load

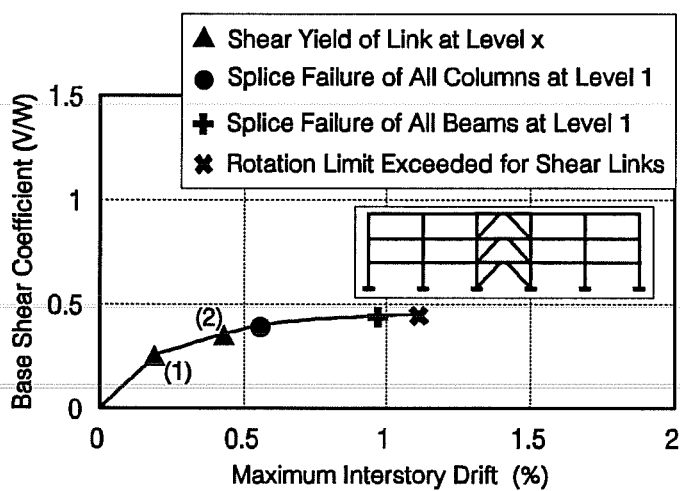


Figure 5.17 Maximum Interstory Drift for EBF4-S
Retrofit Scheme Subjected to Static Load

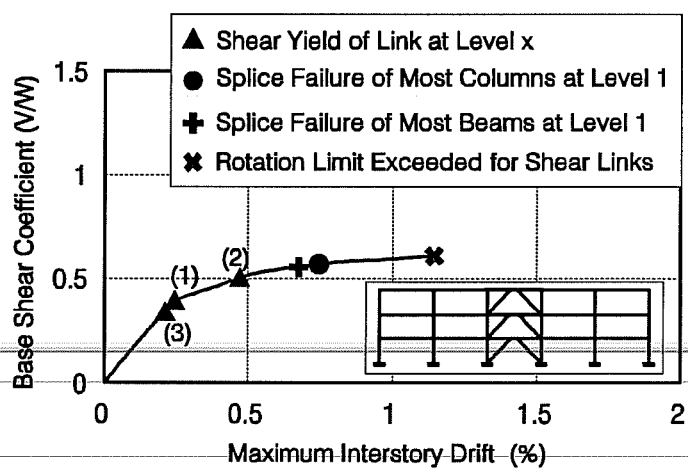


Figure 5.18 Maximum Interstory Drift for EBF4-H Retrofit Scheme Subjected to Static Load

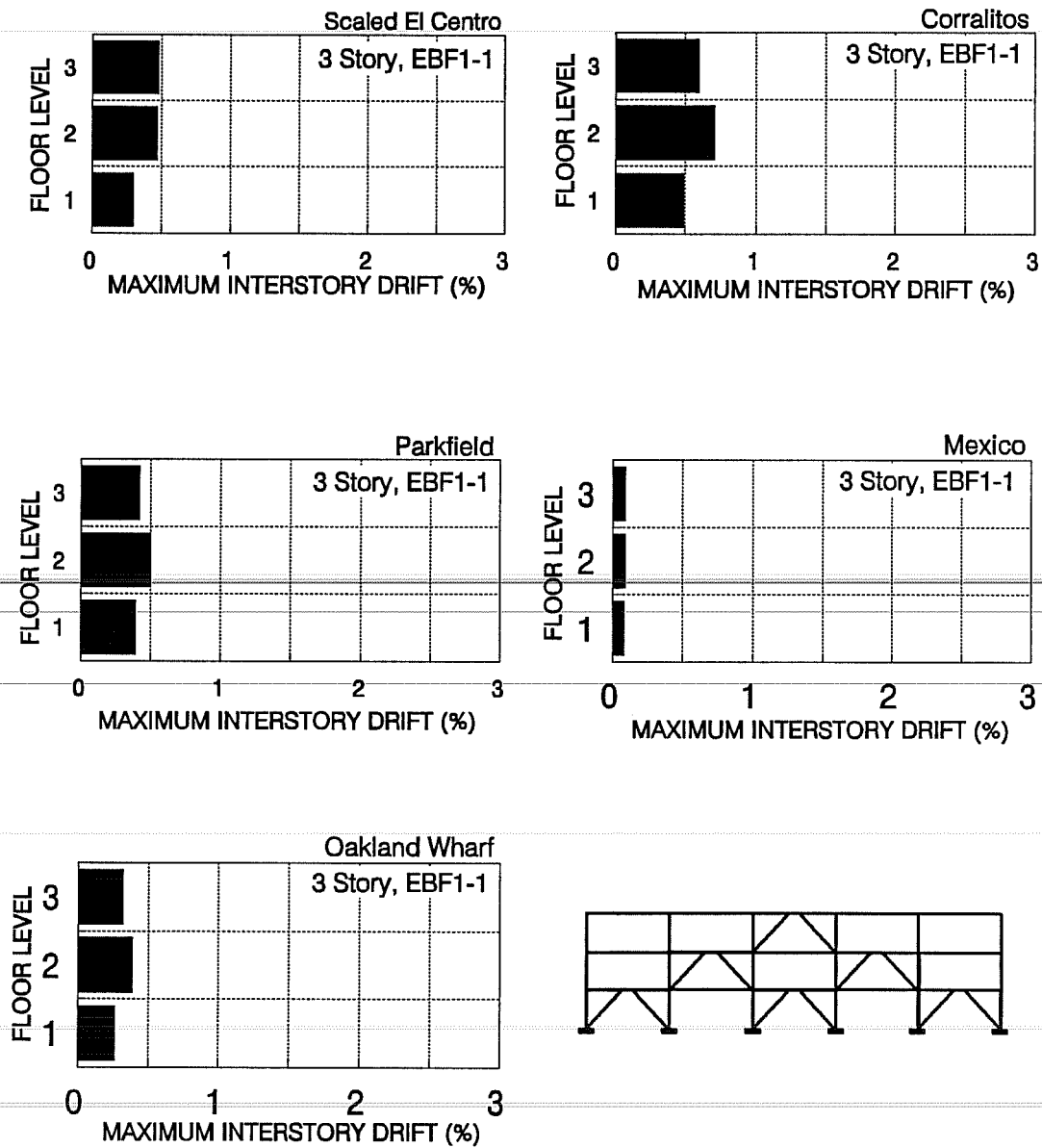


Figure 5.19 Maximum Interstory Drifts for the EBF1-1 Retrofit Scheme Subjected to the Selected Acceleration Records

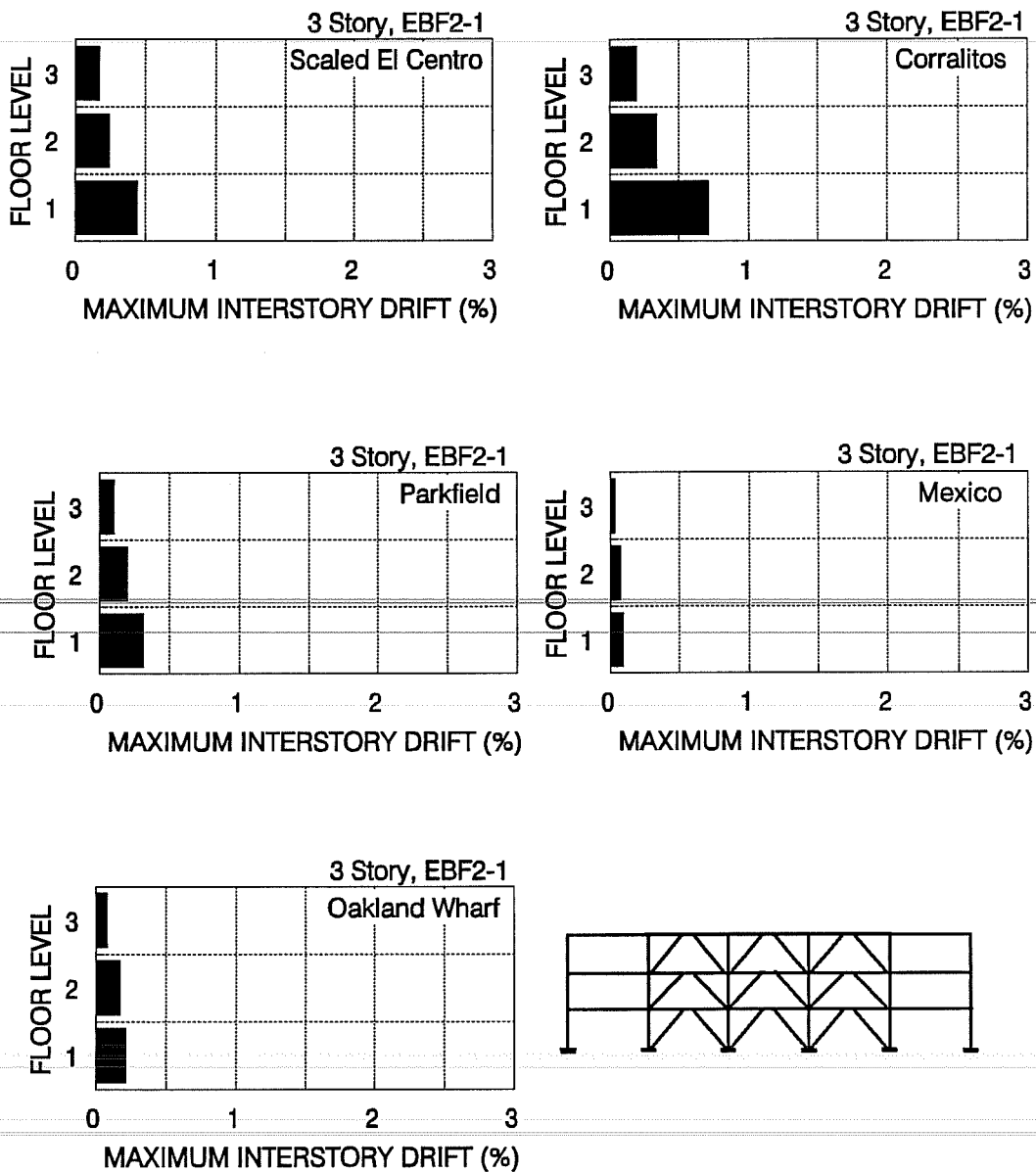


Figure 5.20 Maximum Interstory Drifts for EBF2-1 Retrofit Scheme Subjected to the Selected Acceleration Records

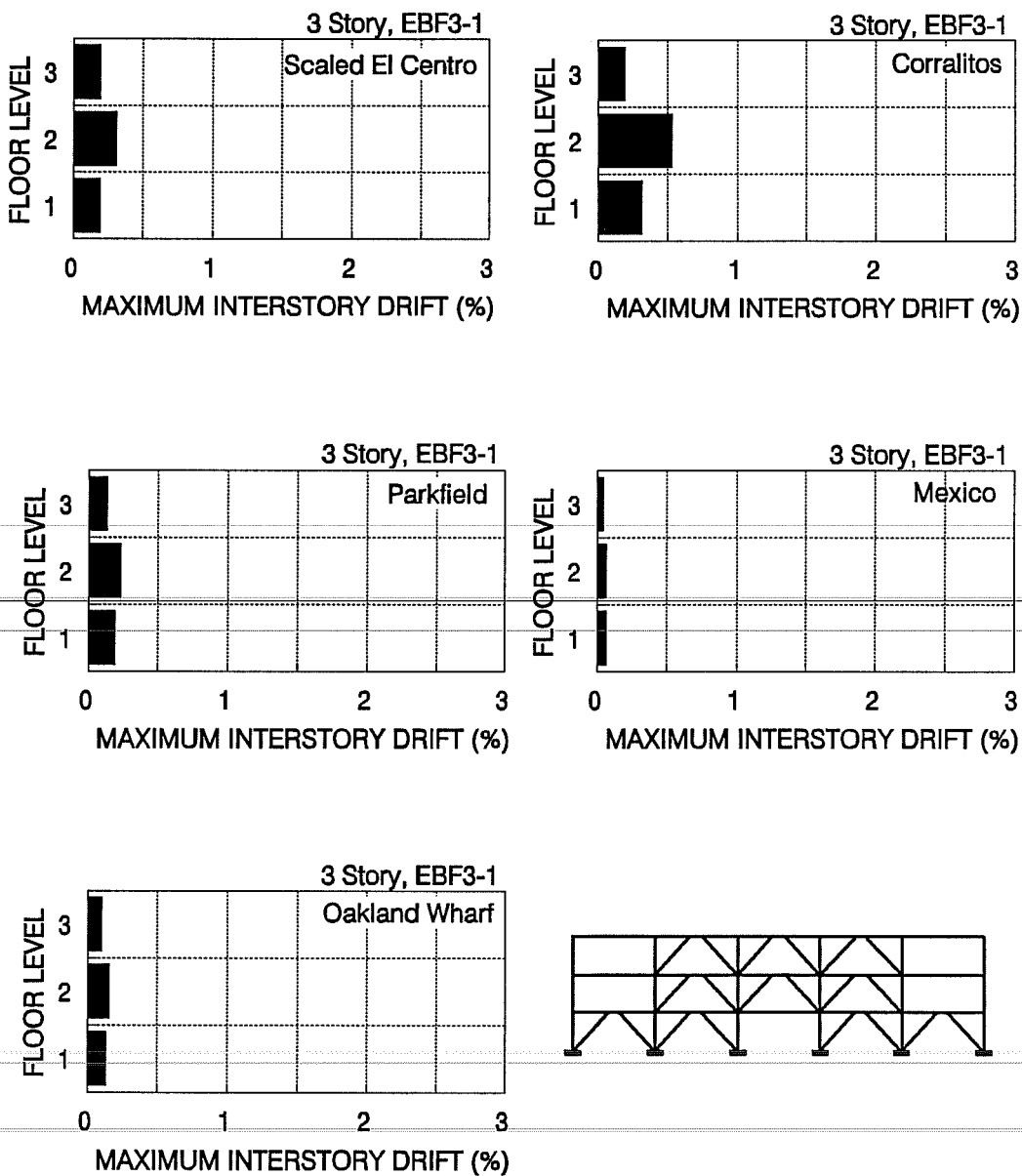


Figure 5.21 Maximum Interstory Drifts for EBF3-1 Retrofit Scheme Subjected to the Selected Acceleration Records

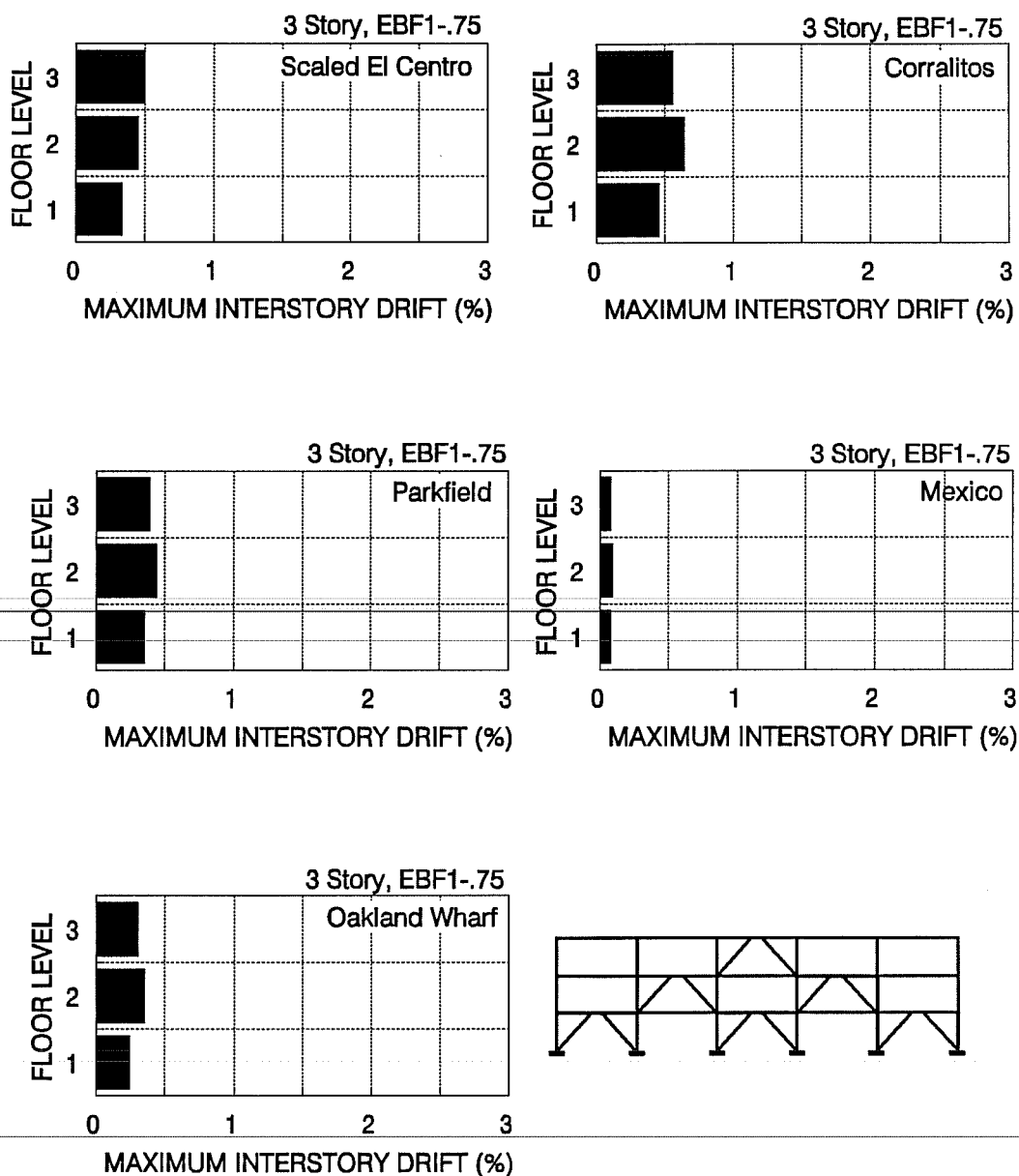


Figure 5.22 Maximum Interstory Drifts for EBF1-.75 Retrofit Scheme Subjected to the Selected Acceleration Records

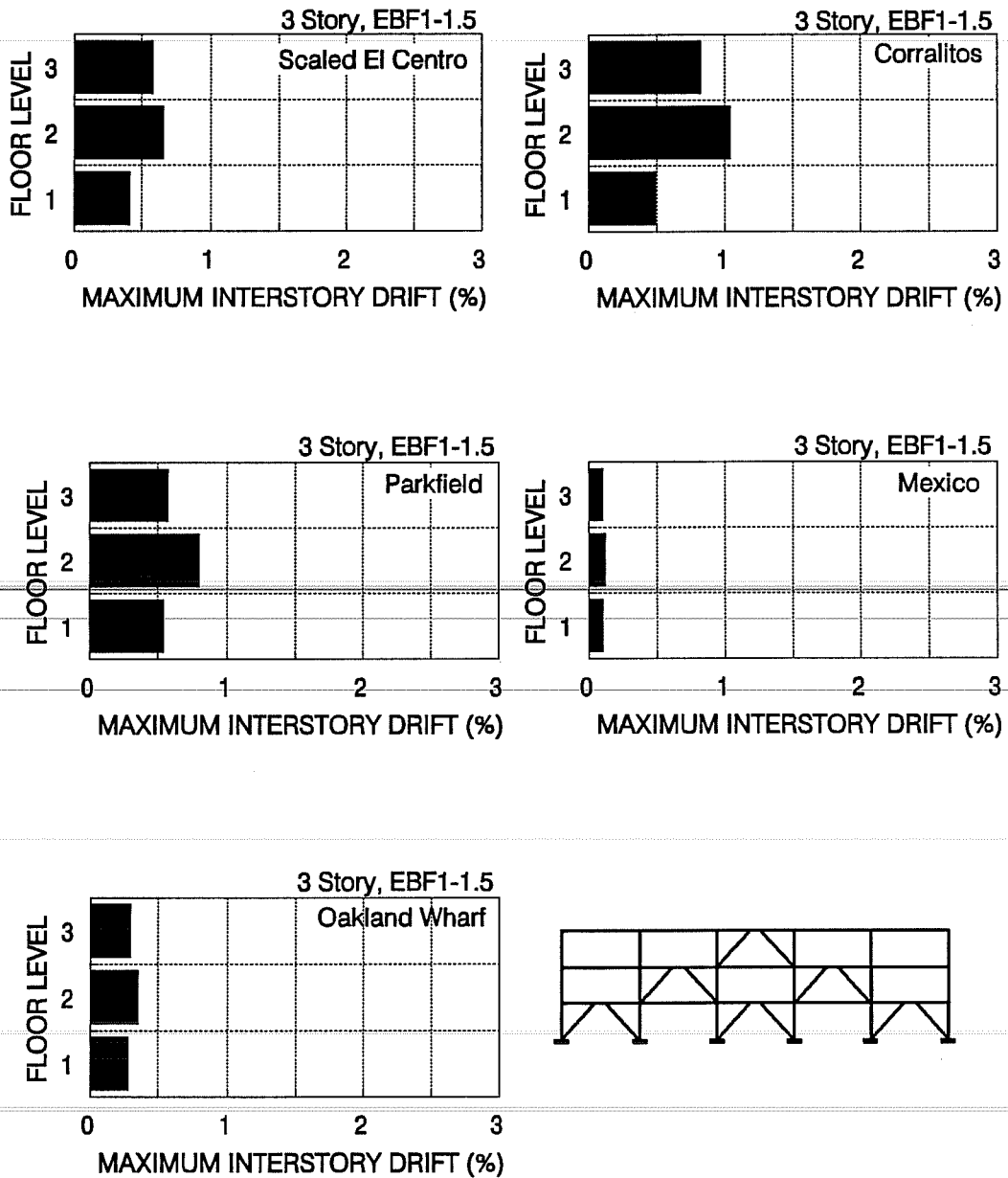


Figure 5.23 Maximum Interstory Drifts for EBF1-1.5 Retrofit Scheme Subjected to the Selected Acceleration Records

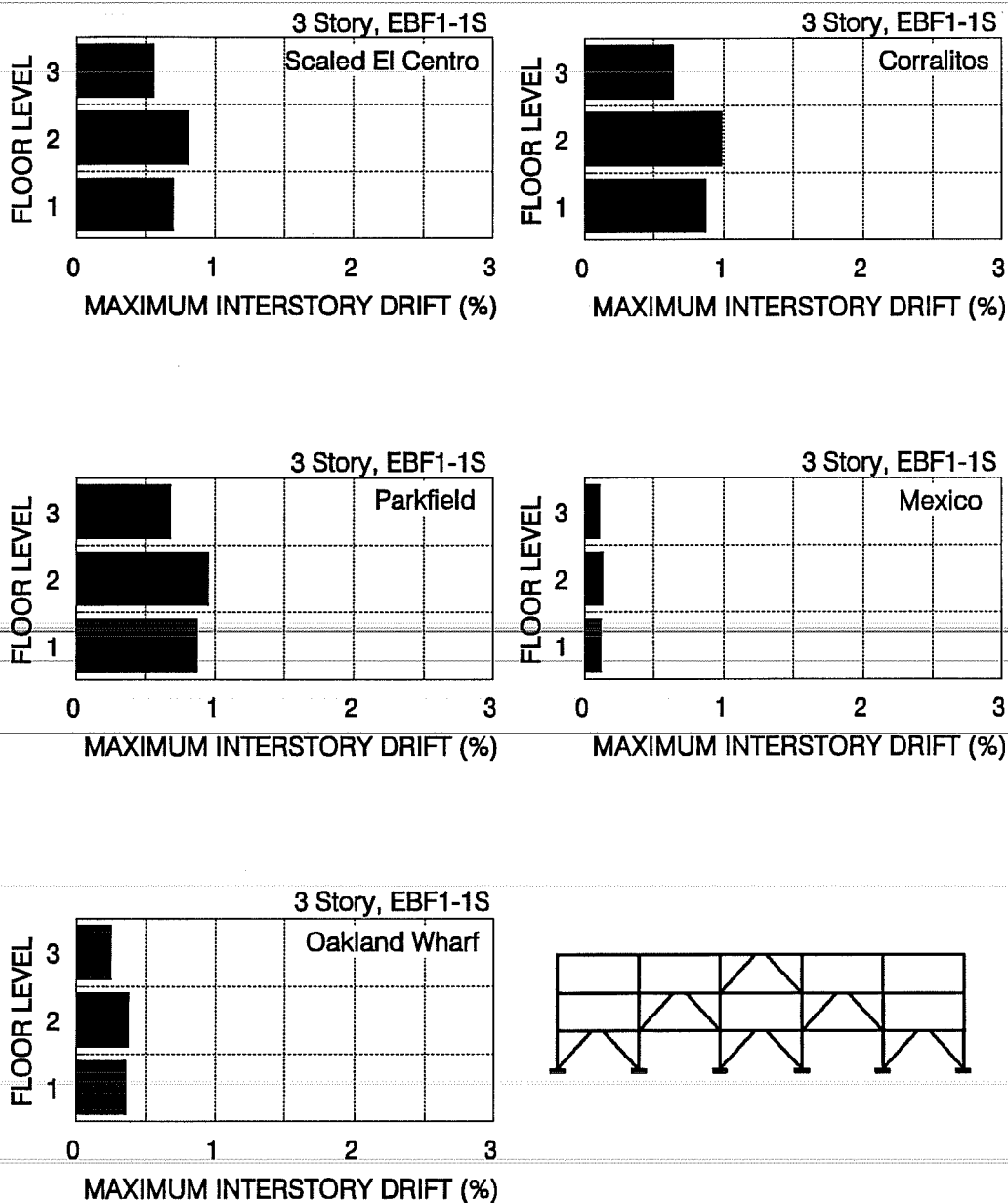


Figure 5.24 Maximum Interstory Drifts for EBF1-1S Retrofit Scheme Subjected to the Selected Acceleration Records

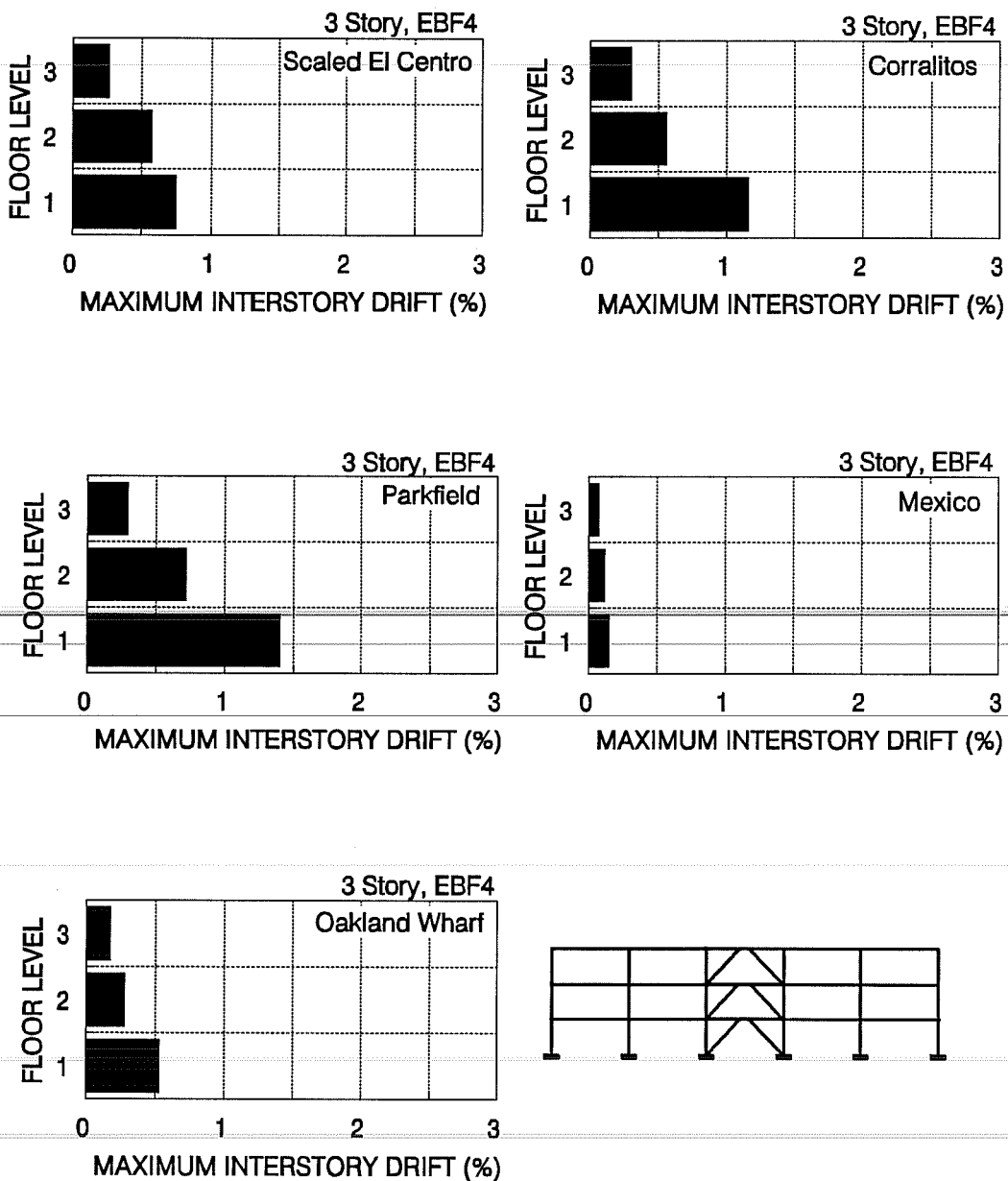


Figure 5.25 Maximum Interstory Drifts for EBF4 Retrofit Scheme Subjected to the Selected Acceleration Records

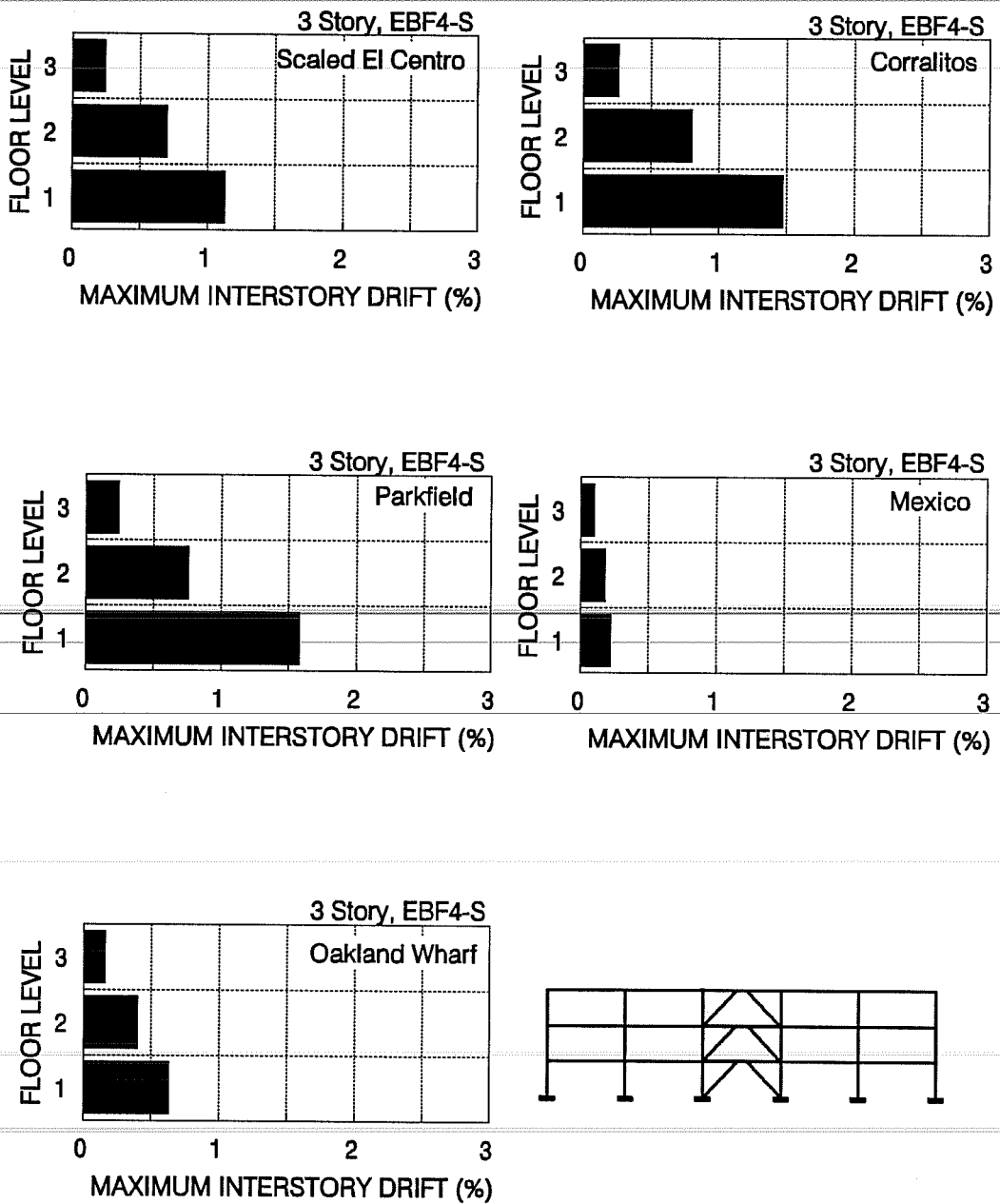


Figure 5.26 Maximum Interstory Drifts for EBF4-S Retrofit Scheme Subjected to the Selected Acceleration Records

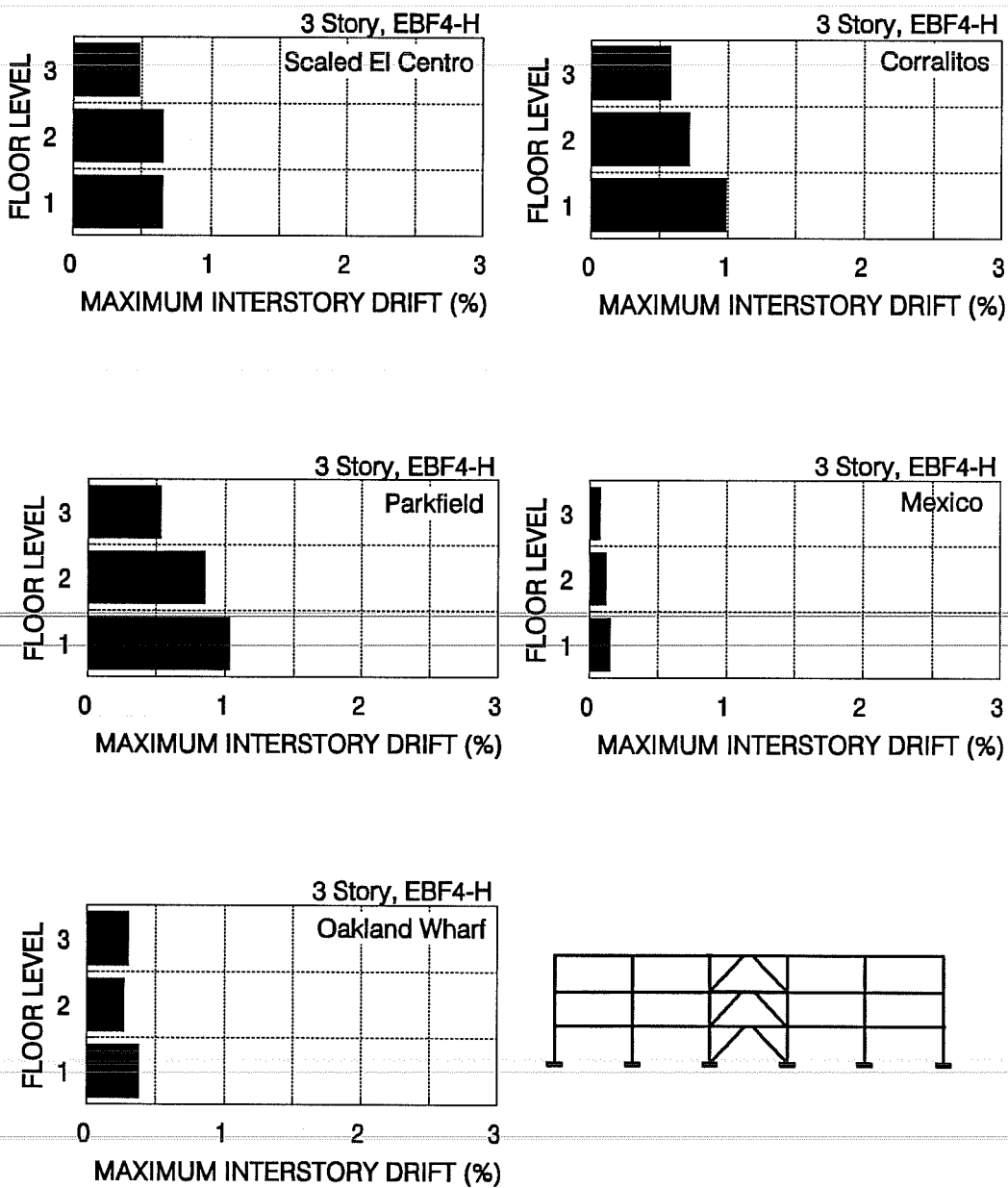


Figure 5.27 Maximum Interstory Drifts for EBF4-H Retrofit Scheme Subjected to the Selected Acceleration Records

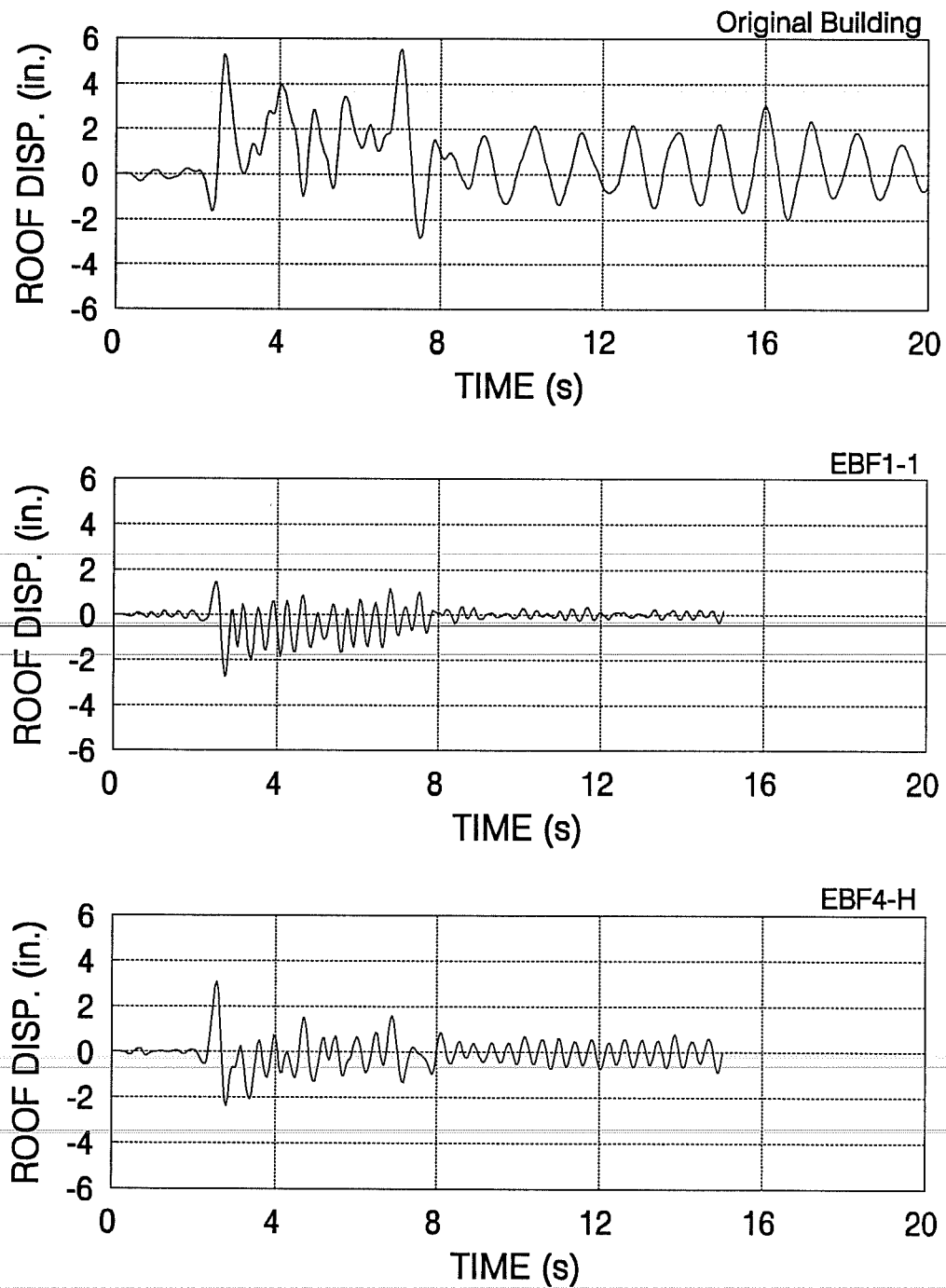


Figure 5.28 Roof Displacement of the Original Three-Story Building and of EBF1-1 and EBF4-H Retrofit Schemes Under Corralitos Record

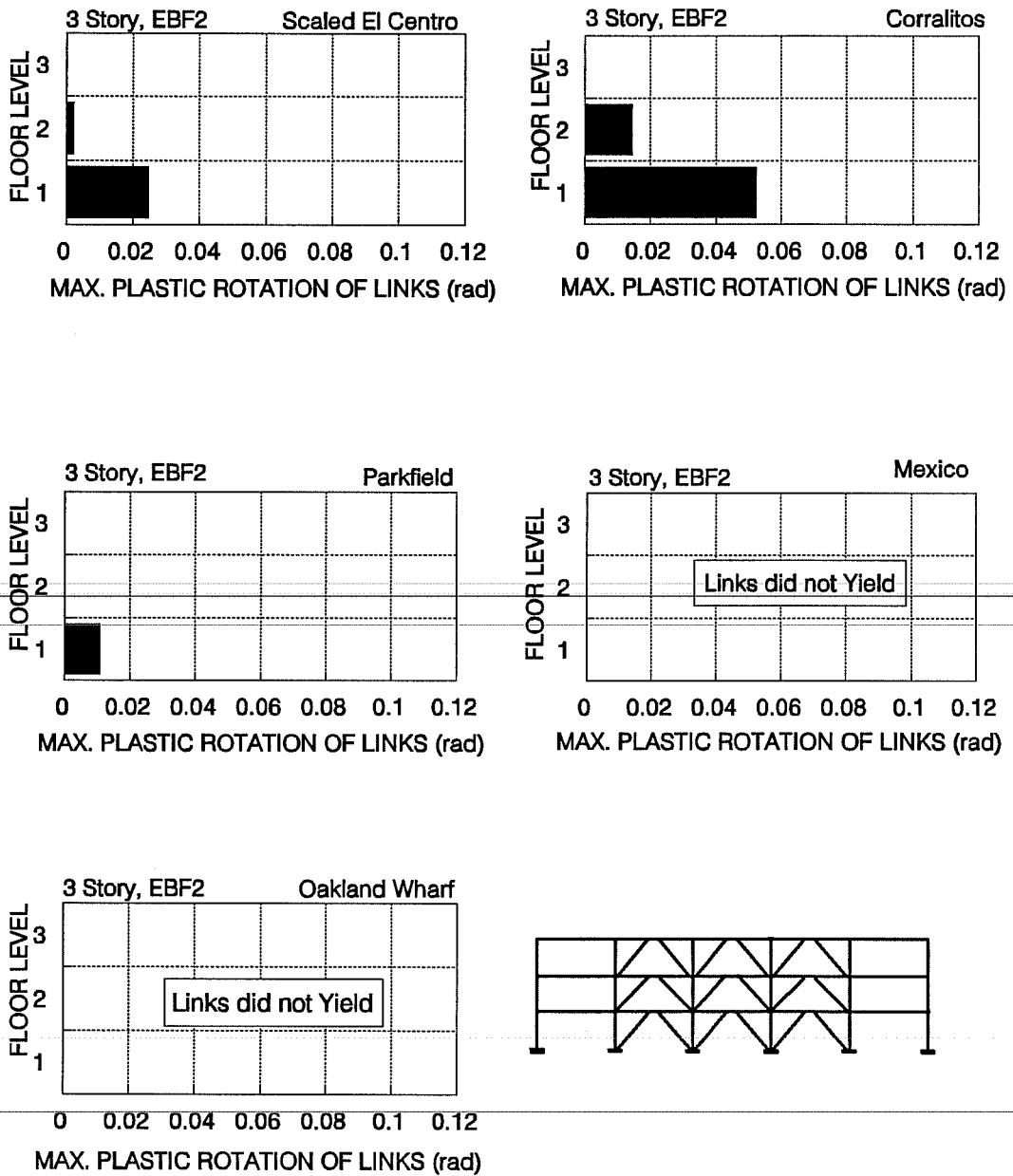


Figure 5.29 Maximum Plastic Rotation in Links of EBF2 Subjected to the Selected Ground Accelerations

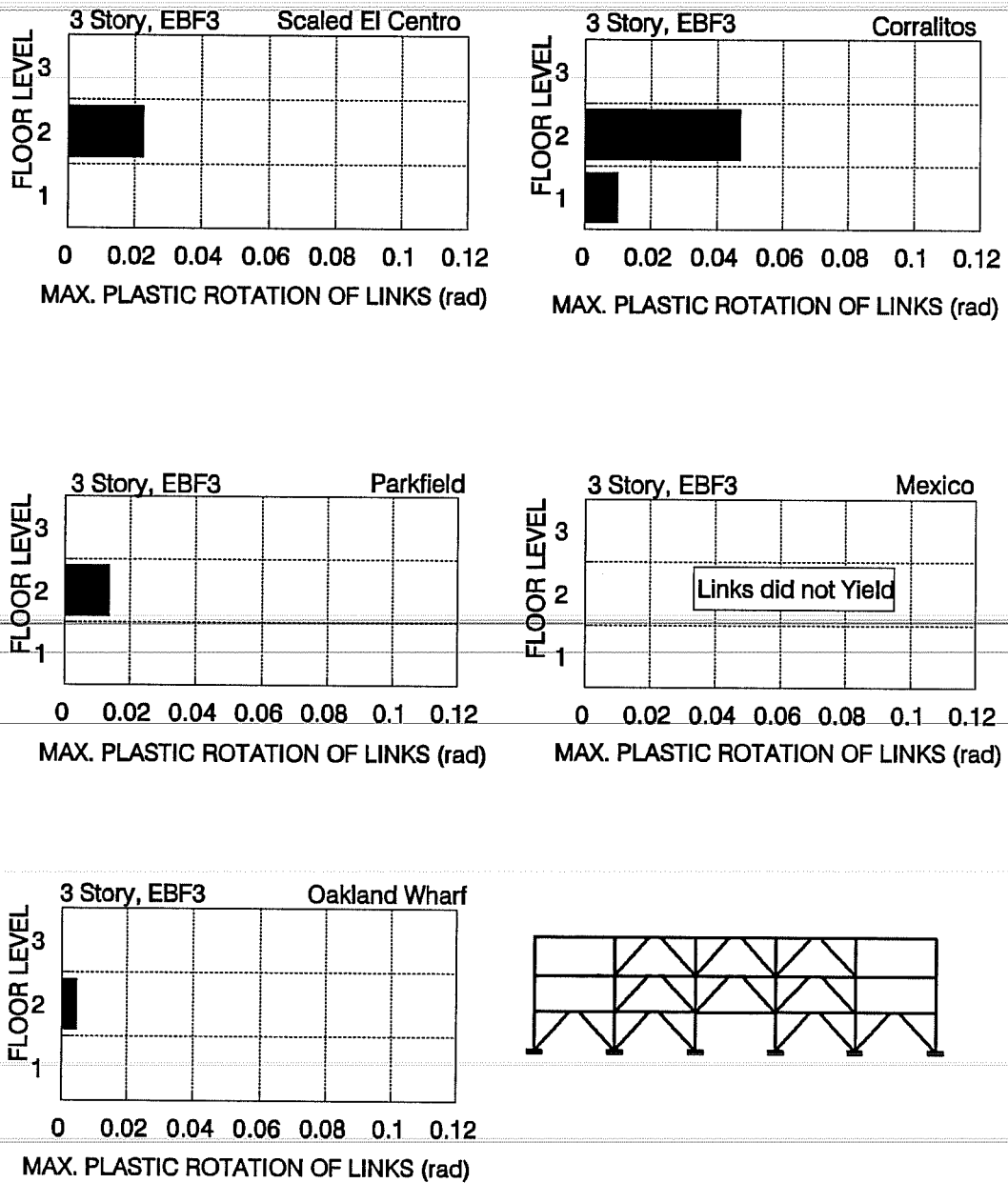


Figure 5.30 Maximum Plastic Rotation in Links of EBF3 Subjected to the Selected Ground Accelerations

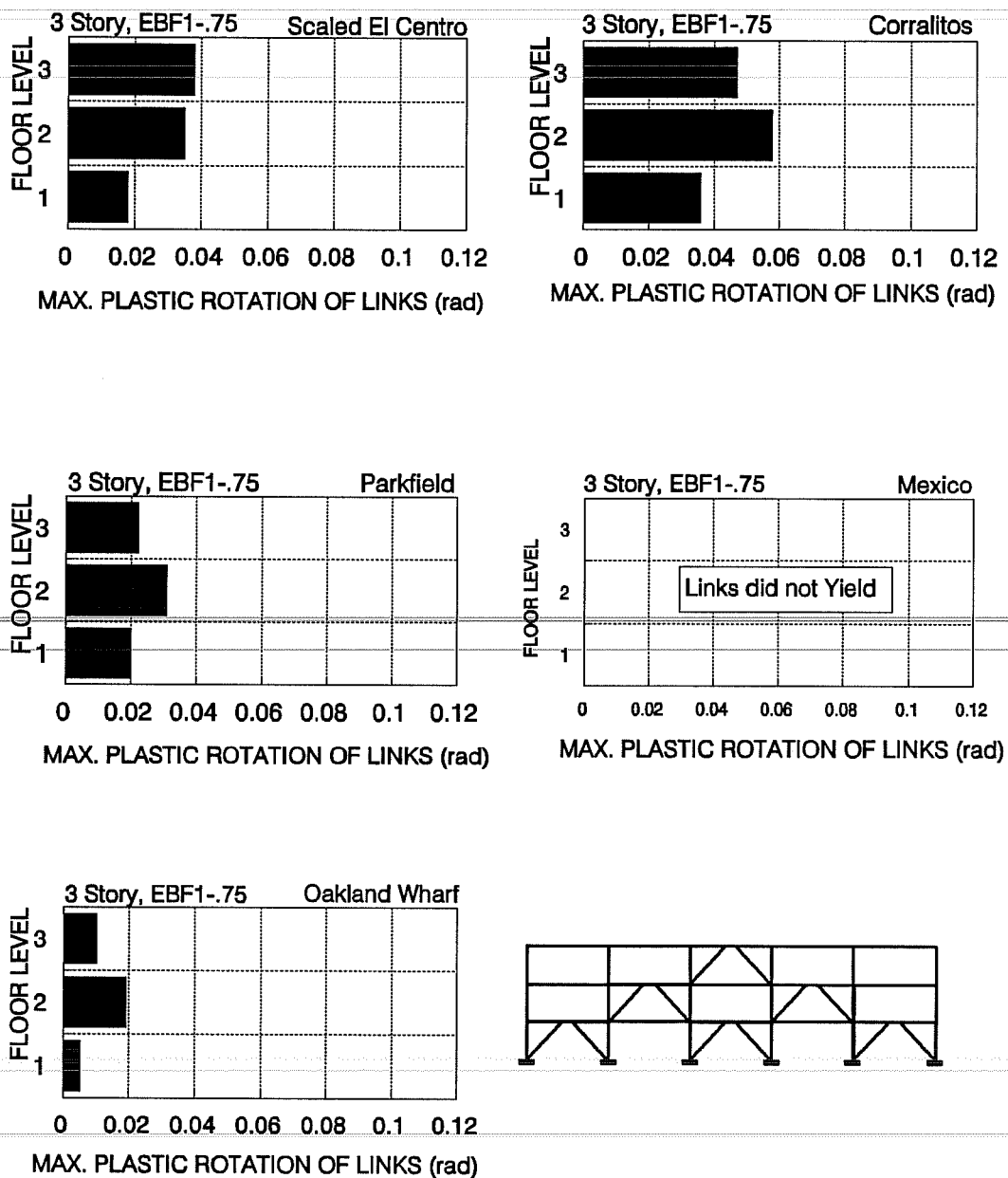


Figure 5.31 Maximum Plastic Rotation in Links of EBF1-.75 Subjected to the Selected Ground Accelerations

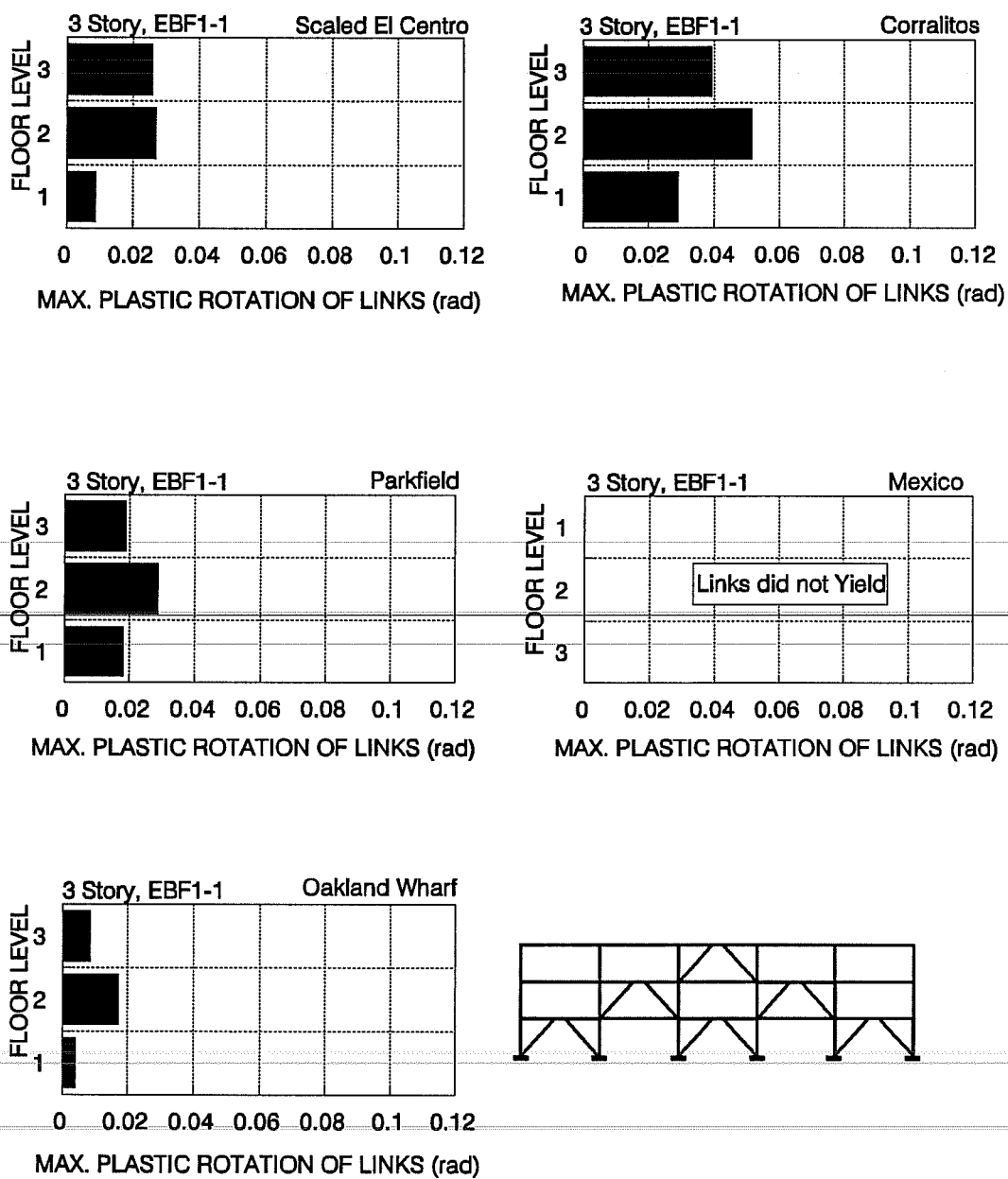


Figure 5.32 Maximum Plastic Rotation in Links of EBF1-1 Subjected to the Selected Ground Accelerations

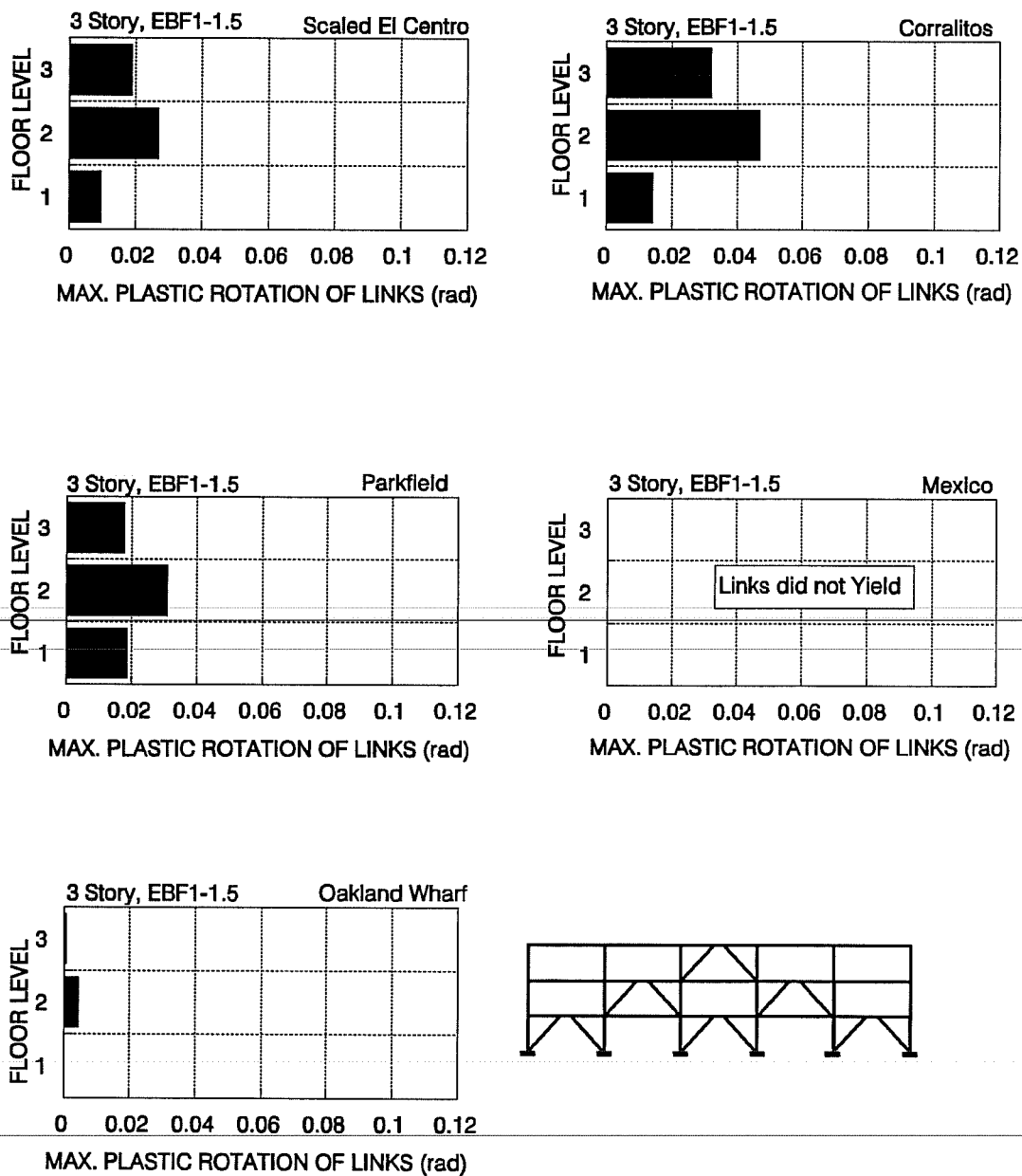


Figure 5.33 Maximum Plastic Rotation in Links of EBF1-1.5 Subjected to the Selected Ground Accelerations

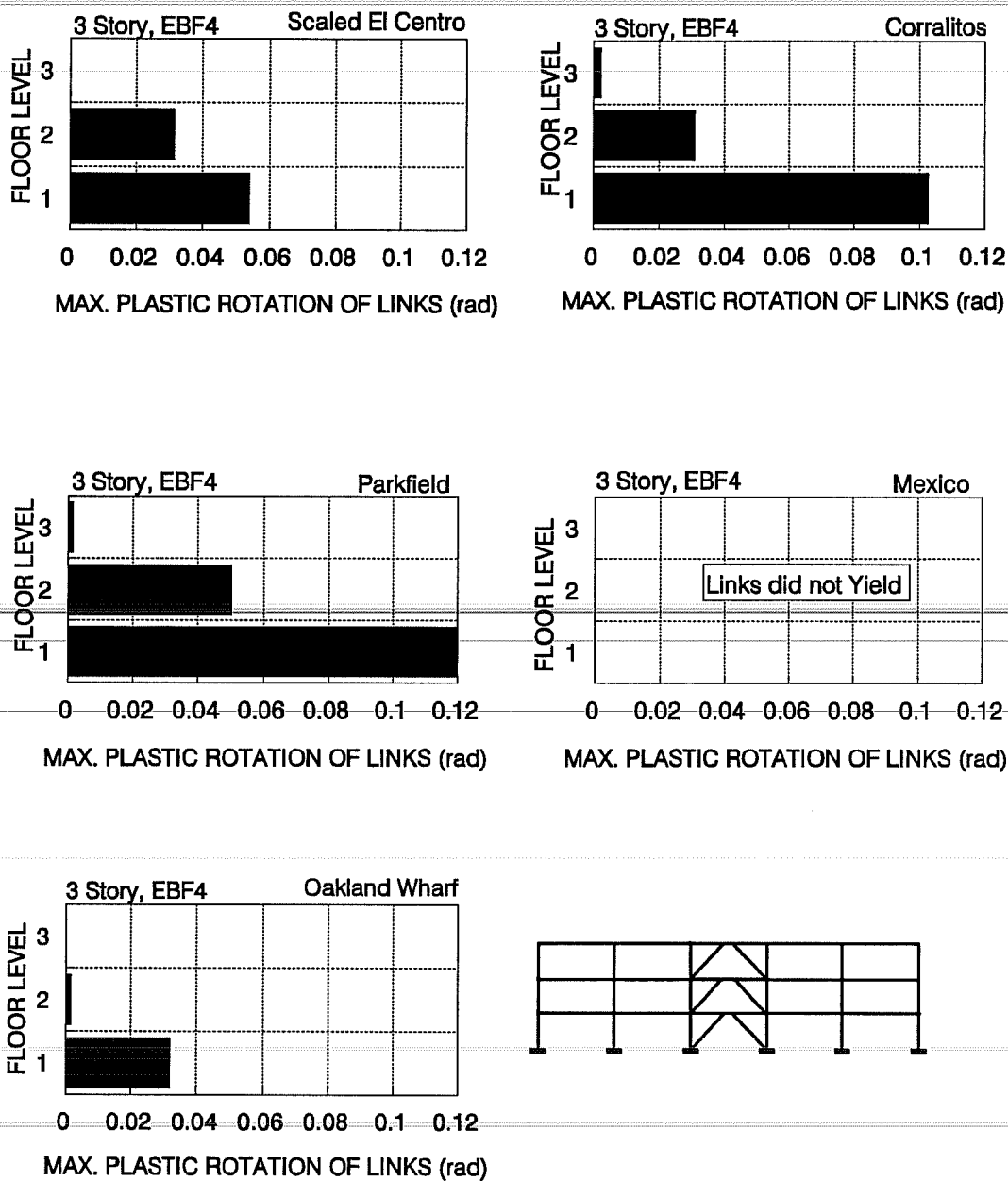


Figure 5.34 Maximum Plastic Rotation in Links of EBF4 Subjected to the Selected Ground Accelerations

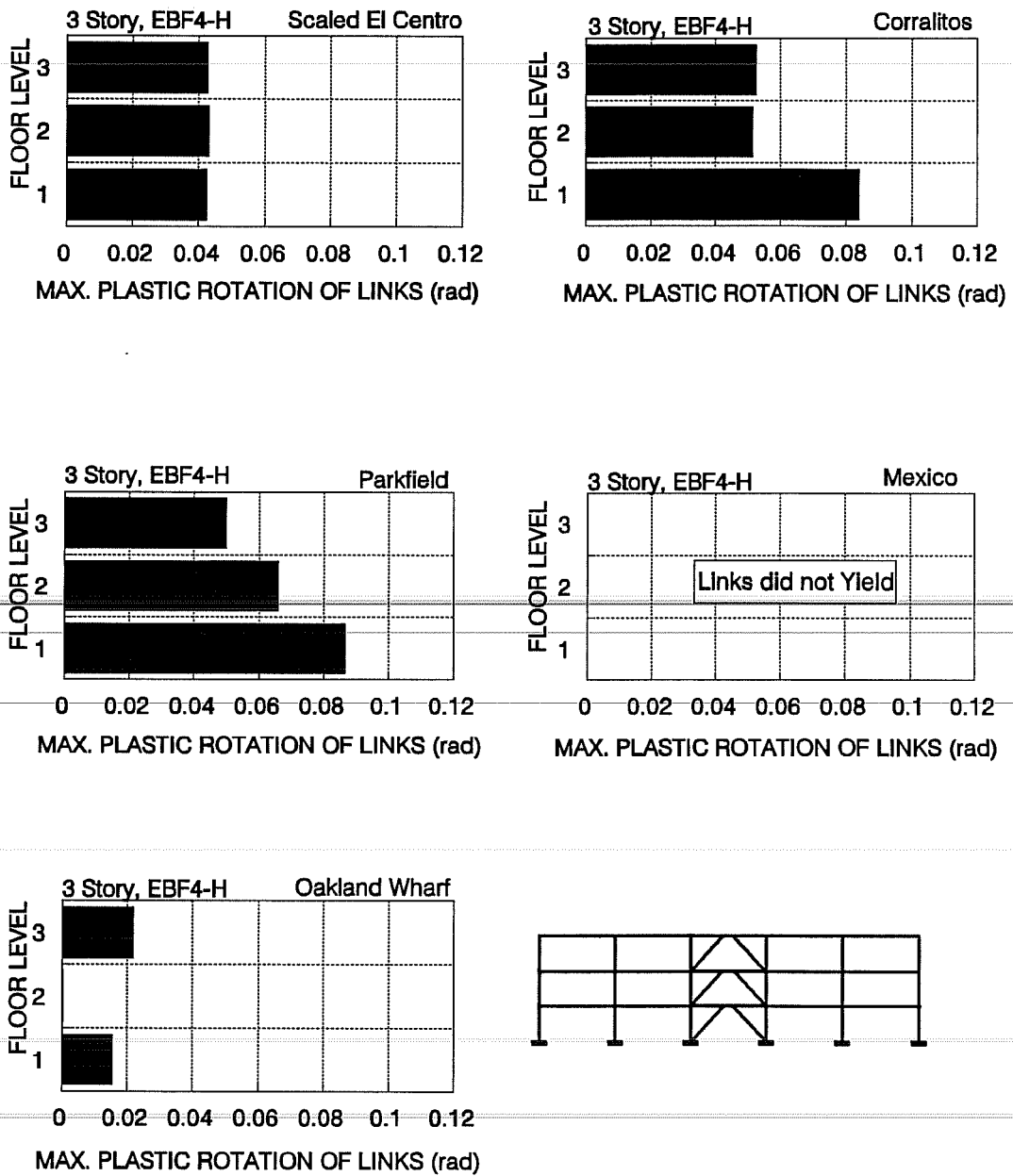


Figure 5.35 Maximum Plastic Rotation in Links of EBF4-H Subjected to the Selected Ground Accelerations

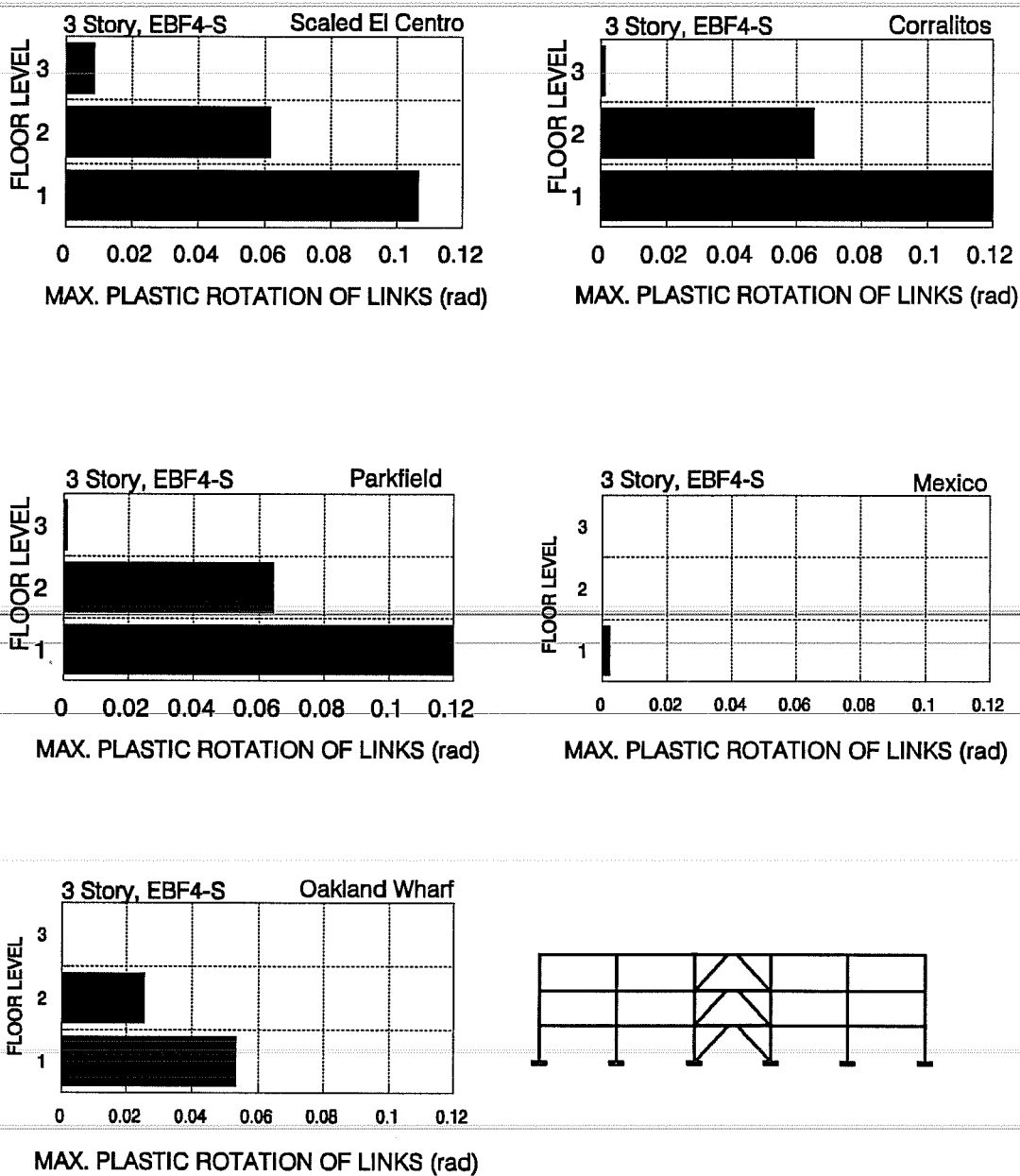


Figure 5.36 Maximum Plastic Rotation in Links of EBF4-S Subjected to the Selected Ground Accelerations

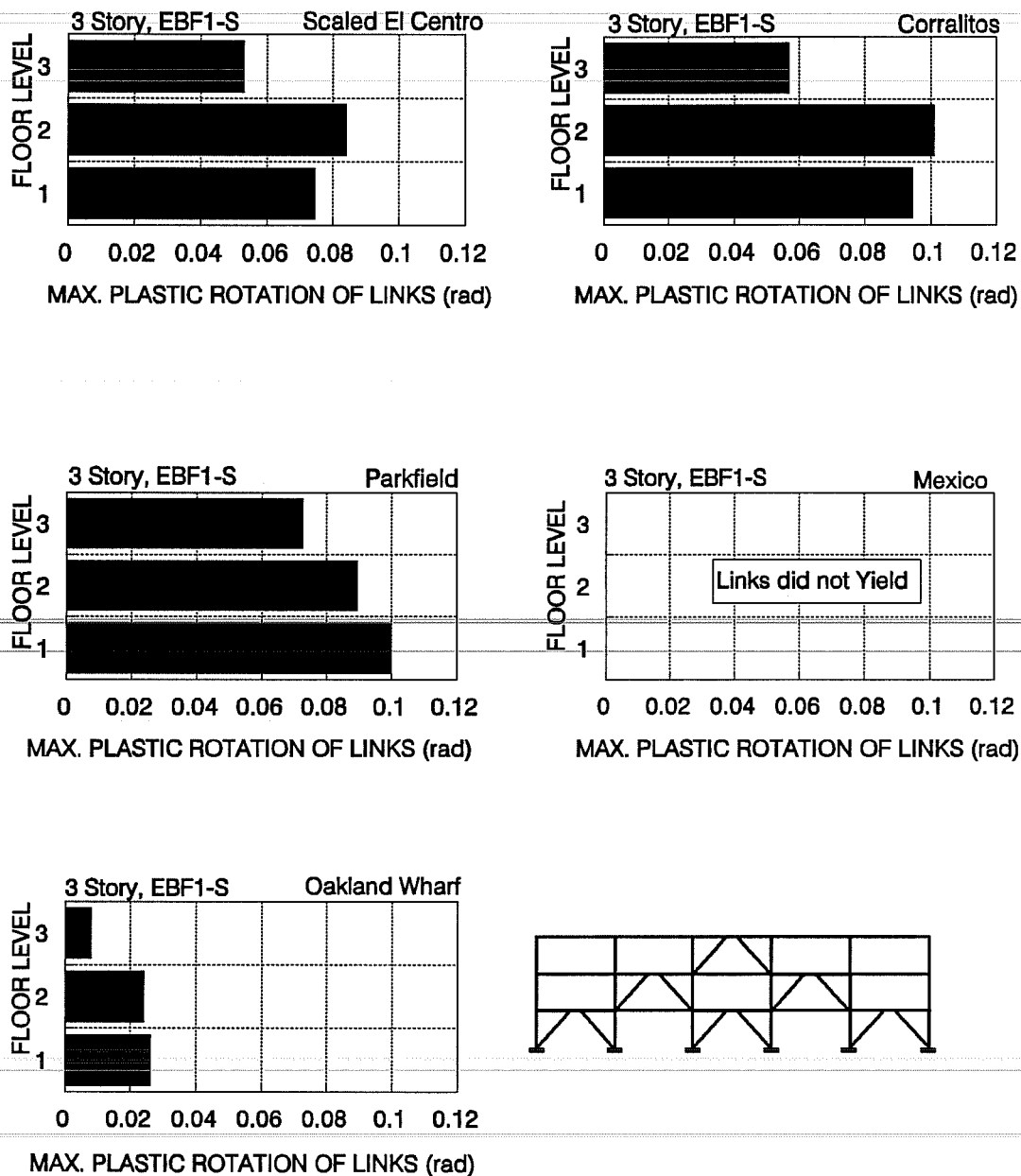


Figure 5.37 Maximum Plastic Rotation in Links of EBF1-S Subjected to the Selected Ground Accelerations

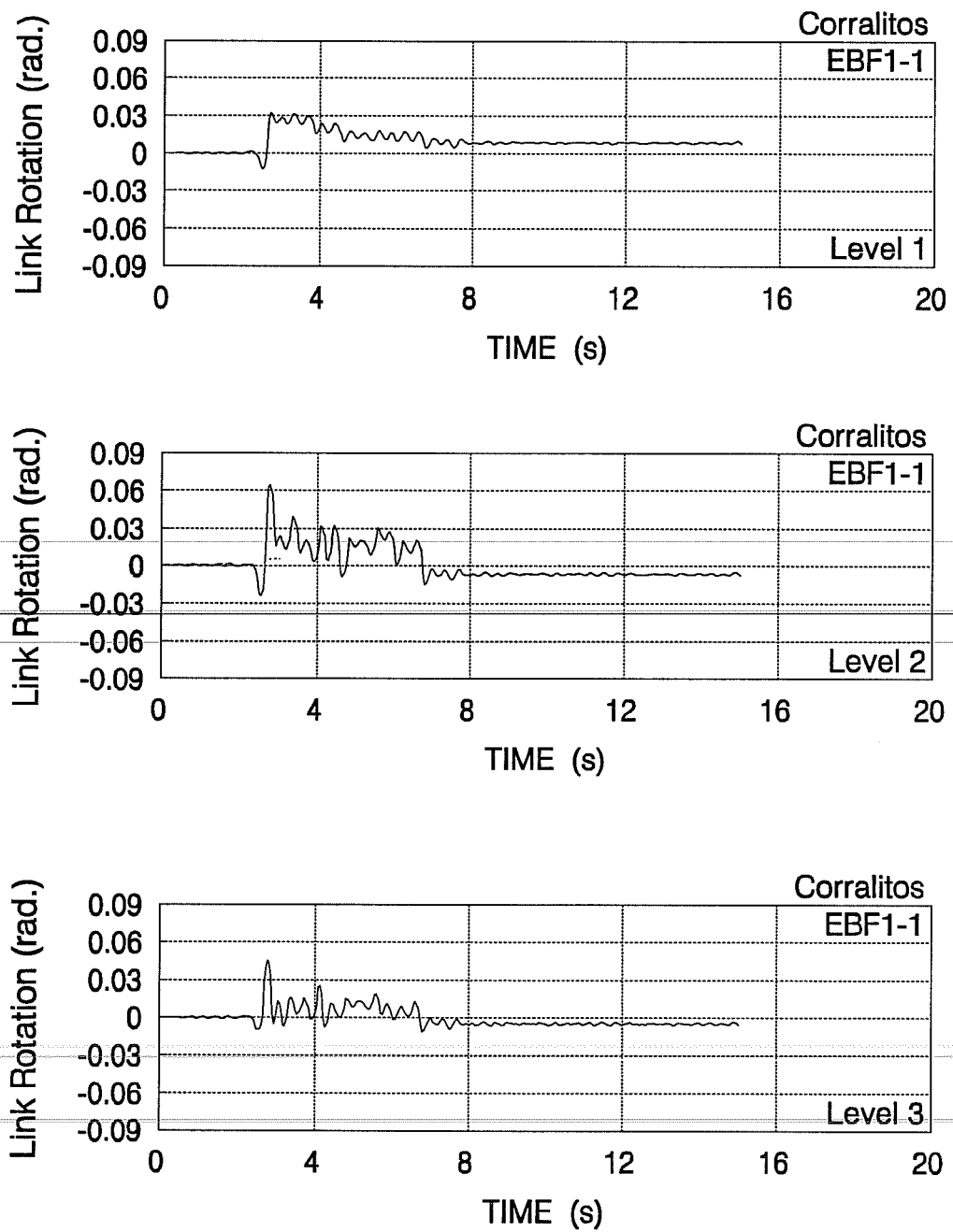


Figure 5.38 Link End Rotations of EBF1-1 Subjected to Corralitos Record

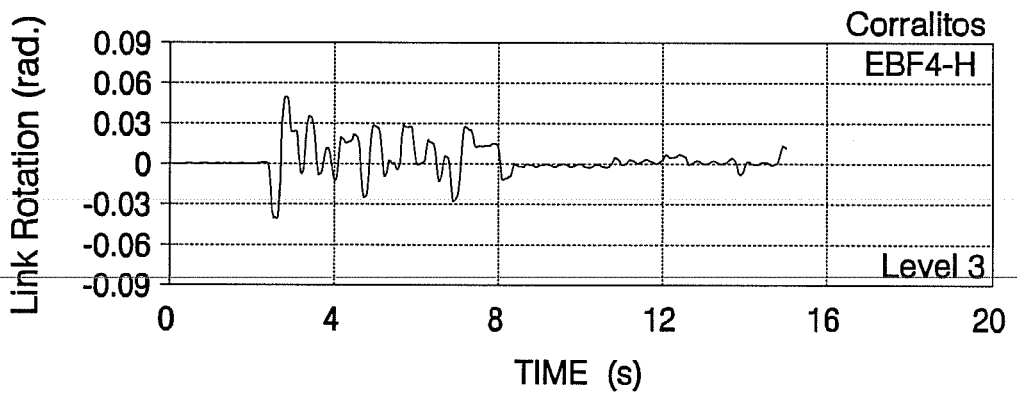
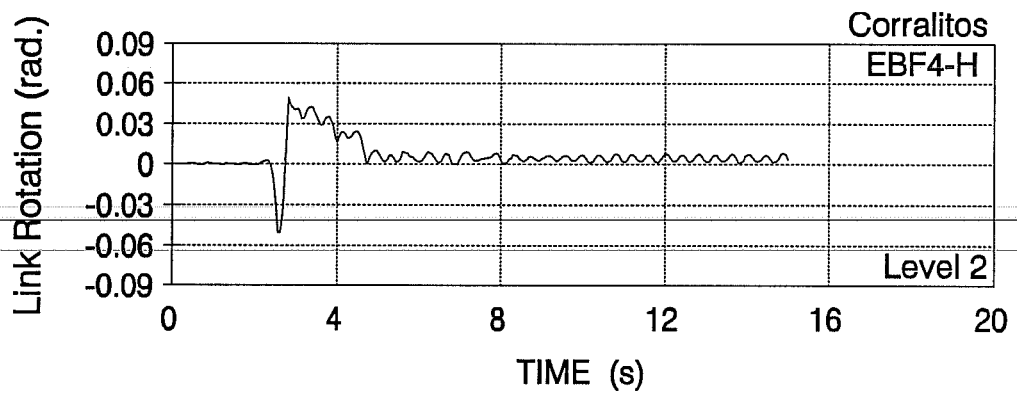
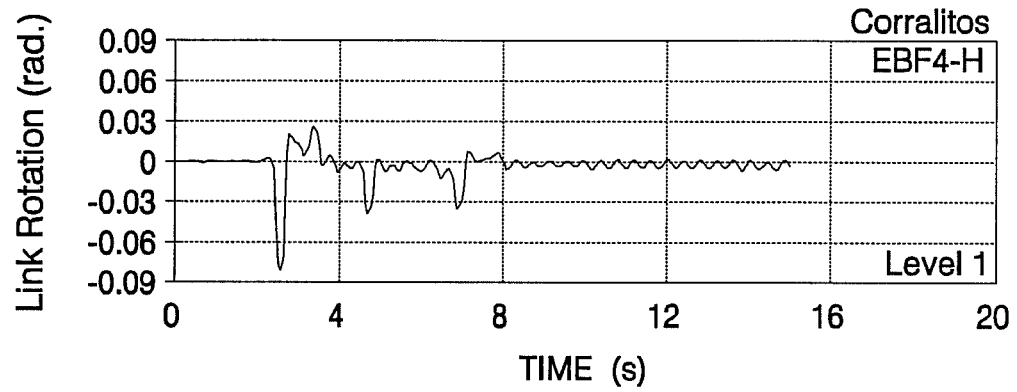
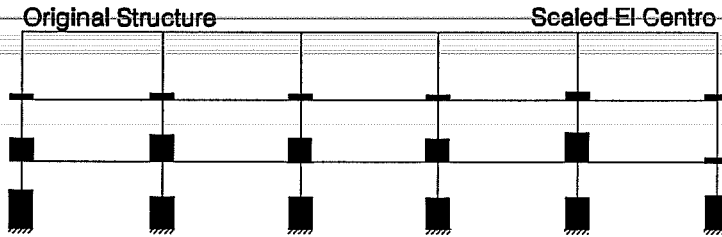
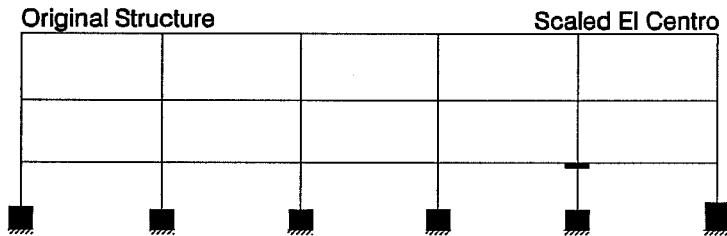


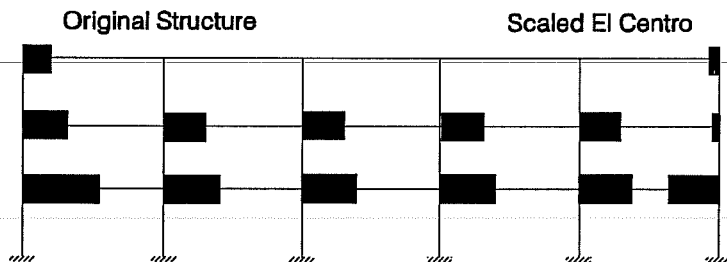
Figure 5.39 Link Rotations of EBF4-H Subjected to Corralitos Record



(a) Columns in Positive Bending



(b) Columns in Negative Bending



(c) Beams in Positive Bending

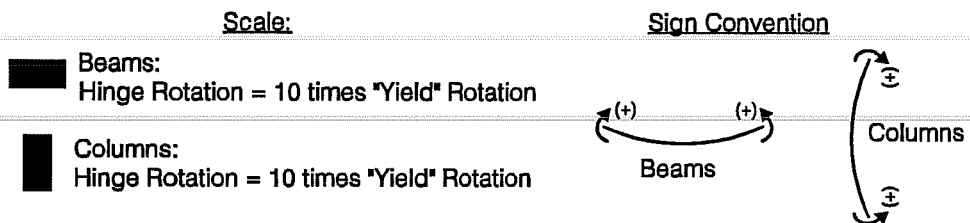
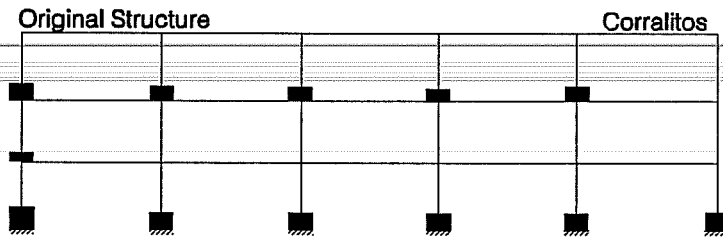
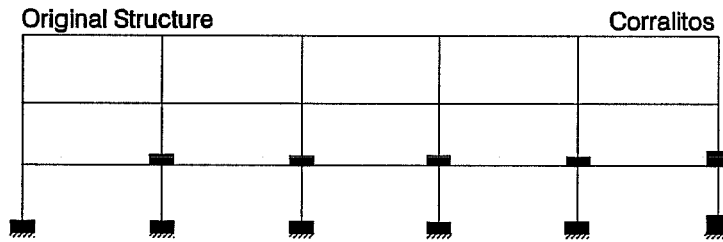


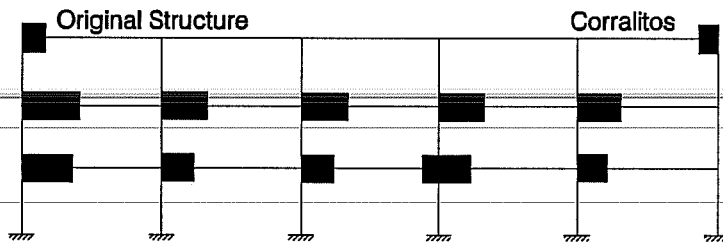
Figure 5.40 Ductility Demands in the Original Three-Story Building Subjected to the Scaled EI Centro Record



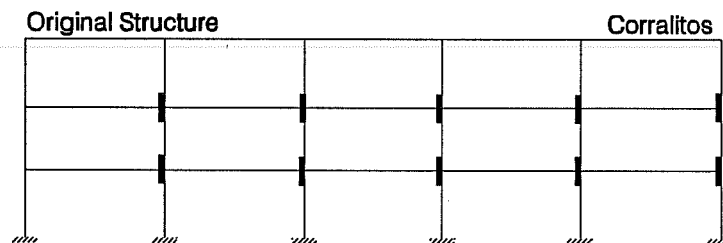
(a) Columns in Positive Bending



(b) Columns in Negative Bending



(c) Beams in Positive Bending



(d) Beams in Negative Bending

Scale:

- Beams:
Hinge Rotation = 10 times "Yield" Rotation
- Columns:
Hinge Rotation = 10 times "Yield" Rotation

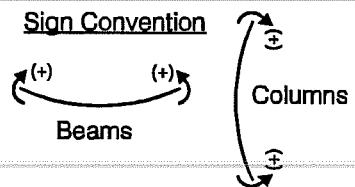


Figure 5.41 Ductility Demands in the Original Three-Story Building Subjected to the Corralitos Record

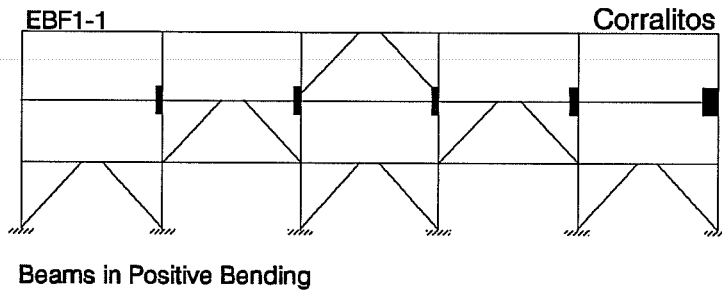


Figure 5.42 Ductility Demands in the Reinforced Concrete Members in EBF1-1 Subjected to the Corralitos Record

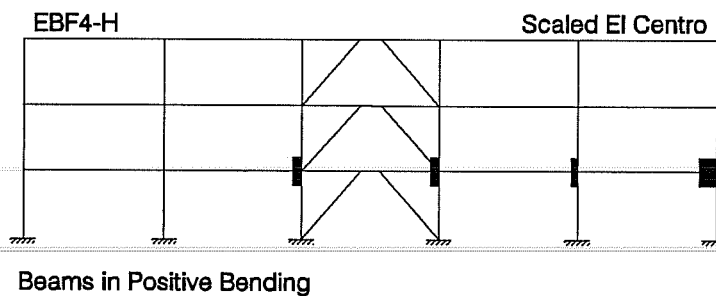
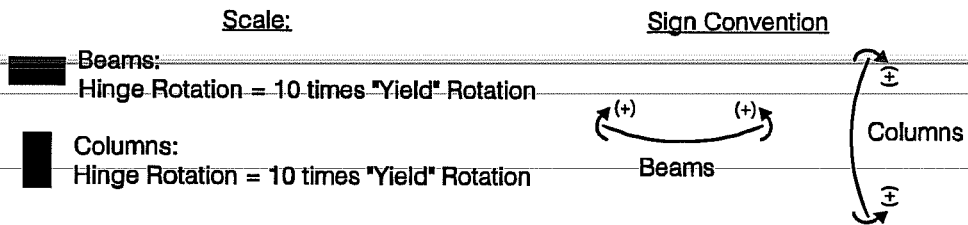
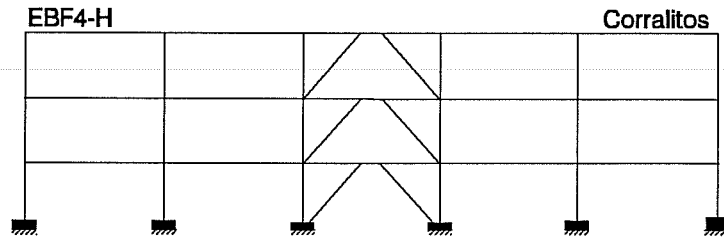
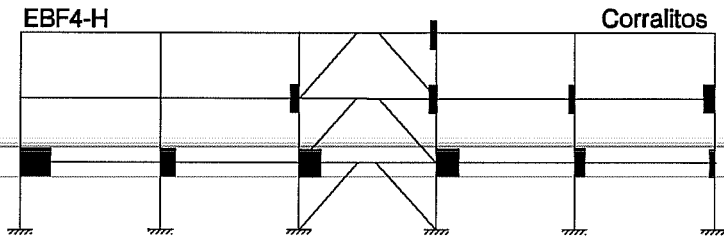


Figure 5.43 Ductility Demands in the Reinforced Concrete Members in EBF4-H Subjected to the Scaled El Centro Record



(a) Columns in Negative Bending



(b) Beams in Positive Bending

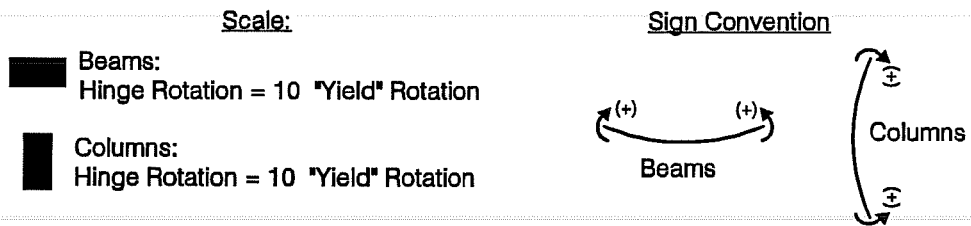


Figure 5.44 Ductility Demands in the Reinforced Concrete Members in EBF4-H Subjected to the Corralitos Record

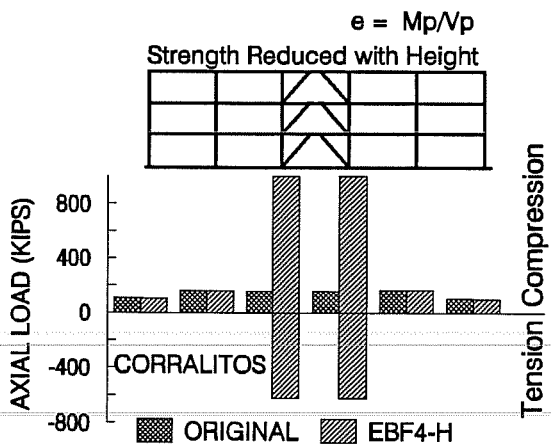
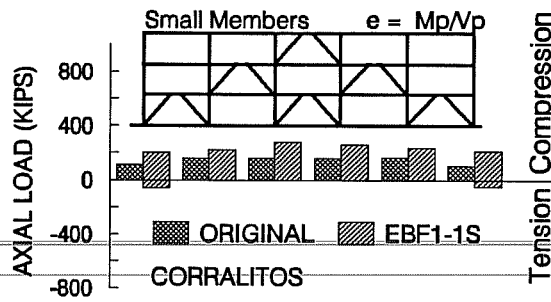
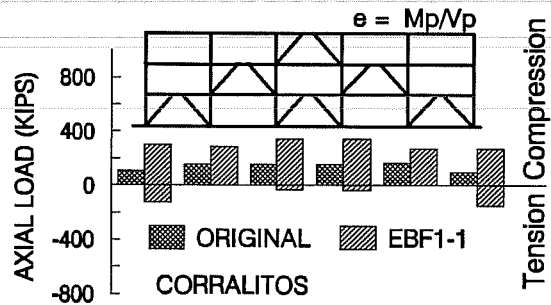
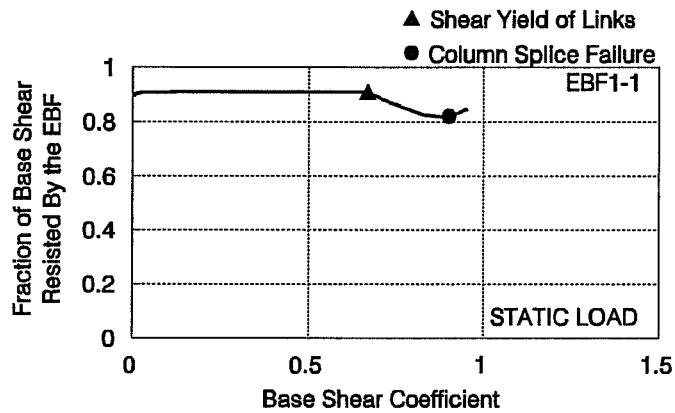
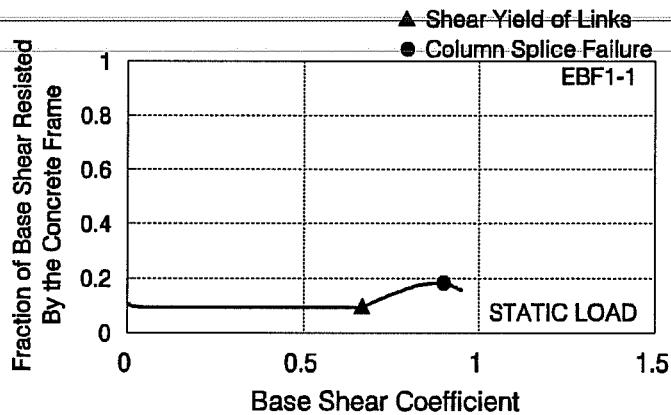


Figure 5.45 Maximum Axial Load on the Foundation of the Three-Story Building Subjected to the Corralitos Record

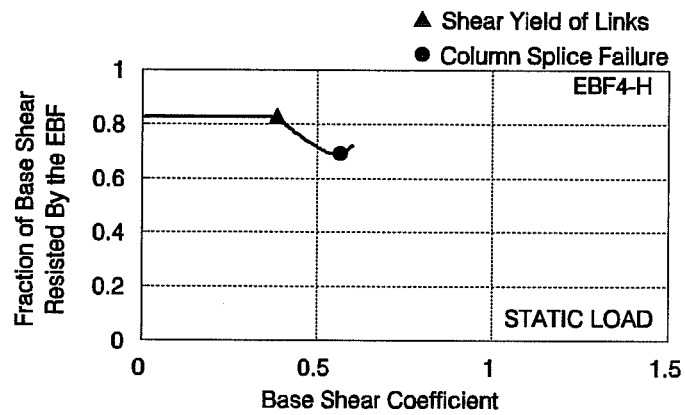


(a) Base Shear Fraction Resisted by the EBF

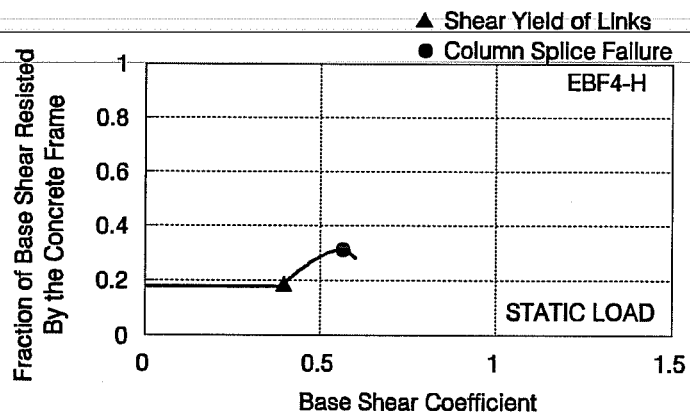


(b) Base Shear Fraction Resisted by the Concrete Frame

Figure 5.46 Fraction of Base Shear Resisted by the Reinforced Concrete Frame and by the EBF in EBF1-1 retrofit scheme Subjected to Static Load

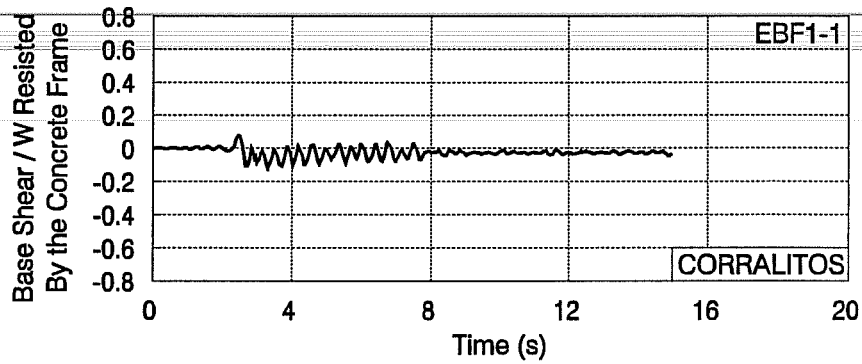


(a) Base Shear Fraction Resisted by the EBF

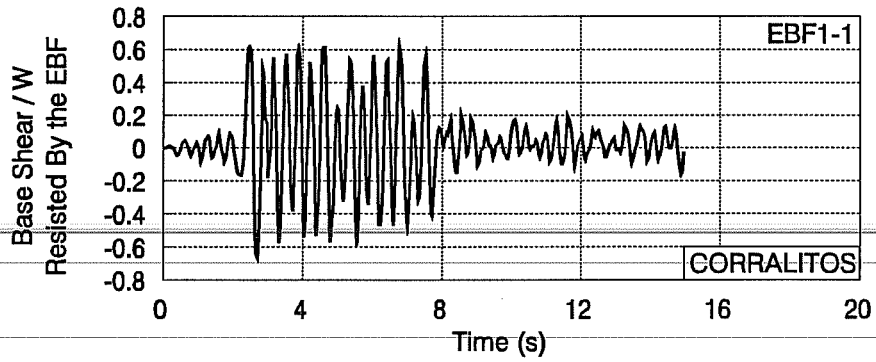


(b) Base Shear Fraction Resisted by the Concrete Frame

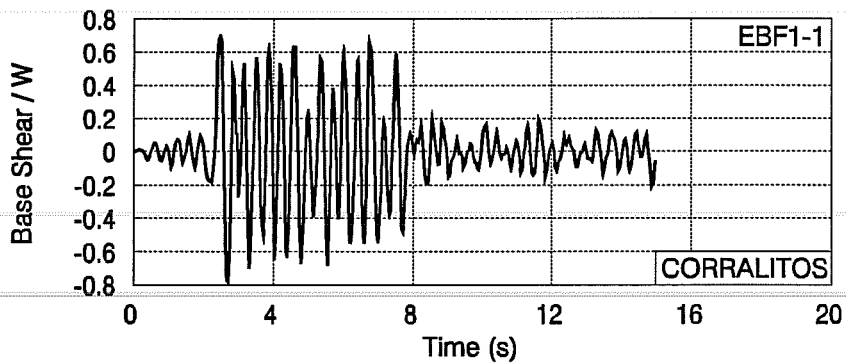
Figure 5.47 Fraction of Base Shear Resisted by the Reinforced Concrete Frame and by the EBF in EBF4-H retrofit scheme Subjected to Static Load



(a) Base Shear Resisted by the Concrete Frame

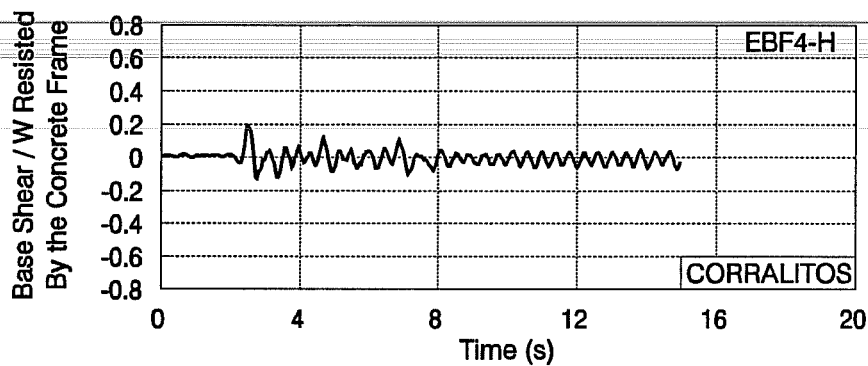


(b) Base Shear Resisted by the EBF

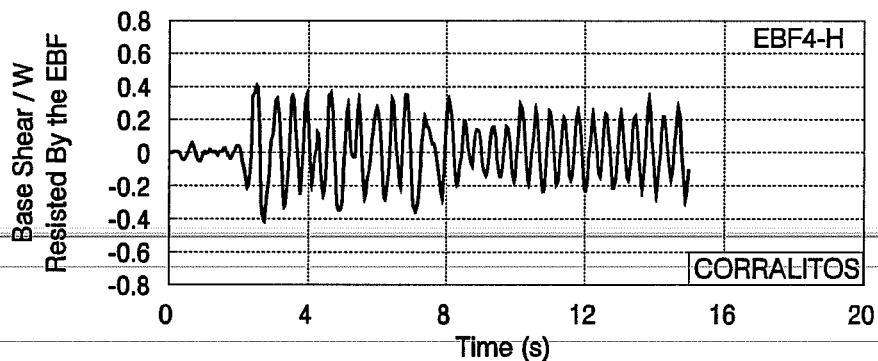


(c) Total Base Shear in the Structure

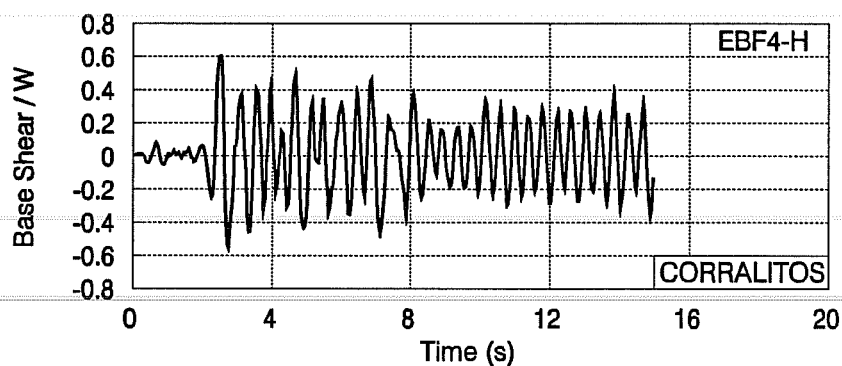
Figure 5.48 Base Shear Distribution for EBF1-1 Subjected to the Corralitos Earthquake Record



(a) Base Shear Resisted by the Columns



(b) Base Shear Resisted by the Bracing Scheme



(c) Total Base Shear in the Structure

Figure 5.49 Base Shear Distribution for EBF4-H Subjected to the Corralitos Earthquake Record

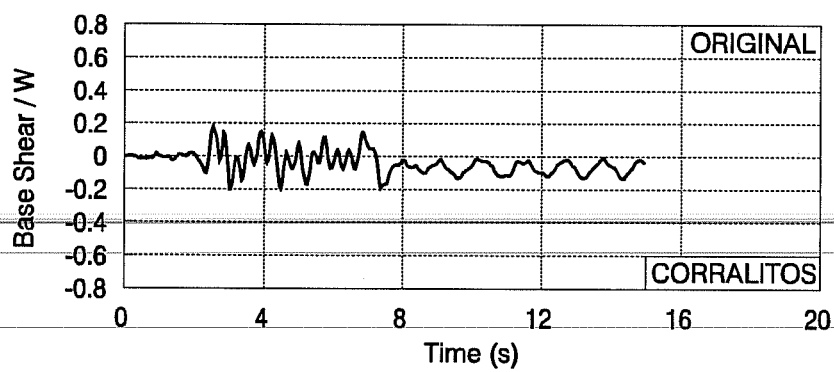


Figure 5.50 Base Shear in the Original Three-Story Building Subjected to the Corralitos Earthquake Record

CHAPTER 6: SEVEN-STORY BUILDING

6.1 General.

The structure presented in this chapter is a seven-story reinforced concrete building representative of medium rise west coast construction of the 1950s and 1960s. The structure has 11 bays in the longitudinal direction and three bays in the transverse direction. In the longitudinal direction, the external frames are formed by six feet deep spandrel beams and by short ("captive") columns. Windows fill the space between spandrels. The corner columns are 18 in. by 18 in. and the remaining columns are 18" by 24". A one way 6 in. deep floor slab spans between the spandrel beams and the internal shallow beams. A normal weight concrete with a compressive strength of 3000 psi was specified. All reinforcing steel is Grade 40 except the column's longitudinal reinforcement which is Grade 50. Figures 6.1 to Figure 6.4 show the building configuration and the members' reinforcement.

The lateral load resisting system consists of shear walls and moment frames in the building's short direction. In the longitudinal direction, the lateral load is resisted by the stiff external frames. Only the behavior in the longitudinal direction was studied here.

6.2 Details of Structural Members.

The seismic design forces were based on the 1955 edition of the UBC and the member design and detailing followed the recommendations of the 1956 ACI 318 code. The use of these old codes resulted in low strength and poor detailing by today's standards. Highlights of the structural details are discussed below.

- **Column Shear Strength.** The floor to floor height of the outer frame columns is 10 ft. However the deep spandrel beams created "captive" columns by reducing their clear

height to only 4 ft. Furthermore, the transverse reinforcement is widely spaced and does not permit the development of the columns' flexural capacity. Poorly detailed "captive" columns are known to exhibit low shear strength, and a rapid deterioration in stiffness and strength under cyclic load (Woodward and Jirsa, 1983). Consequently, brittle shear failure is expected under seismic loading. Also, the transverse reinforcement does not satisfy the current code recommendations on confinement. For these columns, the current ACI 318-89 requires a spacing of 4 in. The actual spacing was 12 in. or larger. Figure 6.2 shows the column's cross section and reinforcement.

● **Lap Splice in Columns.** Due to the low force requirements of the 1955 UBC, tension was not expected in the columns. Consequently, the columns were provided with a short compressive splice in accordance with the recommendations of the ACI 318-56 code. However because of the presence of the deep spandrel beams, the actual development length was larger than the splice length. With the exception of the bottom section of the first three floors of the inside columns, the anchorage length was found adequate to develop the longitudinal steel capacity. Based on Orangun's equation (Eq. 3.9) (Orangun et al., 1977), splice failure was estimated to occur at a steel stress of 62 ksi for the lower section of the first three floors.

● **Anchorage of Beam Reinforcement.** The top and bottom bars in the spandrel beams were provided with a tension splice since moment reversal was expected under the design load. The anchorage length followed the recommendations of the ACI 318-56 code and does not ensure the development of the longitudinal steel capacity. In general anchorage failure was found to occur following steel yielding. The spandrel beams were provided with #7 and #8 bars as shown in Figure 6.3. According to Orangun's equation (Eq. 3.9) (Orangun et al., 1977), anchorage failure for these bars was expected at a stress of 41 ksi and 47 ksi respectively. The yield stress of the longitudinal reinforcement is 40 ksi.

● **Transverse Reinforcement in Beams.** The transverse reinforcement in the spandrel beams consisted of #4 bars spaced at 18" which represents about $0.25 h$, h being the member depth. The shear strength of the beams allows for the development of the flexural capacity and shear failure was not expected. Away from the joint region, the transverse reinforcement was in excess of the recommendations of ACI 318-56 and satisfied the current provisions on minimum spacing. However, in the proximity of the joint, the transverse reinforcement was below current recommendations and does not provide proper concrete confinement.

● **Shear Strength of Joints.** The joints were not provided with transverse reinforcement. However, due to the deep spandrel, the shear capacity of the connections largely exceeded the maximum stress that can be developed. Hence, joint shear failure is not expected.

6.3 Analytical Modeling.

6.3.1 General. The analytical modeling procedure was similar to the one outlined in Section 4.3.2. The columns and spandrel beams were modeled using the DRAIN2D reinforced concrete element.

6.3.2 Column Modeling. The moment curvature diagram of the columns was derived assuming an axial load corresponding to gravity loading. Splice failure was a possibility at the column base for the first three levels of the inside columns, as explained above. For these sections, splice failure was found to occur after yielding. The rate of stiffness softening following splice failure was similar to the one assumed for the three story building (Chapter 5). Figure 6.5 shows the shape of the moment-rotation envelope for the columns. Table 6.1 lists the parameters used to define the moment rotation envelope.

Although shear failure constitutes a possible failure mode for the columns, it was not modeled for the analysis of the original building. However, the analytical output will be examined to determine if column shear failure occurred. This type of failure, viewed as very brittle, will be considered to define failure of the original building. Table 6.2 gives the shear strength of the columns, computed using ACI 318-89 procedure and assuming a strength reduction factor, ϕ of one.

6.3.3 Beam Modeling. The moment curvature diagram of the spandrel beams was derived assuming no axial load. Figure 6.6 shows the shape of the moment-rotation envelope used for modeling the spandrel beams. Splice failure is anticipated for both top and bottom reinforcement of the beams, however yielding was found to occur prior to splice failure. Table 6.3 shows the moment and rotation at yield and splice failure for the beams.

6.4 Static Analysis of the Original Building.

A static incremental load was applied on the structure to estimate the building's lateral strength and stiffness. The load was uniformly distributed with height and was applied at the floor levels. Figure 6.7 shows the relationship between the base shear coefficient and the maximum interstory drift, which was found to occur at the first floor. The first and second level columns failed in shear at a very low drift level of about 0.2% corresponding to a lateral load of 0.18 W; W being the building weight. The brittle shear failure of the columns led to the structure's collapse.

If shear failure were prevented, the structure would continue to deform elastically, as indicated by Figure 6.7, until splice failure of the first level columns. This occurs at an interstory drift level of about 0.3% and a lateral load of about 0.24 W. This event would result in the onset of inelastic deformations. At an interstory drift ratio of 0.5%, splice failure would be initiated at the second level columns and in the beams. This condition would be followed by a rapid degradation in strength and stiffness and can be considered as the capacity limit of

the building. If shear failure is prevented, the lateral strength of this structure is equal to 0.24 W.

Figure 6.7 provides also a comparison between the strength of the building and the minimum strength required by the 1955 edition of the UBC code and by the ATC 22 recommendations. The structure was considered as an Ordinary Moment Resisting Frame resting on firm soil. As expected, the structure was found to satisfy the strength recommendations of the 1955 UBC. However, the strength of the building is lower than the minimum requirement of the current provisions of ATC 22, indicating the seismic inadequacy of the structure. Further discussions on the application of ATC 22 recommendations are presented in Chapter 7.

6.5 Dynamic Analysis of the Original Building.

Inelastic dynamic analysis of the seven-story building was conducted using four earthquake ground acceleration records. These records are the N00E component of the 1940 El Centro record scaled to 0.5 g, the N00E component of the 1989 Corralitos record, the N35E component of the 1989 Oakland Wharf record and the N90E component of the Mexico City SCT1 record. The first two records were on firm soil and the last two records were on soft soil.

The dynamic analyses showed that the original building experienced early column shear failure under all records. Under the Scaled El Centro record and the Corralitos record, column shear failure initiated at the first and second level. Under the Oakland Wharf and Mexico records, the second level columns were the first one to fail in shear. Shear failure can be considered as brittle and leading to the likely collapse of the building.

A dynamic analysis was conducted on the original building assuming column shear failure was prevented. This analysis can reflect the behavior of the original building if jacketing,

for example, was performed on the columns to preclude shear failure. Figure 6.8 show the maximum interstory drift of the building subjected to the selected earthquake records. The maximum interstory drift was in the vicinity of 1.3% under the scaled El Centro record and under the Oakland Wharf record and around 1% under the Corralitos record. Under the Mexico record, the maximum interstory drift was around 0.5%. The interstory drifts under the Scaled El Centro record, the Corralitos record, and the Oakland Wharf record appeared excessive. Based on the static analysis, the ability of the building to withstand the load due to these records appears doubtful.

6.6 Concluding Observations.

The seismic adequacy of a seven-story reinforced concrete building was evaluated by a static and dynamic analyses. The lateral load resisting system of the building was formed by ~~moment resisting frames that featured deep spandrel beams and short columns with low shear strength~~. This structure was designed for low lateral forces and was not detailed for seismic behavior. The static analysis was conducted by applying a static incremental load and the dynamic analysis was performed using four acceleration records.

The static analysis indicated that the structure has a low capacity and is subject to column shear failure, leading to the structure's collapse, at very low drift. The dynamic analysis showed the building inadequacy to resist the forces due to the selected earthquake records. Structural collapse due to column shear failure is expected for all records. Strengthening of this building appears necessary to enhance its seismic behavior. A dynamic analysis that assumed column shear failure prevented, was performed. The results of this analysis also showed the inadequacy of the building to resist the earthquake loading.

The seven-story building was retrofitted with the addition of steel EBFs to improve the seismic performance. The results of the analyses on the retrofitted structure are presented below. The presentation was divided into four parts. A first series of retrofit schemes were analyzed assuming that shear failure was prevented. This analysis can be valid if the columns

are protected against shear failure by jacketing or if the added steel EBFs can keep the drifts at very low levels to avoid column shear failure. The dynamic analysis showed that the EBFs alone could not prevent column shear failure. A second series of retrofit schemes was analyzed to assess the effect of column shear failure. For that analysis the approximate shear model element was included. In the third series of retrofit schemes, the column behavior was changed to a more flexural and ductile behavior. To that end, the spandrel beams were cut below the floor level in the vicinity of the columns to permit the development of flexural strength in the columns prior to shear failure and to force hinging into the beams. Finally, an analysis was performed to determine an EBF retrofit scheme having the minimum strength required to resist the strong ground motions.

6.7 Retrofit Schemes I: Column Shear Failure Prevented.

6.7.1 Description of Retrofit Schemes I. Steel EBFs, with different configurations, were selected to retrofit the existing building. The EBFs were added to the external frames only. The outer bays, which were smaller than the inner bays, were not braced for practical and economical reasons. The strength and stiffness of the selected schemes were reduced with height to allow for uniform yielding of links at the different levels.

Three configurations were selected. EBF1 and EBF2 configurations had three braced bays. EBF3 had 5 braced bays. The geometric configurations of EBF1 and EBF2 were similar but EBF2 had larger member sizes. Figures 6.9a and 6.9b show the geometric configuration of the bracing schemes and the member properties are summarized in Table 6.4. The links used were short links yielding primarily in shear. Vertical steel channels, acting as collectors, were attached to the existing reinforced concrete columns. The vertical collectors used in EBF1 and EBF2 were formed of C9x15 sections of A572 Gr 50 steel. The vertical collectors used for EBF3 were formed of C8x18.75 sections of A572 Gr. 50 steel. The beams and braces of the EBFs are attached at their ends to the steel channels. The steel channels are assumed connected to the existing reinforced concrete columns by means of epoxy grouted dowels (Figure 4.6).

A concentrically braced frame labeled CBF3, was also selected to retrofit the seven-story building. This scheme was designed to have an initial stiffness comparable to that of EBF3. The strength and stiffness of the CBF3 scheme were gradually reduced with height. The braces, added to the external frames only, were attached by means of horizontal and vertical collectors connected to the existing reinforced concrete members by epoxy grouted dowels. Figure 6.9c shows the configuration of CBF3 and Table 6.5 gives the member properties. The vertical collectors attached to the columns were made of C10x30 sections of A572 Gr. 50 steel.

6.7.2 Modeling of Retrofit Schemes I. The concrete columns in the braced bays were strengthened by the addition of steel channels as vertical steel collectors. The strengthened columns were modeled assuming full composite action between the reinforced concrete columns and the added vertical collectors for flexural behavior. The shape of the moment rotation diagram of the strengthened columns is shown in Figure 6.5a. Table 6.6 and Table 6.7 give the moments and end rotations at yield and ultimate.

The addition of steel channels was experimentally shown to increase column shear strength; however the increase was difficult to quantify (Bush, 1987). In this study, an estimate of the shear strength of these columns was taken as sum of the reinforced concrete column shear strength and the steel channel shear strength.

For the EBF schemes, the shear links were modeled using the DRAIN2D shear link element. The beams and braces were modeled using the beam column element. This element was deemed appropriate to model the braces since they were designed to remain elastic and were not expected to buckle.

For the CBF3 retrofit scheme, the steel beams were modeled using the beam column element and the braces were modeled using the brace buckling element. The initial buckling load and the post buckling strength of the braces are given in Table 6.8.

In the following static and dynamic analyses of the retrofit frames, several results will be presented:

- The point at which the unstrengthened columns fail in shear will be identified. These are the columns that are not part of a braced bay, i.e. those columns where no steel channels have been added. Shear failure is expected to lead to a dramatic loss of stiffness and strength of these columns. It may also lead to the loss of the columns' gravity load carrying capacity. Shear failure of these columns may therefore be considered as defining failure of the frame.
- The analysis will be continued past the point where the unstrengthened columns fail in shear. This will indicate the expected behavior of the frame if shear failure of the columns is prevented. This could be accomplished for example by the addition of steel jackets to the unstrengthened columns. Recent research has demonstrated that a thin rectangular jacket is highly effective for shear strengthening of concrete columns (Aboutaha and Engelhardt, 1994).
- The point at which the columns with added steel channels are expected to fail in shear will also be identified. These are the columns that are part of a braced bay. As noted earlier, the shear strength of these columns is estimated simply as the sum of the shear strength of the original column and the shear strength of the steel channels. The actual shear strength of these columns is quite uncertain. The rate of stiffness and strength degradation is also uncertain.
- The analyses will be continued past the point where the columns with the added steel channels are predicted to fail in shear. This will indicate the expected behavior of the frame if the columns with added steel channels have greatly shear strength than estimated. It will also predict the frame behavior if more certain measures are taken to strengthen the columns in the braced bays, such as the addition of steel jackets.

6.7.3 Static Analysis of Retrofit Schemes I. A static inelastic analysis was conducted on the retrofit schemes of Series I by applying a static incremental load. The load was uniformly distributed with height and was applied at the floor levels.

Figure 6.10 shows the relation between the base shear coefficient and the maximum interstory drift for EBF1 and EBF2. The analysis showed that the unstrengthened columns experienced a shear failure at a drift ratio of about 0.2%. This is essentially the same drift at which column shear failure occurred in the original, unretrofitted building. Since half of the columns in this configuration are not strengthened by the addition of vertical steel collectors, column shear failure will result in a significant loss of lateral strength and stiffness and may lead to a building collapse.

Figure 6.10 shows also the expected behavior if column shear failure is prevented. Strengthening schemes EBF1 and EBF2 provided approximately the same level of stiffness and strength but EBF1 exhibited a higher ductility. The initial stiffness of both schemes was about twice that of the original building. The retrofitted structures behaved elastically until yielding of the first level links at a drift of about 0.23% corresponding to a lateral load of 0.3W. Additional reduction in stiffness was observed with the yielding of the second level link which occurred at a drift of about 0.4%, corresponding to a base shear of about 0.4W. EBF1 and EBF2 reached their deformation capacity at an interstory drift of 1.5% and 1.3% respectively. These drifts correspond to a lateral load of about 0.54W.

The relationship between the lateral load and the maximum interstory drift for EBF3 is shown in Figure 6.11. This scheme resulted in a substantial increase in strength and stiffness and provided the building with an appreciable ductility. Assuming that column shear failure is prevented, inelastic action in EBF3 was initiated at yielding of the first and second level links. Link yielding occurred at a drift of 0.2% and corresponded to a lateral load level of about 0.5W. Further increase in load resulted in shear yielding of links at the third and fourth level at 0.5% and 0.9% drift respectively. These drifts correspond to a load level of 0.62W and

0.69W. The maximum lateral load capacity of EBF3 was found equal to 0.75W and was attained at a drift of 1.3%. A link rotation of 0.10 rad. was assumed to limit the EBF capacity.

The behavior of the CBF3 scheme under static incremental lateral load is shown in Figure 6.12. The static analysis showed that EBF3 and CBF3 had about the same strength and a comparable initial stiffness. The first level braces buckled at a drift of 0.23% corresponding to a load level of 0.52W. Buckling of the first level braces initiated a stiffness reduction of the structure. At a drift level of 0.33%, the second and third story braces buckled causing further reduction in the stiffness. At a drift of about 0.4%, most of the braces yielded in tension. This event resulted in a plateau in the load-drift response. The maximum load capacity of the structure was equal to 0.64W. Note that the maximum deformation that can be sustained by the braces without extensive damage or fracture cannot be evaluated with the current model. Hence, the maximum drift that can be experienced by the building without collapse or severe damage cannot be estimated.

Shear failure of the corner, unstrengthened columns in EBF3 and CBF3 occurred at the same drift level as for the original structure (approximately 0.2%) but a substantially higher load. Since only a very limited number of columns failed, these retrofit schemes may be able to carry additional lateral load. An analysis that includes approximate shear failure modeling can indicate the behavior of the structure following shear failure of the corner columns. At a drift level of about 0.4% and 0.75%, all first levels columns of CBF3 and EBF3 respectively failed in shear. To prevent this mode of failure an increase in the size of the steel collectors or the use of steel jackets may be required.

The static analyses showed that the retrofit schemes of Series I provided an increase in stiffness and strength but could not prevent column shear failure which was predicted to occur at very a low drift level.

6.7.4 Dynamic Analysis of Retrofit Schemes I.

6.7.4.1 Period of Vibration. Table 6.9 shows the first and second period of vibration of the original structure and the retrofit schemes of series I. A reduction in the fundamental period was observed for all retrofit schemes. This was particularly significant for EBF3 and CBF3 indicating a substantial stiffness increase for these schemes. This increase in stiffness may result in similar or lower demand for the buildings on soft soils as suggested by the response spectra shown in Figure 4.2. For the buildings on firm soil, the reduction in the fundamental vibration period will probably cause an increase in the seismic demands.

6.7.4.2 Maximum Interstory Drift. Figures 6.13 to 6.16 show the maximum interstory drifts for the retrofit schemes of Series I for which column shear failure was assumed prevented. Overall the drifts were kept within acceptable limits. The maximum interstory drifts for EBF1 and EBF2 subjected to the records on firm soil (Scaled El Centro and Corralitos) were maintained below or in the vicinity of 1%. For EBF3, with five braced bays, the maximum drift for the firm soil records was equal to 0.6% under the scaled El Centro record and to 0.7% under the Corralitos record. The maximum interstory drift for CBF3 under these records was in the vicinity of 0.65%. This is comparable to the drifts imposed on EBF3, however, the largest drift occurred at the second and third floor which may indicate a larger participation of higher modes of vibration in the response of the structure.

Maximum interstory drifts for the records on soft soil were very low for all the retrofit schemes of Series I. This may be due to the increase in stiffness combined with a reduction in demand. The maximum drift under Oakland record were below 0.5% while the drift under Mexico record were below 0.25%.

The interstory drifts of the original building, assuming that shear failure is prevented is shown in Figure 6.8. EBF3 and CBF3 appear very effective in controlling the interstory drifts under the soft and firm soil records. EBF1 and EBF2 let to a substantial reduction in

interstory drifts under the soft soil records, particularly under the Oakland Wharf record. EBF1 and EBF2 do not appear however, to be very effective in reducing the deformation of the building under the firm soil records. Under the Corralitos record, the maximum interstory drift at the first level of EBF1 and EBF2 was similar to that of the original building. Under the scaled El Centro, EBF1 reduced the maximum interstory drift by about 0.3%. The maximum interstory drifts for EBF2 was similar to that of the original building. The increase in stiffness provided by EBF1 and EBF2 may be offset by the higher seismic demands under the firm soil records and the increase in strength.

6.7.4.3 Link Rotation. Inelastic action and energy absorption in EBFs is best indicated by the link plastic rotations. The maximum link rotation for EBF1, EBF2, and EBF3 are shown in Figures 6.17, 6.18, and 6.19. Under the Mexico record, the EBF schemes remained elastic. Under Oakland, EBF1 and EBF2 experienced very small plastic link rotations at the lower floors. The largest rotations were in the vicinity of .02 rad for EBF2. For EBF3 the link remained essentially elastic.

For the firm soil records, the maximum link rotation for EBF1 and EBF2 was in the vicinity of 0.07 rad, indicating large plastic activity. The plastic rotation of the links of EBF3 under the same record was in the vicinity of 0.04 rad. The low deformations at the higher floor levels indicate a small participation of these floors in the energy dissipation mechanism. Smaller link sizes at higher levels, may promote a more uniform yielding of the links.

6.7.4.4 Performance of Concentric Braces. Analytical results indicated that for the soft soil earthquake records, braces of CBF3 retrofit scheme remained elastic or experienced limited inelastic deformation. Under the Mexico record, all braces remained elastic and under the Oakland record some brace buckling was predicted. Buckling, however was limited to few braces at the first floor and the level of plastic deformation was very small.

The firm soil records subjected CBF3 retrofit scheme to relatively large inelastic deformation. Under the Corralitos record, the CBF3 braces buckled at all levels except at the roof. The largest permanent axial compressive deformation occurred at the first and second floor and measured approximately 0.8 in. which represents four times the axial deformation at first buckling. For the scaled El Centro record, brace buckling was limited to the three lower stories. The maximum compression deformation was in the vicinity of 0.9 in. and represents 4.5 times the axial deformation at first buckling. Braces yielding occurred in the first three floors under the Corralitos record, and in the first four floors under the scaled El Centro record. The maximum plastic extension measured 2.5 times the extension at yield for the Corralitos record and 3.0 times the extension at yield for the scaled El Centro record.

6.7.6 Column Shear. For the soft soil records, EBF3 and CBF3 successfully ~~prevented column shear failure by drastically reducing the drifts and limiting the forces in the~~ columns. Column shear failure, however was observed for EBF1 and EBF2 under the Oakland record. The dynamic analyses also showed that proposed the schemes were unable to prevent column shear failure for the firm soil records. The results of the static analysis indicated that interstory drifts need to be kept below the very small value of 0.2% to preclude column shear failure. The stiffness increase provided by the selected retrofit schemes was not sufficient to limit the drifts to such a small level.

6.7.5 Concluding Remarks. Dynamic and static analyses were carried on a series of three EBF and one CBF retrofit schemes. Three, out of 11, bays were braced in two EBF retrofit schemes. One EBF retrofit scheme and the CBF retrofit scheme considered bracing five bays. The retrofit schemes provided a significant increase in stiffness, strength, and ductility. The schemes with five braced bays effectively prevented column shear failure and limited drifts to very small levels for the soft soil earthquake records. The schemes with three braced bays could not prevent shear failure of the columns under the Oakland record. For the firm soil earthquake records, the retrofit schemes could not prevent column shear failure.

Assuming the columns are strengthened to prevent shear failure, the analyses indicate the retrofitted frames will show acceptable performance under strong ground motion records. In the following sections, new analyses will be conducted, assuming columns are strengthened against shear failure. The approximate post-shear failure behavior of the columns will be included in the model.

6.8 Retrofit Schemes II: Shear Failure Not Prevented.

6.8.1 General. A second series of retrofit schemes were analyzed to assess the effect of column shear failure on the overall response of the building. This analysis will indicate if column shear failure will cause limited, isolated damage or will lead to more extensive damage or even collapse. The analysis was performed on the EBF2, EBF3 and CBF3 schemes. Analytical modeling of these schemes was similar to that presented above, except that column shear failure was included. The DRAIN-2D model assumes that after shear failure, a reinforced concrete member loses its lateral load capacity but can still carry axial load, as discussed in Section 3.6.2. This model can give an indication of the structure's behavior following column shear failure.

6.8.2 Static Analysis of Retrofit Schemes II. The static analysis was conducted by applying a static incremental lateral load on the structure. The lateral load was concentrated at the floor levels and was uniformly distributed with height. Figures 6.20 and 6.21 summarize the results of the static analyses. All retrofit schemes provided an increase in strength and stiffness. EBF3 and CBF3 had the same ultimate lateral load capacity of $0.65W$. The strength level of EBF2 was limited to $0.42W$.

At a low drift of about 0.23%, unstrengthened columns in several levels of the EBF2 retrofit scheme failed in shear causing a sudden and large increase in displacement. The loss in stiffness due to column shear failure combined with the transfer of the lateral forces of the failed columns to the bracing scheme can explain the abrupt increase in displacement. The first

and second level links yielded at a drift of 0.35% and resulted in an apparent reduction in stiffness. The interstory drift limit of EBF2 was estimated equal to 1.30%.

Shear failure of the unstrengthened columns in EBF3 occurred at a drift level of 0.23% but was limited to the two lower stories. At 0.37% interstory drift, external columns at all levels failed in shear causing some increase in the drifts. Yielding of the first and second level links reduced the stiffness of the structure. Shear failure of the strengthened columns (columns with steel channels attached) occurred at a drift level of 0.72% and resulted in a significant increase in the structure's displacement. The lateral deformation capacity of EBF3 was reached at a drift of 2.4%.

CBF3 had the same initial stiffness and strength capacity as EBF3. Shear failure of the columns was initiated at a low drift of about 0.23%. Inelastic action in the braces started at 0.22% drift upon buckling of the first and second story braces, causing a gradual reduction of stiffness. At a drift level of approximately 0.6%, most of the braces of the first three stories have either buckled or yielded in tension. Shear failure of the unstrengthened columns occurred at a drift of about 0.75% and led to a substantial increase in deformation.

Shear failure of the unstrengthened columns for all retrofit schemes occurred at about the same drift as the original building but at a much higher base shear. Shear failure of the strengthened columns led to large drift and may cause excessive damage in the structure.

6.8.3 Dynamic Analysis of Retrofit Schemes II. The dynamic analysis was conducted for the Corralitos and the scaled El Centro records. The series I analyses showed that these records led to column shear failure in all retrofit schemes.

6.8.3.1 Maximum Interstory Drift. Figure 6.22 shows the maximum interstory drifts for EBF2 under the Corralitos and the scaled El Centro records.

Under the Corralitos records, the interstory drifts, although relatively high, remained within acceptable limits. Maximum interstory drifts for EBF2 retrofit scheme under Corralitos ground acceleration record were below 1.5%. Shear failure of the unstrengthened columns was predicted at 2.42 s. However, the strengthened columns did not fail in shear.

The El Centro record subjected the four lower levels of EBF2 to relatively large interstory drifts. The largest drift occurred at the first floor and was around 2% indicating extensive damage. Columns of internal frames, that are not detailed for ductile behavior and are not retrofitted, may not be able to sustain such large displacements. The analysis showed that the unstrengthened columns of the external frames failed in shear at 1.51 s., while the strengthened columns experienced a shear failure at 1.90 s., resulting in a large reduction of the structure's stiffness.

Figure 6.23 shows the maximum interstory drifts for EBF3. The stiffness of this retrofit scheme appears to keep the drift within reasonable limits. Maximum interstory drifts were below 1.5% for both records. The dynamic analysis predicted shear failure of the unstrengthened columns at the first three stories at 2.41s. Strengthened columns at the first three levels failed in shear at 2.78s.

CBF3 experienced drift levels in excess of 1.5% under Corralitos and the scaled El Centro records (Fig. 6.24). Maximum interstory drift occurred at the first level for the scaled El Centro record and at the third level for the Corralitos record. These drifts may be considered large and can result in substantial damage to the structure. The analysis predicted shear failure of the unstrengthened columns at the first five stories under both records. Shear failure of the strengthened columns was predicted for the lower four stories under the Corralitos record and for the lower three floors under the scaled El Centro record.

In summary, shear failure of the strengthened and unstrengthened columns of the external frames was observed for the three retrofit schemes. EBF2, which had only three braced bays, experienced very large drifts, leading to extensive damage. The adequacy of this

scheme to sustain the earthquake load due to the scaled El Centro record and to the Corralitos record appeared doubtful. Despite column shear failure, EBF3 experienced interstory drifts below 1.5%. Based on the observations on interstory drifts, it is expected that EBF3 retrofit scheme will provide safety against collapse. However the columns may experience heavy damage. The seismic behavior of EBF3 appeared somewhat better than that of CBF3. The latter was found to experience larger displacements under both strong earthquake records.

6.8.3.2 Link Rotations. Figure 6.25 shows the plastic link rotations for EBF2. Under the scaled El Centro records, the rotations of the four lower level links far exceeded the rotation capacity of 0.10 rad. This indicates the inadequacy of EBF2 to resist the earthquake load due to this record. Under the Corralitos record, the link rotations were very high but remained essentially below 0.10 rad. The largest plastic rotations were experienced at the first three stories and at the sixth story.

Link rotations of EBF3 were in excess of 0.10 rad for the Corralitos and the scaled El Centro records (Fig. 6.26). This indicates the inadequacy of EBF3 to sustain the seismic forces due to these severe earthquake records. The figure also indicates that link plastic deformations were concentrated in the three lower levels and deformations in the higher floors remained low. The link sizes of the top four stories can be reduced.

6.8.3.3 Brace Inelastic Deformations in CBF3. The dynamic analysis showed the braces of CBF3 are subject to extensive inelastic deformation at some stories. Consequently, a high level of damage may be expected. Analytical results showed that for the scaled El Centro record, brace yielding and brace buckling is limited to the lower three stories. The braces at the first and second stories experienced extensive inelastic excursions. The maximum plastic compressive deformation at the first and second level was equal to eight and four times the deformation at first buckling. The respective brace extensions were equal to five and four times the yield extension. Under the Corralitos record, brace buckling and brace

yielding occurred in the lower five and four levels respectively. Maximum brace compressive deformation at the first level was equal to four times the deformation at first buckling. At the remaining four lower levels, the ratio of maximum brace compressive deformation over deformation at first buckling was in the vicinity of three. Maximum plastic extension at the three lower levels measured two times yield extension.

6.8.4 Concluding Observations. Static and dynamic analyses, that included simplified column shear failure modeling, were conducted for the EBF2, EBF3 and CBF3 retrofit schemes. Column shear failure was observed for all three schemes. The analytical results showed that these schemes may not be able to perform adequately under the seismic loads due to the scaled El Centro record and the Corralitos record. Large interstory drifts were predicted for all schemes. The link deformations for EBF2 and EBF3 schemes were high and may result in link failure and extensive damage. Also, the braces of the CBF scheme experienced large inelastic excursions.

The above analyses were based on the assumption that after shear failure, a column's lateral strength and stiffness are reduced to zero, but its axial load resisting capacity is maintained. The ability of a column which has failed in shear, and has been subjected to large cyclic lateral deformations, to continue to resist axial load is doubtful. Considering the large lateral drifts and extensive damage to the bracing systems, combined with the uncertain axial capacity of the columns, permitting column shear failure appears inadvisable. Strengthening the columns to prevent shear failure will provide a more acceptable performance under strong ground motions. As an alternative to strengthening the columns, shear failure can be prevented by cutting the deep spandrel beams. Cutting the deep beam has also the advantage of changing the joint to a strong column-weak beam joint. This alternative is considered in the following section.

6.9 Retrofit Schemes III: Weaker Spandrels.

In view of the above results, some additional retrofit schemes were considered to provide safety against column shear failure and ensure adequate seismic behavior for the seven-story building. For these schemes, labeled series III, the spandrel beams were weakened by removing the concrete below the slab level in the vicinity of the joints, and by cutting the lower reinforcing bars at the same location. It was decided to cut the lower part of the beams since the existing positive moment capacity of the spandrel beams was already low. Removal of the upper part would have led to a drastic reduction in the negative flexural capacity of the beams. Weakening the beams eliminates the possibility of column shear failure by changing the behavior of the columns to a flexural and more ductile behavior. Also, the flexural capacity of the columns becomes higher than that of the beams, forcing the potential hinging area to the beams. Adversely, the development length of the column bars is reduced.

A similar concept was implemented to repair an eight story building with deep spandrel beams and short columns with low shear strength (Kawamata and Ohnuma, 1980). The repair scheme considered the addition of concentric braces along with beam weakening. The adequacy of the system was demonstrated experimentally. More information on this work has been presented in Chapter 2.

The Series III retrofit schemes were labeled EBF3W and CBF3W. They were similar to EBF3 and CBF3 respectively, except that the spandrel beam was cored below the slab in the vicinity of the columns as explained above.

6.9.1 Modeling of Retrofit Schemes III. The added steel members of EBF3W and CBF3W were modeled as previously explained for EBF3 and CBF3 respectively. Columns and spandrel beams were modeled using the DRAIN-2D reinforced concrete element. Shear failure was not modeled since it was not anticipated. The reduction in the spandrel beam depth adversely reduced the development length of the column's longitudinal reinforcement. Splice failure was now anticipated for the outside columns and for the top sections of the inside

columns. For the outside columns and for the second and third levels of the inside columns, splice failure was predicted to occur prior to column yielding. The shape of the moment rotation diagram for these column sections is shown in Figure 6.27. Figure 6.5b shows the model used for the remaining top sections of the inside columns. The bottom section of the inside column, where splice failure was not anticipated, were modeled as shown in Figure 6.5a. Tables 6.10 provides the values of the moment and rotation used to define the moment rotation envelopes of the columns.

The moment capacity of the spandrel beam sections at the column face was reduced. This reduction was particularly significant for positive bending. The bottom reinforcement was not properly anchored and bar pullout was expected. Anchorage failure was not expected for the upper reinforcement. Figure 6.28 shows the moment rotation envelope of the spandrel beams and Table 6.11 gives the value of the moments and rotations at yield at ultimate.

6.9.2 Static Analysis of Retrofit Schemes III. Figures 6.29 and 6.30 summarize the results of the static analysis of EBF3W and CBF3W. These retrofit schemes provided approximately the same level of initial stiffness and the same ultimate strength. The static analysis showed that reducing the beam depth prevented shear failure in the columns.

In EBF3W, reduction in the structure's stiffness was noted at a drift level of 0.25% upon shear yielding of the links at the lower two stories. Further loading resulted in yielding of other level links without a major effect on the structure's stiffness. Maximum link rotation, which was considered an indication of the ultimate deformation capacity of the building, was reached at a drift level of 1.21% corresponding to lateral load level of 0.56W.

In CBF3W, inelastic activity in the structure started at a drift level of 0.23%, corresponding to a lateral strength of 0.38W, upon buckling of the second level braces. At a drift level of 0.35%, the three lower story's braces either yielded or buckled.

6.9.3 Dynamic Analysis of Retrofit Schemes III. The dynamic analysis was conducted using four ground acceleration records. These records were the N00E component of the 1940 El Centro record scaled by 1.5, the N00E component of the 1989 Corralitos record, the N35E component of the 1989 Oakland Wharf record and the N90E component of the Mexico City SCT1 record. The results of these analyses are summarized below.

6.9.3.1 Period of Vibration. Table 6.12 shows the period of vibration of EBF3W and CBF3W. The fundamental period of vibrations of the Series III retrofit schemes were quite close to that of the original building. These schemes are consequently not expected to result in a major change in the seismic demands. This is particularly advantageous for the building on firm soil, where for the previous cases, the addition of a retrofit scheme increased the demands. Thus in addition to precluding column shear failure, weakening the beams can improve the seismic behavior of the building while keeping the demands at about the same level.

6.9.3.2 Maximum Interstory Drift. Figures 6.31 and 6.32 show the maximum interstory drift for EBF3W and CBF3W. In general, CBF3W had slightly larger drifts than EBF3W. For the records on firm soil, the drifts were maintained below 1%. The largest drifts were predicted at the third level for both structures. For EBF3W, the highest interstory drift measured 0.77% under the scaled El Centro and 0.95% under Corralitos. For the CBF3W scheme, the largest drift was 0.94% and 0.88% respectively.

The drift under the soft soil records (Mexico and Oakland) were kept at very low levels and appear essentially uniform with height. For both schemes, maximum interstory drifts averaged 0.3% under the Oakland record and 0.2% under Mexico record.

Based on the results of the interstory drifts under dynamic loads, it appears that weakening the beam led to improved seismic performance. EBF3W and CBF3W prevented

column shear failure and maintained drifts within acceptable levels. Furthermore, the interstory drifts for these two schemes were smaller than the drifts of EBF3 and CBF3 respectively.

6.9.3.3 Performance of EBF3W Scheme. Plastic rotations in the structural members provide a good indication of the damage level. To evaluate the inelastic deformations of EBF3W, the maximum link plastic rotation will be presented since plastic activity is limited to the links. The rotational ductility demand on the reinforced concrete members will also be shown. As explained in Chapter 5, the rotational ductility demand can constitute a good indication of damage for reinforced concrete member. Based on Table 6.10, the bottom section of the internal columns reach ultimate capacity at a rotational ductility of around five. The top section of the internal columns that are not subject to splice failure prior to yielding, can achieve rotation ductility of about two before reaching ultimate capacity. The remaining columns sections are found to reach ultimate capacity at a rotation ductility equal to one. The spandrel beams reach their ultimate capacity at a rotation ductility of about 2.5 in positive bending and of about 3.0 in negative bending (Table 6.11).

- **Links.**

Figure 6.33 shows the maximum link rotation for the different levels of EBF3W. The soft soil records imposed very low demands on the links. Under Mexico record, the links remained elastic. Under the Oakland record, plastic link deformation was limited to the lower four floors. The link rotation for these floors was relatively low and varied between 0.003 and 0.014 rad.

Under the firm soil records, relatively large plastic rotations were predicted for the four lower stories. These rotations however, did not approach the link rotation capacity of 0.10 rad., indicating that the link size may be reduced. Relatively low plastic link rotations occurred at the fifth and sixth level and the links at the roof level remained elastic. The largest plastic

rotation measured 0.07 rad under the Corralitos record and 0.05 rad under the scaled El Centro record.

- **Columns.**

Figure 6.34 shows the rotational ductility demands in the columns of EBF3W. Hinging, due to splice failure, was limited to some sections of the external columns. The ductility demand averaged 1.5 and reached a maximum value predicted of 2.25. These rotational values can be considered relatively small, and can be sustained by the building's columns without significant damage.

- **Beams.**

Rotational ductility demands in the spandrel beams are shown in Figure 6.35. In positive bending hinges were formed in almost all beams. The rotational ductility demand remained very low and averaged 1.0 at the roof and 2.0 at the remaining levels. Under negative bending, hinging in beams was essentially limited to the lower four stories. The rotational ductility demand in negative bending varied between 1.1 and 2.0. A rotational ductility demand of 2.5 or higher is needed for the beam to attain ultimate moment.

- **Conclusions.**

In summary, the plastic deformations in EBF3W show that energy dissipation was mainly due to the inelastic activity in the links. The links experienced relatively large deformations. However, these deformations remained within a safe level and a reduction in the link size may even be envisioned to obtain a more economical design. The rotation ductility demands in the reinforced concrete members were relatively low and do not appear to endanger the integrity of the columns or of the beams.

6.9.3.4 Performance of CBF3W scheme.

- **Braces.**

Figure 6.36a shows the maximum extension in the braces of CBF3W under the Corralitos acceleration record. Brace yielding was predicted for the first five stories. The smallest plastic extensions were expected at the first level. This was in accordance with the previous results that showed lower interstory drifts at the first floor. The ratio of maximum plastic extension over yield extension averaged 2.5 at the third level and 2.0 at the fourth floor. This ratio was around 1.8 at the second level and below 1.4 at the fifth and first floor. These extensions can be considered relatively moderate.

The maximum compressive deformation in the braces of CBF3W subjected to the Corralitos record are shown in Figure 6.36b. Brace buckling was predicted for all levels. In compression, large plastic excursions were expected for the braces of levels two to five. The largest deformations occurred at the third level where the ratio of plastic compressive deformation over deformation at first buckling was around four. At the second, fourth, and fifth levels this ratio was around three. At the remaining floors these ratios were below a relatively low value of 1.5.

- **Columns.**

Figure 6.37 shows the maximum plastic rotations in the columns of CBF3W under the Corralitos record. This scheme prevented plastic deformations in the internal columns. Column hinging was limited to the external columns which were not strengthened. The maximum plastic rotational ductility demands were relatively low and varied between 1.2 and 2.6. Such rotational demands are not expected to jeopardize the column integrity.

- **Beams.**

Figure 6.38a shows the maximum plastic rotations of the CBF3W reinforced concrete beams in positive bending for the Corralitos record. The largest rotational ductility demands were predicted at the third level and varied between five and six. At the first two levels, rotational ductility demands were between 2.2 and 6. The rotation ductility demands for the beams above the fourth floor were below two. Table 6.11 indicates that splice failure occurs at a rotation ductility of 2.5 for the two lower levels and at a rotation ductility of about three for the remaining floor levels. Pullout of the bottom bars is expected for several beams.

Figure 6.38b shows the rotation ductility demand in the beams under negative bending for the Corralitos record. Plastic hinging occurred in most of the beams. However the deformations were very low. The ductility demand ranged between 1.3 and 2.2. The beams yielded in flexural but did not reach their ultimate moment capacity. Table 6.11 indicates that ~~maximum moment is attained in the beams at a ductility demand ranging between 2.7 and 3.9.~~

- **Conclusions.**

Energy dissipation of CBF3 was mainly due to brace buckling and yielding. Large excursions in the inelastic range are expected for most braces. CBF3W prevented column shear failure and maintained low inelastic rotations in the columns. The beams in positive bending were subjected to high deformations and bottom beam reinforcement pullout was predicted. In general the beams of CBF3W were subjected to higher plastic rotations than of EBF3W.

6.9.3.5 Maximum Axial Load at the Foundation of EBF3W. The addition of a seismic retrofit scheme to an existing building may often cause an increase in the foundation axial loads. In this section, the axial load at the foundation of EBF3W will be examined and compared to the axial load at the foundation of the original building, assuming shear failure prevented.

Figure 6.39 shows the distribution of the maximum load in the columns at the foundation level for the EBF3W and for the original building (if shear failure is prevented). The axial load shown in the figure is due to the combined effect of gravity and earthquake loads. EBF3W substantially increased the compression load acting on the foundation of the braced bays. Compared to the original building, this increase average 400%. The compression acting on the unbraced bay decreased. This is mainly due to the fact that the in EBF3W, the lateral load is essentially resisted by the braced bays. In the original building, tension load was limited to foundation under the external columns only. EBF3W introduced tension load in the foundation of all the internal columns (which are part of braced bays).

No information was available on the existing foundation and its effectiveness was, consequently not numerically assessed. The use of EBFs was found to drastically increase the axial load on the foundation. The existing foundation would probably be unable to resist the increased load, and foundation strengthening may be required.

6.9.3.6 Distribution of Lateral Load. Figure 6.40 shows the fraction of the base shear resisted by the braces and by the columns for EBF3W under static load. During the elastic response, the braces resisted 75% of the lateral load, while the columns resisted the remaining 25%. Shear yielding of the links resulted in a loss of EBF stiffness, leading to a gradual reduction in the fraction of base shear resisted by the braces. This fraction reached a minimum of about 60%. Splice failure in the column reduced the ratio base shear resisted by the columns and increased the part of the base shear resisted by the added EBF.

Figure 6.41 shows that the braces of CBF3W contributed 60% of the strength of the structure for most of the loading. Inelastic action in the braces (buckling and tension yield) led to a reduction of the contribution of the braces to the lateral strength. At ultimate the portions of the base shear resisted by the braces and by the columns was equal to about 50% of the total base shear.

Figure 6.42 and Figure 6.43 show the amount of brace shear resisted by the columns and the braces for EBF3W and CBF3W under the Corralitos ground motion which subjected the building to the largest seismic demands. For both schemes, the braces resisted about 65% of the base shear throughout the earthquake loading. The maximum component of base shear resisted by the braces in EBF3W and CBF3W was equal to 0.28 W and 0.33 W respectively. The base shear in the columns reached a maximum of 0.15 W and 0.23 W respectively.

The distribution of the lateral load for the static and dynamic case showed that although the braces resisted most of the base shear, the contribution of the columns to the lateral strength is relatively important. The high contribution of the columns to the lateral resistance may be due to the increase in column stiffness due to the added vertical collectors. It is useful to note again that for the seven-story building, full composite action was assumed between the existing reinforced concrete columns and the added channels.

6.10 Retrofit Scheme IV: Minimum Requirements.

The results of the static and dynamic analyses summarized above showed that amongst the retrofit schemes that considered the addition of an EBF, only EBF3W can be considered as adequately designed to resist seismic loading. This scheme proved effective in avoiding shear failure in the columns and maintaining low deformations. Plastic link rotations were well below their of 0.10 rad. Consequently the link sizes of EBF3W could be reduced somewhat without endangering the bracing system. A new EBF retrofit scheme was designed. This new scheme, labeled EBF4W, exhibited the minimum strength and stiffness required to resist the selected earthquake records. EBF4W was designed following a trial and error procedure. The trials were evaluated with a dynamic inelastic analysis. The scheme with the smallest link sizes that maintained plastic rotations below 0.10 rad. was selected.

The design of EBF4W considered the need to prevent column shear failure. This was accomplished by weakening the spandrel beams as was done for EBF3W. EBF4W had the same geometric configuration as EBF3W but the link and beam sections were reduced. Table

6.13 shows the member sizes used for EBF4W. The modeling procedure was similar to the one outlined for EBF3W. Note that schemes designed with smaller member sizes than EBF4W were found inadequate to resist the selected earthquake records without exceeding the rotation capacity of links.

6.10.1 Static Analysis of Retrofit Scheme IV. Figure 6.44 summarizes the results of the static analysis for EBF4W. The figure shows that shear failure in the columns was prevented. However, due to the reduction in splice and anchorage length, some beams and columns experienced splice failure. Similar to the other EBF schemes, a significant reduction in the stiffness of the structure occurred upon first yielding of the shear links. First and second story links yielded at 0.28% drift corresponding to lateral load of 0.20W. The third story link yielded at an interstory drift of 0.30% corresponding to a lateral load of 0.22W. Ultimate lateral load capacity was reached at a drift of 1.15% and was equal to 0.43W. EBF4W had 75% of the strength of EBF3W, but maintained a comparable level of deformation capacity.

6.10.2 Dynamic Analysis. For the dynamic analysis, EBF4W was subjected to the scaled El Centro record and to the Corralitos record.

6.10.2.1 Period of vibration. The periods of the first and second vibration modes were equal to 0.62 s and 0.21 s respectively. These periods were very close to the those of the original building (see Table 6.9). This indicates that EBF4W did not provide a substantial increase in the initial stiffness. The stiffness increase due to the addition of the an EBF system was offset by reduction in the spandrel beam depth. Advantageously, the seismic demands on the retrofit structure are expected to be almost similar to those of the original building. Similar to EBF3W, EBF4W appears to increase the strength and ductility of the building without increasing the seismic demands for the records on firm soils.

6.10.2.2 Interstory Drift. Figure 6.45 shows the maximum interstory drifts for EBF4W under the Corralitos and the scaled El Centro records. In general, Corralitos subjected EBF4W to higher drifts. Maximum drift under the Corralitos record and the scaled El Centro record were respectively 1.02% and 0.73%. Such drifts levels can be considered as acceptable and do not appear to endanger the integrity of the structure.

The dynamic analysis showed that column shear failure was prevented. Splice failure was predicted for the outside (non-strengthened) columns. The beams and inside columns did not experience splice failure. Interstory drifts for EBF4W under dynamic loading were similar to those of EBF3W, although the former had higher stiffness. This may be due to possible lower demands on EBF4W. This observation indicates that, for the earthquake records on firm soil records, it may be advantageous to limit the increase in stiffness provided by the retrofit scheme.

6.10.2.3 Plastic Rotation of Links. Figure 6.46 shows the maximum plastic rotation of the links under the Corralitos and the scaled El Centro records. Link rotations were, in general, higher under Corralitos. The maximum rotation occurred at the third level. Maximum rotation under the Corralitos and the El Centro records measured 0.09 rad. and 0.05 rad. respectively. Note that the maximum plastic link rotation due to the Corralitos record was very close to the capacity limit of 0.10 rad. Relatively large rotations were predicted for levels two to five under the Corralitos and for the four lower stories under the scaled El Centro. As shown by the link rotations, the design of EBF4W was controlled by the seismic forces due to the Corralitos record.

6.10.3 Summary on EBF4W. The EBF4W retrofit scheme combined the addition of an EBF system with a reduction of the spandrel beam depth. The original building had a low lateral strength and experienced column shear failure under dynamic loading. The

beam weakening was performed to change the column behavior to a more flexible mode and to avoid a brittle shear failure.

EBF4W was found adequately designed to resist the seismic loads due to the selected strong earthquake records. This scheme increased the strength of the original building and provided a good level of ductility. Also, it successfully prevented column shear failure. The link rotations of EBF4W under the Corralitos record were very close to their capacity. Schemes with smaller member sizes were analyzed and found inadequate to resist the loads due to the selected records, as mentioned earlier. EBF4W was, therefore considered to provide the lowest strength required to resist the selected strong motion earthquake records.

6.11 Summary on the Study of the Seven-Story Building.

An existing seven-story reinforced concrete building was analyzed to evaluate its adequacy to resist strong ground motions. The existing building lateral carrying system was formed by ordinary moment resisting frames that had deep spandrel beams and short ("captive") columns with low shear strength.

A design review showed that the beams and columns were poorly detailed. The longitudinal reinforcement was not properly anchored and shear failure in the column was expected to occur prior to flexural yielding. Static and dynamic analyses were carried out. The static analysis was performed by applying a static incremental load and the dynamic analyses were performed using a set of two firm soil earthquake records and two soft soil records. The original building was found to have a low lateral strength and stiffness and a limited ductility. Under dynamic loading, the columns failed in shear at a very low drift, likely causing a structural collapse.

Several schemes that consisted of the addition of eccentric or concentric braced frames were proposed and investigated. Although most schemes exhibited high stiffness and limited the drifts, they were unable to prevent column shear failure. It was concluded that, in addition

to providing a bracing scheme, it was necessary to strengthen the columns against shear failure or change their failure mode to a more ductile flexural mode.

The solution adopted in this study to prevent column shear failure consisted in adding an EBF or a CBF scheme and weakening the spandrel beams. The reduction in the spandrel beam depth allowed for the columns to develop their flexural strength prior to shear failure. However, the splice and anchorage length of the beam and columns were reduced. Such schemes were found to perform adequately and to prevent column shear failure. An EBF retrofit scheme having the lowest strength required to resist the dynamic load due to the selected records was designed following a trial and error procedure. The trials designs were checked using a dynamic inelastic analysis.

Like most retrofit schemes, the added bracing systems were found to increase the axial load acting on the foundation. Foundation strengthening may be required.

Table 6.1 Moment Rotation for the Columns of the Original Structure

Lev.	Location	Sect.	M_y (k in)	θ_y (rad.)	M_u (k in)	θ_u (rad.)
1	Ext. Col.	Both	2150	.00360	2420	.00621
	Int. Col.	Base ¹	7840	.00315	8000	.00340
		Top	7840	.00315	8335	.00393
2-3	Ext. Col.	Both	2020	.00270	2330	.00538
	Int. Col.	Base ¹	6790	.00234	7500	.00357
		Top	6790	.00234	8000	.00444
4-Roof	Ext. Col.	Both	2190	.00306	2445	.00476
	Int. Col.	Both	3230	.00234	3770	.00447

¹ Splice Failure

Table 6.2 Column Shear Strength

Level	1-3		4-Roof	
Location	Int. Col.	Ext. Col.	Int. Col.	Ext. Col.
V (kips)	101	45	79	38

Table 6.3 Moment Rotation Relationship for the Beams

Level	Bay	Postive Bending Direction				Negative Bending Direction			
		M_y (k in)	M_p (k in)	θ_y (rad.)	θ_p (rad.)	M_y (k in)	M_p (k in)	θ_y (rad.)	θ_p (rad.)
1-2	Ext.	7840	10630	.00176	.00999	8700	11412	.00176	.00867
	Int.	7840	10630	.00189	.01076	8700	11412	.00189	.00934
3-Roof	Ext.	7780	10575	.00176	.00998	7780	10575	.00176	.00998
	Int.	7780	10575	.00189	.01074	7780	10575	.00189	.01074

Table 6.4 Member Properties for EBF retrofit Schemes

	Level	Beams, Links Gr. 36	Braces Gr. 46	Link		
				Length (e)	M_p/V_p	$\frac{e}{(M_p/V_p)}$
EBF1	1, 2	W21x50	TS 6x6x1/2	23 in.	25 in.	.92
	3, 4	W18x35	TS 7x7x1/4	23 in.	23 in.	1.00
	5- Roof	W16x26	TS 7x7x3/16	20 in.	20 in.	1.00
EBF 2	1, 2	W24x55	TS 10x10x3/8	26 in.	26 in.	1.00
	3, 4	W21x50	TS 8x8x5/16	23 in.	25 in.	.92
	5-Roof	W16x31	TS 6x6x1/4	23 in.	23 in.	1.00
EBF3	1, 2	W24x55	TS 10x10x3/8	26 in.	26 in.	1.00
	3, 4, 5	W21x50	TS 8x8x5/16	23 in.	25 in.	.92
	6- Roof	W16x31	TS 6x6x1/4	23 in.	23 in.	1.00

Table 6.5 Member Properties for the CBF3 Retrofit Scheme

	Level	Beams Gr. 36	Braces Gr. 46
CBF3	1, 2	W12x26	TS 6x6x3/8
	3, 4	W12x22	TS 6x6x5/16
	5-Roof	W12x19	TS 5x5x5/16

Table 6.6 Moment Rotation Relationship for the Strengthened Columns of EBF1, EBF2, and EBF3 Retrofit Schemes

Lev.	My (k in)	θ_y (rad.)	Mu (k in)	θ_u (rad.)
1	13655	.00370	16580	.01516
2-3	13810	.00252	18480	.01835
4-Roof	9080	.00270	13840	.02938

Table 6.7 Moment Rotation Relationship for the Strengthened Columns of CBF3 Retrofit Scheme

Lev.	My (k in)	θ_y (rad.)	Mu (k in)	θ_u (rad.)
1	18665	.00332	19445	.00380
2-3	17730	.00234	19030	.00307
4-Roof	11675	.00198	14920	.00496

Table 6.8 Buckling and Post Buckling Capacity of the CBF3 Braces

	Level	Braces Gr. 46	P_b	P_{pb}/P_b
CBF3	1, 2	TS 6x6x3/8	270	.23
	3, 4	TS 6x6x5/16	230	.23
	5-Roof	TS 5x5x5/16	163	.40

Table 6.9 Period of Vibration of the Original Building and of Sries I Retrofit Schemes

Structure	Period of Vibration (s)	
	First Mode	Second Mode
Original	0.687	0.238
EBF1	0.537	0.188
EBF2	0.510	0.179
EBF3	0.434	0.151
CBF3	0.431	0.146

Table 6.10 Moment Rotation Relationship for the Columns of EBF3W and CBF3W Retrofit Schemes

Scheme	Lev.	Location	Section	M_y (k in)	θ_y (rad.)	M_{max} (k in)	θ_{max} (rad.)	
EBF3W	1	Ext. Col.	Both	*	*	1810	.00404	
			Top	12755	.00480	14020	.01133	
		Int. Col. ¹	Base	12755	.00480	16600	.02466	
	2-3	Ext. Col.	Both	*	*	1970	.00329	
			Top	*	*	13780	.00314	
		Int. Col. ¹	Base	13810	.00315	16240	.01345	
	4-Roof	Ext. Col.	Both	*	*	1900	.00332	
			Top	9080	.00338	9315	.00502	
		Int. Col. ¹	Base	9080	.00338	11430	.01984	
	CBF3W	1	Ext. Col.	Both	*	*	1810	.00404
				Top	*	*	18500	.00387
			Int. Col. ¹	Base	18665	.00390	19445	.00447
2-3		Ext. Col.	Both	*	*	1970	.00329	
			Top	17730	.00293	18060	.00315	
		Int. Col. ¹	Base	17730	.00293	19030	.00383	
4-Roof		Ext. Col.	Both	*	*	1900	.00332	
			Top	11675	.00619	14000	.00514	
		Int. Col. ¹	Base	11675	.00619	14920	.00619	

* Splice failure occurs prior to yielding

Table 6.11 Moment Rotation Relationships for the Spandrel Beams of EBF3W and CBF3W

Level	Bay	Positive Bending Direction				Negative Bending Direction			
		M_y (k in)	M_{max} (k in)	θ_y (rad.)	θ_{max} (rad.)	M_y (k in)	M_{max} (k in)	θ_y (rad.)	θ_{max} (rad.)
1-2	Ext.	1020	1250	.00644	.01637	4800	5130	.00351	.00953
	Int.	252	1250	.00693	.01763	4800	5130	.00378	.01026
3-Roof	Ext.	234	1200	.00643	.01899	4310	4890	.00410	.01568
	Int.	252	1200	.00693	.02045	4310	4890	.00441	.00441

Table 6.12 Period of Vibration of the Original Building and of EBF3W and CBF3W

Structure	Period of Vibration (s)	
	First Mode	Second Mode
Original	0.687	0.238
EBF3-W	0.587	0.204
CBF3-W	0.562	0.191

Table 6.13 Member Properties for the EBF4W retrofit Scheme

Level	Beams, Links Gr. 36	Braces Gr. 46	Link			
			Length (e)	M_p/V_p	$\frac{e}{(M_p/V_p)}$	
EBF4W	1, 2	W18x46	TS 6x6x1/2	26 in.	25 in.	1.04
	3, 4	W18x35	7x7x1/4	23 in.	23 in.	1.00
	5- Roof	W16x26	7x7x3/16	23 in.	20 in.	1.15

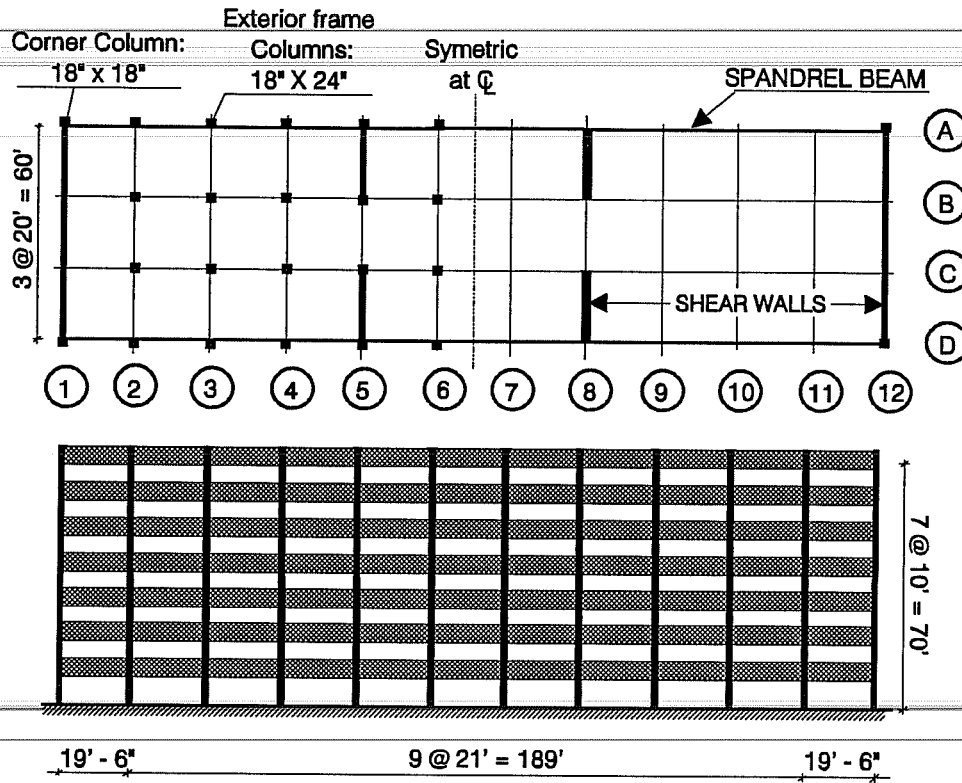


Figure 6.1 Elevation and Plan Views of the Seven-Story Building

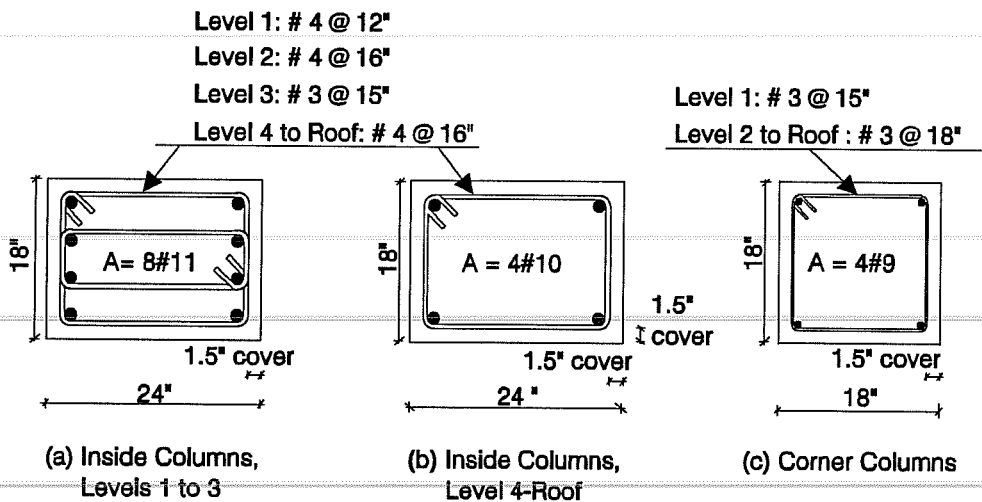


Figure 6.2 Reinforcement Details of the Columns of the Seven Story Building

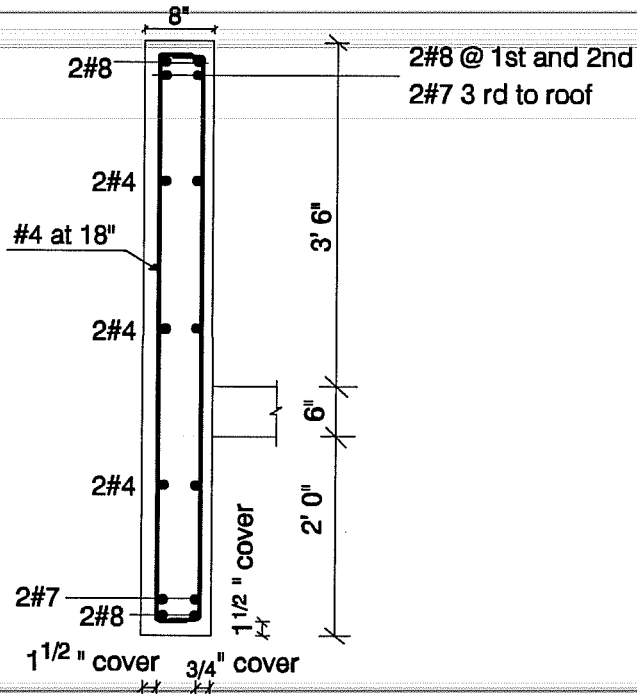


Figure 6.3 Cross Section of the Seven-Story Building's Spandrel Beams

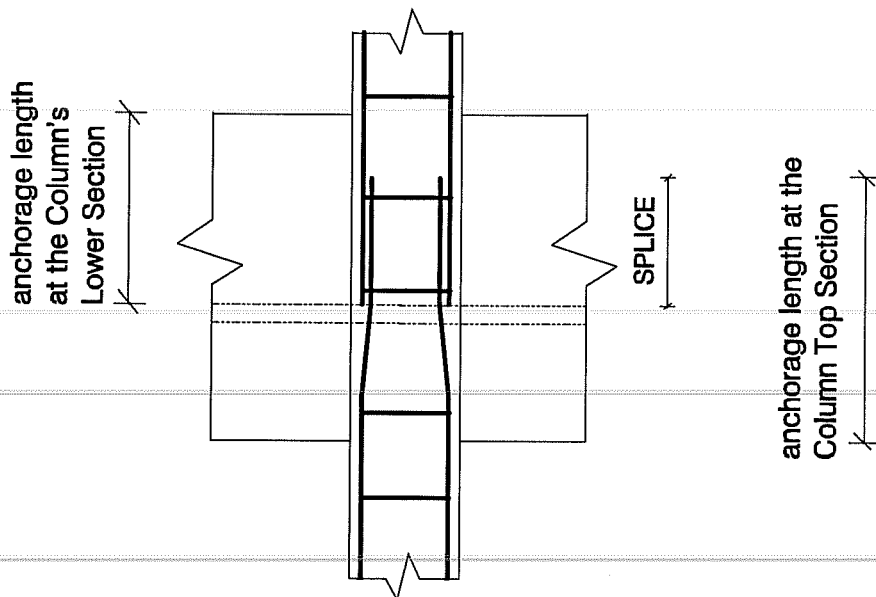
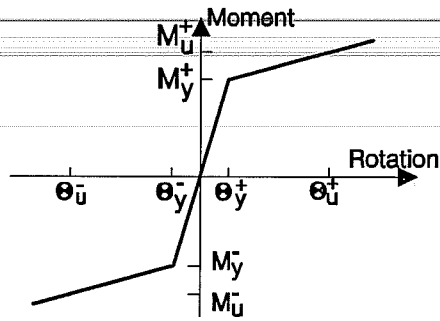
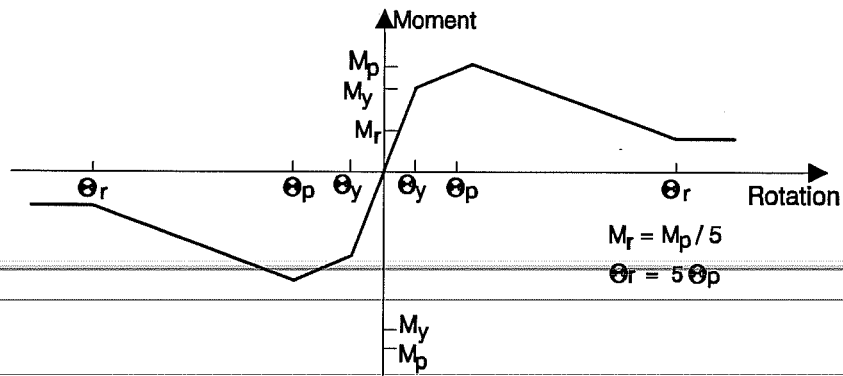


Figure 6.4 Column Reinforcement at the Beam-Column Connection for the Seven-Story Building



(a) Column Sections with Proper Splice



(b) Column Sections with Splice Failure

Figure 6.5 Moment Rotation Envelopes for the Columns of the Original Seven-Story Building

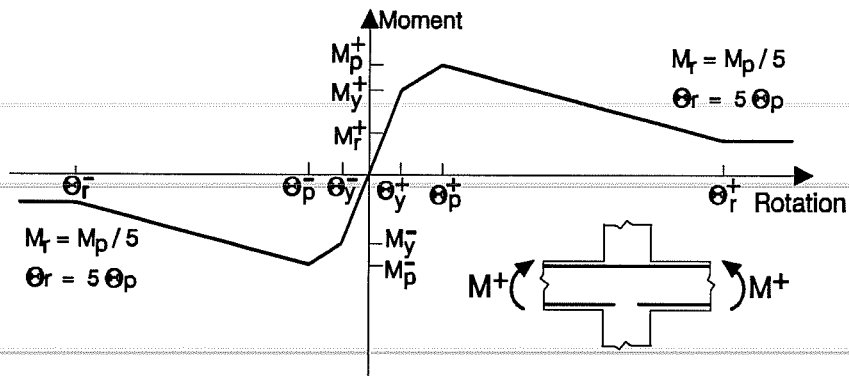


Figure 6.6 Moment Rotation Envelopes for the Spandrel Beams of the Original Seven-Story Building

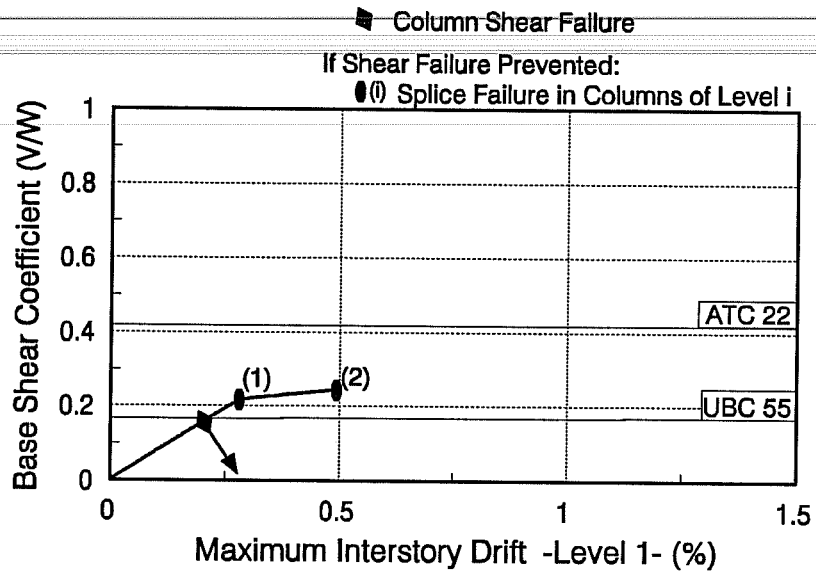


Figure 6.7 Maximum Interstory Drift for the Original Seven-Story Building Under Static Load

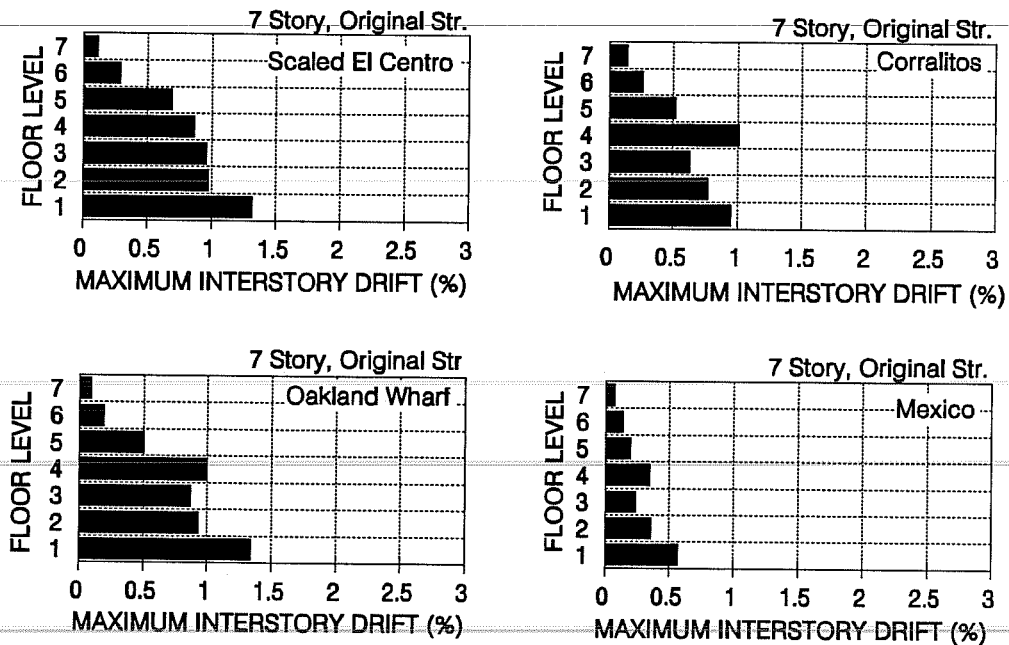


Figure 6.8 Maximum Dynamic Interstory Drifts for the Original Seven-Story Building, assuming shear failure is prevented

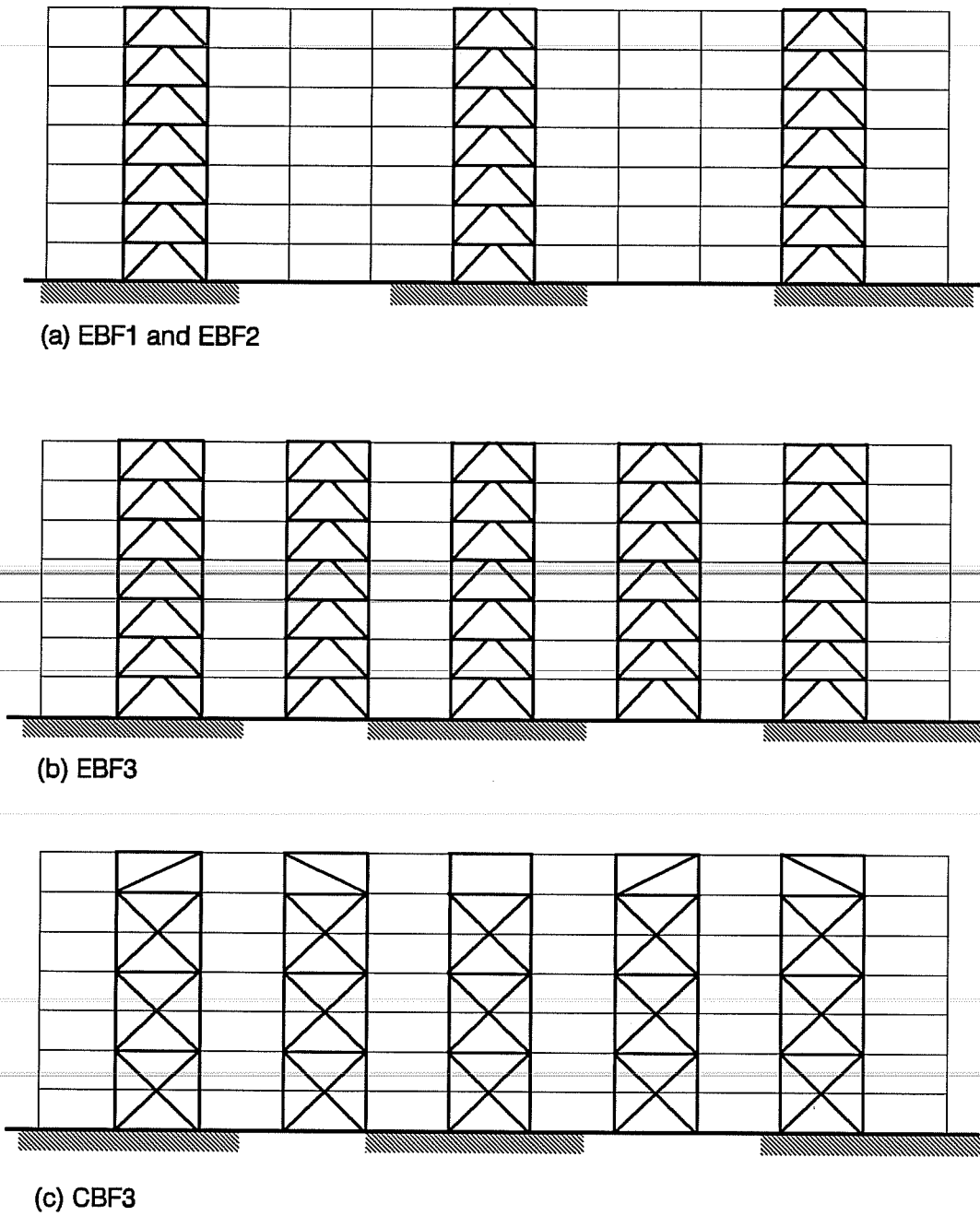


Figure 6.9 Retrofit Scheme Configurations Used for the Seven-Story Building

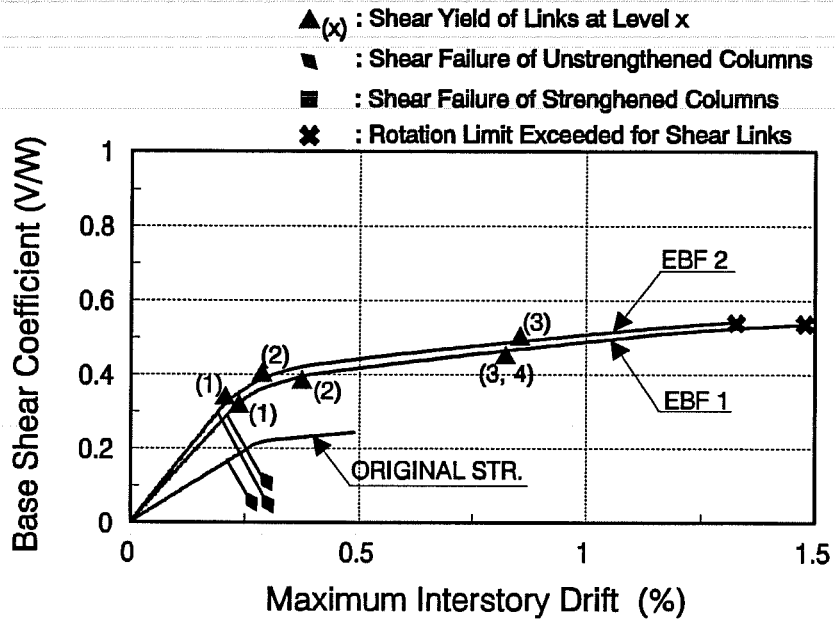


Figure 6.10 Maximum Interstory Drift for EBF1 and EBF2 Retrofit Schemes Subjected to Static Load

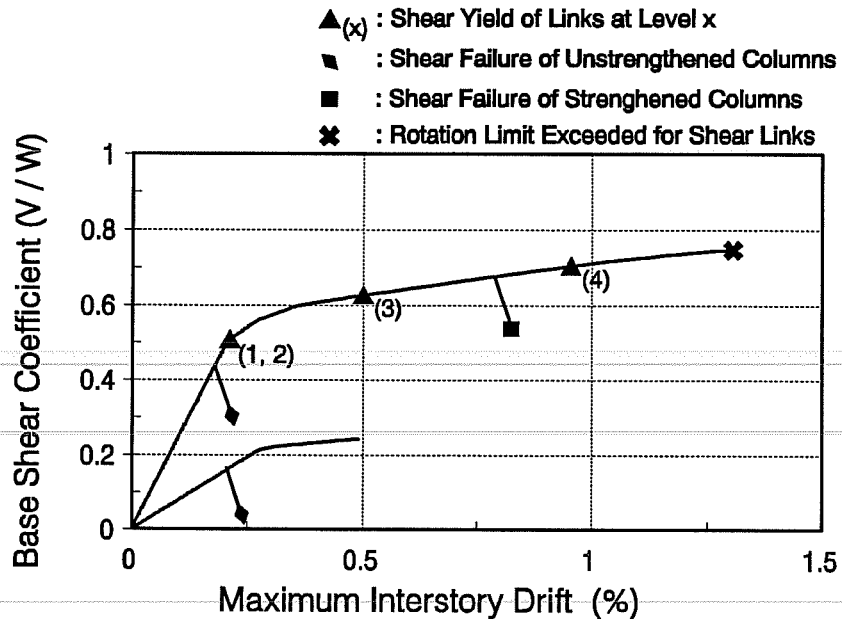


Figure 6.11 Maximum Interstory Drift for EBF3 Retrofit Scheme Subjected to Static Load

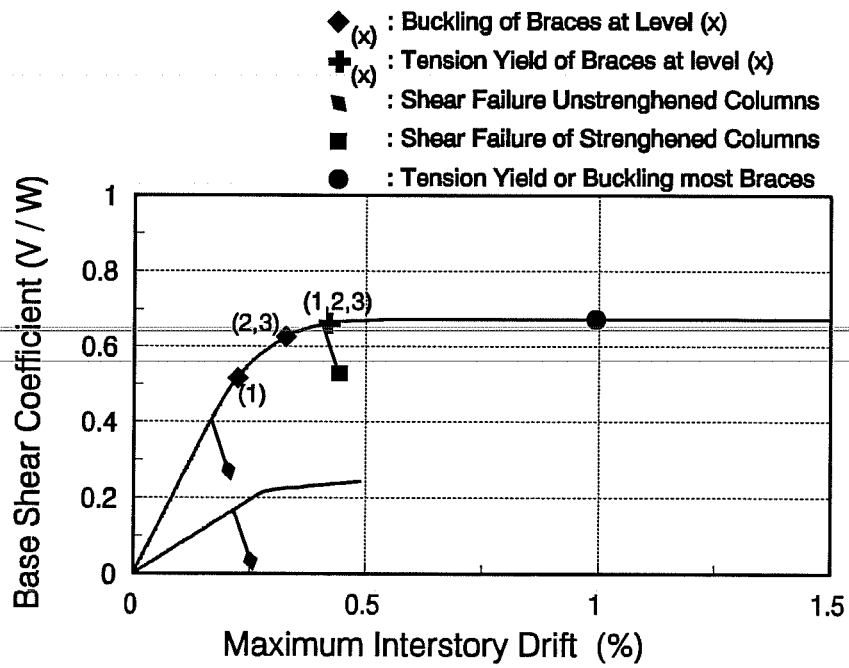


Figure 6.12 Maximum Interstory Drift for CBF3 Retrofit Scheme Subjected to Static Load

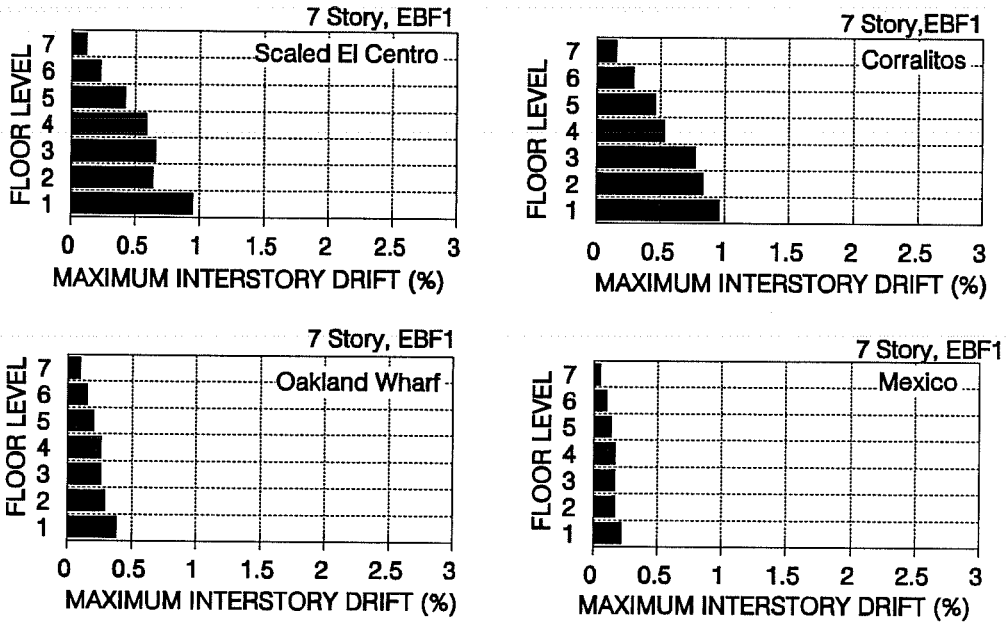


Figure 6.13 Maximum Interstory Drifts for EBF1 Retrofit Scheme Subjected to the Selected Acceleration Records

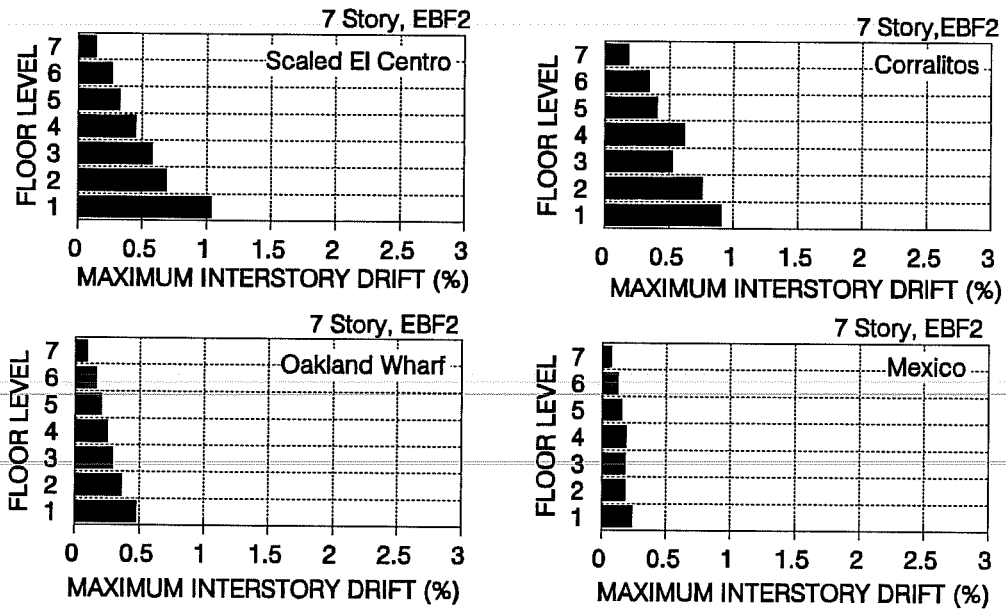


Figure 6.14 Maximum Interstory Drifts for EBF2 Retrofit Scheme Subjected to the Selected Acceleration Records

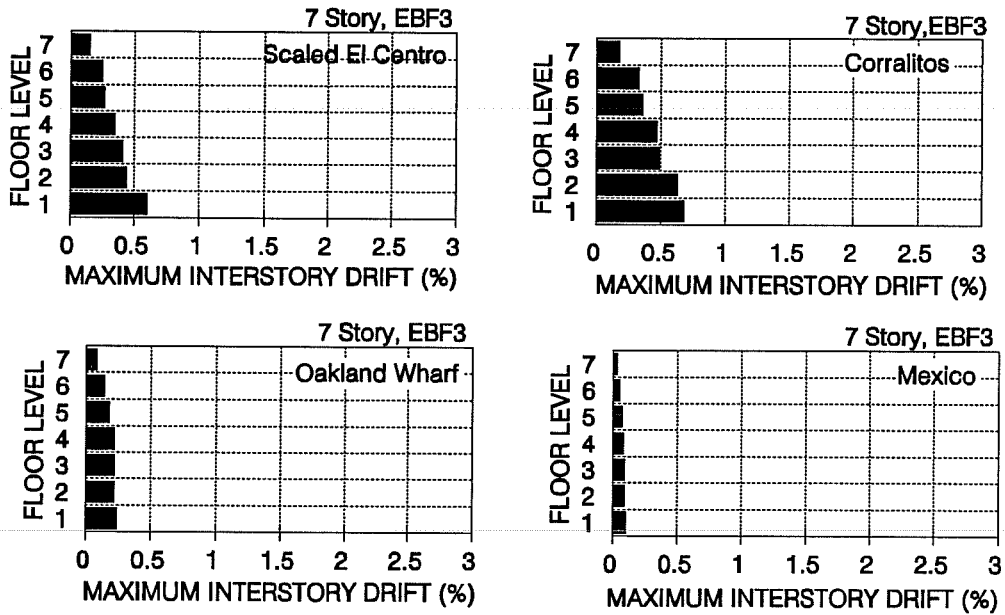


Figure 6.15 Maximum Interstory Drifts for EBF3 Retrofit Scheme Subjected to the Selected Acceleration Records

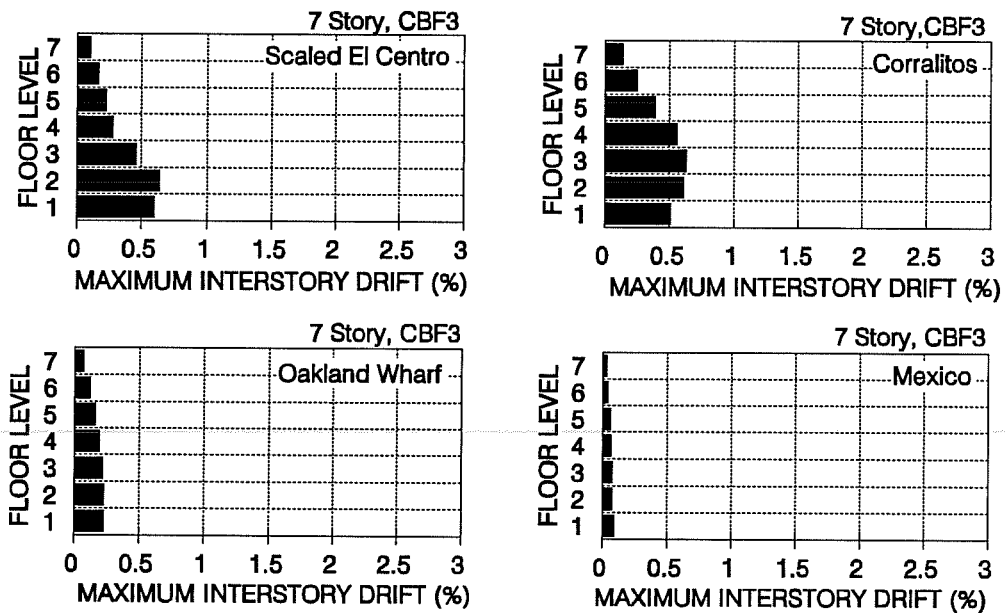


Figure 6.16 Maximum Interstory Drifts for CBF3 Retrofit Scheme Subjected to the Selected Acceleration Records

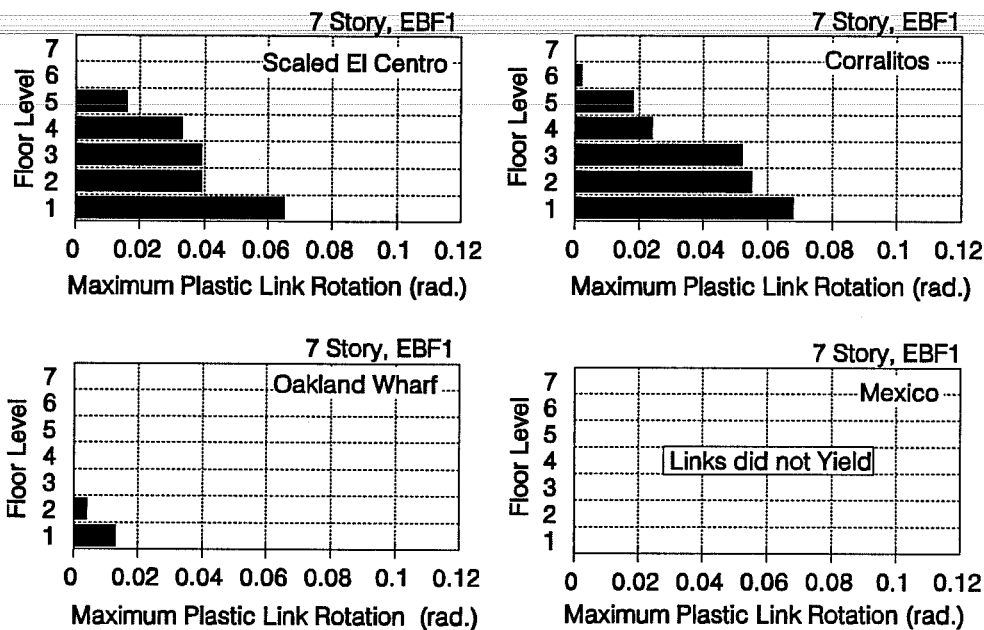


Figure 6.17 Maximum Plastic Rotation in Links of EBF1 Subjected to the Selected Ground Acceleration Records

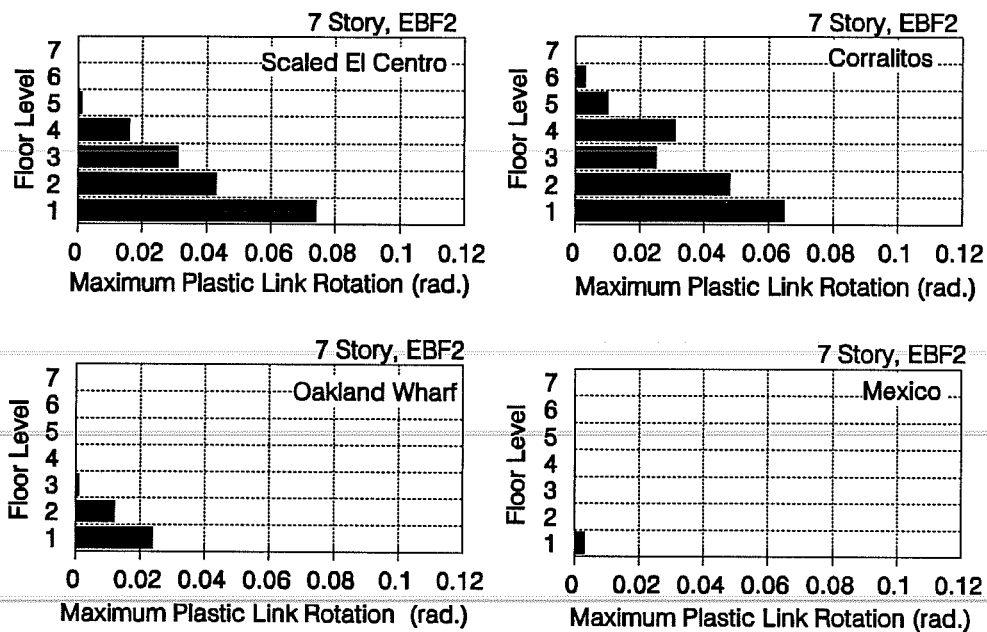


Figure 6.18 Maximum Plastic Rotation in Links of EBF2 Subjected to the Selected Ground Acceleration Records

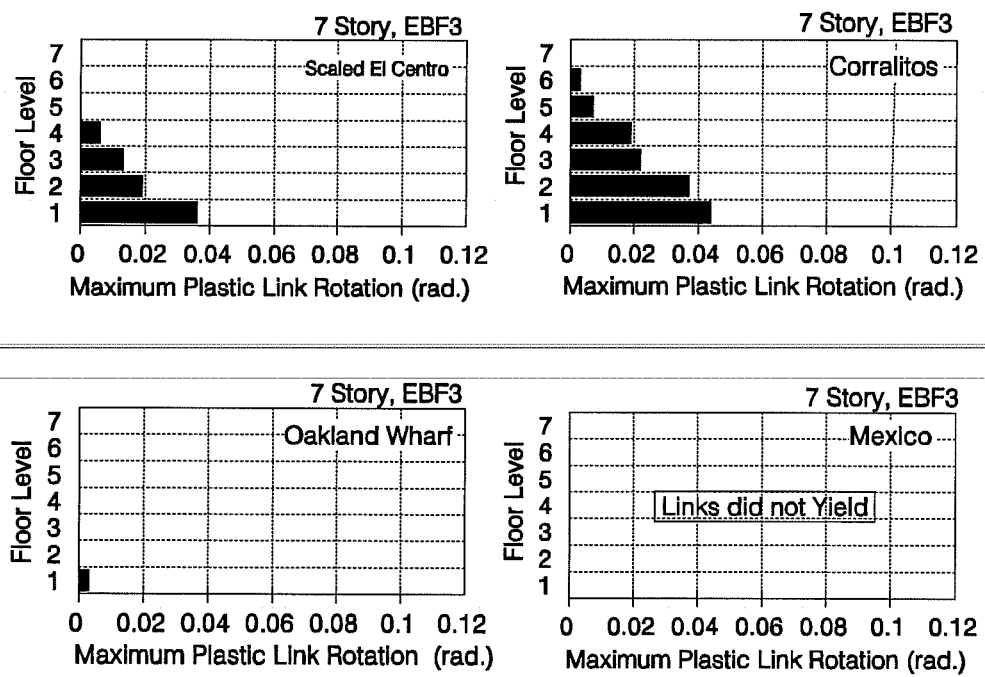


Figure 6.19 Maximum Plastic Rotation in Links of EBF3 Subjected to the Selected Ground Acceleration Records

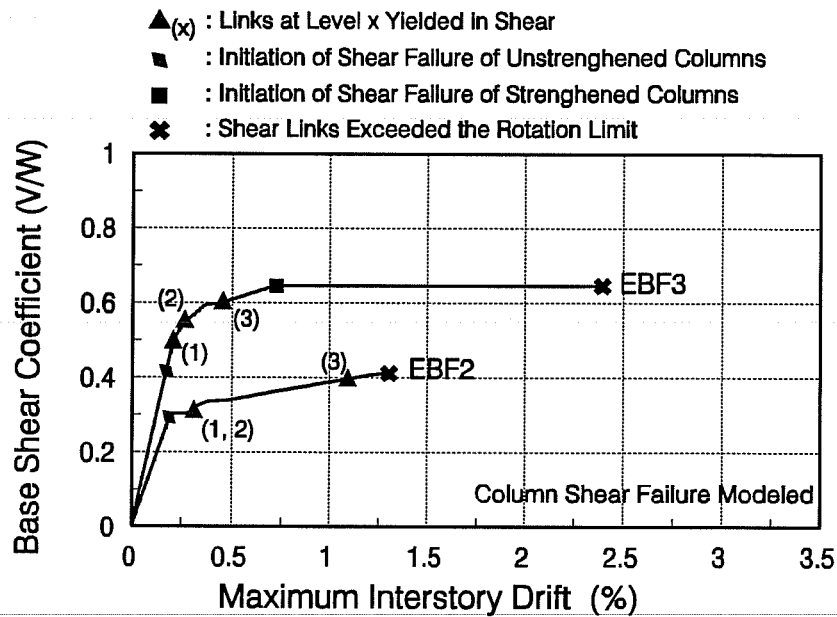


Figure 6.20 Maximum Interstory Drift for EBF2 and EBF3 Subjected to Static Load and with Column Shear Failure Modeled

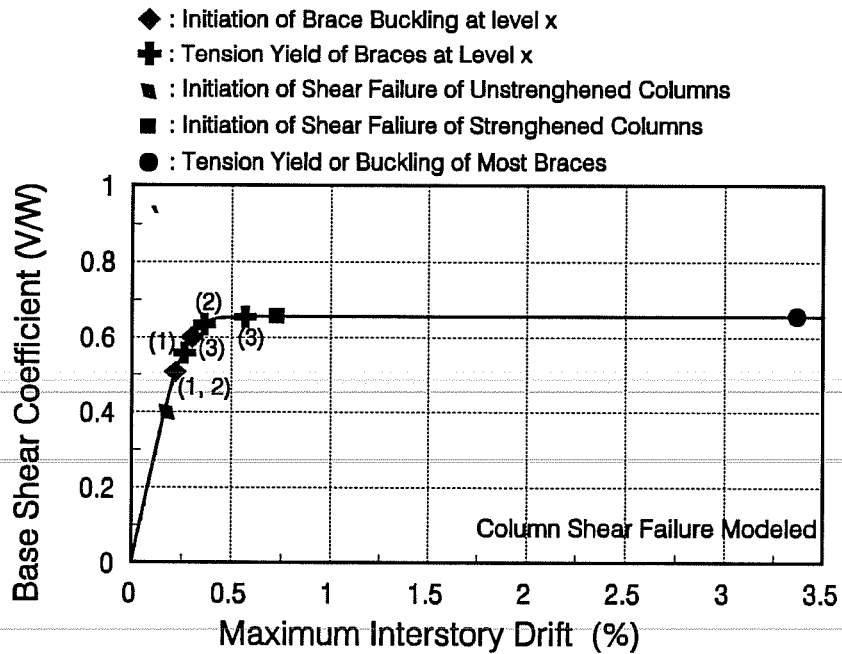


Figure 6.21 Maximum Interstory Drift for CBF3 Subjected to Static Load and with Column Shear Failure Modeled

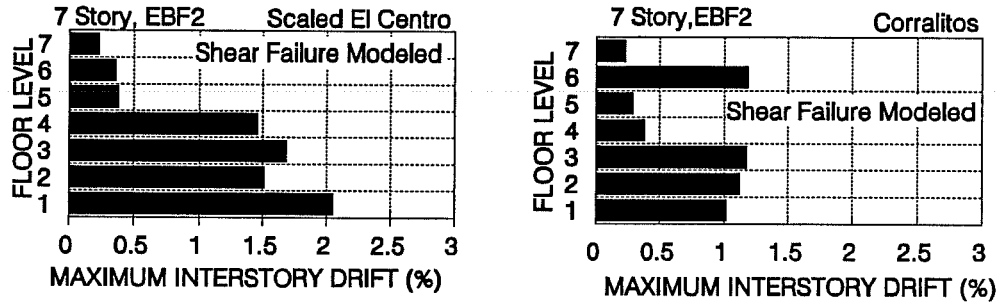


Figure 6.22 Maximum Interstory Drifts for EBF2 Retrofit Scheme Subjected to the Selected Records and with Column Shear Failure Modeled

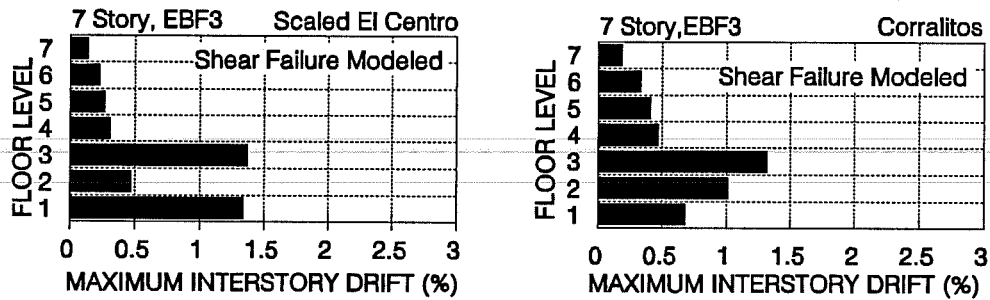


Figure 6.23 Maximum Interstory Drifts for EBF3 Retrofit Scheme Subjected to the Selected Records and with Column Shear Failure Modeled

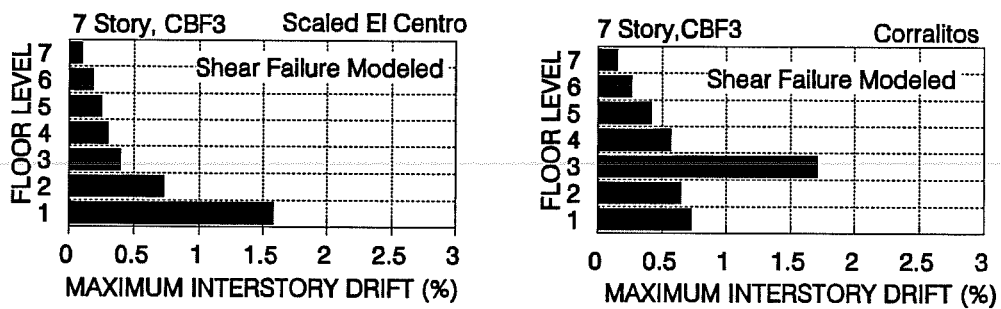


Figure 6.24 Maximum Interstory Drifts for CBF3 Retrofit Scheme Subjected to the Selected Records and with Column Shear Failure Modeled

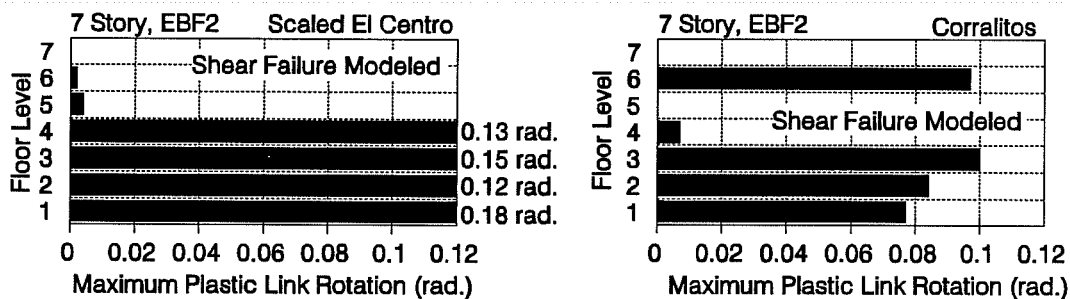


Figure 6.25 Maximum Plastic Rotation in Links of EBF2 Subjected to the Selected Ground Acceleration Records

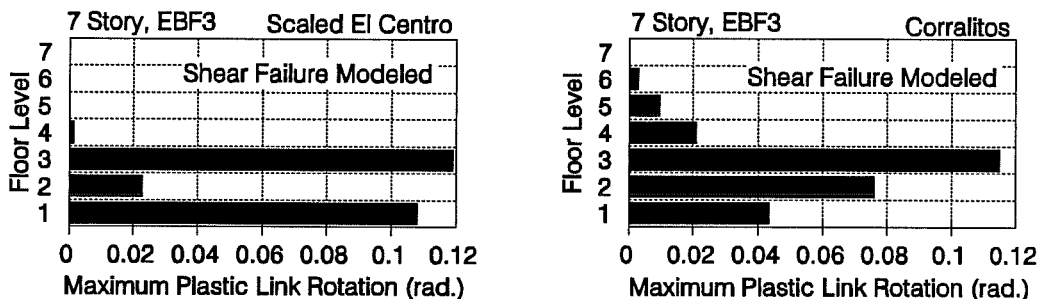


Figure 6.26 Maximum Plastic Rotation in Links of EBF3 Subjected to the Selected Ground Acceleration Records

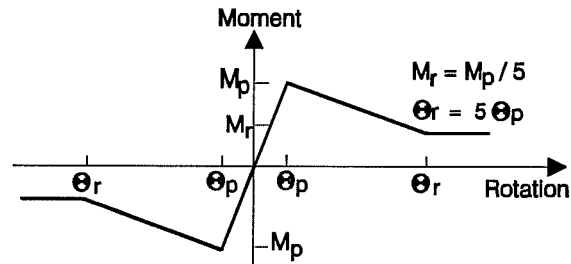


Figure 6.27 Moment Rotation Envelope for EBF3W and CBF3W Columns Sections Subjected to Splice Failure Prior to Yielding

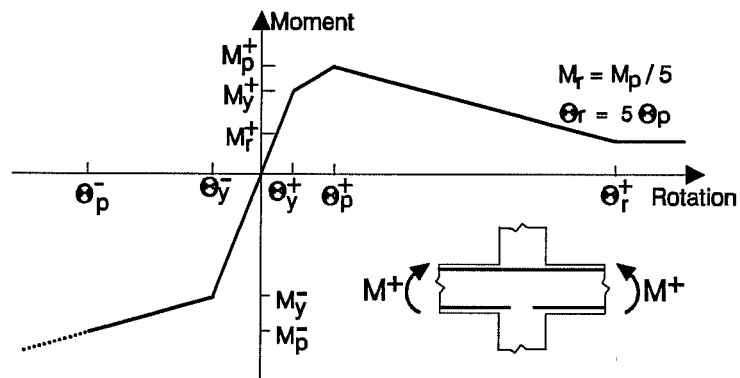


Figure 6.28 Moment Rotation Envelope for the Spandrel Beams with Reduced Depth (EBF3W and CBF3W Retrofit Schemes)

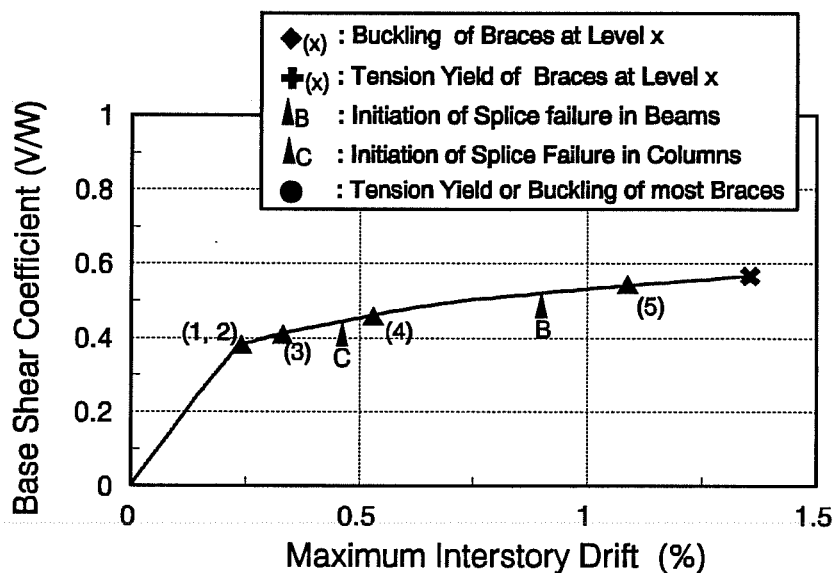


Figure 6.29 Maximum Interstory Drift for EBF3W Subjected to Static Load

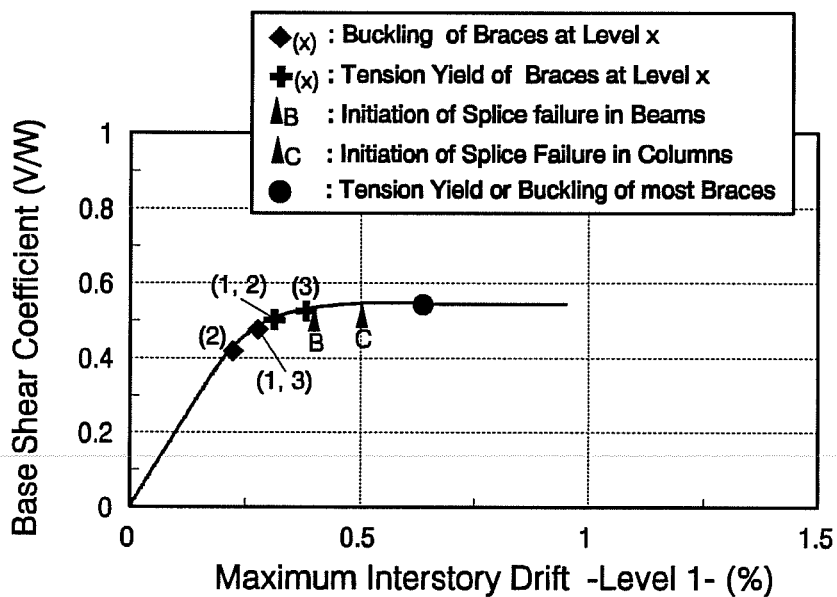


Figure 6.30 Maximum Interstory Drift for CBF3W Subjected to Static Lateral Load

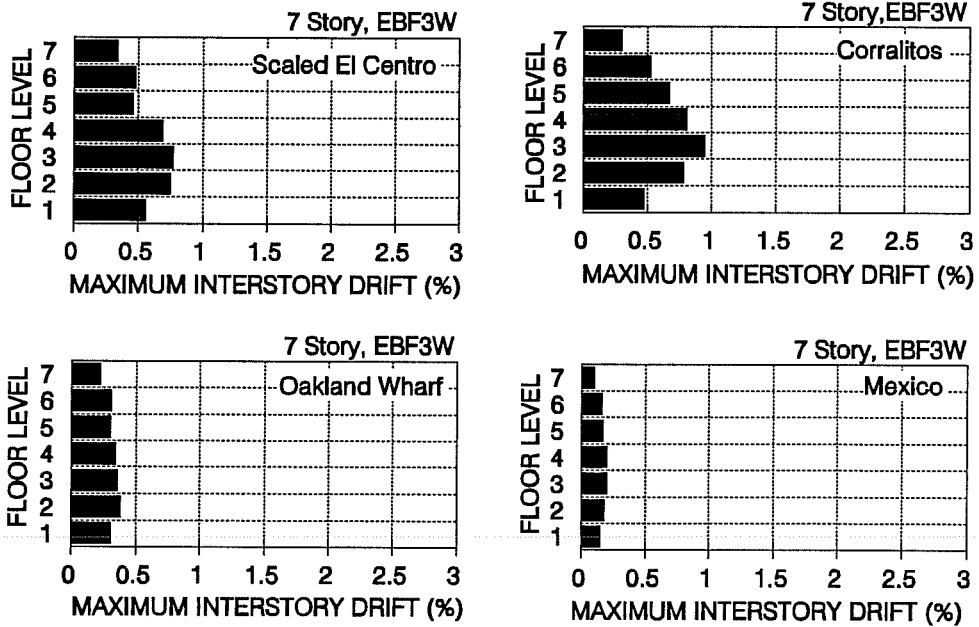


Figure 6.31 Maximum Interstory Drifts for EBF3W Retrofit Scheme Subjected to the Selected Acceleration Records

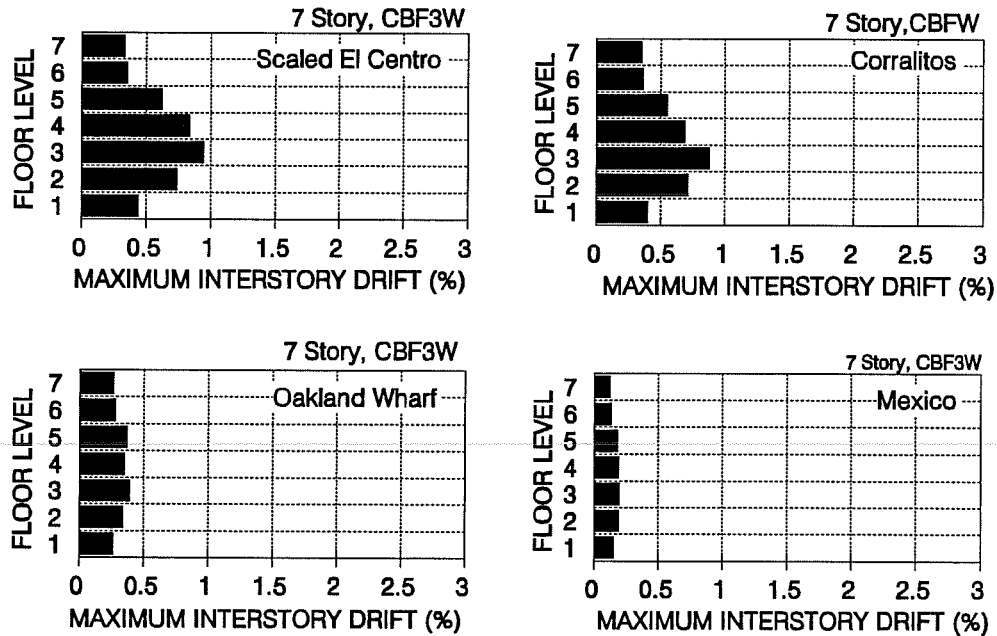


Figure 6.32 Maximum Interstory Drifts for CBF3W Retrofit Scheme Subjected to the Selected Acceleration Records

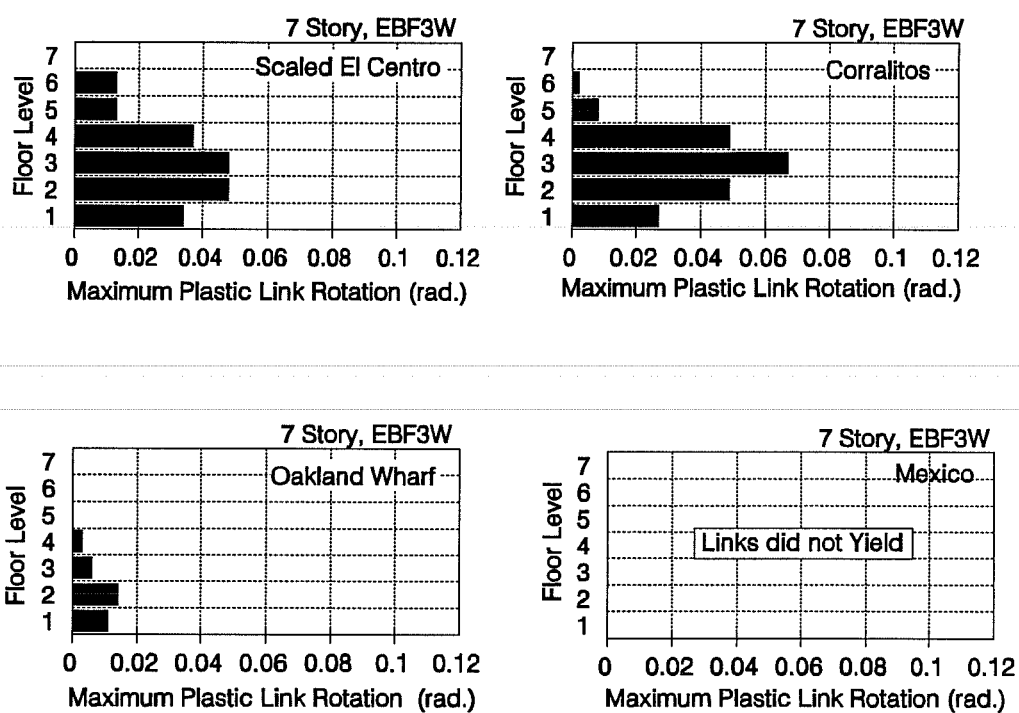
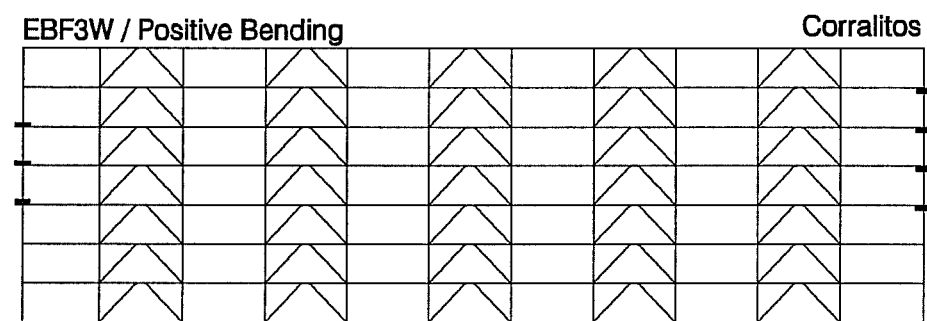
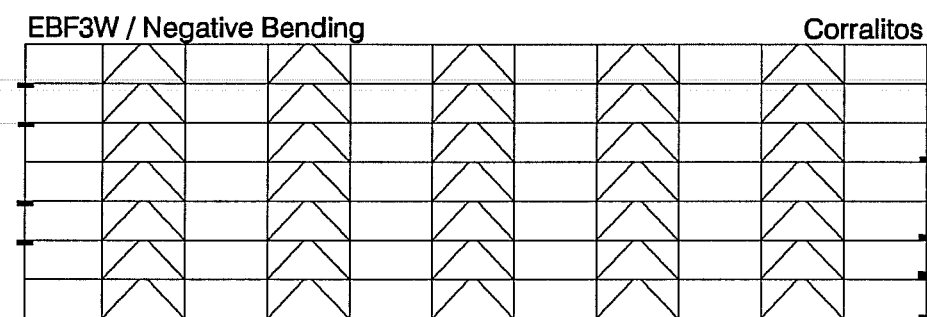


Figure 6.33 Maximum Plastic Rotation in Links of EBF3W Subjected to the Selected Ground Acceleration Records



(a) Positive Bending



(b) Negative Bending

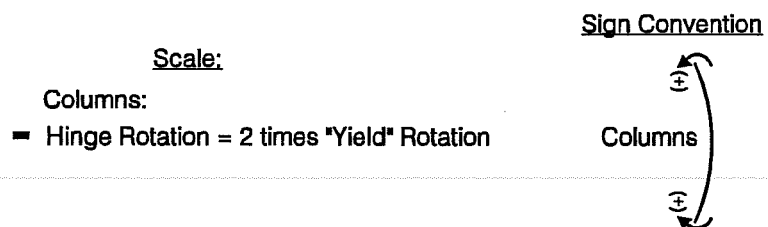
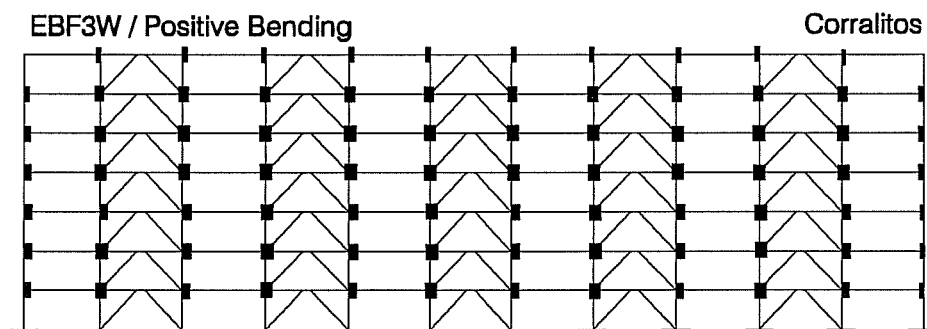
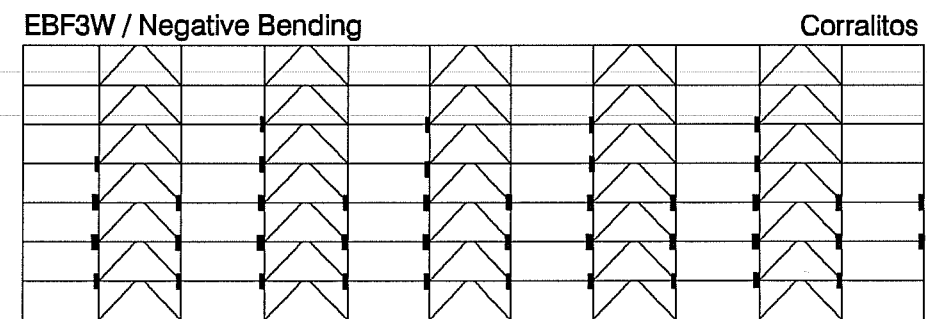


Figure 6.34 Maximum Ductility Demands for Columns of EBF3W Under the Corralitos Acceleration Record



(a) Positive Bending



(b) Negative Bending

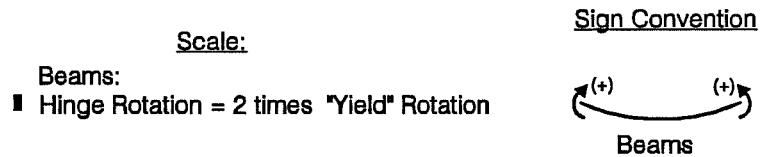
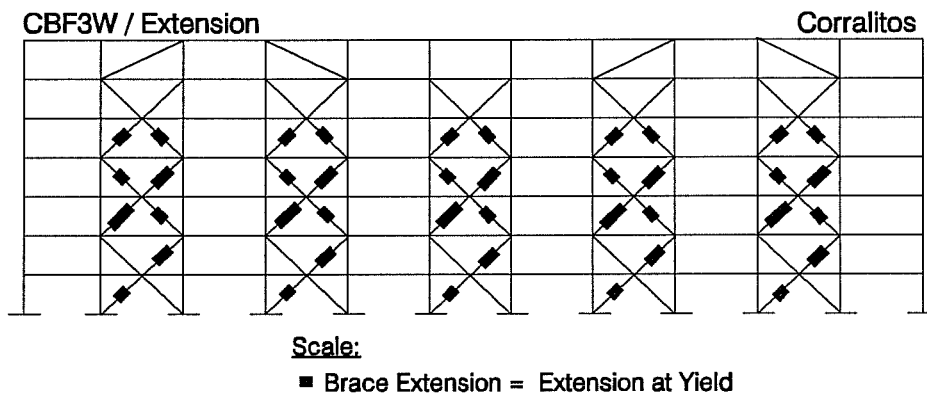
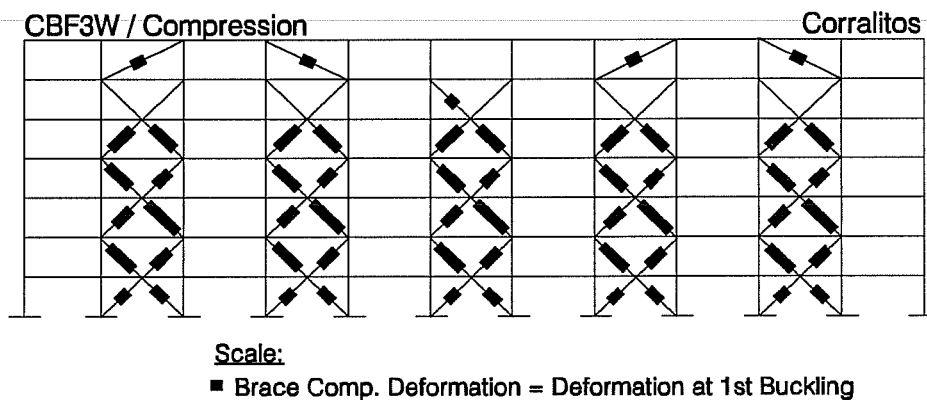


Figure 6.35 Maximum Ductility Demands for the Beams of EBF3W Under the Corralitos Acceleration Record

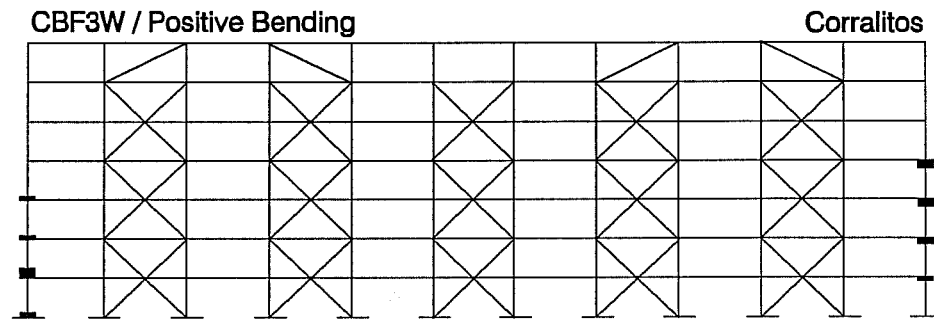


(a) Brace Extension

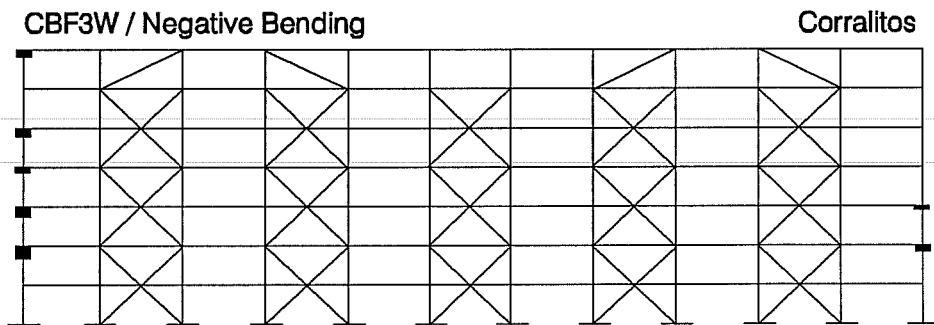


(b) Brace Compression

Figure 6.36 Maximum Plastic Deformations in CBF3W Braces Under Corralitos Acceleration Record



(a) Positive Bending



(b) Negative Bending

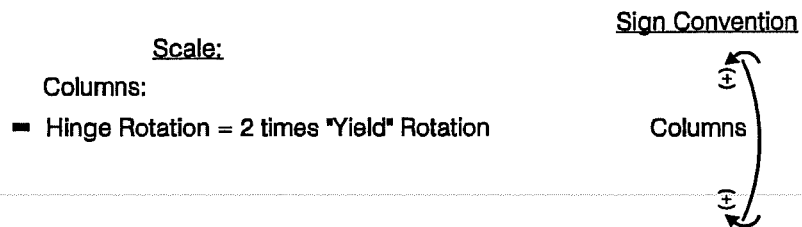
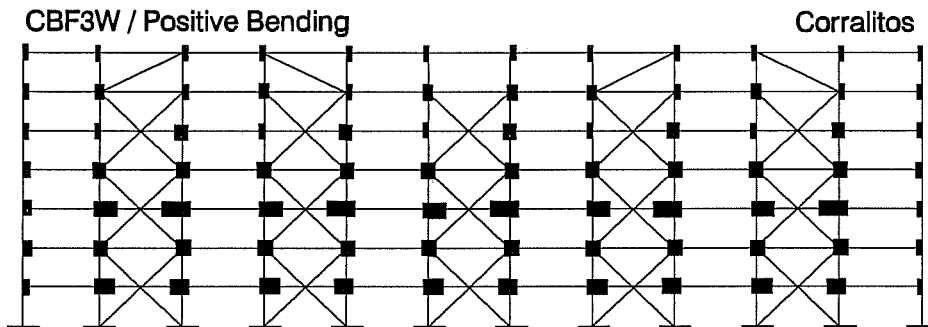
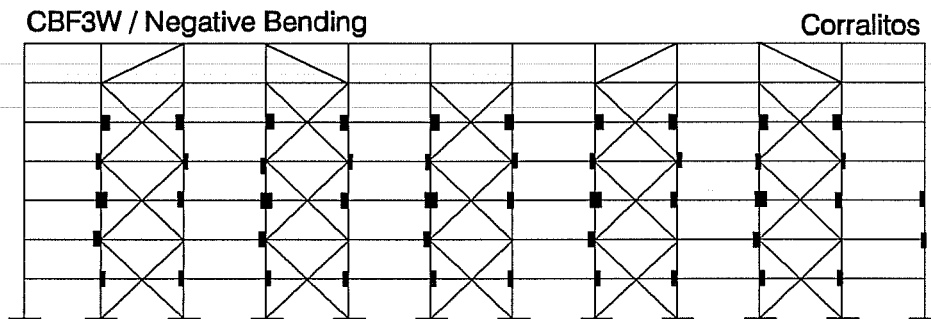


Figure 6.37 Maximum Plastic Rotations in Columns of CBF3W Under the Corralitos Acceleration Record



(a) Positive Bending



(b) Negative Bending



Figure 6.38 Maximum Plastic Rotations in Beams of CBF3W Under the Corralitos Acceleration Record

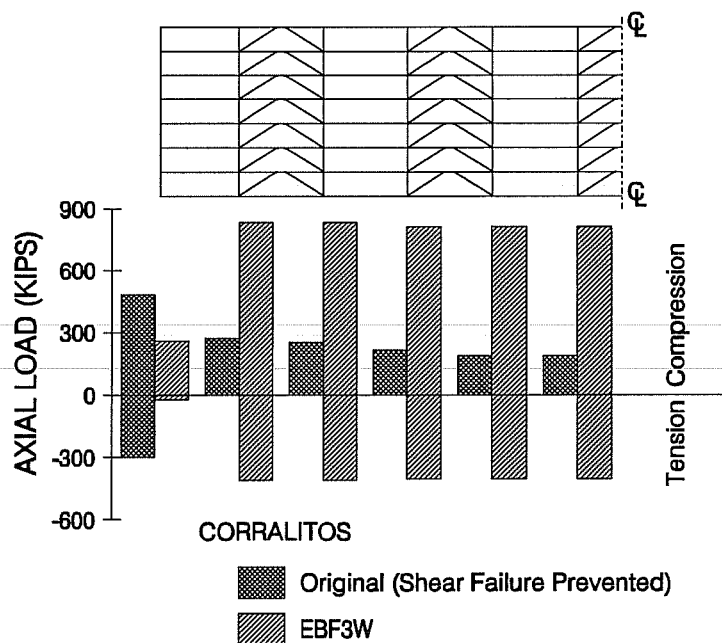


Figure 6.39 Maximum Foundation Axial Load for the Original Seven-Story Building (with Shear Failure Prevented) and for the Retrofit Scheme EBF3W Subjected to the Corralitos Record

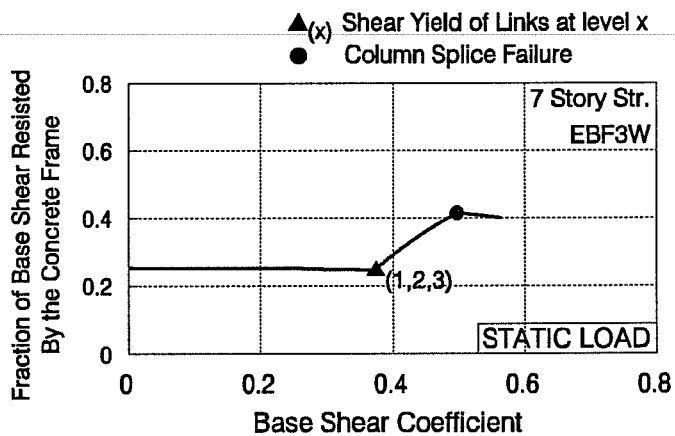
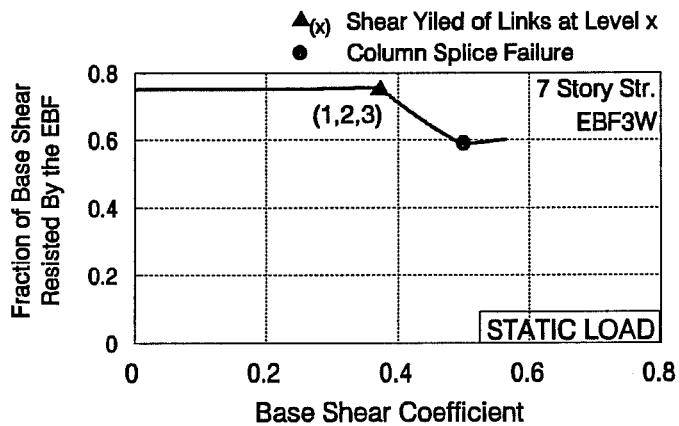


Figure 6.40 Distribution of Base Shear Between the existing R/C Frame and the EBF for the EBF3W Retrofit Scheme Under Static Load

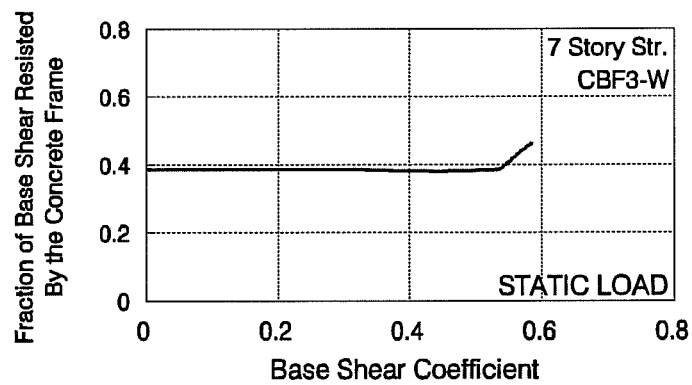
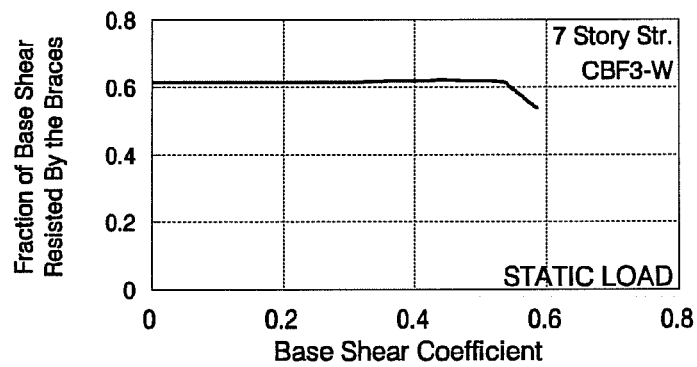


Figure 6.41 Distribution of the Base Shear Between the existing R/C Frame and the Braces for the CBF3W Retrofit Scheme Under Static Load

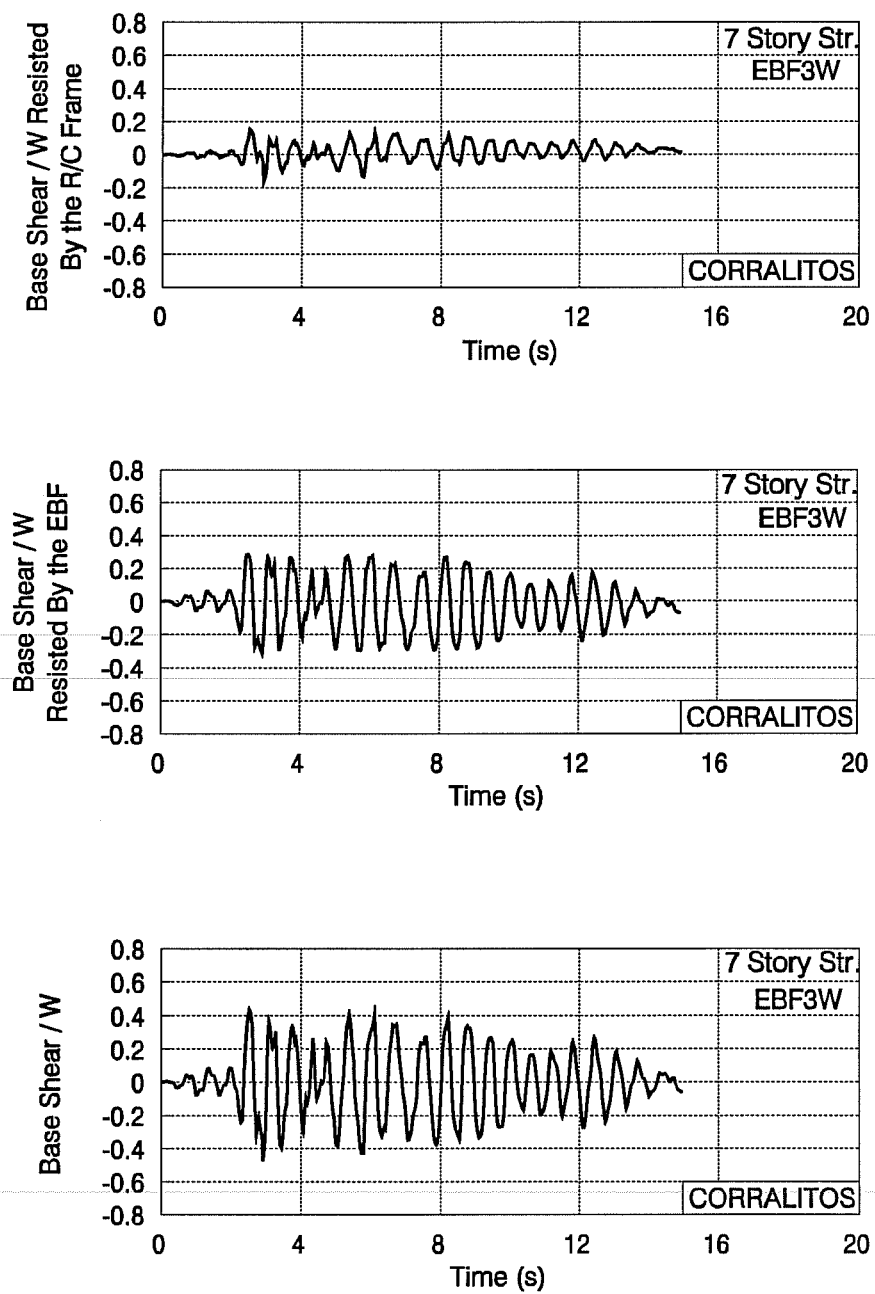


Figure 6.42 Base Shear Distribution for EBF3W Subjected to the Corralitos Record

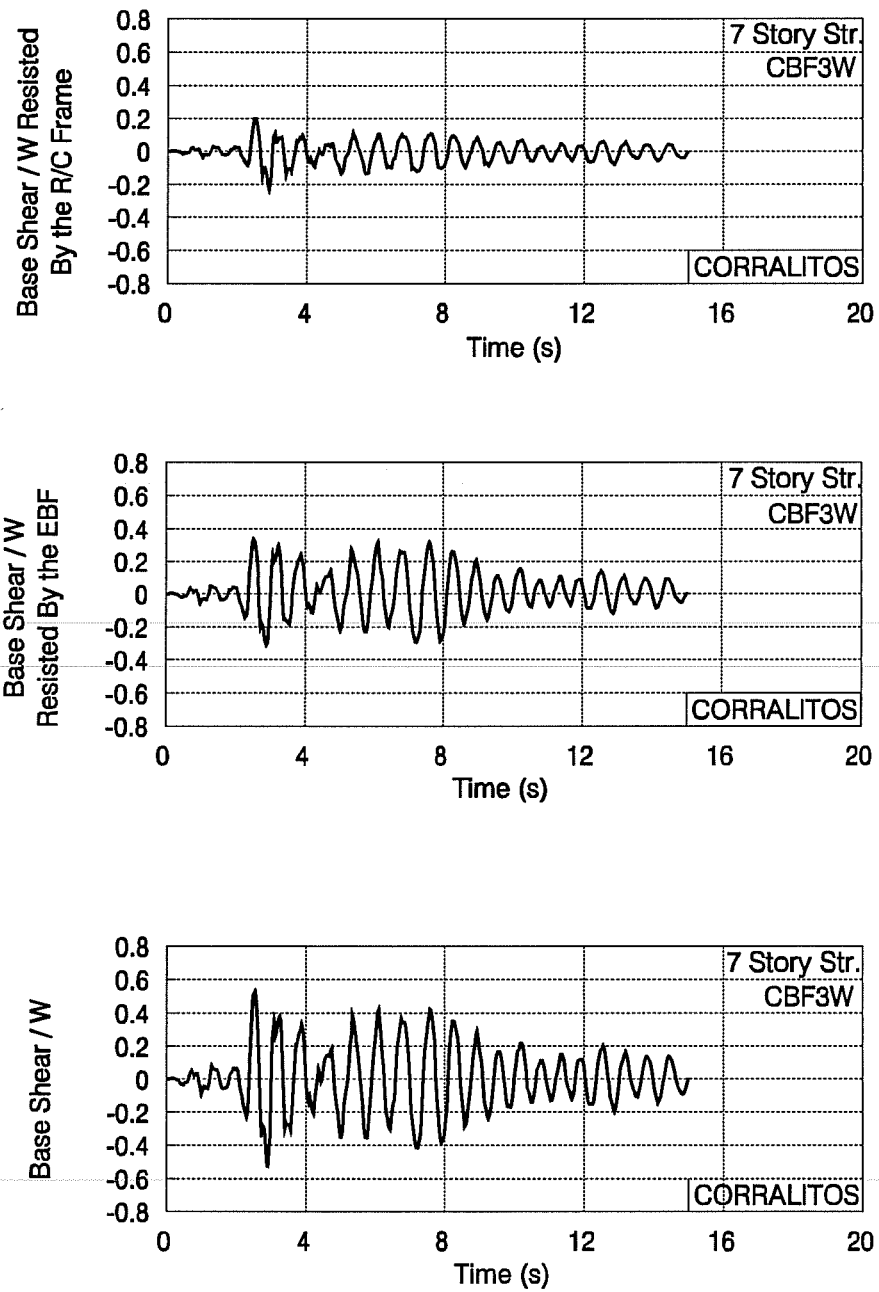


Figure 6.43 Base Shear Distribution for EBF3W Subjected to the Corralitos Record

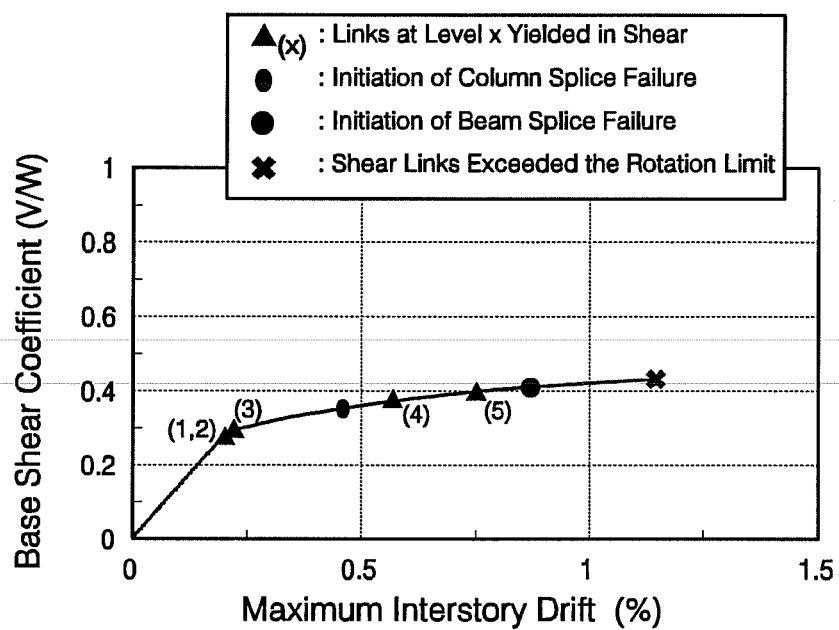


Figure 6.44 Maximum Interstory Drift for EBF4W Subjected to Static Load

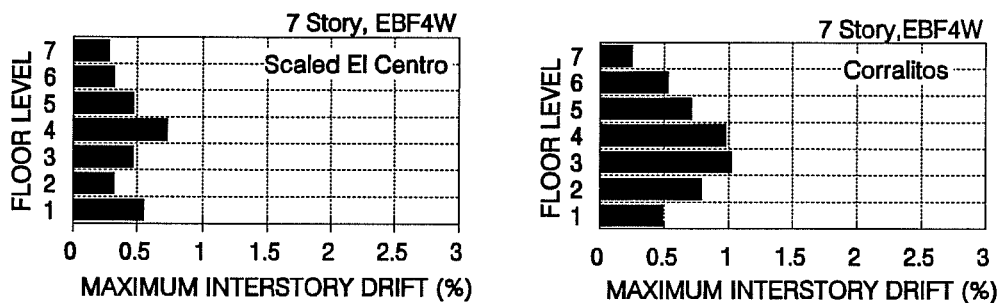


Figure 6.45 Maximum Interstory Drifts for the EBF4W Retrofit Scheme Subjected to the Scaled El Centro and to Corralitos Records

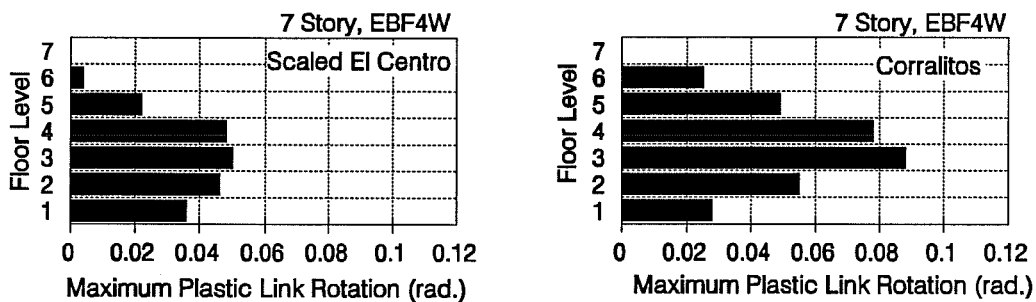


Figure 6.46 Maximum Plastic Rotation in Links of EBF4W Subjected to the Scaled El Centro and to the Corralitos Records

CHAPTER 7:

DISCUSSION OF RESULTS AND DESIGN RECOMMENDATIONS

7.1. Introduction.

In this section, the analytical results will be reviewed to assess the effectiveness of steel eccentrically braced frames (EBFs) as a seismic retrofit scheme for reinforced concrete moment frame buildings. The advantages and drawbacks of EBFs as a retrofit scheme will be summarized. Also, the performance of EBF and concentrically braced frame (CBF) retrofit schemes will be compared by examining the strength and energy dissipation capacity of both systems. The adequacy of ATC 22 recommendations for evaluation of existing buildings will be examined for the case studies. The possibility of using ATC 22 for evaluating the adequacy of EBF and CBF strengthening schemes will also be discussed. Finally, practical recommendations for the design of EBFs used as a retrofit scheme for reinforced concrete moment frame buildings will be suggested.

7.2. General Observations.

Static and dynamic inelastic analyses were conducted on two reinforced concrete buildings, representative of the 1950s and 1960s low rise and medium rise west coast construction. The lateral load resisting system of both buildings consisted of ordinary moment resisting frames. The static analyses were performed by applying lateral incremental loads. The dynamic analyses were conducted by subjecting the buildings to the ground acceleration from three firm soil earthquake records and two soft soil earthquake records. The firm soil records are the 1940 El Centro record scaled to a peak ground acceleration of 0.5g, the 1989 Corralitos record, and the 1966 Parkfield record. The soft soil earthquake records are the 1989 Oakland Harbor Wharf record, and the 1985 Mexico City SCT-1 record.

The first structure considered in this study was a three-story building with 24 ft long bays and 12 ft story heights. The building was designed according to the lateral load levels of

the 1964 Uniform Building Code (UBC). The structural components were proportioned and detailed according to the provisions of the 1963 edition of the ACI 318 code. The building exhibited several deficiencies that included inadequate column and beam splices, inadequate concrete confinement, low strength, and poor ductility.

The second structure was a seven-story building. The lateral load was resisted by stiff external frames that were formed by deep spandrel beams and by short (or "captive") columns. The seismic design forces were based on the 1955 edition of the UBC and the member design followed the recommendations of the 1956 ACI 318 code. The floor to floor height of the outer frame columns was 10 ft. However the deep spandrel beams created "captive" columns by reducing the column's clear height to 4 ft. Furthermore, the transverse reinforcement was widely spaced and did not permit the development of the columns' flexural capacity. Other deficiencies included poor concrete confinement and inadequate splice length.

The analyses showed that the addition of the EBF retrofit schemes increased the strength and stiffness of the buildings and significantly reduced the structure's interstory drifts under dynamic loading. It should be noted that the increase in the structure's stiffness changed the dynamic characteristics of the structure and increased the seismic force demands on the structure. Such increase in demand needs to be considered in the design process

For the seven-story building with low column shear strength, the addition of a bracing system alone was unable to prevent column shear failure. The analyses showed that in addition to the bracing, it was necessary to protect the columns against shear failure. In this study, column shear failure was prevented by reducing the size of the spandrel beams. The spandrel beams were cut below the floor level in the vicinity of the columns to force hinging into the beams and to permit the development of the flexural strength of the columns prior to shear failure. Adversely, the development length of the column bars was reduced. The retrofit scheme that combined steel EBFs with cut spandrel beams showed very good performance under the selected earthquake records. Column shear failure can also be prevented by

jacketing the columns rather than cutting the spandrel beams (Jara et al., 1989, Pincheira, 1992).

Lateral load response of the retrofitted frames was dominated by the EBFs. In all EBF schemes, substantial yielding of the structure occurred with the formation of the first shear hinge in the links. Shear yielding of additional links led to additional reduction in stiffness. Flexural hinging of the reinforced concrete members or splice failure in the beams and columns did not cause a significant effect on the stiffness of the retrofitted buildings.

Variation in the link length was found to affect response of the retrofitted structure. The static analyses showed that increasing the link length leads to higher ductility and that reducing the link length leads to higher strength and to higher rotation demands. The dynamic analyses showed however, that due to the increase in stiffness, the plastic rotations of EBFs with short links remained within acceptable levels. Notice that short links transmits lower moments to the braces and adjoining steel beams. Hence, the requirements of the lateral bracing for the beam segment outside of the link are reduced and the brace end connection details are easier to achieve, with the use of short links.

Changing the link size over the height of the frame was also found to affect the performance of the retrofitted building. Reducing the link size with height improved the performance of the structure by promoting a more uniform distribution of yielding among links and by avoiding a concentration of inelastic deformations at the lower stories.

Similarly to most retrofit schemes, the addition of a steel EBF to an existing reinforced concrete building caused an increase in the column and foundation axial load. Vertical steel collectors or column jacketing may be required to provide the column with the strength needed to resist the added axial loads. Foundation strengthening may also be required. Limiting the strength of the added bracing system and distributing the braces to several bays limits the increase in column and foundation axial load.

In summary, the use of steel EBFs for strengthening of nonductile reinforced concrete frames resulted in good seismic performance of the retrofitted frames under severe ground motion records. For the three-story building, the addition of the EBFs alone was adequate. For the seven-story building that had low column shear strength, it was necessary to combine the addition of steel EBFs to the frame, together with cutting of the spandrel beams, in order to achieve acceptable performance. For both buildings, increasing the strength of the EBF resulted in lower drifts under the earthquake records, and therefore greater damage control. For each building, EBF schemes that provided the minimum strength needed to survive the strong ground motions were identified. Bracing systems with the minimum required strength do not, of course, provide as much drift and damage control as the stronger schemes. However the minimum strengths schemes may be economically advantageous by minimizing the need for strengthening the existing columns and foundations, and by minimizing the connection requirements between the bracing system and the existing frame.

7.3. Comparison of EBF and CBF schemes.

7.3.1. Introduction. For new steel buildings, EBFs are generally considered to perform better than CBFs under cyclic loading, exhibiting higher energy dissipation capacity and more stable hysteretic behavior. This view is reflected by current seismic codes for new construction which require higher design lateral forces for CBFs compared to EBFs. To try to assess the advantages of each bracing scheme in retrofit applications, first a comparison between the analytical behavior of reinforced concrete buildings retrofitted with steel EBFs and steel CBFs will be made. Then, observations and experimental research related to the behavior of EBFs and CBFs will be reviewed. Finally, conclusions will be drawn.

7.3.2. Analytical Behavior of EBF and CBF Retrofit Schemes.

7.3.2.1. General. In this research study, a three-story and a seven-story reinforced concrete building were evaluated and were found to be inadequate to sustain severe

seismic loads. These buildings were retrofitted with various EBF and CBF schemes. The analytical performance of these schemes is compared here.

7.3.2.2 Seven-Story Building. The successful schemes used to retrofit the seven-story reinforced concrete building included EBF3W and CBF3W. The former consisted of the addition of an EBF bracing system, while the latter involved the addition of a CBF system. For these strengthening schemes, the depth of the spandrel beams was reduced and the braces were added to five out of eleven, bays. Full description can be found in Chapter 6.

The static analyses summarized in Chapter 6 showed that EBF3W and CBF3W retrofit schemes provided a comparable level of initial stiffness and strength. However, the inelastic deformation capacity of these schemes could not be compared since the ductility of CBF3W could not be analytically predicted. The deformation capacity of an EBF system corresponds to the rotation capacity of the link and can be, reasonably well, predicted by an analysis. The deformation capacity a CBF system may be limited by brace fracture or connection failure and is difficult to predict analytically.

The dynamic analysis showed that both schemes maintained a similar level of interstory drift. Also, both retrofit schemes resulted in a similar column axial load. However, larger beam rotations were predicted for CBF3W indicating a possibility of higher structural damage for this scheme.

7.3.2.3. Three-Story Building. The three-story building analyzed in this study was retrofitted with several EBF schemes. Pincheira (1992) analyzed the same structure and considered the addition of CBF retrofit schemes. In his study, he used two CBF schemes in which the braces were made of double angle sections and were referred to as DA1 and DA2. (Fig. 7.1). The results of the static analysis performed on DA1 and DA2 are shown in Figure 7.2 and are compared to the behavior of EBF1-1.5, and EBF2-1 respectively (Fig. 7.3). Note

that the plots for the static analysis show the base shear as a function of drift at the *centroid of inertia forces*. The centroid of inertia forces corresponds to the application point of the inertia forces resultant in the fundamental vibration mode. The bracing configuration for EBF1-1.5 and EBF2-1 are detailed in Section 6.9.

The initial stiffness of DA1 and EBF1-1.5 are essentially similar. However, EBF1-1.5 has higher strength and appears to have better energy dissipation capacity. EBF1-1.5 was designed with a link length of about $1.5 M_p/V_p$. This allowed this scheme to withstand large drift and to have large ductility (see Chapter 6). The initial stiffness of DA2 appears comparable to EBF2-1 but DA2 has higher strength.

Overall, the static analysis does not indicate a strong advantage of one bracing system over the other. The analyses demonstrate, however, that different procedures in selecting the scheme's configurations and small differences in the member sizes may result in large difference in strength and ductility.

Interstory drifts under dynamic seismic load for DA1 and DA2 configurations and for EBF1-1.5 and EBF2-1 are shown in Figure 7.4 and Figure 7.5, respectively. As noted above, EBF1-1.5 and DA1 have similar initial stiffness. Under the scaled El Centro record, the performance of EBF1-1.5 and DA1 are comparable, although somewhat lower drifts were predicted for EBF1-1.5. Under the Corralitos record, larger interstory drift occurred for the DA1 scheme. This suggests that somewhat better performance is expected with EBF1-1.5, likely attributed to the somewhat higher strength of EBF1-1.5. A similar drift level under seismic loading was predicted for DA2 and EBF2-1.

7.3.2.4. Concluding Observations. The above comparison between the analytical behavior of EBF and CBF retrofit schemes did not provide a clear indication on the performance differences between the two systems. For the buildings studied, a comparable global behavior was, in general, observed for retrofit schemes involving either bracing type.

However, the analysis did not allow a proper estimation of the deformation capacity of the CBF schemes since a failure criteria for the braces is not incorporated in the brace model. Limitations in the modeling and their implications are discussed below.

7.3.3. Analytical Modeling of EBFs and CBFs. As discussed in Section 3.9, available analytical models can satisfactorily predict EBF behavior but present some limitations in predicting the inelastic behavior of CBFs due to the complexity of brace modeling. In particular energy dissipation capacity cannot be predicted with confidence for CBFs. Also, stiffness and strength reduction due to local buckling, brace fracture, and connection failure which limits the deformation capacity of CBFs, cannot yet be modeled with confidence.

Analytical modeling of EBFs depends mainly on the shear link modeling. Numerous test data of link behavior (Hjelmstad et al. 1983, Kasai et al., 1986b, Malley et al., 1984) indicate that hysteretic behavior of links is stable and predictable and can be represented with a simple model (Roeder and Popov, 1977) such as the one used in this study. The deformations capacity of EBFs is limited by the rotation capacity of the links and can be predicted with a good degree of confidence.

The performance of CBFs is primarily controlled by the brace behavior which is generally more complex and not as well understood as shear links (Khatib et al., 1988, Popov et al. 1993). Brace behavior depends on several parameters that include slenderness ratio, local buckling, type of cross section and brace fracture. Uncertainties and complexity involved in estimating the slenderness ratio makes brace modeling uncertain. In addition brace local buckling and its effect on the strut behavior is not, as yet, incorporated in known brace models including the one used in this study. This limits the ability of the brace model to properly predict strut behavior and can result in overestimating the energy dissipation capacity. In addition, the deformation capacity of CBFs, is often limited by brace fracture which cannot be predicted as yet by the existing models. Also, experimental research showed that the cyclic behavior of the braces depends also on the type of section (Popov and Black, 1981, Jain and

Goel, 1978). The brace model used in this study and in the study conducted by Pincheira (1992) was developed by Jain and Goel (1987) to model the behavior of tubular sections with Kl/r larger than 60. Hence, it can not be readily applied to other brace sections.

7.3.4. Review of Experimental Work on EBF and CBF Behavior. Several experimental investigations have been conducted on the behavior of EBF and CBF steel buildings. A review of such investigations can help overcome some limitations of the analytical study and assess the comparative performance of CBFs and EBFs.

Roeder and Popov (1977) tested two one-third scale models of eccentrically braced frames. Their tests demonstrated the excellent behavior of EBFs under dynamic load. The hysteretic loops remained stable and did not deteriorate in strength or stiffness until large link rotations. In EBF structures, energy dissipation is limited to the links and brace buckling is avoided which permits stable hysteretic behavior. On the other hand, brace buckling in CBF structures is known to cause deterioration in strength and stiffness with repeated loading (Nakashima, 1992, Khatib et al., 1988, Lee and Lu, 1989).

Full scale tests on six-story structures, conducted at the Building Research Institute (BRI) in Japan, provide a valuable experimental basis for comparing the seismic performance of EBFs and CBFs. In Phase I, a concentric braced frame was tested. The braces were made of tubular members. In the final tests, which simulated a major earthquake, seven out of 12 braces experienced extensive buckling and yielding (Roeder, 1989). Continued loading, led to brace fracture at the third level and to significant reduction in strength and stiffness (Foutch et al., 1986, Roeder, 1989). Figure 7.6 illustrates the behavior at the third floor, which was the most critically loaded. In Phase II, an eccentrically braced frame was tested. The tests showed that the EBF possessed an excellent ductility and energy dissipation despite gusset plate failure due to improper detailing (Foutch, 1988, Roeder et al. 1986). The hysteretic loops were very stable (Nishiyama, 1988) as shown by Figure 7.7. Based on the experimental results, Roeder et al. (1986) concluded that the EBF achieved a superior seismic performance.

Whittaker et al. (1987) tested a one-third scale model that replicated the structure tested at BRI, but the connections detailing was improved. Connection failure was prevented and the building exhibited excellent behavior under a number of simulated strong earthquake records. The tests by Whittaker (1987) showed very stable hysteretic behavior and high ductility of EBFs. The capacity of the structure was limited by link web fracture which occurred when the links reached a rotation of around 0.10 rad.

As an extension of the full scale tests performed in BRI, Lee and Lu (1989) conducted an experimental study on 1/3 scale model of EBF and CBF structures subjected to cyclic loading. Their results indicated the better performance of EBFs with regard to ductility and energy dissipation.

In summary, the available experimental research conducted on CBFs and EBFs shows that EBFs exhibit higher energy dissipation capacity, and hence better performance under cyclic loading. Energy absorption capacity of CBFs is reduced by strength and stiffness deterioration due to brace buckling. The deformation capacity of CBFs is limited by brace local buckling or fracture. EBFs exhibit stable hysteretic behavior until very large displacements.

7.3.5. Post Earthquake Repair in EBFs and CBFs. A potential advantage of EBFs, as compared to CBFs, is the possibility of significantly less cost required to repair the bracing system following an earthquake. In the case of an EBF retrofit, yielding of the bracing system will be restricted to the links. As observed in Chapter 5, the permanent inelastic rotations of the link following earthquake are expected to be very small and visually undetectable. Thus, even after a very strong earthquake, there will be little or no visual damage to the EBF. Further, as long as link web buckling did not occur during the earthquake (i.e link plastic rotation did not exceed 0.10 rad.), the structural capabilities of the links will be essentially the same as the link prior to the earthquake. Links are capable of sustaining a very large number of inelastic loading cycles with essentially no loss of strength and stiffness (Kasai and Popov, 1986c). Consequently, as long as web buckling is prevented, a link can sustain

several severe earthquakes without loss of strength. Thus, both from an aesthetic and from a structural point of view, little or no repair may be needed following a strong earthquake.

In the case of a CBF retrofit, considerable repair may be required after an earthquake. As indicated by the analyses in Chapter 5 and 6, brace buckling is anticipated under the earthquake records used in this study. This brace buckling, which will certainly be visually apparent, also causes a significant loss of brace strength and stiffness. Thus, both from an aesthetic and from a structural point of view, repair of buckled braces will likely be needed following a strong earthquake.

7.3.6 Conclusions. Both the static and dynamic analyses show largely similar global performance of reinforced concrete frames retrofitted with EBFs or with CBFs. Thus good performance can be expected from either type of bracing system, if the systems are well designed and detailed, and if the systems behave as predicted. Nonetheless EBFs may offer some advantages over CBFs.

EBFs have very simple, predictable hysteretic behavior with well established failure criteria. They can be expected to perform as predicted by the analysis with a high degree of confidence. On the other hand, CBF behavior, which is controlled by brace hysteretic behavior, is considerably more complex and difficult to predict. There is less confidence that the CBF will behave as predicted.

An additional potential advantage of EBFs as compared to CBFs is that the maximum strength of the EBF can be predicted with greater certainty than that of the CBF. The maximum strength of a shear link can be estimated with considerable confidence. Brace buckling and post-buckling strength cannot be predicted with as high degree of confidence. Thus, the maximum load that will be transferred to the existing frame members and foundations can be predicted with greater certainty for an EBF. Finally, EBFs offer the potential for less costly post-earthquake repair.

In this study, no attempts were made to develop cost estimates for the retrofit schemes. Thus, it is not possible to compare the cost of an EBF with that of a CBF. However both type of bracing systems represent conventional fabricated steel construction, with similar types of members and connection details. Thus it is anticipated that the cost of the fabricated steel framing would be quite similar for both systems.

7.4. Comparison of Analytical Results to ATC 22 provisions.

7.4.1. Introduction to ATC 22. ATC 22 (Applied, 1989) recommendations were developed to provide engineers with practical guidelines in evaluating the strength of existing buildings for seismic resistance. The primary objective of these provisions is to determine if a structure, or structural components, present "unacceptable risk to human life" under severe ground motions. In other words, the provisions are intended to identify life safety hazards and not to evaluate serviceability.

A building is considered adequate to resist dynamic loading if its nominal strength at "first significant yield" is higher than a minimum specified base shear. The base shear required by ATC 22 is computed as $V = LF C_s W$ where W is the weight, or dead load of the building, LF is a load factor, and C_s is defined as follow:

$$C_s = 0.67 \frac{1.2 A_v S}{R T^{2/3}} = \frac{0.80 A_v S}{R T^{2/3}} \quad (7.1)$$

The value of C_s need not be greater than:

$$C_s = 0.85 \frac{2.5 A_a}{R} = 2.12 \frac{A_a}{R} \quad (7.2)$$

Where A_a is an acceleration coefficient that depends on the building location, A_v is defined as a velocity-related acceleration coefficient and depends on the building location, S is a soil profile coefficient, R is a response modification factor that depends on the structural system, and T is the fundamental period of vibration of the building.

ATC 22 was based on NEHRP (Building, 1991) recommendations for new buildings but changes were introduced to consider the characteristics of existing constructions. The base shear coefficient, C_s , was reduced to 67% and the upper limit of the base shear coefficient was reduced to 85% of the corresponding values of new buildings. ATC 22 accepts a reduced demand on existing buildings because they can be strengthened "only at substantial cost in money and disruption of use". The value of the base shear adopted by ATC 22 corresponds to the mean value of the response spectra instead of the mean value plus one standard deviation as in the NEHRP provisions. On the other hand, the lateral forces specified in ATC 22 are increased for structures that do not exhibit ductile behavior. NEHRP provisions were developed for structures properly detailed for ductile behavior. The increase in lateral forces specified in ATC 22 are necessary since existing buildings often exhibit a reduced ductility level. The lateral load is increased by a load factor, LF equal to $0.75 C_d$ for "brittle elements" and to $0.375 C_d$ for "semi-ductile elements". C_d represents the deflection (or displacement) amplification factor and is function of the structural system.

7.4.2. Evaluation of Case Study Buildings by ATC 22.

7.4.2.1. General ATC 22 recommendations are intended for the evaluation of existing buildings and are not necessarily applicable to the design or evaluation of retrofit schemes. Nevertheless, the evaluation process of ATC 22 was applied here to both the original buildings and the retrofitted structures. Note that currently, no codes are available for the design of retrofit schemes. The analytical results of the retrofitted structures were compared to ATC 22 requirements to evaluate the possibility of extending the use of this document to the design of strengthening schemes.

The yield strength of the structure (C_y), obtained from elastic analysis, was compared to the minimum base shear coefficient required by ATC 22 ($LF C_s$). ATC 22 defines C_y as the onset of "significant yielding" of the structure. For the EBF schemes, C_y was considered as the load level corresponding to first yielding in a shear link. In the evaluation of C_s the original structure was assumed as an Ordinary Moment Resistant Frame (OMRF). The retrofit

schemes were considered as a dual system formed of an Intermediary Moment Resisting Frame (IMRF) and a Concentrically Braced Frame (CBF). The load reduction factor R , was then taken equal to two for the original building and to five for the retrofit scheme. ATC 22 contemplates a limited number of structural systems and does not consider a dual system formed of an OMRF combined with an EBF or a CBF. Such a system would most adequately represent the retrofit schemes investigated here and would probably have a smaller reduction factor R , since an OMRF has less ductility than an IMRF.

The design lateral load in ATC 22 depends also on the ductility of the structural members as explained previously. For the original building and for the retrofit schemes that did not prevent column shear failure, the columns were considered to be "brittle", and LF was taken equal to $0.75 C_d$. For the retrofit schemes not subject to column shear failure, the columns were considered as "semi-ductile" to better represent ductility improvement provided by the addition of steel collectors. In this case, LF was taken equal to $0.375 C_d$. Note that C_d was set equal to 2.0 for the original building and to 5.0 for the retrofitted structure.

Tables 7.1 and 7.2 show the ratio of the structure's yield strength over the yield strength required by ATC 22. A ratio below one indicates the structure is inadequate. The main observations on the comparison of the buildings studied to ATC 22 requirements are summarized below.

7.4.2.2. Three-Story Building. The $C_y/(LF C_g)$ ratio for the original building was less than 1.0 indicating that it was inadequately designed according to ATC 22. This conclusion is in agreement with the dynamic analysis.

With the exception of EBF4-S, all retrofit schemes were found to meet ATC 22 strength criteria. In general, this corresponds to the results of the dynamic analysis. The dynamic analysis showed that EBF4-S was inadequately designed to resist the Parkfield and Corralitos records and would undergo extensive damage under the scaled El Centro record.

The dynamic analysis also showed that the remaining schemes had the needed strength and ductility to resist the selected earthquake records. Notice that the ratio $C_y/(LF C_s)$ was found equal to 1.18 for EBF1-S and equal to 1.32 for EBF4-H. The dynamic analysis showed these schemes provided the minimum strength required to resist the selected records. If a weaker EBF have been provided so that $C_y/(LF C_s)$ were closer to 1.0, the scheme would likely have been inadequate. Hence $LF C_s$ was underestimated in this case by 20% to 30%. This underestimation may be due to the system assumed in the calculation, as explained above. Based on these data a load reduction factor (R) of four, instead of five, is suggested when the retrofit is treated as a dual EBF and reinforced concrete IMRF system with semi-ductile elements.

7.4.2.3. Seven-Story Building. As shown in Table 7.2, the ATC 22 evaluation procedure indicated that the original seven-story building is inadequate. This conclusion agrees with the result of the dynamic analysis which indicated that this building was likely to collapse under the seismic loading due to the selected earthquake records.

ATC 22 provisions indicate the adequacy of the EBF3W and CBF3W retrofit schemes. The EBF2 retrofit scheme was found inadequate by ATC 22. These observations correlate with the results of the dynamic analysis. The dynamic analysis indicated that EBF4W had the minimum strength required to resist the seismic loading. ATC 22 recommendations appear to overestimate this scheme's strength by approximately 20%. Calculations made with a load reduction factor equal to four resulted in a more appropriate value of about one for $C_y/(LF C_s)$. The $C_y/(LF C_s)$ ratio was found equal to about one for EBF3 and CBF3. Hence, according to ATC 22, these schemes provide the minimum required strength. However the dynamic analysis showed that they were inadequately designed. As with the three-story building these results also indicate that the ATC 22 evaluation procedure overestimates the strength when using a load reduction factor of five for this type of structure, considering the severe earthquake records used in this study.

7.4.2.3. Concluding Observations

The comparison made herein between ATC 22 recommendations and the dynamic analyses led to the following conclusions:

- 1) ATC 22 predictions for the original reinforced concrete buildings are in good agreement with the outcome of the dynamic analyses.
- 2) ATC 22 recommendations were found to overestimate the strength of the retrofit schemes by about 20%. This observation appears to be due the load reduction factor, R associated with the structural system assumed. ATC 22 provisions contemplate a dual system formed of a steel bracing system and a reinforced concrete IMRF. However a dual system that is combination of a steel bracing system and an OMRF is not considered. Based on the above results an R value equal to four is suggested for this type of structure.

7.5. Preliminary Design Recommendation for EBF Retrofit Schemes.

7.5.1. Introduction. ~~As yet there is no code available for the design of seismic retrofit schemes.~~ Based on the analytical results obtained in this study, preliminary recommendations for the design of EBF retrofit schemes will be made in this section. These recommendations are considered preliminary, since they are based on a rather limited number of analyses. The recommendations are intended to provide some guidance to designer until further research results are available. The design methodology of the 1991 edition of the UBC will be followed since designers are very familiar with this code.

7.5.2. Estimation of Required Strength. The buildings studied were retrofitted with several EBF schemes. As explained in Chapters 5 and 6, a trial and error procedure was followed to obtain the retrofit scheme having the minimum strength needed to survive the selected ground motion records. The trial schemes were tested against dynamic inelastic analyses. The retrofit schemes with the smallest link sizes that maintained plastic rotation below 0.10 rad. were selected. For the three-story building, EBF1-S and EBF4-H configurations were found to provide the minimum strength. For the seven-story building,

EBF4W was shown to have the lowest required strength. These schemes will be referred herein as *minimum strength schemes*.

The minimum strength schemes would result from a design based on UBC 91 using an acceleration factor, Z of four, a soil coefficient, S of one, a period of vibration, T from an elastic dynamic analysis, and a load reduction factor, R_w of 4.5. The UBC forces obtained from this procedure need to be applied to the added EBF only when designing the steel members of the EBF retrofit scheme. The soil coefficient was taken equal to one since the most critical dynamic effect was due to the scaled El Centro record or Corralitos record, both of which were on firm soil.

The period of vibration was based on the dynamic analysis of the retrofitted system (original frame and added EBF), to reflect better the vibration characteristic of the retrofitted structure. ~~The UBC simplified procedure for period evaluation, valid for "regular" buildings only, is based on the building's geometric configuration and does not consider the effect of the added retrofit scheme. Consequently the simple period calculations of UBC 91 would result in the same vibration period for a given building irrespective of the retrofit scheme used. However, the analyses showed that for a given building, large variation in the vibration period can be obtained depending on the stiffness of the added EBF.~~

The minimum strength schemes were obtained by applying the UBC design forces to the added steel EBF only. The existing reinforced concrete frame was assumed to carry gravity load only.

The value of the strength reduction factor R_w was obtained by comparing the capacity of the minimum strength schemes to the capacity required by UBC. In accordance with the UBC provisions, the base shear provided by the added bracing scheme was computed using the allowable stress method. The base shear capacity was then divided by the building weight to obtain the seismic coefficient C_s . Finally the UBC equation for C_s was solved for R_w . Table 7.3 summarizes the computations performed for the minimum strength schemes. This Table

shows that the value obtained for R_w varies between 4.0 and 4.8. An average value of 4.5 is proposed here. Although the proposed R_w value is seemingly low, it was justified by the analysis. Notice that the proposed R_w value for the repair scheme considers the effect of the existing non-ductile reinforced concrete frame that may limit deformation. Furthermore, an experimental study of a full scale six-story concentrically braced frame and a full scale six-story eccentrically braced frame showed that the R_w value given in the UBC are large and need to be reviewed and perhaps reduced (Foutch, 1989).

Note that the procedure proposed here was based on the study of two reinforced concrete buildings. These buildings are representative of a low rise and medium rise 1950s and 1960s West Coast construction. Due to the limited number of buildings examined here, the proposed method needs to be confirmed by additional research work.

Note also that the proposed design procedure may not be directly applicable to buildings with low column shear strength. For this type of buildings, the addition of an EBF scheme is not sufficient. Studies on the use of concentric steel bracing and post-tensioned braces to retrofit reinforced concrete buildings with inadequate column shear strength led to similar conclusions (Pincheira, 1992, Kawamata and Ohnuma, 1980). Thus, in addition to bracing, additional measures must be taken to prevent column shear failure. This may be done by counting on the vertical steel collectors attached to the columns to improve column shear strength. However, as noted earlier, the effect of steel collectors is uncertain and difficult to quantify. Other alternatives for preventing column shear failure include cutting spandrel beams, as was done in this study, or column jacketing (Jirsa and Alcocer, 1991, Aboutaha and Engelhardt, 1993).

7.5.3. Estimation of Ultimate Drift. In design practice, the actual maximum drift expected under an earthquake is estimated by multiplying the drift obtained under code design forces by a displacement amplification factor. The UBC 91 code specifies an amplification factor of $3/8 R_w$. Estimation of the maximum drift in a structure is needed to check for

example, for the likelihood of non structural damage, for P- Δ effects, or for the deformations of critical structural members. In retrofit design applications, drift estimates can also indicate if the structural members that are not retrofitted can withstand the expected deformations. For instance, in case of a retrofit structure that involves strengthening the external frame and columns only, maximum interstory drift can be helpful in evaluating the safety of the internal columns (not retrofitted). For EBF retrofit schemes, maximum frame deformation will indicate if the shear links, which control the EBF's deformation capacity, did not exceed their rotation limit.

The minimum strength schemes were selected to investigate the correlation between elastic drift under the proposed UBC force level (δ_U^e) and ultimate drift that may occur under the expected seismic loading (δ_D^m). The main objective is to verify the adequacy of the displacement amplification factor recommended by the current UBC. Figures 7.8 and 7.9 show the maximum interstory drift ratio under the selected ground motion and the maximum drift (δ_U^m) predicted using UBC. δ_U^m corresponds to δ_U^e amplified by $3/8 R_w$. In general, UBC estimates for maximum interstory drifts are very unconservative. The ultimate drift ratio predicted by UBC for the EBF1-S and EBF4-H configurations of the three-story building were equal to 0.22% and 0.29% respectively. However the dynamic analyses indicated that maximum interstory drift ratio was in excess of 0.80% for EBF1-S and between 0.65% and 1.03% for EBF4-H. Similarly for the seven-story building, UBC recommendations predict a maximum story drift ratio of 0.25%, while the dynamic analyses resulted in drift levels between 0.73% and 1.02%.

In an attempt to make more accurate prediction of interstory drift, δ_U^e was amplified by a displacement factor equal to $1.2 R_w$. The drifts, δ_M^m , computed with this higher amplifications are shown in Figure 7.8 and Figure 7.9 and are referred to as "modified UBC". With such amplification of the elastic displacement due to code level forces, better correlation was obtained with the computed drift under dynamic loading. For EBF1-S of the three-story building, drift estimations were still somewhat unconservative but were closer to the computed values than the drifts given by UBC calculations. For EBF4-H of the three-story building, δ_M^m

was very close to the computed drifts under Parkfield and Corralitos records and larger than the maximum drift under the scaled El Centro. Similar observations were made for the seven-story building. The maximum interstory drift predicted using the "modified UBC" procedure exceeded the drifts under the scaled EL Centro and was close to the maximum interstory drift expected under the Corralitos record.

In summary, the current UBC displacement amplification factor of $3/8 R_w$ is low and yields unconservative estimates of the ultimate drift for the buildings studied herein. For this case study, an amplification factor of $1.2 R_w$ was found to provide more accurate estimates of the ultimate drift under severe earthquakes. These observations on the use of displacement amplification factor higher than the one currently adopted by UBC, were also noted in a study by Uang and Maarouf (1993). They analyzed a series of four buildings subjected to eight earthquake records. Their investigation showed that the displacement amplification factors varied between $1.0 R_w$ and $1.5 R_w$ and that the UBC factors are too small and should be revised.

7.5.4. Estimation of Maximum Link Rotation.

7.5.4.1. Introduction Links can be considered the most critical member in an EBF structure. Energy dissipation under seismic loading is limited to the links and the capacity of an EBF is controlled by the link's strength and deformation capacity. Proper estimation of link rotation is thus essential.

In current practice, ultimate link rotation is estimated using a simplified energy dissipation mechanism, as explained in Section 2.4.3. The energy dissipation mechanism assumes plastic rigid deformations. Furthermore, the link deformations are assumed uniform throughout the height and all floors are assumed to have the same drift ratio. The validity of this approach for the retrofit design is checked below. Design recommendations for estimating the ultimate plastic deformation of the links are drawn.

7.5.4.2. Estimation of Maximum Link Rotation Under Static Load Table 7.4 summarizes the ultimate interstory drift (θ), and the link rotation (γ) of the different retrofit schemes studied under static load. For each scheme, the value of θ and γ are given for the floor with the largest interstory drift. Table 7.4 also gives an estimated value of the link rotations computed according to the above model. For the EBF configuration selected in this study, the link rotation is estimated equal to $\theta L/e$. L is the span length and e is the link length. Note that 0.10 rad. represents the shear link rotation capacity under cyclic load. In general the plastic model gave a good estimation of the link rotation. The use of the rigid-plastic model to estimate link deformation of an EBF retrofit appears justified.

7.5.4.3. Application to the UBC Design Code The above discussion showed that under static load, the plastic model provides reasonably good estimates for the link deformations. The UBC design procedure involves computing elastic interstory drifts under code level forces and estimating ultimate drift by multiplying the elastic drifts by a displacement amplification factor, currently set equal to $3/8 R_w$. The corresponding link deformations are estimated from geometric compatibility assuming the plastic mechanism outlined above. In the following, this method will be checked for the case studies.

Figures 7.10 and 7.11 show the computed plastic link rotations under dynamic loading and the estimated rotations using UBC recommendations. For both buildings, the UBC design procedures greatly underestimated the link rotations. This is primarily due to UBC's underestimation of maximum story drift. To improve predictions of the link rotations, calculations were made using a displacement amplification factor of $1.2 R_w$. The corresponding results are also shown in Figure 7.10 and 7.11 and are referred to as "Modified UBC". Overall, this procedure resulted in satisfactory prediction for link rotations. For the EBF4W configuration of the seven-story building, the predicted maximum rotation exceeded the maximum computed rotation under the scaled El Centro record and was close to the maximum rotation under the Corralitos record. For the three-story EBF4-H configuration, the proposed

procedure led to conservative estimates. For EBF1-S, the predicted link rotation was within 15% of the measured rotation.

The rigid-plastic model results in a satisfactory estimate of the maximum link rotation provided an appropriate value is selected for the displacement amplification factor when computing maximum story drift. This study and the work conducted by Uang and Maarouf (1993) support the conclusion that the current displacement amplification factor of $3/8 R_w$ underestimates the maximum frame deformation. A value of $1.2 R_w$ is suggested here.

7.5.5. Estimation of Maximum Axial Load in the Columns. The actual forces generated in the columns of a frame during a severe earthquake may significantly exceed those predicted from a code lateral force analysis, due to the presence of overstrength in the yielding elements of the frame. An estimate of the actual forces are important for protecting against nonductile column failures. To avoid unsafe column design, codes amplify the specified lateral forces for column axial load calculations. Estimation of a reasonable amplification factor is difficult and may depend on several parameters including the building's structural system, dynamic characteristics of the structure, and structure configuration. The 1991 edition of the UBC considers amplified column loads by requiring a minimum column strength to resist the effect due to the following load combinations:

$$1.0 DL + 0.8 LL + 3 (R_w/8) E \quad (7.3)$$

$$0.85 DL + 3 (R_w/8) E \quad (7.4)$$

where DL is the dead load, LL is the live load, and E is the design earthquake load.

The above equations indicate that the basic code design load is essentially amplified by a factor of $3 (R_w/8)$. The adequacy of the UBC load combinations for determining column

axial loads is checked below and is compared to a proposed capacity design method that is based on the following assumptions:

- 1) Links at the first level are assumed to reach their ultimate capacity, $1.5 V_p$
- 2) Shear force at the top level links is assumed equal to $0.5 V_p$
- 3) Shear force at intermediate links is computed following a linear interpolation.
- 4) Contribution of links that result in a reduced column load is ignored.

Note that the proposed method is used to compute the effect of earthquake loading only. Gravity loads must of course be included in the column design.

A capacity design procedure was selected since it relies less on approximate, and not well justified, amplification factors and more on the structure's behavior. Also, the links of an EBF allow for a control of the forces transferred to the remaining members which makes a capacity design a more suitable procedure. Different yield levels were assumed for the links since under dynamic loads, the links may not reach their maximum rotation at the same time. Calculations made with the assumption that all links yielded at the same time resulted in very conservative estimates of the column axial load. The contribution of links that result in a reduction of the column loads was ignored to avoid unconservative design loads.

To illustrate the procedure, calculations made for the columns of EBF1-S are detailed here. Figure 7.12. shows a simplified free body diagram of a braced bay. Vertical force equilibrium shows that the shear forces in the links are balanced by the axial load in the columns.

Column axial loads due to $(1.0 DL + 0.8LL)$ acting at the base of column lines 1, 2, and 3 are equal to 66 kips, 142 kips and 140 kips respectively. The axial loads due to $0.85 DL$ are equal to 51 kips, 110 kips, and 110 kips respectively. Axial load due to earthquake forces are computed using the proposed capacity design method. As explained above, first level links were assumed to reach ultimate capacity, i.e. $1.5 V_{p,1}$. Shear force at the third level links was assumed equal to $0.5 V_{p,3}$. Finally the second level link shear was taken as $1.0 V_{p,2}$ following

the linear interpolation rule. Numerically, the shear force in the first, second, and third level links are equal to 130 kips, 87 kips, and 44 kips.

Maximum compressive load was computed by combining the earthquake effect with the gravity load effect due to (1.0 DL + 0.8 LL). For column line 1, the effect of gravity load was combined with lateral load transferred by the first level link. For column line 2, the effect of gravity load was combined with the axial load due to first level or second level link, whichever is larger. Notice that for column line 2, a combination of first level and second level link forces was avoided as explained in rule (4) above. For column line 3, axial load due to gravity loading was combined with the load transferred by either the second level link or the first and third level link. The most conservative value was retained.

Numerical application of the procedure led to the following maximum axial compression forces at column line 1, 2, and 3:

$$P_1 = 66 + 130 = 196 \text{ kips}$$

$$P_2 = 142 + 130 = 272 \text{ kips}$$

$$P_3 = 140 + (44 + 130) = 314 \text{ kips}$$

The corresponding maximum tension force in the columns was computed by combining gravity load effect due to 0.85DL with the earthquake load resulting from the capacity design procedure outlined above. The calculations resulted in the following tension forces:

$$P_1 = 51 - 130 = -78 \text{ kips}$$

$$P_2 = 110 - 130 = -20 \text{ kips}$$

$$P_3 = 110 - (44 + 130) = -64 \text{ kips}$$

Column forces computed with the proposed procedure are discussed below for the minimum strength schemes at the base of the first floor columns. Column forces at the second level for the three-story building and at the third level for the seven-story building are also considered.

Figure 7.13 and 7.14 show the column axial load at the foundation level on EBF1-S and EBF4-H configurations of the three-story building under dynamic loading and under UBC design load (Eqs 7.3 and 7.4). These figures also show column axial load estimates using the proposed capacity design method. The axial load shown in figures 7.13 and 7.14 considers the effect of earthquake loading only. In general, the proposed procedure gave better estimation of the maximum axial load than the UBC procedure. The UBC procedure greatly overestimated the axial load for some columns.

Figure 7.15 shows the same type of graph for the EBF4W configuration of the seven-story building. In general, UBC procedure resulted in somewhat unconservative estimates of column load. The capacity design procedure somewhat overestimated column loads.

Figure 7.16 and 7.17 show the axial load on the second level columns for EBF1-S and EBF4-H schemes of the three-story building, subjected to earthquake loading. The figures show also the axial load estimated using the proposed method and the UBC procedure. For EBF1-S, both the UBC computations and the proposed capacity design procedure gave reasonable estimates of the load in column lines 1 and 2. However, the UBC procedure greatly overestimated the axial load at column line 3, while the proposed method resulted in a fairly good estimate. For EBF4-H, the UBC method overestimated the axial load by a factor of about eight. The proposed method also overestimated the load but by a lesser factor of about two.

Figure 7.18 shows a similar graph for the third level of the EBF4W scheme of the seven-story building. For the braced bays, the UBC procedure underestimated the load. Compression load was underestimated by about 30%, and the tensile load by about 70%. The capacity design gave conservative, yet reasonable, estimates of the compression load. The proposed capacity design overestimated the tensile load by a factor of about two.

The proposed capacity design method appears to yield better estimates of the column axial load than the UBC method. The proposed capacity design method relies on the transfer

of force mechanisms and takes advantage of the characteristics of an EBF. This method generally resulted in a better estimate of column axial load than the UBC procedure. The UBC procedure, based on an arbitrary force amplification factor, resulted in unconservative estimates in some cases, and in overly conservative estimates in others.

7.5.6. Summary of Suggested Design Procedure. A procedure to design an EBF retrofit scheme was proposed. It was based on the 1991 edition of the UBC but involved some modification. The design base shear is computed assuming a force reduction factor R_w , of 4.5. For the selection of the member sizes, the design lateral load is applied to the added EBF only. Ultimate story drifts are obtained by amplifying the elastic deformations under code level forces by a displacement amplification factor equal to $1.2 R_w$. Maximum link rotations are obtained assuming a plastic-rigid mechanism at ultimate. A capacity design procedure was proposed to estimate the maximum axial load in the columns. The design procedure was based on the analytical results of a limited number of buildings and further research is needed to validate the procedure. Also, the objective of the dynamic analysis was to provide safety against collapse under relatively strong earthquake records, with a maximum acceleration varying between 0.5 g and 0.6 g. These earthquake records were considered in the present study to be representative of the west coast ground motions. If other objectives, or lower forces are expected, some adjustments in the proposed factors are needed.

7.5.7. Observations on Link Connections Details. Detailing requirements for EBFs are well established and are included in the current model building codes, including the 1991 UBC and the AISC seismic provisions (AISC, 1990b). EBF detailing requirements, including connection details, link stiffener requirements, and lateral bracing requirements are summarized by Popov and Engelhardt (1988). Most of the detailing provisions developed for new EBFs are directly applicable to retrofit applications. An item which require special considerations in retrofit applications, however, is that of lateral bracing of the EBF.

Previous research (Popov and Engelhardt, 1988) showed that lateral bracing must be provided at the link ends (both top and bottom flanges) to maintain the stability of the link, the beam and the brace (see Section 2.4.7). The lateral bracing must prevent out-of-plane movement of the links, but should not restrict vertical, in-plane movement of the link ends. Similar lateral braces may be required at interval along the length of the beam outside of the link, in order to prevent lateral buckling of this member. In new EBF steel construction, link and beam lateral bracing is usually provided by the floor slab and/or by cross beams. In retrofit applications, these elements will not be present. Consequently providing lateral bracing will generally require special consideration in retrofit applications.

For the buildings considered in this study, the EBF was added to the outside of the building. Consequently lateral support of the EBF links and beams can be provided by braces running between the EBF and the adjoining concrete beams. As noted above, these braces must prevent out-of-plane movement but should not restrict in-plane movement of the links or beams. This can likely be accomplished through the use of plates with slotted holes, or perhaps by the use of rods or plates that are flexible in the vertical direction.

Table 7.1 Comparison Between computed Strength and ATC 22 Required Strength for the Three Story Building

Bldg.	ATC 22 Application		C_y	$\frac{C_y}{C_{req}}$	Observations From Dynamic Analysis
	System Assumed	LF C_{req}			
Orig.	R/C OMRF Brittle	.36	.12	.33	Low Strength. Failure Expected
EBF1-.75	CBF & R/C IMRF Semi-Brittle	.29	.70	2.44	
EBF1-1	CBF & R/C IMRF Semi-Brittle	.29	.67	2.33	
EBF1-1.5	CBF & R/C IMRF Semi-Brittle	.29	.70	2.44	
EBF2-1	CBF & R/C IMRF Semi-Brittle	.29	.65	2.67	
EBF3-1	CBF & R/C IMRF Semi-Brittle	.29	.90	3.13	
EBF4	CBF & R/C IMRF Semi-Brittle	.29	.38	1.32	
EBF1-S	CBF & R/C IMRF Semi-Brittle	.29	.34	1.18	Links Reached Capacity.
EBF4-S	CBF & R/C IMRF Semi-Brittle	.29	.26	.91	Links Exceeded Capacity.
EBF4-H	CBF & R/C IMRF Semi-Brittle	.29	.38	1.32	Links Reached Capacity.

Table 7.2 Comparison Between Computed Strength and ATC 22 Required Strength
for the Seven Story Building

Bldg.	ATC 22 Application		C_y	$\frac{C_y}{C_{req}}$	Observations From Dynamic Analysis
	System Assumed	LF C_{req}			
Orig.	R/C OMRF Brittle	.3	.18	.60	Col. Shear Failure. Bldg. Collapse Expected.
EBF2	CBF & R/C IMRF Brittle	.5	.3	.60	Col. Shear Failure. Bldg. Collapse Expected.
EBF3	CBF & R/C IMRF Brittle	.5	.5	1.00	Link. Capacity Exceeded.
CBF3	CBF & R/C IMRF Brittle	.5	.5	1.00	Col. Shear Failure. Extensive Damage.
EBF3W	CBF & R/C IMRF Semi-Brittle	.25	.38	1.52	No Col. Shear Failure.
CBF3W	CBF & R/C IMRF Semi-Brittle	.25	.41	1.64	No Col. Shear Failure.
EBF4W	CBF & R/C IMRF Semi-Brittle	.25	.30	1.20	Links Reached Capacity.

Table 7.3 Base Shear Capacity and Computed R_w Values for the Minimum Strength Schemes

		$C_s = V/W$	Computed R_w
3 Story	EBF4-H	.23	4.0
	EBF1-S	.21	4.1
7 Story	EBF4W	.15	4.8

Table 7.4 Approximate Estimation and Analytical Evaluation of the Maximum Link Rotation Under Static Lateral Load

Structure		Static Analysis		
		θ (%)	γ (rad.)	$\theta L/e$ (rad.)
3 Story	EBF1-.75	0.68	0.100	0.109
	EBF1-1	0.96	0.100	0.120
	EBF1-1.5	1.81	0.100	0.130
	EBF2	0.69	0.100	0.083
	EBF3	0.90	0.100	0.108
	EBF4	0.93	0.100	0.111
	EBF1-S	0.90	0.100	0.108
	EBF4-S	0.91	0.100	0.109
	EBF4-H	0.91	0.100	0.109
7 Story	EBF3W	1.10	0.100	0.122
	EBF4W	0.96	0.100	0.118

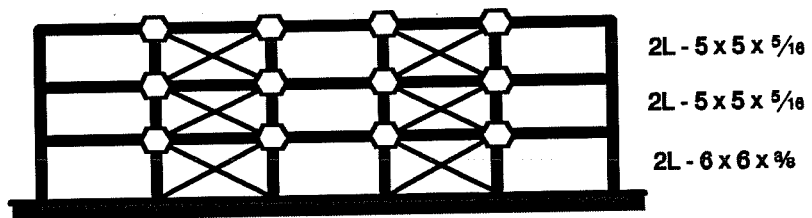
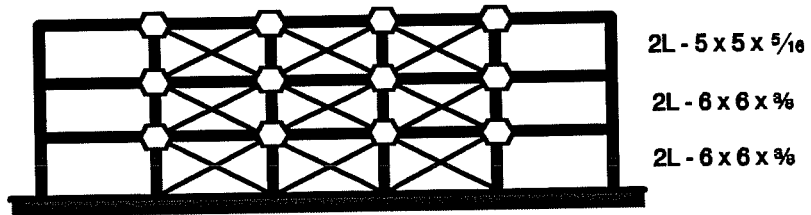
*DA1**DA2*

Figure 7.1 Configuration of CBF Retrofit Schemes DA1 and DA2, Used for the Three-Story Building in the Study by Pincheira (1992)

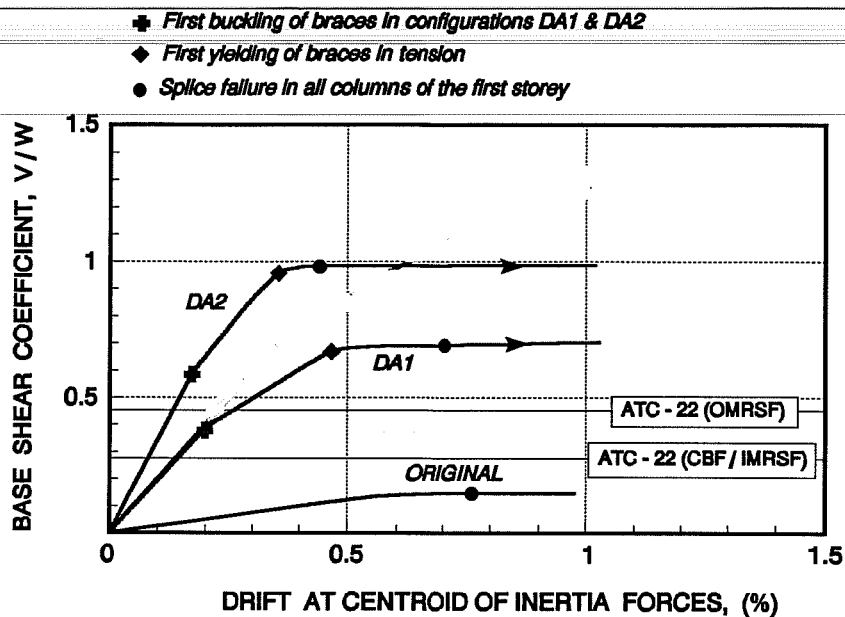


Figure 7.2 Static Behavior of the Original Three-Story Building and of DA1 and DA2 Retrofit Schemes (Adapted from Pincheira, 1992)

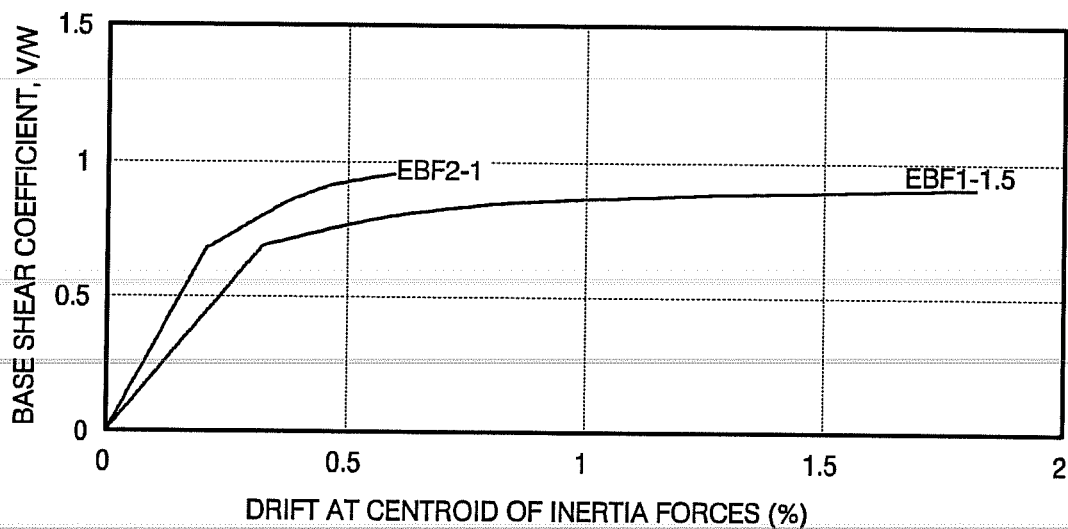


Figure 7.3 Static Behavior of Selected EBF Schemes Used to Retrofit the Three Story Building

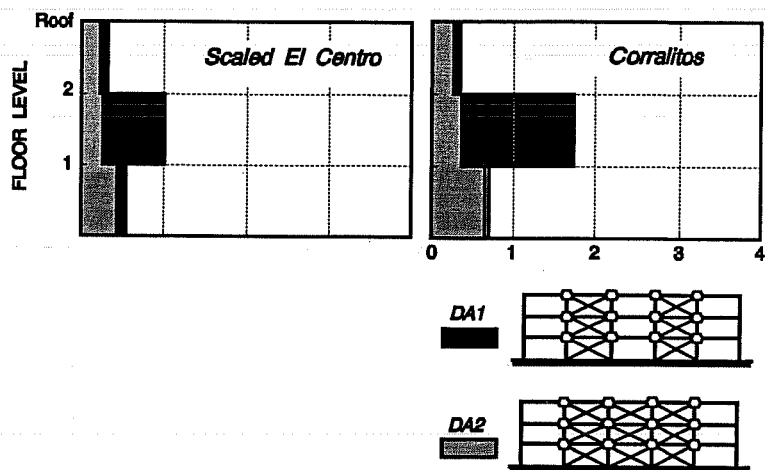


Figure 7.4 Maximum Interstory Drift Ratio For Retrofit Configuration DA1 and DA2 of the Three-Story Building Subjected the Scaled El Centro and Corralitos Earthquake Records (Pincheira, 1992)

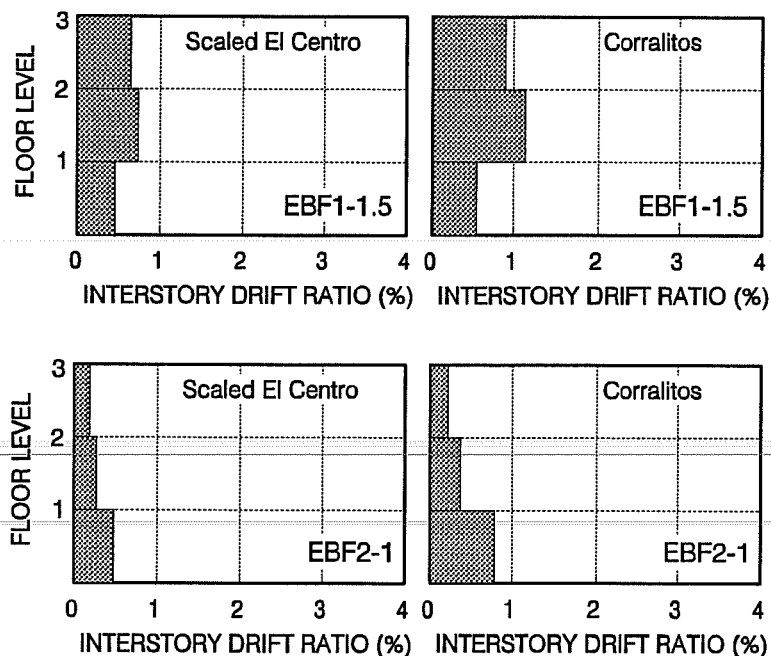


Figure 7.5 Maximum Interstory Drift Ratio For retrofit Configuration EBF1-1.5 and EBF2-1 of the Three-Story Building Subjected the Scaled El Centro and Corralitos Earthquake Records

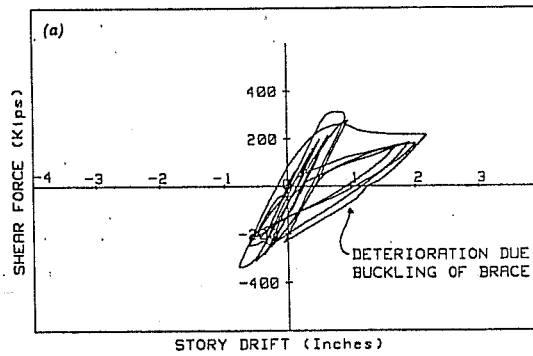


Figure 7.6 Story Shear versus Story Drift at the Third Level of the Concentrically Braced Frame in the Tests on Full Scale Six-Story Building (Foutch et al., 1987)

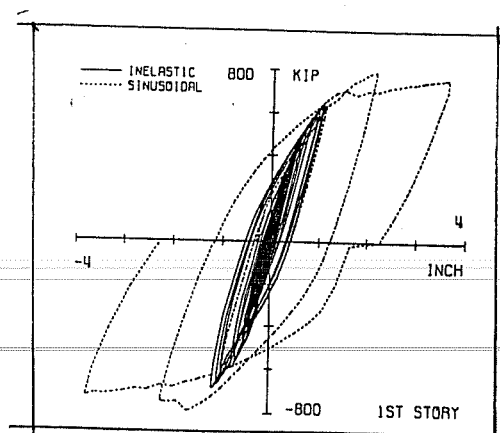


Figure 7.7 Story Shear Versus Story Drift at the First Level of the Eccentrically Braced Frame in the Tests on Full Scale Six-Story Building (Foutch, 1989)

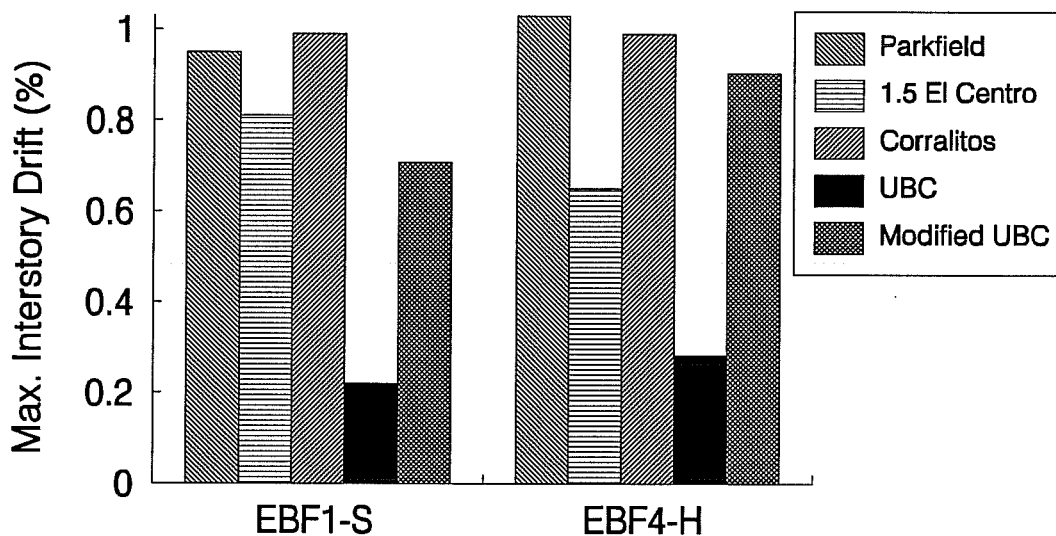


Figure 7.8 Maximum Interstory Drift for EBF1-S and EBF4-H Configuration of the Three-Story Building

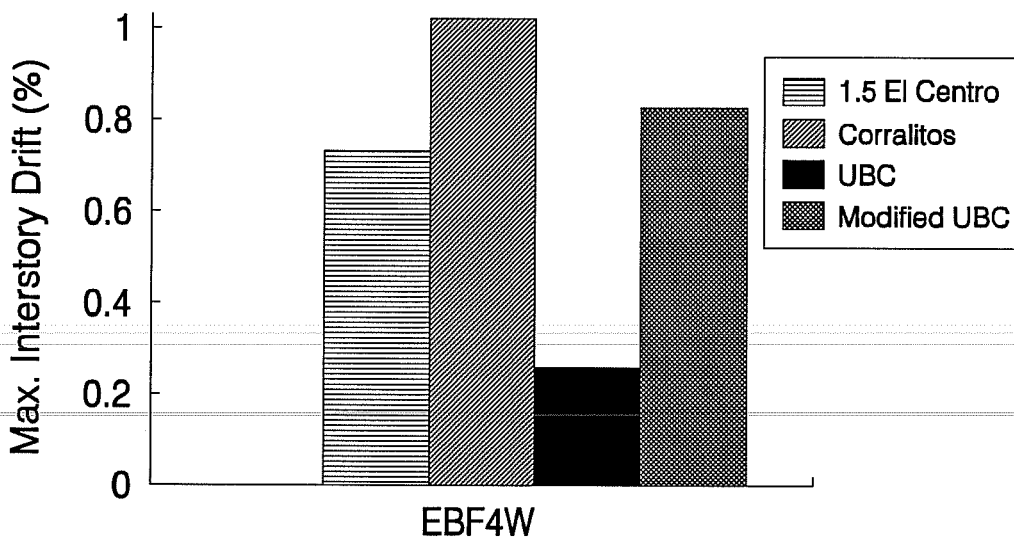


Figure 7.9 Maximum Interstory Drift for EBF4W Configuration of the Seven-Story Building

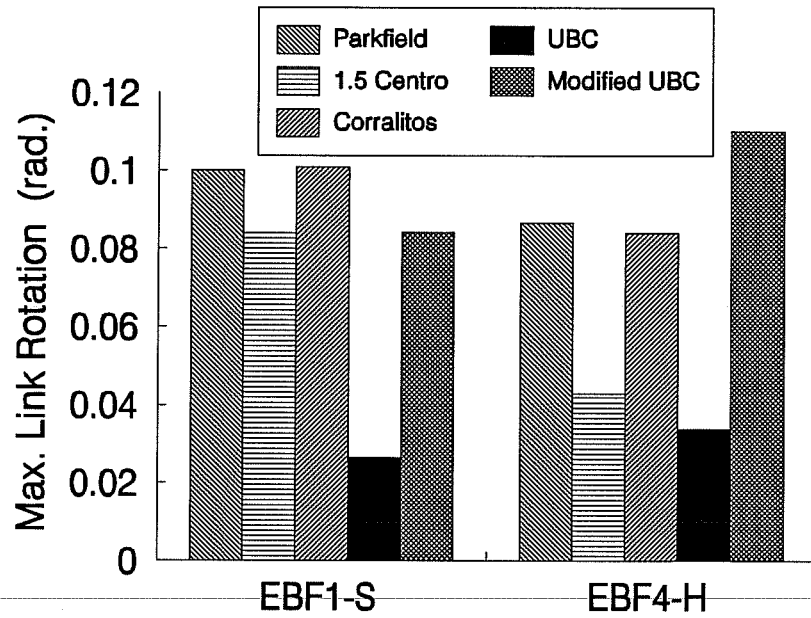


Figure 7.10 Maximum Plastic Link Rotations for EBF1-S and EBF4-H Configurations of the Three-Story Building

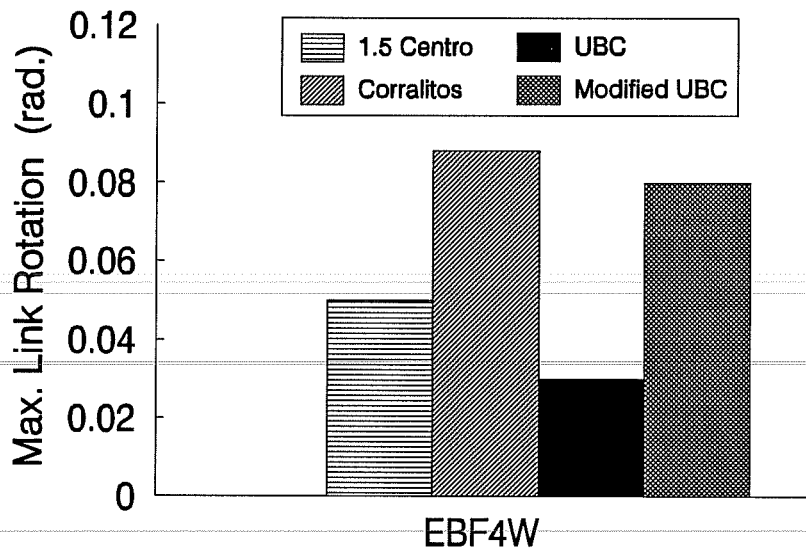


Figure 7.11 Maximum Plastic Link Rotations for EBF4W Configuration of the Seven-Story Building

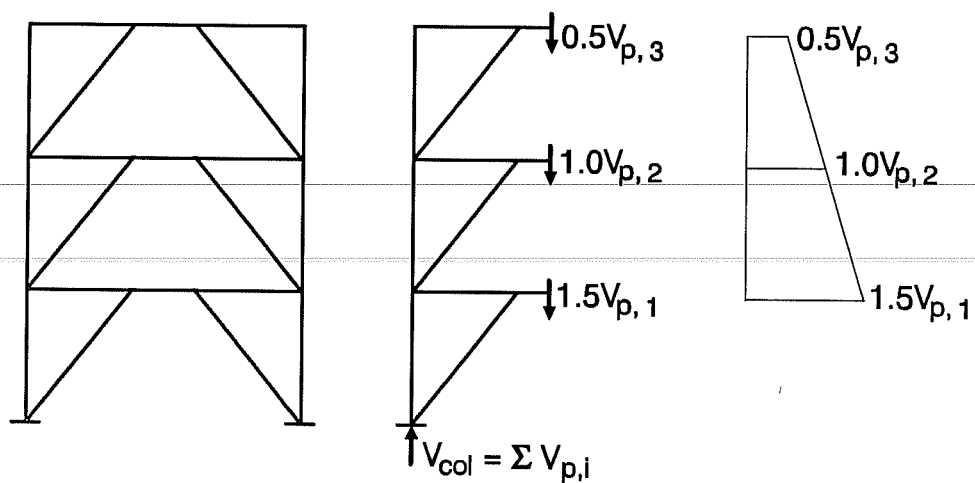


Figure 7.12 Schematic Representation for the Proposed Capacity Design Method for Column Axial Load

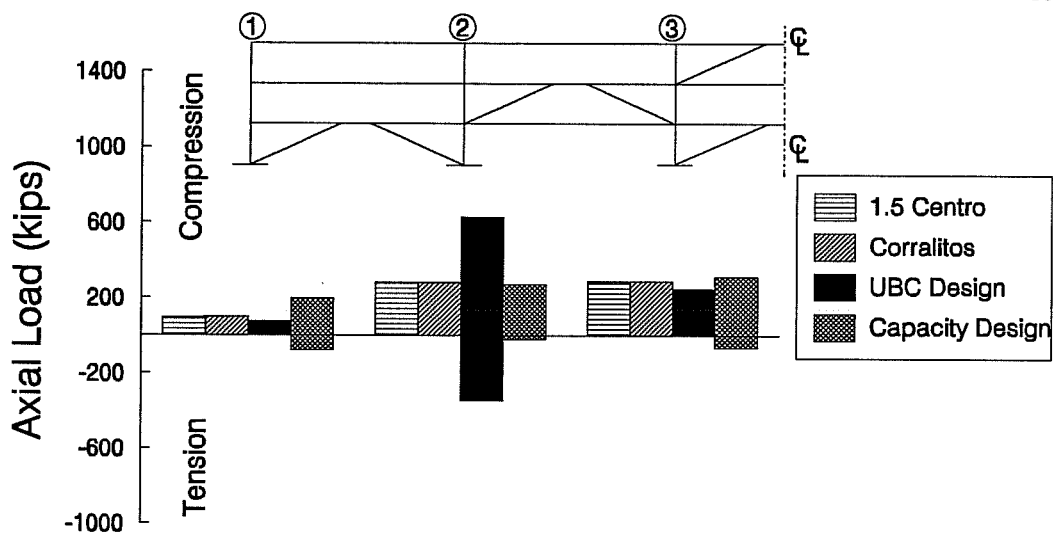


Figure 7.13 Maximum Axial Load at the Base of EBF1-S configuration for the Three-Story Building

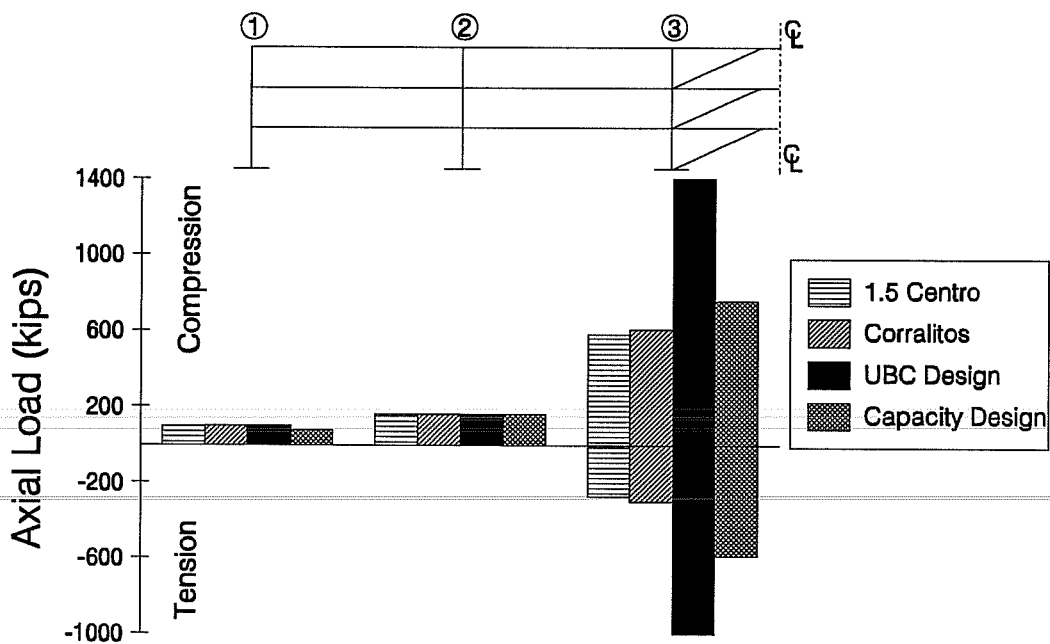


Figure 7.14 Maximum Axial Load at the Base of EBF4-H configuration for the Three-Story Building

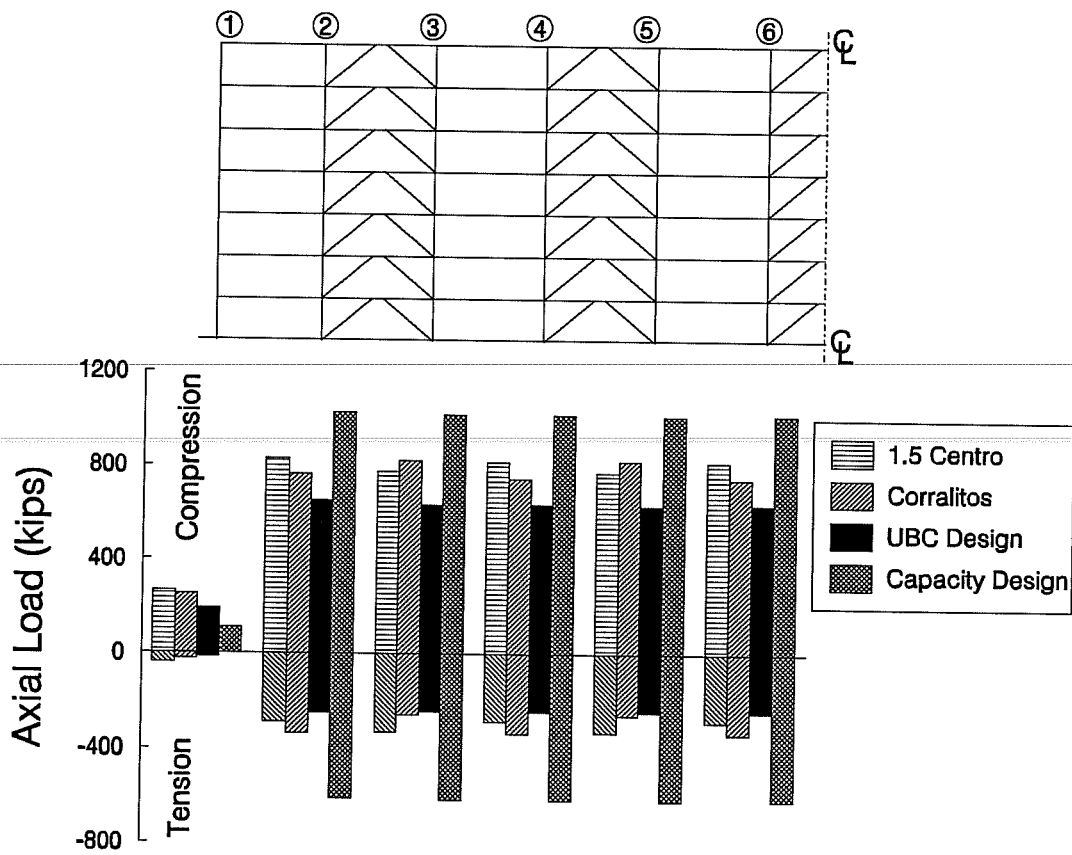


Figure 7.15 Maximum Axial Load at the Base of EBF4W configuration for the Seven-Story Building

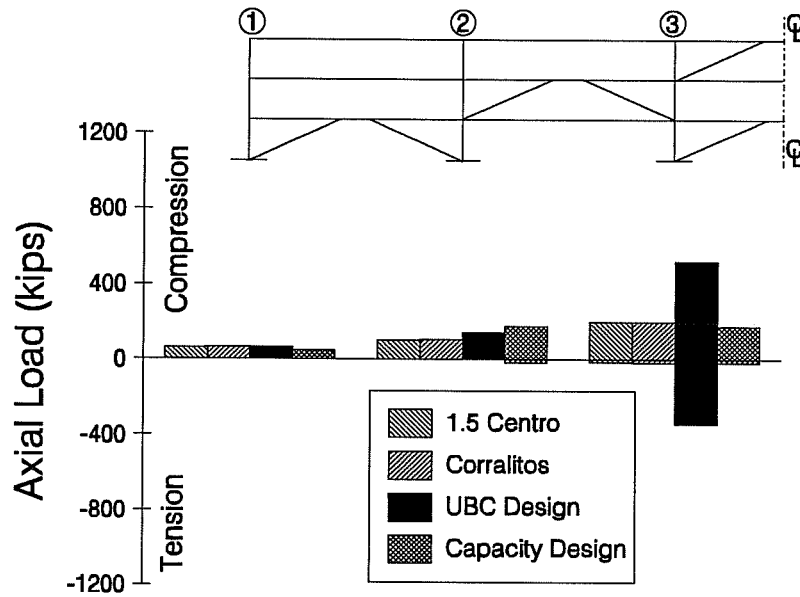


Figure 7.16 Maximum Axial Load at the Lower Section of the Second Level Columns for the EBF1-S Scheme of the Three-Story Building

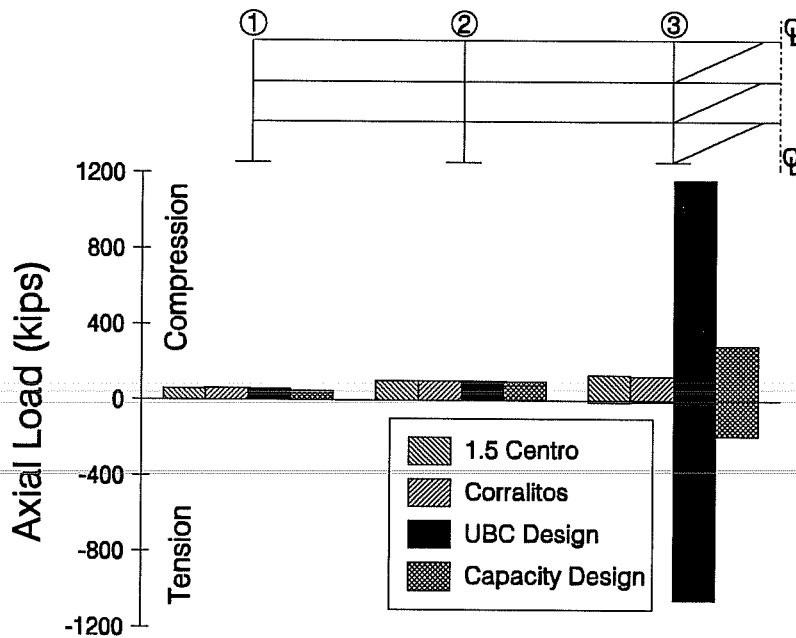


Figure 7.16 Maximum Axial Load at the Lower Section of the Second Level Columns for the EBF4-H Scheme of the Three-Story Building

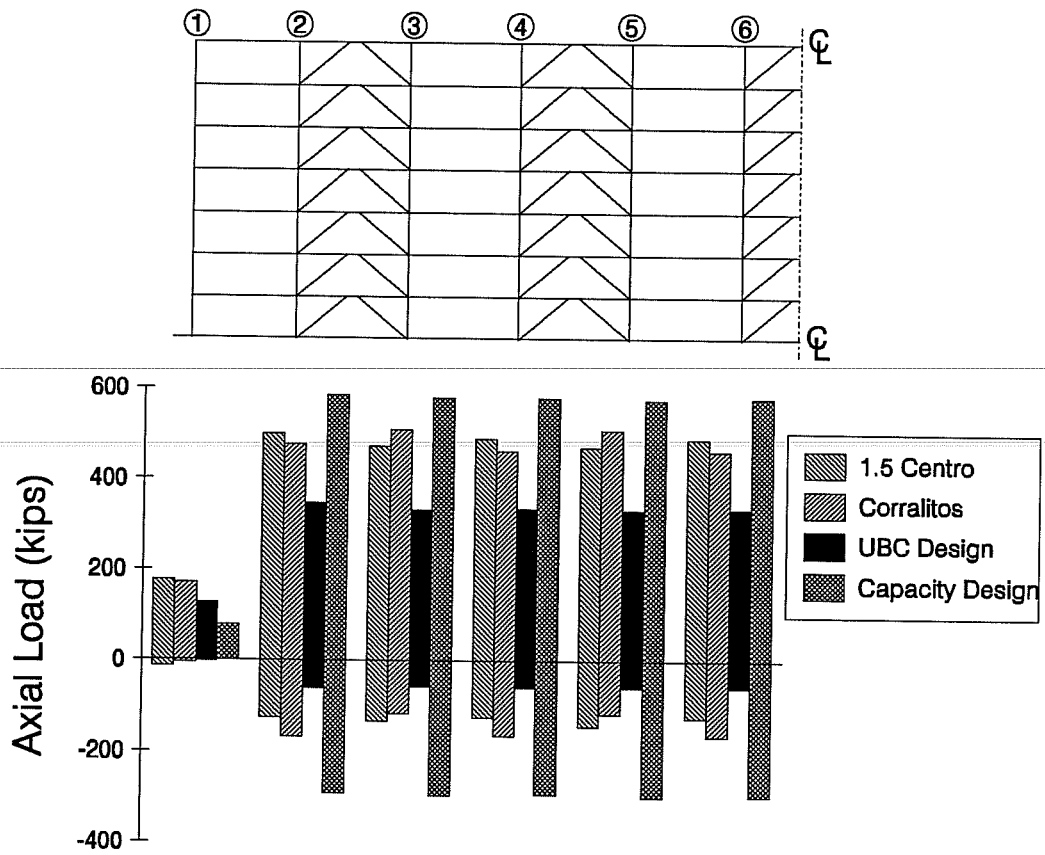


Figure 7.18 Maximum Axial Load at the Lower Section of the Third Level Columns for the EBF4W Scheme of the Seven-Story Building

CHAPTER 8: CONCLUSIONS

8.1. Summary.

The present research was conducted to study the feasibility of steel eccentrically braced frames (EBFs) as a retrofit scheme for existing reinforced concrete frames that are inadequately designed to resist seismic load. EBFs are known to be an effective lateral load resisting system in new steel structures subject to seismic loading. However as yet, EBFs have received little attention as a retrofit scheme. They combine high stiffness and strength and large ductility and exhibit stable hysteretic behavior under cyclic load. This can be a major benefit over concentrically braced frames (CBFs) which possess a high initial stiffness but have limited ductility and exhibit strength and stiffness degradation after brace buckling.

In EBFs, the inelastic deformations are limited to the links that are characterized by stable hysteretic behavior and high energy dissipation capacity. The rest of the structural members are designed to remain elastic under the forces generated by the fully plastic links. This design principle eliminates the possibility of brace buckling and results in high ductility for the entire system.

An analytical study was conducted to investigate the seismic performance of reinforced concrete buildings retrofitted with EBFs. A low-rise building and a medium-rise building, representative of the 1950s and 1960s west coast construction, were selected. The lateral load resisting system of both structures is formed by reinforced concrete moment frames. The main deficiencies of the low rise building consisted of inadequate column splices, very short embedment of the beams' bottom reinforcement, and widely spaced transverse reinforcement. The medium rise building featured deep spandrel beams and short columns with low shear strength.

Both buildings were found inadequate to resist high seismic forces and were retrofitted with several EBF schemes. The EBFs were added to the external frames only to limit disruption to the building during construction. The schemes investigated considered the use of different configurations and provided different levels of strength and stiffness. Possible effects of changes in the link length were investigated. The effect of reducing the strength with height to better match the seismic demand was also studied. The seismic behavior of the EBFs was compared to the behavior of similar CBF retrofit schemes.

The original reinforced concrete buildings and the retrofit schemes were analyzed under static and dynamic load. For the static analysis, a lateral incremental load was applied at the floor level. The dynamic analysis was carried out using two earthquake records on soft soils and three earthquake records on firm soil. The soft soil records were the N90E component of the 1985 Mexico SCT-1 record, and the N35E component of the 1989 Oakland Harbor Wharf record. The firm soil records were the N00E component of the 1940 El Centro record scaled to a peak acceleration of .5g, the N00E component of the 1989 Corralitos record, and the N65E component of the 1966 Parkfield record, Cholame array 5 station.

The analyses were conducted using the computer program DRAIN-2D that allows for nonlinear analysis of two-dimensional frames under gravity load and earthquake excitation. The program is composed of a base program and a set of element subroutines. Each subroutine models a specific type of member. The reinforced concrete member model used in this study considered stiffness degradation and splice failure. Shear failure was idealized by a simplified procedure that assumes that a member loses its lateral strength and stiffness after shear failure but maintains its axial stiffness. The purpose of the simple model was to provide some indication of the behavior of the structure after shear failure of some columns. The steel braces were modeled assuming elastic perfectly plastic behavior in tension and a stiffness and strength reduction after first buckling in compression. The brace model did not consider the effect of local buckling and could not predict brace failure.

In the original program, viscous damping was expressed as a combination of the mass matrix and the tangent stiffness matrix following the Rayleigh formulation. However, this and other studies suggested that EBFs modeled with conventional Rayleigh damping developed unrealistically high forces in the braces. A modified formulation was introduced in the program to avoid such unrealistic forces. In this formulation, viscous damping was expressed as a linear combination of the mass matrix and the initial stiffness matrix. Furthermore, damping for the shear links was assumed proportional to the mass only. In the analyses, the viscous damping was considered using this modified formulation of Rayleigh damping and assuming 2% of critical for the first and second vibration period.

8.2. Conclusions.

Based on the analyses performed on the selected buildings under severe ground motion, the following conclusions were reached:

- EBFs constitute an effective retrofit scheme and can control drift, and provide an increase in strength, stiffness, and ductility.
- EBFs alone may not be sufficient in preventing shear failure in columns. For a structure exhibiting low column shear strength, in addition to the EBFs, it may be necessary to either increase the shear capacity of the columns or change their mode of failure to a ductile flexural mode.
- The EBF retrofit schemes changed the dynamic characteristics of the structures and hence, affected the seismic demands. For the soft soil records, the increase in stiffness was accompanied by a reduced demand. However, for the California firm soil records, the increase in stiffness provoked an increase in the demand.
- Significant yield in the retrofitted structures started with first shear yielding in the links.

- Link length was found to affect the seismic behavior of the retrofitted structure. In general very short links provide for the best overall behavior.
- To obtain better behavior of the retrofitted structure, the strength and stiffness of the added EBF should be reduced with height in an attempt to match the demand. Failure to do so may lead to concentrated deformations at the lower levels and result in the formation of soft stories.
- The addition of EBFs to an existing structure leads to an increase in the axial load acting on the columns and foundation. These members may need to be strengthened to resist the additional load. Keeping the EBF strength to a minimum and distributing the braces to several bays limits the axial load increase.
- For the case studies, and if column shear failure is prevented, the added EBF can be designed to resist severe ground motions using the general procedures of the 1991 edition of the UBC but taking a force reduction factor, R_w , of 4.5 and a period of vibration, T , from a dynamic analysis. The design lateral load should be applied to the added steel EBF only.
- The deformation amplification factor (DAF) of $3/8 R_w$ used in the current UBC was found to be too low. A higher value for the DAF is needed to obtain a satisfactory estimate of the interstory drift and plastic link deformation under earthquake loads. A value of $1.2 R_w$ was proposed here.
- The maximum axial load in the columns can be estimated using a proposed capacity design method that relies on the building behavior. The links of an EBF allow for a control of the forces transferred to the remaining members which make a capacity design very suitable. The proposed method was found to yield better estimates of the column axial load than the current UBC procedure.

8.3. Need for Further Research.

Following are some suggestions for additional research:

- Additional case studies of existing buildings retrofitted with steel EBFs would be beneficial. Such studies would provide additional data on features such as the required R_w factor for an EBF, deflection amplification factors, forces developed at the foundations, etc...
- Steel collectors are often used to attach a bracing retrofit system to an existing reinforced concrete frame. The increase in stiffness and strength provided by these collectors cannot be properly estimated at present. Experimental research on isolated elements is needed to understand the behavior of reinforced concrete members strengthened by steel collectors.
- Experimental studies on connection details between the EBF link and the existing concrete member could be desirable. This connection must prevent lateral movement of the link, but should permit free vertical movement.
- The study presented here assumed two-dimensional behavior and neglected torsional effects. Torsion due to unsymmetric configuration or accidental eccentricities may affect the behavior of the EBF retrofit schemes. A three-dimensional analysis is needed to investigate the effects of torsional deformation.

BIBLIOGRAPHY

- Aboutaha, R.S., and Engelhardt M.D. (1994). "Seismic Strengthening of Non Ductile Reinforced Concrete Members Using Steel Jacketes", Ongoing Research, The University of Texas at Austin.
- ACI Committee 318, (1956). *Building Code Requirements for Reinforced Concrete (ACI 318-63)*, American Concrete Institute, Detroit, Michigan.
- ACI Committee 318, (1963). *Building Code Requirements for Reinforced Concrete (ACI 318-71)*, American Concrete Institute, Detroit, Michigan.
- ACI Committee 318, (1989). *Building Code Requirements for Reinforced Concrete (ACI 318-89)*, American Concrete Institute, Detroit, Michigan.
- ACI Committee 408. (1979). " Suggested Development, Splice, and Standard Hook Provisions for Deformed Bars in Tension." *Concrete International Journal*, July 1979, 44-46.
- AISC (1990a). *Load and Resistance Factor Design Manual for Steel Construction*.
- AISC (1990b). *Seismic Provisions for Structural Steel Buildings - Load and Resistance Factor Design*.
- Alcocer, S.M., and Jirsa, J.O., (1991). "Reinforced Concrete Frame Connections Rehabilitated by Jacketing." *PMFSEL Report 91-1*, Phil M. Ferguson Structural Engineering Laboratory, The University of Texas at Austin.
- Applied Technology Council, (1989). *ATC-22, A Handbook for Seismic Evaluation of Existing Buildings (Preliminary)*, Washington, D.C.
- Banon, H., Biggs, J.M., and Irvine H.M., (1981). Seismic Damage in Reinforced Concrete Frames." *Journal of the Structural Division*, Proceedings, ASCE, Vol. 107(9), 1713-1729.
- Bass, R. A. (1985). "Interface Shear Capacity of Concrete Surfaces Used in Strengthening Structures." PMFSEL Report No 85-4, Phil M. Ferguson Structural Engineering Laboratory, Department of Civil Engineering, The University of Texas at Austin.
- Bertero, V. V., Uang, C. M., Lopiz, C. R., and Igarashi, K. (1989). "Earthquake Simulator Testing of Concentric Braced Dual System." *Journal of Structural Division*, ASCE, Vol. 115 (No 8), 1877-1894.
- Building Seismic Safety Council, (1991). *NEHRP Recommended Provisions for the Development of Seismic Regulations for New Buildings*, Washington D.C.

- Bush, T. D. (1987). *Seismic Strengthening of a Reinforced Concrete Frame*, Ph.D. diss., The University of Texas at Austin.
- Bush, T. D., Roach, C. E., Jones, E. A., and Jirsa, J. O. (1986). "Behavior of Strengthened Reinforced Concrete Frame." *Third US Conference on Earthquake Engineering*, Charleston, 1203-1214.
- Clough R.W. and Penzien J. (1975). *Dynamics of Structures*, McGraw-Hill Book Company, New York.
- Del Valle, E. (1980). "Some Lessons From the March 14, 1979 Earthquake in Mexico City." *Proceedings, Seventh World Conference on Earthquake Engineering*, Istanbul.
- Engelhardt, M.D., (1987). "Long Links in Eccentrically Braced Frames: A Preliminary Assessment." *CE229 Report*, University of California, Berkeley, Department of Civil Engineering.
- Engelhardt, M.D., and Popov, E.P., (1989a). "On Design of Eccentrically Braced Frames." *Earthquake Spectra*, Vol. 5 (3).
- Engelhardt, M.D., and Popov, E.P., (1989b). "Behavior of Long Links in Eccentrically Braced Frames." *Report No UCB/EERC-89/01*, Earthquake Engineering Research Center, University of California, Berkeley.
- Engelhardt, M.D., and Popov, E.P., (1992). "Experimental Performance of Long Links in Eccentrically Braced Frames." *Journal of Structural Engineering*, ASCE, Vol. 118 (11), 3067-3088.
- Federal Emergency Management Agency (1989). "Techniques for Seismically Rehabilitating Existing Buildings (Preliminary)." *FEMA 172*.
- Foutch, D. A. (1989). "Seismic Behavior of Eccentrically Braced Steel Building." *Journal of Structural Division*, ASCE, Vol. 115 (No 8), 1857-1876.
- Foutch, D.A., Goel, S.C., Roeder, C.W., (1987). "Seismic Testing of Full Scale Steel Building - Part I." *Journal of Structural Engineering*, ASCE, Vol. 113 (11).
- Foutch, D. A., Hjelmstad, K.D., Del Val Caldéron, E., Figueriez Gutiérrez, and Downs R.E. (1989). "The Mexico Earthquake of September 19, 1985 - Case Studies of Seismic Strengthening of Two Buildings in Mexico City." *Earthquake Spectra*, Vol. 15, (1), 153-174.
- Gaynor, P.J. (1988). *The Effect of Openings on the Cyclic Behavior of reinforced Concrete Infilled Shear Walls*, Master Thesis, The University of Texas at Austin.

- Giberson, M. F. (1969). "Two Nonlinear Beams with Definition of Ductility." *Journal of Structural Division*, Proceedings, ASCE, 95 (ST2), 137-157.
- Hjelmstad, K. D., and Popov, E. P. (1983a). "Cyclic Behavior and Design of Link Beams." *Journal of Structural Engineering*, 109 (ST10), 2387-2403.
- Hjelmstad, K. D., and Popov, E. P. (1983b). "Seismic Behavior of Active Beam Links in Eccentrically Braced Frames." *Report No UCB/EERC 83/15*, Engineering Earthquake Research Institute, University of California at Berkeley.
- Hjelmstad, K. D., and Popov, E. P. (1984) "Characteristics of Eccentrically Braced Frames." *Journal of Structural Engineering*, ASCE, 110 (ST2), 340-353.
- International Conference of Building Officials, (1955). *Uniform Building Code*, Whittier, California.
- International Conference of Building Officials, (1964). *Uniform Building Code*, Whittier, California.
- International Conference of Building Officials, (1991). *Uniform Building Code*, Whittier, California.
- Jain A.K., and Goel S.C. (1978) "Hysteresis Model for Steel Members Subjected to Cyclic Buckling." *Report Research No UMEE 78R6*, The University of Michigan, Ann Arbor.
- Japan Building Disaster Prevention Association (1990). *Standard for Evaluation of Seismic Capacity of Existing Reinforced Concrete Buildings*.
- Jara, M., Hernández, C., García, R., and Robles, F. (1989). "The Mexico Earthquake of September 19, 1985 - Typical Cases of Repair and Strengthening of Concrete Buildings." *Earthquake Spectra*, Vol. 15, No 1, 175-193.
- Jimenez, L.R. (1989). *Strengthening of Reinforced Concrete Frame Using an Eccentric Wall*, Master Thesis, The University of Texas at Austin.
- Jiménez-Pacheco, J. (1992). *Behavior of Steel -to-Concrete Connections for Use in Repair and Rehabilitation of Reinforced Concrete Structures*, Master Thesis, The University of Texas at Austin.
- Jirsa, J.O, LeRoy, A.L., and Gergely, P. (1979). "Rational for Suggested Development, Splice, and Standard Hook Provisions for Deformed Bars in Tension." *Concrete International*, July 1979, 47-61.

- Jones, E. A., and Jirsa, J. O. (1985). Seismic Strengthening of a Reinforced Concrete Frame Using Steel Bracing." *Report PMFSEL 86-5*, The University of Texas at Austin, Bureau of Engineering, Department of Civil Engineering.
- Kanaan, A.E., and Powell G.H. (1975). "DRAIN-2D" EERC *Report No 73-6 and &3-22*, The University of California, Berkeley.
- Kasai, K. S., and Popov, E. P. (1986a). "Cyclic Web Buckling Control For Shear Link Beams." *Journal of Structural Engineering*, 112 (ST3), 505-523 experimental behavior of links.
- Kasai, K. S., and Popov, E. P. (1986b). "General Behavior of WF Steel Shear Link Beams." *Journal of Structural Engineering*, ASCE, 112 (ST2), 362-382
- Kasai, K. S., and Popov, E. P. (1986c). "A Study of Seismically Resistant Eccentrically Braced Steel Frame Systems." *EERC Report 86/01*, Earthquake Engineering Research Center, The University of California at Berkeley.
- Kawamata S, and Ohnuma M. (1980). "Strengthening Effect of Eccentric Steel Braces to Existing Reinforced Concrete Frames." *Proceedings of the Seventh World Conference on Earthquake Engineering*, Istanbul, 513-520.
- Kent, D.C., and Park R., (1971). "Flexural Members with Confined Concrete." *Journal of the Structural Division*, ASCE, Vol. 97 (7), 1969-1989.
- Khatib, I.F., Mahi, S. A., and Pister K.S. (1988). "Seismic Behavior of Concentrically Braced Steel Frames." *Report UCB/EERC-88/01*, Earthquake Engineering Research Center, The University of California at Berkeley.
- Lee S, and Goel, S.C. (1987). "Seismic Behavior of Hollow and Concrete-Filled Square Tubular Bracing Members." *Research Report UMCE 87-11*, Department of Civil Engineering, The University of Michigan Ann Arbor.
- Lee, S. J., and Lu, L. W. (1989). "Quasi-Static Tests of Scaled Model Building." *Journal of Structural Engineering*, ASCE, Vol. 15 (8), 1895-1916.
- Lew, H.S., Leyendecker, and Dikkers, R.D., (1971). *Engineering Aspects of the 1971 San Fernando Earthquake*, National Bureau of Standards, Washington D.C.
- Mahin, S.A., and Bertero, V.V., (1977). *RCCOLA, A Computer Program for Reinforced Concrete Column Analysis, User's Manual and Documentation*, Department of Civil Engineering, University of California, Berkeley.
- Maison, B.F., and Popov, E.P. (1980). "Cyclic Response Prediction for Braced Steel Frames." *Journal of Structural Division*, ASCE Proceedings, Vol 106 (ST7), 1401-1416.

- Malley, J. O., and Popov, E. P. (1984). "Shear Links in Eccentrically Braced Frames." *Journal of Structural Engineering*, 110 (ST9), 2275-2295.
- Malley, J. O., and Popov, E. P. (1983). "Design Considerations for Shear Links in Eccentrically Braced Frames." Report No UCB/EERC 83/24, Earthquake Engineering Research Center, The University of California at Berkeley.
- Manhein, D. N., and Popov, E. P. (1983). "Plastic Shear Hinges in Steel Frames." *Journal of Structural Engineering*, 109(ST10), 2404-2419.
- Midorikawa, M., Nishiyama, I., and Yamanouchi, H. (1989). "Analytical Evaluation of K-Braced Structure Seismic Test." *Journal of Structural Engineering*, ASCE, Vol. 15 (No. 8), 1930-1948.
- Miranda, E. (1990). "Upgrading of a School Building in Mexico City." *Proceedings, Fourth US National Conference on Earthquake Engineering, Palm Springs, California*, 109-118
- Moehle, J.P., Kreger, M.E., and Leon, R. (1988). "Background to Recommendations for Design of Reinforced Concrete Slab-Columns Connections." *ACI Structural Journal*, Vol. 85 (6), 636-644.
- Mondkar, D.P. and Powell, G.H. (1975). "ANSR-I General Purpose Computer Program for Analysis of Non-Linear Structural Response." *EERC Report No 75-73*, Earthquake Engineering Research Center, the University of California, Berkeley.
- Nakashima, M. (1992). "Analysis and Design of Steel Braces and Braced Frames in Building Structures." *Stability and Ductility of Steel Structures Under Cyclic Loading*, CRC Press, Boca Raton, Florida.
- Newmark, N.M. (1959). "A Model of Computations for Structural Dynamics." *Journal of the Engineering Mechanics Division*, ASCE, Vol. 85 (EM3), 67-94.
- Nishiyama, I., Midorikawa, M., and Yamanouchi, H. (1988). "Inelastic Behavior of Full Scale Eccentrically K-Braced Building." *Proceedings, Ninth World Conference on Earthquake Engineering*, Volume IV, 261-266.
- Okada T., and Bresler B. (1976). "Strength and Ductility Evaluation of Existing-Low Rise Reinforced Concrete Buildings -Screening Method-." *EERC Report No 76-1*, The University of California, Berkeley.
- Orangun, C.O., Jirsa, J.O., and Breen, J.E. (1977). "A Reevaluation of Test Data on Development Length and Splices." *ACI Journal*, March 1977, 114-122.
- Pessiki, S. P., Conley C., White, R. N., and Gargely, P. (1990). "Seismic Resistance of the Beam Column Connection Region in Lightly Reinforced Concrete Frame Structures." *Proceedings*

- of the Fourth U.S. National Conference on Earthquake Engineering, Palm Springs, California, 707-716.*
- Pincheira, J., (1992). *Seismic Strengthening of Reinforced Concrete Frames Using Post-Tensioned Bracing Systems*, Ph.D. Dissertation, The University of Texas at Austin.
- Popov, E. P., and Black, R. G. (1981). "Steel Struts Under Cyclic Loadings." *Journal of Structural Engineering Division*, ASCE, 107(ST9), 1857-1881.
- Popov, E. P., and Engelhardt M. D. (1988). "Seismic Eccentrically Braced Frames." *Journal of Construction Steel Research*, No 10, 321-354.
- Popov, E.P., Kasai, K., and Engelhardt, M.D. (1993). "Some Unresolved Issues in Seismic Steel Codes." *ASCE Structures Congress '93 Proceedings*, Irvine California.
- Roeder, C.W., and Popov, E.P. (1977). "Inelastic Behavior of Eccentrically Braced Steel Frames Under Cyclic Loadings." *Research Report No UCB/EERC-77/18*, Earthquake Engineering Research Center, University of California, Berkeley.
- Roeder, C.W., and Popov, E. P. (1978). "Eccentrically Braced Steel Frames for Earthquakes." *Journal of Structural Division*, proceedings, ASCE, 104 (ST3), 391-413.
- Roeder, C.W. (1989). "Seismic Behavior of Concentrically Braced Frame." *Journal of Structural Engineering*, ASCE, Vol. 115 (8), 1837-1856.
- Seismic Provisions for Structural Steel Buildings*, (1990). Load and Resistance Factor Design, LRFD. American Institute of Steel Construction, Chicago, Illinois.
- Scott, B.D., Park R., and Priestley, N.J. (1982). "Stress-Strain Behavior of Concrete Confined by Overlapping Hoops at Low and High Strain Rates.", *ACI Journal*, Vol. 79(2), 13-27.
- Sugano, S., (1982). "An Overview of the State-of-the-Art in Seismic Strengthening of Existing Reinforced Concrete Buildings in Japan." *Proceedings of the Third Seminar on Repair and Retrofit*, US-Japan Cooperative Research Program, The University of Michigan at Ann Arbor, 328-349.
- Takeda, T., Sozen M.T., and Nielson N.N. (1970). "Reinforced Concrete Response to Simulated Earthquakes." *Journal of Structural Division*, ASCE, 96(ST12), 2558-2572.
- Tang, X., and Goel, S.C. (1987). "Seismic Analysis and Design Considerations of Braced Steel Structures." *Research Report UMCE 87-4*, Department of Civil Engineering, The University of Michigan Ann Arbor.

- Tang, X., and Goel, S.C. (1988). "DRAIN-2DM - Technical Notes and User's Guide." *Research Report UMCE 88-1*, Department of Civil Engineering, The University of Michigan Ann Arbor.
- Trembley, R. (1991). "Toward a Comprehensive Seismic Design Approach for Concentrically Braced Steel Frames." *Seismic Design of Steel Structures*, CSCE Seismic Seminar, Vancouver.
- Uang, C.M. (1991). "Establishing R (or R_w) and C_d Factors for Building Seismic Provisions." *Journal of Structural Engineering*, ASCE, Vol. 117 (1), 19-28.
- Uang, C.M., and Maarouf A. (1993). "Displacement Amplification Factor for Seismic Design Provisions." *Proceedings, 1993 ASCE Structures Congress*, Irvine, California., 211-216.
- Umehara, H. and Jirsa, J.O., (1982). "Shear Strength and Deterioration of Short Reinforced Concrete Columns under Cyclic Deformations." *PMFSEL Report 823*, The University of Texas at Austin.
- Umemura H. (1980). "A guideline to Evaluate Seismic Performance of Existing Medium and Low-Rise Reinforced Concrete Buildings and Applications." *Proceedings of the Seventh World Conference on Earthquake Engineering*, Istanbul, 505-512.
- Valluvan, R. (1993). Issues Involved in Seismic Retrofit of Reinforced Concrete Frames Using Infilled Walls, Ph.D. Dissertation, The University of Texas at Austin.
- Whittaker, A.S., Uang, C.M., Bertero, V.V. (1987). "Earthquake Simulation Tests and Associated Studies of a 0.3-Scale Model of a Six-Story Eccentrically Braced Steel Structure." *Report No UCB/EERC-87/02*, Earthquake Engineering Research Institute, The University of California at Berkeley.
- Wakabayashi, M. (1986). *Design of Earthquake-Resistant Buildings*, McGraw-Hill Book.
- Wyllie, L.A., Dal Pino, J.A., Cohen, J., (1991). "Seismic Upgrade Preserves Architecture." *Modern Steel Construction*, January 1991, 20-23.
- Woodward, K.A., and Jirsa, J.O. (1984). "Influence of Reinforcement on RC Short Column Lateral Resistance." *Journal of Structural Engineering*, Vol. 110(1), 90-104.

VITA

Abdelhakim Bouadi was born on November 4, 1961 in Algiers, Algeria, the son of Mohand Bouadi and Taos Messara. After completing his high school, he entered the Ecole Polytechnique d'Alger where he received his *Ingéniorat* (B.Sc.) in June 1985. He obtained a Master of Sciences in Civil Engineering from the University of Texas at Austin in Fall 1989.

Permanent Address: 68 Rue Jean Jaures
El Mouradia, 16070
Algiers, Algeria

This dissertation was typed by the author

